A light in the dark: Using cabled seafloor observatories to study abundance and behaviour of seafloor megafauna in response to environmental change

by

©Rylan J. Command B.Sc.

A thesis submitted to the School of Graduate Studies in partial fulfillment of the requirements for the degree of Master of Science in Fisheries Science and Technology

Marine Institute

School of Fisheries

Memorial University of Newfoundland and Labrador

June 14, 2022

St. John's, Newfoundland and Labrador

Table of Contents

Table of Contents ii

Abstract vi

Acknowledgments vii

List of Tables ix

List of Figures xi

List of Appendices xiv

Co-authorship Statement xv

Chapter 1: Introduction 1

1.1 Scales of variability in the ocean 1

1.2 Sampling the seafloor 4

1.3 Seafloor observatories 5

1.4 Objectives 7

1.5 References 9

1.6 Figures 16

Chapter 2: Temporal dynamics of the deep-sea pink sea urchin *Strongylocentrotus fragilis* on the Northeast Pacific continental margin 17

2.1 Introduction 18

2.2 Methods 23

2.2.1 Study site 23

2.2.2 Estimating *S. fragilis* densities from imagery 24

2.2.3 Environmental data from the seafloor and sea-surface 26

2.2.4 Bottom Trawl Surveys (2004-2018) 28

2.2.5 Data analysis 29

2.2.5.1 Environmental predictor variables and density of S. fragilis 29

2.2.5.2 Trawl surveys 32

2.3 Results 33

2.3.1 Temporal patterns of sea urchin density 33

2.3.2 Pink sea urchin density model fit / model selection 33

2.3.3 Environmental models 34

2.3.3.1 Seafloor dissolved oxygen GAMM 34

2.3.3.2 Surface chlorophyll-a GAMM 35

2.3.4 Trawl Survey data (2004-2018) 35

2.4 Discussion 36

2.4.1 Within- and between-year variation of sea urchin density 38

2.4.2 *S. fragilis* response to the 2013-2016 marine heatwave 42

2.4.3 Decadal distribution shifts (from bottom trawl surveys) 45

2.5 Conclusion 46

2.6 Acknowledgements 46

2.7 References 49

2.8 Tables 58

2.9 Figures 67

Chapter 3: A first look at megabenthic community responses to seasonal change using the new Holyrood Subsea Observatory in Conception Bay, NL. 82

3.1 Introduction 83

3.2 Methods and Materials 89

3.2.1 Study site 89

3.2.2 Data collection 89

3.2.2.1 Holyrood Subsea Observatory System 89

3.2.2.2 Environmental data collection and processing 91

3.2.2.3 Video collection and faunal characterization 92

3.2.3 Statistical analysis 92

3.2.3.1 Community characterization 93

3.2.3.2 Biological rhythms and tidal periodicity 94

3.2.3.3 Changepoint analysis 95

3.3 Results 97

3.3.1 Spring bloom conditions 97

3.3.1.1 Temperature and salinity 97

3.3.1.2 Chlorophyll-a and turbidity 98

3.3.2 Benthic community 99

3.3.2.1 Whole-community response 99

3.3.2.2 Psolus phantapus emergence 101

3.3.3 Tidal periodicity, currents, and biological rhythms 102

3.4. Discussion 103

3.4.1 Spring bloom dynamics 103

3.4.2 *Psolus* emergence and phenology 106

3.4.3 Tidal periodicity 109

3.4.4 Other taxa 110

3.5 Conclusions and future directions 112

3.6 Acknowledgements 114

3.7 References 115

3.8 Tables 123

3.9 Figures 130

Chapter 4: Conclusion 143

4.1 References 149

Appendix 1: Field of view calculations 153

A1.1 Barkley Canyon Upper Slope 153

A1.2 Holyrood Subsea Observatory 158

Appendix 2: Drowning in Data: How artificial intelligence could throw us a life ring 159

Abstract

Surface primary productivity forms the base of most marine food webs and contributes significantly to global carbon cycling, providing a key link from surface to seafloor. High seasonal primary productivity along temperate latitude coastlines provides crucial nutrients for seafloor communities, driving spatiotemporal patterns in abundance, behaviour, biodiversity, and distribution of benthic megafauna. Many factors, including ocean warming, deoxygenation, and increasing frequency and duration of marine heatwaves (MHW), may alter the dynamics governing primary production, threatening benthic organisms that depend on the seasonal input of phytodetritus for food. The focus of this thesis is to make use of two seafloor observatories, NEPTUNE near Vancouver Island, British Columbia, and a new platform in Conception Bay, NL, to examine variability in abundance, behaviour, and composition of seafloor communities in response to environmental change across temporal scales. First, the response of the deep-sea pink urchin *Strongylocentrotus fragilis* to a recent MHW on the continental margin off the coast of Vancouver Island was investigated using a combination of benthic trawls (2004-2018) and seafloor observatory data (2013-2020). Sea urchin density declined during the MHW, likely in response to reduced kelp subsidies from coastal waters. Next, the new Holyrood Underwater Observatory in Conception Bay was used to study benthic community response to the spring phytoplankton bloom. High-frequency variability in seafloor environmental dynamics was documented during the winter-spring transition, and the unexpected emergence of >200 sea cucumbers (*Psolus* sp.) coinciding with the arrival of phytodetritus at the seafloor was observed. These data will provide a baseline against which to monitor changes in phenology as climate change progresses. This work comes at a critical point in ocean observing as we approach global climate tipping points. Now more than ever, it is essential to document the current state of marine communities to understand and predict community responses to changing ocean conditions, and to sustainably manage ocean resources.

Acknowledgments

I would like to acknowledge the immense amount of support I received throughout my program, without which I could not have completed this degree. First, I thank my supervisor Dr. Katleen Robert for accepting me into the lab and giving me the opportunity to work on this project. I am very grateful for your calm and thoughtful mentorship and guidance as I venture into the academic world. Thank you to my co-supervisor Dr. Cynthia McKenzie for making me feel welcome at Fisheries and Oceans, and for sharing your wisdom and local knowledge. I also thank my committee member Dr. Fabio De Leo for always taking the time to meet with me and exchange thoughts and ideas, as well as your thorough and ever-helpful feedback on all my writing. I promise I now understand how to calculate field of view.

I would also like to acknowledge field and technical support from so many people. Thank you to Adam Templeton and Kirk Regular for deploying and recovering the sonde in Holyrood, and for your patience and kindness when presented with a less-than-seaworthy graduate student. I am grateful for your endless expertise, and especially your seasickness cures. Thank you also to Phil Sargent, Megan Mews, Kyle Matheson, and Haley Lambert for sonde support and calibration, as well as collecting phytoplankton samples during the spring bloom. I also thank Sally Faulkner for analyzing these samples and for your unwavering kindness and friendship whenever we cross paths (not to mention a seemingly endless supply of home baking that I could never eat enough of).

I extend my sincere gratitude to everyone at Ocean Networks Canada who has ever worked on the NEPTUNE and Holyrood Subsea Observatory observatories. I do not have space to list everyone by name, but I am grateful for all you do to make research like this possible. I would like to give a special thank you to Dwight Owens and Grant Garner who, although we have never actually met in person, provided steady support in everything form of troubleshooting flickering observatory lights to writing code to process ADCP data in R.

Ok, now for the big ones. I would like to thank, in no particular order, Shreya, Kate, Poppy, Julia, Aaron, Ben, Xiaodong, Belen, Emme, and Zach from the 4D Oceans Lab for fostering such a wonderful and supportive community inside and outside the lab. I am so grateful for all the kitchen parties and pizza nights, hikes and adventures, and I am so excited to see where everyone ends up.

My parents, Bonnie and Chris Command, without whom I, for obvious reasons, would not be here writing this thesis (thanks a lot). You always push me to be the best version of myself, and you don't mind telling me when I stray. I never feel as though you doubt me, even though I often doubt myself. Your support has always been steadfast, and I will always be grateful for that.

Finally, to my loving partner, Mary. These last three years have not gone by easily. Both of us working on graduate degrees and working part-time simultaneously, making time to explore Newfoundland, maintain our sanity, fitness, and a social life, and still enjoy each others company. All this while sharing a room that has been one-part bedroom, one-part yoga studio, and two-parts home office. Through all the challenges this time has brought, you have always been my rock. You always challenge me, and push me to stand up for myself and to speak my mind. You always proof-read the emails I am overly stressed about, and make them seem light and easy.

I know that I drive you crazy, especially when I'm coding and I don't breathe for a few minutes and then inhale really loudly. That must be super annoying. But all the while you stuck by me, and for that I will be forever grateful.

List of Tables

Table 2.1. Video camera deployments for each time-series sampling period at the Barkley Canyon Upper Slope.

Table 2.2. List of instruments, sampling frequencies, measured environmental variables, and their units for data collected at the upper slope of Barkley Canyon (48° 25' 37.2"N, 126° 10' 29.7"W), weather data collected from the La Perouse Bank buoy (48° 49' 48"N, 126° 0' 0"W), Tofino, British Columbia and MODIS satellite. Data were collected from August 15, 2013 to February 3, 2014, August 15, 2014 to January 15, 2015, August 15, 2018 to November 24, 2018, and September 11, 2019 to February 3, 2020.

Table 2.3. Akaike Information Criteria (AIC) table comparing Generalized Additive Model fits for Barkley Canyon Upper Slope sea urchin density. ΔAIC refers to the difference in AIC between each model and the best model for Temporal models and Temporal + environmental covariate (Env. Cov.) models. Global smooths in Temporal model + Env. Cov. are dissolved oxygen, current magnitude, and ADCP backscatter.

Table 2.4. Model summary table for parametric and smooth terms of final generalized additive model for sea urchin abundance at Barkley Canyon Upper Slope.

Table 2.5. Model summary table for parametric and smooth terms of final generalized additive mixed-model for benthic dissolved oxygen at Barkley Canyon Upper Slope.

Table 2.6. Dunn's post-hoc multiple comparisons with Bonferroni correction for S. fragilis density over time from the West Coast Vancouver Island synoptic bottom trawl surveys. Komolgorov-Smirnov (K-S) comparison of S. fragilis depth distributions for each pair of survey years. Bold rows indicate statistical significance at the $\alpha = 0.05$ level.

Table S2.1. Model summary table for linear regression models for depth distribution parameters as a function of time, trawl contents (sea urchins only vs all species), and an interaction between time and trawl contents. Bold-face p-values indicate significance at the alpha = 0.05 level.

Table 3.1. Average (+/- standard deviation) and maximum count and density (abundance/area where area is 0.89 m^2) observed per video at the Holyrood Subsea Observatory over the study period (Feb 21 – Jun 16, 2021).

Table S3.1. Range and mean +/- SD for environmental variables from the Holyrood Underwater Observatory over the entire study period (Feb 21 – Jun 16, 2021).

Table S3.2. SIMPER analysis results.

Table S3.3. Chlorophyll-*a* change points. Mean, Lower, and Upper represent the average and the 95% confidence interval around each variable. For the change points (cp 1 to cp 5) the values are given as a "time step", where a one-unit increase in time step equals one hour and time zero is February 21st, 2021 at 00:00:00 UTC.

Table S3.4. Temperature change points. Mean, Lower, and Upper represent the average and the 95% confidence interval around each variable. For the change points (cp 1 to cp 5) the values are given as a "time step", where a one-unit increase in time step equals one hour and time zero is February 21st, 2021 at 00:00:00 UTC.

Table S3.5. *Psolus phantapus* change points. Mean, Lower, and Upper represent the average and the 95% confidence interval around each variable. For the change points (cp 1 to cp 5) the values are given as a "time step", where a one-unit increase in time step equals one hour and time zero is February 21st, 2021 at 00:00:00 UTC.

List of Figures

Figure 1.1. Spatial and temporal scales of physical environmental (left) and biological (right) processes. Adapted from Chelton et al. (2007).

Figure 2.1. Map of the study area showing the NEPTUNE cabled observatory infrastructure at Barkley Canyon and Upper Slope (A). Examples of two seafloor camera fields of views for November 2013 (B), and January 2020 (C).

Figure 2.2. Observed pink sea urchin density (points) and predicted (solid lines) values from the highest-ranking environmental hierarchical generalized additive model for each year. Solid lines are the smooth mean trend of sea urchin abundance for each year, the ribbon is +/- pointwise 95% confidence interval.

Figure 2.3. Global smooths for the effects of oxygen (A) and ADCP backscatter (B) on *S. fragilis* density from the final temporal and environmental covariate GAM.

Figure 2.4. Weekly benthic dissolved oxygen concentration (solid black line) at Barkley Canyon Upper Slope from 2013-2020. Solid red line is the smoothed temporal trend of oxygen over time, grey ribbon is +/- standard error around the trend, and horizontal dashed line is the mean dissolved oxygen across the entire study period. Orange overlay represents the duration of the 2013-2016 warm blob.

Figure 2.5. Smooth effects of week of year (A) and surface chlorophyll-a concentration (B). Lines are mean oxygen concentration, grey ribbons are +/- 95% confidence interval around the mean. Parametric fixed-effect of year (C), points represent the mean effect of each year relative to 2013, vertical lines are +/- 95% confidence interval around the mean effect. Vertical dashed lines in (A) are the average week of the onset of summer (blue) and winter (grey).

Figure 2.6. Predicted values of oxygen for weekly surface chlorophyll-a concentration on benthic dissolved oxygen at Barkley Canyon Upper Slope across the entire study period (2013-2020). Points are a scatter plot of dissolved oxygen and chlorophyll-a, solid red line is the smooth effect, grey ribbon is +/- 95% CI around the smooth. Horizontal dashed line is the mean dissolved oxygen concentration across the entire study period.

Figure 2.7. Smooth effects of week of year (A) and sea-surface temperature anomaly (B). Lines are mean chlorophyll-a concentration, grey ribbons are +/- 95% confidence interval around the mean. Parametric fixed-effect of year (C), points are the mean effect of each year relative to 2002, vertical lines are +/- 95% confidence interval around the mean effect.

Figure 2.8. Mean +/- standard deviation of density of *S. fragilis* found in the West Coast Vancouver Island bi-annual trawl surveys from 2004-2018 considering the entire depth range of trawl samples. The orange band indicates the 2013-2016 “Warm Blob”.

Figure 2.9. Depth-distribution statistics from 2004-2018 from the West Coast Vancouver Island bi-annual trawl surveys for trawls where pink sea urchins were caught (blue points) and for all trawls (red points). Coloured lines represent the least squares fitted line for a simple linear model

for all trawls (red line) and trawls where pink sea urchins were caught (blue line). Grey bands represent 95% confidence intervals around the fitted line.

Figure 2.10. Box plot of depth distribution of *S. fragilis* obtained from the bi-annual West Coast Vancouver Island synoptic trawl survey from 2004-2018. Solid horizontal line indicates median depth, + symbol indicates mean depth, and dots indicate outliers that are greater than 1.5 times the distance between the 25% and 75% quartiles. Numbers above each box indicates the number of trawls in which *S. fragilis* was present for each survey year. Orange band indicates the 2013-2016 "Warm Blob". Two trawls found pink sea urchins at 800 m depth but were considered outliers and were subsequently excluded from analysis.

Figure S2.1. Map of the West coast of Vancouver Island. Depth contours shown at 400m and 2000m. Green box indicates the area from which Chlorophyll-a values were extracted from the MODIS OceanColour satellite (bottom-left corner at 48˚N, 128˚W, top-right corner at 49˚30'N, 124° 35' 59.99451"). Orange point indicates the location of the Barkley Canyon Upper Slope platform of the NEPTUNE observatory. Dots indicate the start position of all trawls from the 2004-2018 biannual West Coast Vancouver Island synoptic bottom trawl surveys, where black dots represent trawls that did not find any Strongylocentrotus fragilis and red dots represent those trawls that recorded at least one S. fragilis, including those for which 1) a count was recorded, or 2) a weight was recorded and a count was not (see Methods section 2.4 for more details). GEBCO Gridded Bathymetry data retrieved from https://download.gebco.net/.

Figure S2.2. Autocorrelation plot for residuals of sea urchin temporal model I.

Figure S2.3. Autocorrelation function of benthic oxygen Generalized Additive Mixed-Model residuals. Dotted blue line indicates the threshold for significance at the alpha = 0.05 level.

Figure S2.4. Predicted versus observed values (points) for temporal sea urchin model I (A) and final temporal + environmental covariate sea urchin model (B). Points are transparent to illustrate overlap between points. 1:1 line added for reference.

Figure S2.5. Benthic boundary layer currents (BBLc) magnitude (m/s) at Barkley Canyon Upper Slope. Red dashed line indicates the threshold above which resuspension of phytodetritus and other organic matter can occur.

Figure 3.1. Map of the Holyrood Inlet of Conception Bay. Black triangle represents the location of the Holyrood Subsea Observatory (82 m depth). Bathymetry measured at 10 m resolution.

Figure 3.2. Observed environmental time series over the study period at the Holyrood Underwater Observatory at 82 m depth. (A) temperature (˚C), (B) salinity (psu), (C) near-seabed chlorophyll-*a* (µg mL^{-3}), (D) near-surface chlorophyll-*a* (µg mL^{-3}), and (E) backscatter (Hz).

Figure 3.3. Photographic atlas of the most common taxa observed at the Holyrood Subsea Observatory between February 21 and June 16, 2021. (A) *Anarhichas lupus*, (B) Nudibranchia sp.1, (C) Ophiuroidea spp., (D) *Solaster endeca*, (E) *Psolus* cf. *phantapus*, (F) Zoarcidae sp., (G)

Caridea spp., (H) *Phoca* sp., (I) school of Clupeidae, (J) Osmeridae (*Mallotus villosus*), (K) *Hyas* sp., (L) *Chionoecetes opilio*.

Figure 3.4. Time series of abundance of the most common morphotaxa over the study period at the Holyrood Subsea Observatory. (A) *Psolus phantapus*, (B) Caridean shrimp, (C) Ophiuroidea, (D) Clupeidae, (E) Osmeridae, and (F) *Chionoecetes opilio.*

Figure 3.5. Graphical ordination of daily observations using the Bray-Curtis dissimilarity matrix, based on Hellinger-transformed visual count data from the Holyrood Subsea Observatory. (A) Dendrogram. (B) Non-metric multidimensional scaling showing groups (coloured ellipses) identified by the dendrogram. Environmental variables were fitted onto the ordination. Arrows show direction of increasing values of each variable and the magnitude is proportional to the amount of correlation between the environmental variable and the ordination.

Figure 3.6. Abundance of dominant taxa during the spring phytoplankton bloom, and pre-and-post bloom (A). *In-situ* image from the Holyrood Subsea Observatory pre- (B) and during (C) the 2021 spring phytoplankton bloom.

Figure 3.7. Daily averaged time series of *Psolus phantapus* (A), temperature (B), and chlorophyll-*a* (C), at the Holyrood Subsea Observatory. Black lines are time series, vertical dashed lines are the mean change points identified from the models.

Figure 3.8. Data from the 400kHz ADCP at Holyrood Subsea Observatory. Time series of (A) pressure (dbar), and (B) current velocity magnitude (m s^{-1}) and (C) direction (˚True) between 1.49m and 2.0m above bottom. Bar plots show mean current velocity (D), and variation (E) over the entire time series for East-West (red) and North-South (blue) velocity components. All current data represent the near-seabed currents, and are the average values between 1.49m and 2.0m above bottom.

Figure 3.9. Waveform analysis for Caridean shrimp. Points and vertical lines represent hourly measurements (pressure or abundance) averaged over 28 days and standard error, respectively. Horizontal dashed line indicates the Midline Estimating Statistic of Rhythm, and the yellow rectangle denotes daylight hours.

Figure 3.10. Waveform analysis for *Psolus phantapus*. Points and vertical lines represent hourly measurements (pressure or abundance) averaged over 28 days and standard error, respectively. Horizontal dashed line indicates the Midline Estimating Statistic of Rhythm, and the yellow rectangle denotes daylight hours.

Figure S3.1. Wavelet transform of U (East-West) near seabed current velocity time series.

Figure S3.2. Wavelet transform of V (North-South) near seabed current velocity time series.

Figure S3.3. Wavelet transform of pressure time series.

List of Appendices

Appendix 1 Field of view calculations.

Appendix 2 Drowning in data: How artificial intelligence could throw us a life ring.

Co-authorship Statement

I, Rylan J. Command, declare that this thesis titled, "A light in the dark: Using cabled seafloor observatories to study abundance and behaviour of seafloor megafauna in response to environmental change" and the work presented in it are my own. This work was carried out by me, with supervision and guidance from Drs. Katleen Robert, Cynthia H. McKenzie, and Fabio C. De Leo. Chapters 2 and 3 were written as journal manuscripts with co-author contributions in the following order:

Authorship for **Chapter 2** is Command, R.J., De Leo, F.C., Robert, K.

Authorship for **Chapter 3** is Command, R.J., De Leo, F.C., McKenzie, C.H., Robert, K.

Chapter 2 is currently undergoing peer-review in the journal Deep-Sea Research I.

Chapter 3 is currently undergoing peer-review in the journal Progress in Oceanography.

Appendix 2 has been published in the Journal of Ocean Technology and has been reproduced here with permission.

Chapter 1: Introduction

1.1 Scales of variability in the ocean

Ocean systems are inherently dynamic, and their processes operate across many spatial and temporal scales (Levin 1998). Physical processes such as currents and waves, vertical mixing, and coastal upwelling vary across space and time (Figure 1.1; Chelton et al. 2007), contributing to biogeochemical cycling and primary production (Tian et al. 2003). Photoperiod, the light-dark cycle produced by the Earth's rotation, varies seasonally and across latitudes and drives atmospheric and oceanographic processes that influence the ecology and behaviour of animals and plants globally (Naylor 2005). Tides generated by the lunar cycle on semi-daily, daily, monthly, and seasonal scales influence nearly all life in the ocean; in coastal ocean regions, tides produce extreme variation in habitat (substrate and physicochemical environment), which translates to morphological and behavioural adaptations that ultimately contribute to biodiversity (Martin 1995; Mariani et al. 2002). In the deep sea, internal tides also play an important role in structuring marine communities (Wagner et al. 2007; Aguzzi and Company 2010). Basin-scale atmospheric and oceanographic processes such as the El Niño Southern Oscillation (ENSO), the Pacific Decadal Oscillation (PDO), and the North Atlantic Oscillation (NAO) operate on interannual-decadal scales, influencing coastal upwelling processes and weather patterns across oceans and continents (Sutton and Allen 1997; Yang et al. 2018b), as well as marine population structures and food webs (Mantua et al. 1997). All these physical processes (Figure 1.1) have existed for millennia, contributing to a relatively stable ocean biogeochemistry that ultimately sustains ocean life (McClain et al. 2012; Levin et al. 2015).

In the benthos, patterns in biological processes overlap with, and are driven by, environmental variation across scales. Biological rhythms - regular fluctuations in activity levels in response to internal (endogenous) or external (exogenous) cues - are an integral component of

life in the ocean (Naylor 2005). Exogenously controlled rhythms occur in direct response to environmental cues (e.g., spawning triggered by phytoplankton (Coady 1973; Himmelman 1975; Starr et al. 1990, 1994)) or chemical cues from congeners (Marquet et al. 2018), and generally cease when the cue is removed (Mercier et al. 2007). Other biological rhythms, such as burrow emergence, may be under endogenous control, whereby an internal clock regulates an organisms' physiology and behaviour (Rodríguez-Sosa et al. 2008; Aguzzi and Company 2010). The relative contribution of internal and external mediation to the generation and maintenance of biological rhythms can be difficult to tease apart (Mercier and Hamel 2009), and in many cases a combination of these factors likely influence rhythms on different time-scales (e.g., circadian, circatidal, lunar)(Cohen and Forward 2005; Mercier and Hamel 2014). In these ways, environmental cues and conditions play a key role in driving behaviour of marine organisms.

Megafaunal behaviour and community structure are also influenced by fluctuations in environmental conditions on seasonal and interannual scales (Gage and Tyler 1991; Condal et al. 2012; Batten et al. 2018; Chauvet et al. 2018). For example, phytoplankton blooms that occur in surface waters in temperate and high-latitude regions during spring and summer provide a large pulse of organic matter to the seafloor (Billett et al. 1983; Lampitt 1985). These seasonal phytoplankton blooms are the primary food source for many benthic organisms and can be thought of as a "biological pump" linking surface and seafloor (Volk and Hoffert 1985). This seasonality in food source is thought to lead to seasonality in behaviours of marine organisms (Townsend and Cammen 1988).

In the short-term, seasonal vertical nutrient flux influences the abundance and distribution of benthic megafauna (Billett et al. 1983, 2001; Meyer et al. 2013), and may also influence their behaviour (Company et al. 2003). The timing, duration, and intensity of the spring phytoplankton

bloom has been shown to influence growth rates of the shrimp *Pandalus borealis* off the coast of Newfoundland and Labrador (Fuentes-Yaco et al. 2007). Fresh diatom cells deposited on the seafloor from the spring bloom are important for gonad development and reproduction in *Ctenodiscus crispatus* (Parrish et al. 2009). Spring blooms are also important for suspension-feeding dendrochirote sea cucumbers; *Cucamaria frondosa* feeds more actively during the spring bloom season (Singh et al. 1999), and diatoms provide an important source of carotenoids for vitelogensis in echinoderms (Gianasi et al. 2017). Survival of larval haddock (*Melanogrammus aeglefinus*) is also correlated with the timing of the peak of the spring bloom on the Scotian shelf (Platt et al. 2003). In general, the timing of spring phytoplankton blooms is influenced by light intensity, sea-surface temperature, mixing layer depth, and atmospheric processes linked to large-scale climate indices like the North Atlantic Oscillation (NAO; Townsend and Cammen 1988; Lampitt et al. 2010).

The global ocean is changing rapidly; ocean warming, deoxygenation, and acidification are occurring as a direct result of human activity (IPCC 2014). Warming oceans are causing range-shifts in mobile species (Poloczanska et al. 2013; Bates et al. 2014; Sunday et al. 2015; Cavole et al. 2016; Auth et al. 2018), and high mortality in sessile species (Cavole et al. 2016). Further, warm water has lower oxygen saturation than cold water – a chemical property that is driving deoxygenation in the world's oceans (Whitney et al. 2007; Diaz and Rosenberg 2008; Ross et al. 2020), with consequences for the distribution and fitness of benthic megafauna (Sato et al. 2017, 2018). Increased stratification due to ocean warming inhibits vertical mixing from deep nutrient rich water to the surface, decreasing primary production (Lewandowska et al. 2014). Temperate, high-latitude regions associated with cold-water marine environments and strong seasonality are among the most vulnerable to climate change (Tian et al. 2003). Increasing

frequency and intensity of marine heatwaves (MHW) is also disrupting the upwelling processes that drive surface and coastal primary production (Kintisch 2015; Scannell et al. 2016; Yang et al. 2018a; Oliver et al. 2018), which means less food may be available to seafloor communities (Smith et al. 1996). As ocean conditions change, so too will the timing, duration, and intensity of the spring phytoplankton bloom, which may lead to a mis-match between food availability and the timing of important biological events (Cushing 1990; Ouellet et al. 2007; Koeller et al. 2009). In order to understand the effects of ocean change we require high-frequency monitoring to capture variation on multiple spatial and temporal scales.

1.2 Sampling the seafloor

Collecting ocean data across spatial and temporal scales is challenging, and there is no one-size-fits-all solution – appropriate methods depend on the processes or organisms of interest, and across which scales they operate. Historically, epibenthic megafauna have been collected using bottom-contact fishing gear (e.g., trawls, dredges), whereby captured organisms are counted and measured to assess biodiversity, population size and age-structure, and distribution (Matabos et al. 2016). Biodiversity data from fishing gear can provide information on the distribution and density of a population, and are an important data source for fisheries management and marine conservation (Jørgensen et al. 2022). Similar methods are often used to collect specimens for laboratory studies of biological rhythms and behaviour (Aguzzi and Company 2010). However, trawls are often only conducted during certain seasons or times of day, which can bias sampling efforts (Aguzzi and Bahamon 2009), and not all organisms can be adequately captured with bottom-contact fishing gear (de Mendonça and Metaxas 2021). Additionally, laboratory conditions cannot replicate spatial and temporal heterogeneity in pressure, turbidity, light levels, habitat, substrate, and complex species interactions that influence

behaviour (Matabos et al. 2011; Sato et al. 2018; Aguzzi et al. 2018; Chauvet et al. 2018). Thus, studying an animal outside the context in which it lives is inherently limited in scope.

Advances in underwater cameras and imaging technology have allowed for a rapid expansion of *in situ* biological data collection on the seafloor (Matabos et al. 2016). Remotely Operated Vehicles (ROV) and drop camera systems have become staples of seafloor research (Althaus et al. 2015; Piechaud et al. 2019), offering a less-destructive method for data collection to support the monitoring and study of vulnerable ecosystems and species (Long 2020; Du Preez et al. 2020; de Mendonça and Metaxas 2021). Several long-term monitoring stations have also been established to study the seafloor in the Pacific Ocean (e.g., Station-M), Atlantic Ocean (e.g., PAP-SO), and the Arctic (e.g., HAUSGARTEN). These stations combine drop cameras, sediment cores, and environmental sensors to collect seafloor data, and have enabled significant advances to our understanding of oceanography and ecology in the deep sea (Billett et al. 1983; Huffard et al. 2016; Taylor et al. 2017; Levin 2018; Durden et al. 2020; Ross et al. 2020). Imaging systems also provide low-impact access to vulnerable habitats and ecologically interesting and geomorphologically complex features like submarine canyons, seamounts, and vertical walls that are difficult to sample with fishing gear (De la Torriente et al. 2018; Campanyà-Llovet et al. 2018; Rybakova et al. 2020). However, many organisms cannot be reliably identified from imagery alone a physical specimen must be collected so distinguishing characteristics can be examined, reducing the taxonomic resolution possible for biodiversity studies from images (Howell et al. 2014; Althaus et al. 2015; Piechaud et al. 2019). Further, ship time is expensive and subject to favourable weather and sea state. As with bottom-contact fishing gear, high-frequency temporal patterns and processes cannot be resolved using these methods.

1.3 Seafloor observatories

Over the past two decades, permeant seafloor observatories have been developed and deployed around the world to collect data continuously from the seafloor (Best et al. 2007; Mànuel-Làzaro et al. 2010; Matabos et al. 2011, 2016; Meyer et al. 2013). Seafloor observatories enable continuous, high-frequency sampling of biological (i.e. organic matter in sediment traps, still-frame and video cameras), chemical (i.e. oxygen, salinity, pH) and physical (i.e. current velocity) data *in situ*, previously not possible through traditional at-sea sampling (Matabos et al. 2016). Cabled seafloor observatories are connected to land *via* electro-optical cables that can provide power to instruments from shore stations to enable continuous, high-frequency data collection, and transmit this data in near-real time to data repositories for study. The first cabled seafloor observatories were the JAMSTEC Hatsushima observatory (Momma et al. 1998), the H2O Observatory between Hawaii and California (Duennebier et al. 2002). Along the west coast of North America, the VENUS in Saanich Inlet off Vancouver Island, British Columbia, Canada (Tunnicliffe et al. 2003), MARS in Monterey Bay, California, United States of America (Massion and Raybould 2006), and the NEPTUNE regional ocean network off the west coast of Vancouver Island (Best et al. 2007). Smaller coastal observatories have also been deployed in Bonne Bay, Newfoundland and Labrador, Canada (de Young et al. 2005), in the Canadian Arctic (Juniper et al. 2013b), off the coast of Barcelona, Spain (OBSEA, Mànuel-Làzaro et al. 2010), and recently in Conception Bay, Newfoundland and Labrador, Canada (Command et al. *in prep*). Many ecological studies have been conducted over different time-scales using cabled seafloor observatories in recent years (Matabos et al. 2012, 2014, 2017; Robert and Juniper 2012; Condal et al. 2012; Aguzzi et al. 2013; Juniper et al. 2013a; del Río et al. 2013; Doya et al. 2014; Chauvet et al. 2018, 2019; De Leo et al. 2018; Gasbarro et al. 2019), and such studies will continue to increase in number as more data becomes available and as technology improves.

The high-temporal resolution of still and video imagery possible from fixed observatories comes at a cost of spatial coverage – pan-and-tilt camera systems can only cover a few square meters around the observatory, precluding the study of spatial patterns. However, combining multiple approaches to sample in space and time is key to developing a holistic understanding of benthic systems (Rountree et al. 2020).

1.4 Objectives

The focus of this thesis is to make use of large datasets collected by seafloor observatories to examine variability in abundance, behaviour, community composition, and diversity of seafloor communities in response to environmental change at multiple temporal scales. In Chapter 2, seasonal and interannual population dynamics of the deep-sea pink sea urchin *Strongylocentrotus fragilis* (Jackson, 1914) was examined at the continental margin off the west coast of Vancouver Island, British Columbia. The study investigated 1) how density of *S. fragilis* changed over time, 2) if these changes were environmentally forced and what the driving factors were, and 3) how the population of *S. fragilis* was affected by the 2013-2016 NE Pacific "warm blob" event. In Chapter 3, a new cabled seafloor observatory deployed in Holyrood Inlet, Conception Bay, Newfoundland and Labrador was used to characterize the benthic megafaunal community in the bay and its response to seasonal food input from the spring phytoplankton bloom. The study examined 1) the composition and abundance of the megabenthic community, as well as behaviour of dominant megafauna, and 2) how the community responded to the downward flux of nutrients from the spring phytoplankton bloom. Chapter 4 synthesizes the findings from Chapters 2 and 3 in the broader context of seafloor monitoring and benthic ecology, suggests avenues for future research and presents concluding remarks. This work comes at a critical point in ocean observing as we approach global climate

tipping points. It is essential to document the current state of marine communities to understand and predict community responses to changing ocean conditions, and to sustainably manage our marine resources.

1.5 References

Aguzzi, J., and Bahamon, N. 2009. Modeled day–night biases in decapod assessment by bottom trawling survey. Fisheries Research **100**(3): 274–280. doi:10.1016/j.fishres.2009.08.010.

Aguzzi, J., and Company, J.B. 2010. Chronobiology of Deep-Water Decapod Crustaceans on Continental Margins. *In* Advances in Marine Biology. Elsevier. pp. 155–225. doi:10.1016/B978-0-12-381015-1.00003-4.

Aguzzi, J., Fanelli, E., Ciuffardi, T., Schirone, A., De Leo, F.C., Doya, C., Kawato, M., Miyazaki, M., Furushima, Y., Costa, C., and Fujiwara, Y. 2018. Faunal activity rhythms influencing early community succession of an implanted whale carcass offshore Sagami Bay, Japan. Sci Rep **8**(1): 11163. doi:10.1038/s41598-018-29431-5.

Aguzzi, J., Sbragaglia, V., Santamaría, G., Del Río, J., Sardà, F., Nogueras, M., and Manuel, A. 2013. Daily activity rhythms in temperate coastal fishes: insights from cabled observatory video monitoring. Mar. Ecol. Prog. Ser. **486**: 223–236. doi:10.3354/meps10399.

Althaus, F., Hill, N., Ferrari, R., Edwards, L., Przeslawski, R., Schönberg, C.H.L., Stuart-Smith, R., Barrett, N., Edgar, G., Colquhoun, J., Tran, M., Jordan, A., Rees, T., and Gowlett-Holmes, K. 2015. A Standardised Vocabulary for Identifying Benthic Biota and Substrata from Underwater Imagery: The CATAMI Classification Scheme. PLOS ONE: 18.

Auth, T.D., Daly, E.A., Brodeur, R.D., and Fisher, J.L. 2018. Phenological and distributional shifts in ichthyoplankton associated with recent warming in the northeast Pacific Ocean. Glob Change Biol **24**(1): 259–272. doi:10.1111/gcb.13872.

Bates, A.E., Pecl, G.T., Frusher, S., Hobday, A.J., Wernberg, T., Smale, D.A., Sunday, J.M., Hill, N.A., Dulvy, N.K., Colwell, R.K., Holbrook, N.J., Fulton, E.A., Slawinski, D., Feng, M., Edgar, G.J., Radford, B.T., Thompson, P.A., and Watson, R.A. 2014. Defining and observing stages of climate-mediated range shifts in marine systems. Global Environmental Change **26**: 27–38. doi:10.1016/j.gloenvcha.2014.03.009.

Batten, S.D., Raitsos, D.E., Danielson, S., Hopcroft, R., Coyle, K., and McQuatters-Gollop, A. 2018. Interannual variability in lower trophic levels on the Alaskan Shelf. Deep Sea Research Part II: Topical Studies in Oceanography **147**: 58–68. doi:10.1016/j.dsr2.2017.04.023.

Best, M.M.R., Bornhold, B.D., Juniper, S.K., and Barnes, C.R. 2007. NEPTUNE Canada Regional Cabled Observatory: Science Plan. *In* OCEANS 2007. IEEE, Vancouver, BC. pp. 1–7. doi:10.1109/OCEANS.2007.4449316.

Billett, D.S.M., Bett, B.J., Rice, A.L., Thurston, M.H., Galéron, J., Sibuet, M., and Wolff, G.A. 2001. Long-term change in the megabenthos of the Porcupine Abyssal Plain (NE Atlantic). Progress in Oceanography **50**(1–4): 325–348. doi:10.1016/S0079-6611(01)00060-X.

Billett, D.S.M., Lampitt, R.S., Rice, A.L., and Mantoura, R.F.C. 1983. Seasonal sedimentation of phytoplankton to the deep-sea benthos. Nature **302**(5908): 520–522. doi:10.1038/302520a0.

Campanyà-Llovet, N., Snelgrove, P.V.R., and De Leo, F.C. 2018. Food quantity and quality in Barkley Canyon (NE Pacific) and its influence on macroinfaunal community structure. Progress in Oceanography **169**: 106–119. doi:10.1016/j.pocean.2018.04.003.

Cavole, L.M., Demko, A., Diner, R., Giddings, A., Koester, I., Pagniello, C., Paulsen, M.-L., Ramirez-Valdez, A., Schwenck, S., Yen, N., Zill, M., and Franks, P. 2016. Biological

Impacts of the 2013–2015 Warm-Water Anomaly in the Northeast Pacific: Winners, Losers, and the Future. Oceanog **29**(2). doi:10.5670/oceanog.2016.32.

Chauvet, P., Metaxas, A., Hay, A.E., and Matabos, M. 2018. Annual and seasonal dynamics of deep-sea megafaunal epibenthic communities in Barkley Canyon (British Columbia, Canada): A response to climatology, surface productivity and benthic boundary layer variation. Progress in Oceanography **169**: 89–105. doi:10.1016/j.pocean.2018.04.002.

Chauvet, P., Metaxas, A., and Matabos, M. 2019. Interannual Variation in the Population Dynamics of Juveniles of the Deep-Sea Crab Chionoecetes tanneri. Front. Mar. Sci. **6**: 50. doi:10.3389/fmars.2019.00050.

Chelton, D.B., Schlax, M.G., Samelson, R.M., and de Szoeke, R.A. 2007. Global observations of large oceanic eddies: GLOBAL OBSERVATIONS OF OCEANIC EDDIES. Geophys. Res. Lett. **34**(15). doi:10.1029/2007GL030812.

Cohen, J.H., and Forward, R.B. 2005. Diel vertical migration of the marine copepod Calanopia americana. II. Proximate role of exogenous light cues and endogenous rhythms. Marine Biology **147**(2): 399–410. doi:10.1007/s00227-005-1570-4.

Company, J., Sardà, F., Puig, P., Cartes, J., and Palanques, A. 2003. Duration and timing of reproduction in decapod crustaceans of the NW Mediterranean continental margin: is there a general pattern? Mar. Ecol. Prog. Ser. **261**: 201–216. doi:10.3354/meps261201.

Condal, F., Aguzzi, J., Sardà, F., Nogueras, M., Cadena, J., Costa, C., Del Río, J., and Mànuel, A. 2012. Seasonal rhythm in a Mediterranean coastal fish community as monitored by a cabled observatory. Mar Biol **159**(12): 2809–2817. doi:10.1007/s00227-012-2041-3.

Cushing, D.H. 1990. Plankton production and year-class strength in fish populations: an update of the match/mismatch hypothesis. Advances in Marine Biology **26**: 249–293.

De la Torriente, A., Serrano, A., Fernández-Salas, L.M., García, M., and Aguilar, R. 2018. Identifying epibenthic habitats on the Seco de los Olivos Seamount: Species assemblages and environmental characteristics. Deep Sea Research Part I: Oceanographic Research Papers **135**: 9–22. doi:10.1016/j.dsr.2018.03.015.

De Leo, F.C., Ogata, B., Sastri, A.R., Heesemann, M., Mihály, S., Galbraith, M., and Morley, M.G. 2018. High-frequency observations from a deep-sea cabled observatory reveal seasonal overwintering of Neocalanus spp. in Barkley Canyon, NE Pacific: Insights into particulate organic carbon flux. Progress in Oceanography **169**: 120–137. doi:10.1016/j.pocean.2018.06.001.

Diaz, R.J., and Rosenberg, R. 2008. Spreading Dead Zones and Consequences for Marine Ecosystems. Science **321**(5891): 926–929. doi:10.1126/science.1156401.

Doya, C., Aguzzi, J., Pardo, M., Matabos, M., Company, J.B., Costa, C., Mihaly, S., and Canals, M. 2014. Diel behavioral rhythms in sablefish (Anoplopoma fimbria) and other benthic species, as recorded by the Deep-sea cabled observatories in Barkley canyon (NEPTUNE-Canada). Journal of Marine Systems **130**: 69–78. doi:10.1016/j.jmarsys.2013.04.003.

Du Preez, C., Swan, K.D., and Curtis, J.M.R. 2020. Cold-Water Corals and Other Vulnerable Biological Structures on a North Pacific Seamount After Half a Century of Fishing. Front. Mar. Sci. **7**: 17. doi:10.3389/fmars.2020.00017.

Duennebier, F.K., Harris, D.W., Jolly, J., Babinec, J., Copson, D., and Stiffel, K. 2002. The Hawaii-2 Observatory seismic system. IEEE J. Oceanic Eng. **27**(2): 212–217. doi:10.1109/JOE.2002.1002475.

Durden, J.M., Bett, B.J., Huffard, C.L., Pebody, C., Ruhl, H.A., and Smith, K.L. 2020. Response of deep-sea deposit-feeders to detrital inputs: A comparison of two abyssal time-series sites. Deep Sea Research Part II: Topical Studies in Oceanography **173**: 104677. doi:10.1016/j.dsr2.2019.104677.

Fuentes-Yaco, C., Koeller, P.A., Sathyendranath, S., and Platt, T. 2007. Shrimp (Pandalus borealis) growth and timing of the spring phytoplankton bloom on the Newfoundland?Labrador Shelf. Fisheries Oceanogr **16**(2): 116–129. doi:10.1111/j.1365-2419.2006.00402.x.

Gage, J.D., and Tyler, P.A. 1991. Deep-Sea Biology: A Natural History of Organisms at the Deep-sea Floor. Cambridge University Press, Cambridge.

Gasbarro, R., Chu, J.W.F., and Tunnicliffe, V. 2019. Disassembly of an epibenthic assemblage in a sustained severely hypoxic event in a northeast Pacific basin. Journal of Marine Systems **198**: 103184. doi:10.1016/j.jmarsys.2019.103184.

Gianasi, B.L., Parrish, C.C., Hamel, J.-F., and Mercier, A. 2017. Influence of diet on growth, reproduction and lipid and fatty acid composition in the sea cucumber *Cucumaria frondosa*. Aquac Res **48**(7): 3413–3432. doi:10.1111/are.13168.

Howell, K.L., Bullimore, R.D., and Foster, N.L. 2014. Quality assurance in the identification of deep-sea taxa from video and image analysis: response to Henry and Roberts. ICES Journal of Marine Science **71**(4): 899–906. doi:10.1093/icesjms/fsu052.

Huffard, C.L., Kuhnz, L.A., Lemon, L., Sherman, A.D., and Smith, K.L. 2016. Demographic indicators of change in a deposit-feeding abyssal holothurian community (Station M, 4000 m). Deep Sea Research Part I: Oceanographic Research Papers **109**: 27–39. doi:10.1016/j.dsr.2016.01.002.

IPCC. 2014. Climate change 2014: synthesis report. *Edited By*R.K. Pachauri and L. Mayer. Intergovernmental Panel on Climate Change, Geneva, Switzerland.

Jørgensen, L.L., Logerwell, E.A., Strelkova, N., Zakharov, D., Roy, V., Nozères, C., Bluhm, B.A., Hilma Ólafsdóttir, S., Burgos, J.M., Sørensen, J., Zimina, O., and Rand, K. 2022. International megabenthic long-term monitoring of a changing arctic ecosystem: Baseline results. Progress in Oceanography **200**: 102712. doi:10.1016/j.pocean.2021.102712.

Juniper, S.K., Matabos, M., Mihály, S., Ajayamohan, R.S., Gervais, F., and Bui, A.O.V. 2013a. A year in Barkley Canyon: A time-series observatory study of mid-slope benthos and habitat dynamics using the NEPTUNE Canada network. Deep Sea Research Part II: Topical Studies in Oceanography **92**: 114–123. doi:10.1016/j.dsr2.2013.03.038.

Juniper, S.K., Pirenne, B., McLean, S., Moran, K., and Fissel, D. 2013b. Cambridge Bay observatory: A miniature cabled ocean observatory for science and outreach. Canadian Meteorological and Oceanographic Society, Saskatoon.

Kintisch, E. 2015. 'The Blob' invades Pacific, flummoxing climate experts. Science **348**(6230): 17–18. doi:10.1126/science.348.6230.17.

Koeller, P., Fuentes-Yaco, C., Platt, T., Sathyendranath, S., Richards, A., Ouellet, P., Orr, D., Skúladóttir, U., Wieland, K., Savard, L., and Aschan, M. 2009. Basin-scale coherence in phenology of shrimps and phytoplankton in the North Atlantic Ocean. Science **324**(5928): 791–793. doi:10.1126/science.1170987.

Lampitt, R.S. 1985. Evidence for the seasonal deposition of detritus to the deep-sea floor and its subsequent resuspension. Deep Sea Research Part A. Oceanographic Research Papers **32**(8): 885–897. doi:10.1016/0198-0149(85)90034-2.

Lampitt, R.S., Salter, I., de Cuevas, B.A., Hartman, S., Larkin, K.E., and Pebody, C.A. 2010. Long-term variability of downward particle flux in the deep northeast Atlantic: Causes and trends. Deep Sea Research Part II: Topical Studies in Oceanography **57**(15): 1346–1361. doi:10.1016/j.dsr2.2010.01.011.

Levin, L.A. 2018. Manifestation, Drivers, and Emergence of Open Ocean Deoxygenation. Annu. Rev. Mar. Sci. **10**(1): 229–260. doi:10.1146/annurev-marine-121916-063359.

Levin, L.A., Liu, K.-K., Emeis, K.-C., Breitburg, D.L., Cloern, J., Deutsch, C., Giani, M., Goffart, A., Hofmann, E.E., Lachkar, Z., Limburg, K., Liu, S.-M., Montes, E., Naqvi, W., Ragueneau, O., Rabouille, C., Sarkar, S.K., Swaney, D.P., Wassman, P., and Wishner, K.F. 2015. Comparative biogeochemistry–ecosystem–human interactions on dynamic continental margins. Journal of Marine Systems **141**: 3–17. doi:10.1016/j.jmarsys.2014.04.016.

Levin, S.A. 1998. Ecosystems and the Biosphere as Complex Adaptive Systems. Ecosystems **1**(5): 431–436. doi:10.1007/s100219900037.

Lewandowska, A.M., Boyce, D.G., Hofmann, M., Matthiessen, B., Sommer, U., and Worm, B. 2014. Effects of sea surface warming on marine plankton. Ecol Lett **17**(5): 614–623. doi:10.1111/ele.12265.

Long, S. 2020. Identification of a Soft Coral Garden Candidate Vulnerable Marine Ecosystem (VME) Using Video Imagery, Davis Strait, West Greenland. Frontiers in Marine Science **7**: 19.

Mantua, N.J., Hare, S.R., Zhang, Y., Wallace, J.M., and Francis, R.C. 1997. A Pacific Interdecadal Climate Oscillation with Impacts on Salmon Production. Bull. Amer. Meteor. Soc. **78**(6): 1069–1079. doi:10.1175/1520-0477(1997)078<1069:APICOW>2.0.CO;2.

Mànuel-Làzaro, A., Nogueras, M., and Del Río, J. 2010. OBSEA: an Expandable Seafloor Observatory. Sea Technology **51**(7): 37.

Mariani, S., Piccari, F., and Matthaeis, E.D. 2002. Shell morphology in Cerastoderma spp. (Bivalvia: Cardiidae) and its signicance for adaptation to tidal and non-tidal coastal habitats. Journal of the Marine Biological Association of the United Kingdom **82**: 483–490.

Marquet, N., Hubbard, P.C., da Silva, J.P., Afonso, J., and Canário, A.V.M. 2018. Chemicals released by male sea cucumber mediate aggregation and spawning behaviours. Sci Rep **8**(1): 239. doi:10.1038/s41598-017-18655-6.

Martin, K.L.M. 1995. Time and tide wait for no fish: intertidal fishes out of water. Environmental Biology of Fishes **44**: 65–181.

Massion, G., and Raybould, K. 2006. MARS: The Monterey accelerated research system. Sea Technology **47**(9): 39–42.

Matabos, M., Aguzzi, J., Robert, K., Costa, C., Menesatti, P., Company, J.B., and Juniper, S.K. 2011. Multi-parametric study of behavioural modulation in demersal decapods at the VENUS cabled observatory in Saanich Inlet, British Columbia, Canada. Journal of Experimental Marine Biology and Ecology **401**(1–2): 89–96. doi:10.1016/j.jembe.2011.02.041.

Matabos, M., Best, M., Blandin, J., Hoeberechts, M., Juniper, S.K., Pirenne, B., Robert, K., Ruhl, H.A., Sarrazin, J., and Vardaro, M. 2016. Seafloor Observatories. *In* Biological Sampling in the Deep Sea. *Edited by* M.R. Clark, M. Consalvey, and A.A. Rowden. John Wiley & Sons, Ltd, Chichester, UK. pp. 306–337. doi:10.1002/9781118332535.ch14.

Matabos, M., Bui, A.O.V., Mihály, S., Aguzzi, J., Juniper, S.K., and Ajayamohan, R.S. 2014. High-frequency study of epibenthic megafaunal community dynamics in Barkley Canyon: A multi-disciplinary approach using the NEPTUNE Canada network. Journal of Marine Systems **130**: 56–68. doi:10.1016/j.jmarsys.2013.05.002.

Matabos, M., Hoeberechts, M., Doya, C., Aguzzi, J., Nephin, J., Reimchen, T.E., Leaver, S., Marx, R.M., Branzan Albu, A., Fier, R., Fernandez-Arcaya, U., and Juniper, S.K. 2017. Expert, Crowd, Students or Algorithm: who holds the key to deep-sea imagery 'big data' processing? Methods Ecol Evol **8**(8): 996–1004. doi:10.1111/2041-210X.12746.

Matabos, M., Tunnicliffe, V., Juniper, S.K., and Dean, C. 2012. A Year in Hypoxia: Epibenthic Community Responses to Severe Oxygen Deficit at a Subsea Observatory in a Coastal Inlet. PLOS ONE **7**(9): 15.

McClain, C.R., Allen, A.P., Tittensor, D.P., and Rex, M.A. 2012. Energetics of life on the deep seafloor. Proc. Natl. Acad. Sci. U.S.A. **109**(38): 15366–15371. doi:10.1073/pnas.1208976109.

de Mendonça, S.N., and Metaxas, A. 2021. Comparing the Performance of a Remotely Operated Vehicle, a Drop Camera, and a Trawl in Capturing Deep-Sea Epifaunal Abundance and Diversity. Front. Mar. Sci. **8**: 631354. doi:10.3389/fmars.2021.631354.

Mercier, A., and Hamel, J. 2009. Chapter 3 Spawning. *In* Advances in Marine Biology. Elsevier. pp. 73–168. doi:10.1016/S0065-2881(09)55003-1.

Mercier, A., and Hamel, J.-F. 2014. Lunar Periods in the Annual Reproductive Cycles of Marine Invertebrates from Cold Subtidal and Deep-Sea Environments. *In* Annual, Lunar, and Tidal Clocks. *Edited by* H. Numata and B. Helm. Springer Japan, Tokyo. pp. 99–120. doi:10.1007/978-4-431-55261-1_6.

Mercier, A., Ycaza, R., and Hamel, J. 2007. Long-term study of gamete release in a broadcast-spawning holothurian: predictable lunar and diel periodicities. Mar. Ecol. Prog. Ser. **329**: 179–189. doi:10.3354/meps329179.

Meyer, K.S., Bergmann, M., and Soltwedel, T. 2013. Interannual variation in the epibenthic megafauna at the shallowest station of the HAUSGARTEN observatory (79° N, 6° E). Biogeosciences **10**(6): 3479–3492. doi:10.5194/bg-10-3479-2013.

Momma, H., Iwase, R., Mitsuzawa, K., Kaiho, Y., and Fujiwara, Y. 1998. Preliminary results of a three-year continuous observation by a deep seafloor observatory in Sagami Bay, central Japan. Physics of the Earth and Planetary Interiors **108**(4): 263–274. doi:10.1016/S0031-9201(98)00107-1.

Naylor, E. 2005. Chronobiology: implications for marine resource exploitation and management. Sci. Mar. **69**(S1): 157–167. doi:10.3989/scimar.2005.69s1157.

Oliver, E.C.J., Donat, M.G., Burrows, M.T., Moore, P.J., Smale, D.A., Alexander, L.V., Benthuysen, J.A., Feng, M., Sen Gupta, A., Hobday, A.J., Holbrook, N.J., Perkins-Kirkpatrick, S.E., Scannell, H.A., Straub, S.C., and Wernberg, T. 2018. Longer and more frequent marine heatwaves over the past century. Nat Commun **9**(1): 1324. doi:10.1038/s41467-018-03732-9.

Ouellet, P., Savard, L., and Larouche, P. 2007. Spring oceanographic conditions and northern shrimp Pandalus borealis recruitment success in the north-western Gulf of St. Lawrence. Mar. Ecol. Prog. Ser. **339**: 229–241. doi:10.3354/meps339229.

Parrish, C., Deibel, D., and Thompson, R. 2009. Effect of sinking spring phytoplankton blooms on lipid content and composition in suprabenthic and benthic invertebrates in a cold ocean coastal environment. Mar. Ecol. Prog. Ser. **391**: 33–51. doi:10.3354/meps08148.

Piechaud, N., Hunt, C., Culverhouse, P., Foster, N., and Howell, K. 2019. Automated identification of benthic epifauna with computer vision. Mar. Ecol. Prog. Ser. **615**: 15–30. doi:10.3354/meps12925.

Platt, T., Fuentes-Yaco, C., and Frank, K.T. 2003. Spring algal bloom and larval fish survival. Nature **423**(6938): 398–399. doi:10.1038/423398a.

Poloczanska, E.S., Brown, C.J., Sydeman, W.J., Kiessling, W., Schoeman, D.S., Moore, P.J., Brander, K., Bruno, J.F., Buckley, L.B., Burrows, M.T., Duarte, C.M., Halpern, B.S., Holding, J., Kappel, C.V., O'Connor, M.I., Pandolfi, J.M., Parmesan, C., Schwing, F., Thompson, S.A., and Richardson, A.J. 2013. Global imprint of climate change on marine life. Nature Clim Change **3**(10): 919–925. doi:10.1038/nclimate1958.

del Río, J., Aguzzi, J., Costa, C., Menesatti, P., Sbragaglia, V., Nogueras, M., Sarda, F., and Manuèl, A. 2013. A New Colorimetrically-Calibrated Automated Video-Imaging Protocol for Day-Night Fish Counting at the OBSEA Coastal Cabled Observatory. Sensors **13**(11): 14740–14753. doi:10.3390/s131114740.

Robert, K., and Juniper, S. 2012. Surface-sediment bioturbation quantified with cameras on the NEPTUNE Canada cabled observatory. Mar. Ecol. Prog. Ser. **453**: 137–149. doi:10.3354/meps09623.

Rodríguez-Sosa, L., Calderón-Rosete, G., and Flores, G. 2008. Circadian and ultradian rhythms in the crayfish caudal photoreceptor. Synapse **62**(9): 643–652. doi:10.1002/syn.20540.

Ross, T., Du Preez, C., and Ianson, D. 2020. Rapid deep ocean deoxygenation and acidification threaten life on Northeast Pacific seamounts. Glob Change Biol: gcb.15307. doi:10.1111/gcb.15307.

Rountree, R.A., Aguzzi, J., Marini, S., Fanelli, E., De Leo, F.C., Del Rio, J., and Juanes, F. 2020. Towards an optimal design for ecosystem-level ocean observatories. *In* Oceanography and Marine Biology, 1st edition. *Edited by* S.J. Hawkins, A.L. Allcock, A.E. Bates, A.J. Evans, L.B. Firth, C.D. McQuaid, B.D. Russell, I.P. Smith, S.E. Swearer, and P.A. Todd. CRC Press. pp. 79–105. doi:10.1201/9780429351495-2.

Rybakova, E., Galkin, S., Gebruk, A., Sanamyan, N., and Martynov, A. 2020. Vertical distribution of megafauna on the Bering Sea slope based on ROV survey. PeerJ **8**: e8628. doi:10.7717/peerj.8628.

Sato, K.N., Andersson, A.J., Day, J.M.D., Taylor, J.R.A., Frank, M.B., Jung, J.-Y., McKittrick, J., and Levin, L.A. 2018. Response of Sea Urchin Fitness Traits to Environmental Gradients Across the Southern California Oxygen Minimum Zone. Front. Mar. Sci. **5**: 258. doi:10.3389/fmars.2018.00258.

Sato, K.N., Levin, L.A., and Schiff, K. 2017. Habitat compression and expansion of sea urchins in response to changing climate conditions on the California continental shelf and slope (1994–2013). Deep Sea Research Part II: Topical Studies in Oceanography **137**: 377–389. doi:10.1016/j.dsr2.2016.08.012.

Scannell, H.A., Pershing, A.J., Alexander, M.A., Thomas, A.C., and Mills, K.E. 2016. Frequency of marine heatwaves in the North Atlantic and North Pacific since 1950: FREQUENCY OF MARINE HEATWAVES SINCE 1950. Geophys. Res. Lett. **43**(5): 2069–2076. doi:10.1002/2015GL067308.

Singh, R., MacDonald, B., Thomas, M., and Lawton, P. 1999. Patterns of seasonal and tidal feeding activity in the dendrochirote sea cucumber Cucumaria frondosa (Echinodermata:Holothuroidea) in the Bay of Fundy, Canada. Mar. Ecol. Prog. Ser. **187**: 133–145. doi:10.3354/meps187133.

Smith, C.R., Hoover, D.J., Doan, S.E., Pope, R.H., Demaster, D.J., Dobbs, F.C., and Altabet, M.A. 1996. Phytodetritus at the abyssal seafloor across 10° of latitude in the central equatorial Pacific. Deep Sea Research Part II: Topical Studies in Oceanography **43**(4–6): 1309–1338. doi:10.1016/0967-0645(96)00015-X.

Sunday, J.M., Pecl, G.T., Frusher, S., Hobday, A.J., Hill, N., Holbrook, N.J., Edgar, G.J., Stuart-Smith, R., Barrett, N., Wernberg, T., Watson, R.A., Smale, D.A., Fulton, E.A., Slawinski, D., Feng, M., Radford, B.T., Thompson, P.A., and Bates, A.E. 2015. Species traits and climate velocity explain geographic range shifts in an ocean-warming hotspot. Ecol Lett **18**(9): 944–953. doi:10.1111/ele.12474.

Sutton, R.T., and Allen, M.R. 1997. Decadal predictability of North Atlantic sea surface temperature and climate. Nature **388**(6642): 563–567. doi:10.1038/41523.

Taylor, J., Krumpen, T., Soltwedel, T., Gutt, J., and Bergmann, M. 2017. Dynamic benthic megafaunal communities: Assessing temporal variations in structure, composition and diversity at the Arctic deep-sea observatory HAUSGARTEN between 2004 and 2015. Deep Sea Research Part I: Oceanographic Research Papers **122**: 81–94. doi:10.1016/j.dsr.2017.02.008.

Tian, R., Deibel, D., Thompson, R., and Rivkin, R. 2003. Modeling of climate forcing on a cold-ocean ecosystem, Conception Bay, Newfoundland. Mar. Ecol. Prog. Ser. **262**: 1–17. doi:10.3354/meps262001.

Townsend, D.W., and Cammen, L.M. 1988. Potential Importance of the Timing of Spring Plankton Blooms to Benthic-Pelagic Coupling and Recruitment of Juvenile Demersal Fishes. Biological Oceanography **5**(3): 215–228. doi:https://doi.org/10.1080/01965581.1987.10749514.

Tunnicliffe, V., Dewey, R., and Smith, D. 2003. Research Plans for a Mid-Depth Cabled Seafloor Observatory in Western Canada. oceanog **16**(4): 53–59. doi:10.5670/oceanog.2003.08.

Volk, T., and Hoffert, M.I. 1985. Ocean Carbon Pumps: Analysis of Relative Strengths and Efficiencies in Ocean-Driven Atmospheric CO2 Changes. *In* The Carbon Cycle and Atmospheric CO2: Natural Variations Archean to Present. American Geophysical Union (AGU). pp. 99–110. doi:10.1029/GM032p0099.

Wagner, H.-J., Kemp, K., Mattheus, U., and Priede, I.G. 2007. Rhythms at the bottom of the deep sea: Cyclic current flow changes and melatonin patterns in two species of demersal fish. Deep Sea Research Part I: Oceanographic Research Papers **54**(11): 1944–1956. doi:10.1016/j.dsr.2007.08.005.

Whitney, F.A., Freeland, H.J., and Robert, M. 2007. Persistently declining oxygen levels in the interior waters of the eastern subarctic Pacific. Progress in Oceanography **75**(2): 179–199. doi:10.1016/j.pocean.2007.08.007.

Yang, B., Emerson, S.R., and Peña, M.A. 2018a. The effect of the 2013–2016 high temperature anomaly in the subarctic Northeast Pacific (the "Blob") on net community production. Biogeosciences **15**(21): 6747–6759. doi:10.5194/bg-15-6747-2018.

Yang, S., Li, Z., Yu, J.-Y., Hu, X., Dong, W., and He, S. 2018b. El Niño–Southern Oscillation and its impact in the changing climate. National Science Review **5**(6): 840–857. doi:10.1093/nsr/nwy046.

de Young, B., Brown, K.M., Adams, R.S., and McLean, S.D. 2005. Design and Deployment of the Bonne Bay Observatory (B2O). *In* OCEANS 2005. MTS/IEEE, Washington, DC. pp. 855–860.

1.6 Figures

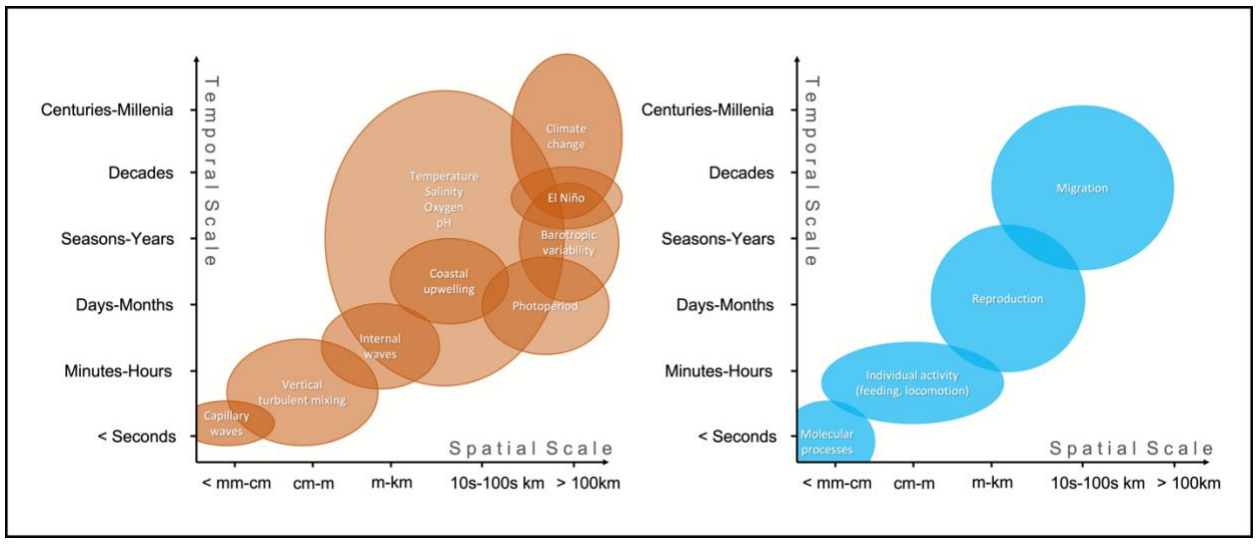

Figure 1.1. Spatial and temporal scales of physical environmental (left) and biological (right) processes. Adapted from Chelton et al. (2007).

Chapter 2: Temporal dynamics of the deep-sea pink sea urchin *Strongylocentrotus fragilis* on the Northeast Pacific continental margin

Abstract

The Northeast Pacific continental margin is characterized by strong seasonal upwelling, which drives high primary productivity, and supports high diversity and biomass of benthic megafauna. The recent occurrence of a marine heat wave ("The Blob", *sensu* Kintisch, 2015) in 2013-2016 resulted in changes to phytoplankton community composition and loss of coastal kelp abundance and diversity, reducing gross primary productivity in the region. However, cumulative effects of marine heat waves and ongoing basin-scale deoxygenation in deep-sea ecosystems remain poorly understood. Here, we use a 7-year time series of physicochemical and video imagery data from Ocean Networks Canada's NEPTUNE observatory to investigate temporal dynamics of the deep-sea pink sea urchin *Strongylocentrotus fragilis* in relation to multi-year environmental variability. Using generalized additive models, we show that local *S. fragilis* density at Barkley Upper Slope (420 m) fluctuated over time and was partially explained by changes in dissolved oxygen concentration and suspended particulate matter in the benthic boundary layer (ADCP backscatter), with high sea urchin density corresponding to high oxygen and low backscatter. Seafloor dissolved oxygen ranged from 0.80-1.89 mL/L and varied seasonally, exhibiting a clear negative correlation with sea surface primary productivity (MODIS satellite Chl-a data), corresponding with the onset of yearly upwelling conditions. However, the anomalously warm years affected by 'The Blob' dampened upwelling and maintained higher dissolved oxygen conditions near the seafloor. *S. fragilis* density declined during 'Blob' conditions, likely in response to reduced kelp and phytodetritus subsidies from coastal waters. We propose a foraging-respiration trade-off hypothesis, whereby *S. fragilis* forages in deeper water during

weak upwelling and migrates to shallower habitats during low oxygen conditions. *S. fragilis* is an important bioturbator and detritivore; changes in the density and distribution of this species may directly affect sediment turnover rates and nutrient cycling on the continental margin, with consequences for surface and coastal productivity.

2.1 Introduction

The continental margin of the Northeast Pacific Ocean (NEP) is characterized as an Eastern Boundary Current Ecosystem, where strong upwelling brings cool, nutrient-rich water from the deep sea up to the surface (Rossi et al. 2009; Chavez and Messié 2009). Seasonal upwelling maintains high primary productivity in offshore surface waters (Arntz et al. 2006) and dense kelp forests along the coast (Edwards 2004), fueling productive fisheries (Ware and Thomson 1991). Phytodetritus eventually sinks to the seafloor, providing a large source of organic carbon and nutrients to deep-sea communities (Billett et al. 1983; Lampitt 1985; Gage and Tyler 1991; Smith et al. 1993, 1994; Ruhl and Smith Jr., Kenneth L. 2004). This organic matter is the primary food source for many benthic megafauna species (Smith et al. 1994; Billett et al. 2010; Glover et al. 2010; Birchenough et al. 2015; Campanyà-Llovet et al. 2018; Durden et al. 2020), that make up much of the biomass (Levin et al. 2015; Fredriksen et al. 2020) and drive biogeochemical cycling (Turner 2015; Thomsen et al. 2017) in the deep sea. Where respiration of decomposers breaking down sinking phytodetritus outweighs natural reoxygenation processes, a region of permanently low dissolved oxygen (< 0.5 mL/L) can form, known as an Oxygen Minimum Zone (OMZ, Helly and Levin 2004). Benthic megafaunal species densities and richness is highest on the OMZ margins, decreasing towards the OMZ core where dissolved oxygen is lowest (Levin 2003). The distribution of oxygen on the continental margin also

influences the spatiotemporal distribution of benthic communities (Levin 2003; Helly and Levin 2004; Papiol et al. 2017), with direct consequences for nutrient cycling and benthopelagic coupling (Lebrato et al. 2010; Levin and Sibuet 2012; Kendzierska et al. 2020).

Organic matter export to the seafloor varies on seasonal, annual, and decadal scales (Billett et al. 1983; Bett et al. 2001; Smith et al. 2018), and the amount of food available to the benthos is directly related to surface productivity (Honjo et al. 2014; Thomsen et al. 2017). Marine heatwaves (MHW) – extended periods of anomalously warm water (Sorte et al. 2010) – cause thermal stratification in the upper ocean, inhibiting upwelling and nutrient flux that drives primary productivity (Kintisch 2015), and reducing the downward flux of organic matter between the surface and benthos along the continental margin. In the NEP, a MHW dubbed "The Blob" was observed off the coast of British Columbia and the western United States at the end of 2013 and persisted until early 2016 (Cavole et al. 2016), with long-lasting ecological and oceanographic effects in some areas (Jackson et al. 2018a; McPherson et al. 2021; Suryan et al. 2021). "The Blob" resulted in the loss of kelp abundance and diversity (Starko et al. 2019), changes to phytoplankton community composition (Cavole et al. 2016), and reduced gross primary productivity (Yang et al. 2018), with likely consequences for benthic megafauna that rely on phytodetritus for food (Brodeur et al. 2019). MHWs are becoming more common and lasting longer (Scannell et al. 2016; Oliver et al. 2018), causing harmful algal blooms (McCabe et al. 2016; McKibben et al. 2017; Trainer et al. 2020), reduced fish recruitment (Cavole et al. 2016), and fisheries closures (Ritzman et al. 2018). Most of the research on the 2013-2016 MHW has focused on the pelagic and nearshore realms (Cavole et al. 2016; Auth et al. 2018; Batten et al. 2018) and abyssal plain (Smith et al. 2018; Kuhnz et al. 2020), however the extent to which benthic megafauna on the continental margin were affected by these events remains

understudied. Many organisms are well adapted to their thermal niche (Bates et al. 2010) and may rapidly recover once conditions return to normal (Heise 2006; Gleason and Burton 2013; Kelly et al. 2017). However, the persistence and increasing prevalence of warm water anomalies is causing potentially permanent damage to marine ecosystems (Couch et al. 2017; Jackson et al. 2018b; Suryan et al. 2021).

The distribution and availability of food and oxygen on the NEP continental margin is further influenced locally by topographic features such as submarine canyons, which steer Ekman-driven current flows enhancing coastal upwelling (Allen and de Madron 2009; Ramos-Musalem and Allen 2019). Submarine canyons also play a key role in structuring slope and deep-sea ecosystems since they affect the distribution of food on the seafloor by trapping and funneling zooplankton, detrital and sedimentary organic matter from shallower shelf areas into the slope (Vetter and Dayton 1999; Puig et al. 2014; De Leo et al. 2018). Perhaps the best studied submarine canyon on British Columbia's coast is Barkley Canyon, in particular after the installation of the NEPTUNE cabled observatory in 2009 (Best et al. 2007). Ocean Networks Canada (ONC) operates and maintains NEPTUNE with several oceanographic sensors permanently installed along the axis of Barkley Canyon, and on the adjacent upper slope. The local current regime affected by the canyon's topography has been extensively studied prior to NEPTUNE, and is known to enhance local upwelling and primary productivity in surface waters above the canyon (Mackas et al. 1997; Allen et al. 2001; Genin 2004). Secondary production resulting from zooplankton aggregations and decomposing organic matter is also transported down into Barkley Canyon's deeper waters (Baker and Hickey 1986; Allen and de Madron 2009; De Leo et al. 2018). A recent study employing a series of molecular markers has demonstrated that sedimentary organic matter quantity and quality are higher at intermediate depths (900-1300

m) in Barkley Canyon when compared to the shallower (200-400 m) canyon head (Campanyà-Llovet et al. 2018). The study points to an interplay of higher current hydrodynamics at shallower depths, a range of degradation processes and the accumulation of dead ontogenetically-migrating zooplankton in determining the deposition of labile vs refractory organic matter along a depth gradient in the canyon (Campanyà-Llovet et al. 2018).

Extensive research on the temporal dynamics of megafauna within Barkley Canyon has identified diel behaviour patterns and seasonal migration of sablefish, *Anopoploma fimbria* (Doya et al. 2014; Matabos et al. 2014; Chauvet et al. 2018) and interannual ontogenetic migration of tanner crab, *Chionoecetes tanneri* (Chauvet et al. 2019). However, considerably less attention has been given to the adjacent slope ecosystem (Robert and Juniper 2012; De Leo et al. 2017; Chauvet et al. 2018). The canyon cuts across the slope impinging the core of the OMZ at about 900 m, where dissolved oxygen can drop as low as 0.16 mL L^{-1} (Domke et al. 2017). In contrast, the adjacent upper slope (400 m) experiences higher, though more variable, oxygen concentrations, ranging from 0.79 mL L^{-1} to 1.94 mL L^{-1}, making this an ideal site to study megafaunal responses to short- and long-term variability in ocean conditions.

One of the dominant megafauna at the upper slope near Barkley Canyon is the deep-sea pink sea urchin *Strongylocentrotus fragilis* (Jackson, 1912; Robert and Juniper 2012; De Leo et al. 2017). *S. fragilis* is a detritivore that forages on a wide range of detritus material, though many studies point to a diet predominantly composed of large macroalgal detritus and other phytodetritus arriving at the seafloor from the surface and coastal waters (Boolootian et al. 1959; Filbee-Dexter and Scheibling 2014; Campanyà-Llovet et al. 2018). It plays an important role in deep-sea nutrient cycling through locomotion and grazing, which contributes to horizontal sediment turnover (15.1 to 21.0 m^2 yr^{-1}, with little subduction; Robert and Juniper 2012) and

enhances nutrient availability in the water column (Thompson and Riddle 2005). *S. fragilis* forms large feeding aggregations on the continental margin (De Leo et al. 2017), influencing the composition and spatial distribution of nutrients and sediment infaunal communities (Campanyà-Llovet et al. 2018). As slow-moving (average 7.31 - 26.9 cm h^{-1}; Robert and Juniper 2012; Barry et al. 2014), calcifying organisms, sea urchins are particularly susceptible to climate change (Delorme and Sewell 2014; Asnaghi et al. 2020; Low and Micheli 2020). Previous research has found that calcification rates and reproductive capacity of *S. fragilis* are affected by food availability, ocean warming, acidification, and deoxygenation, with reduced recruitment and survival already occurring under current ocean conditions (Sato et al. 2018).

In this paper, we used long-term (7-year) and high-frequency (5 minutes every 6 hours) video and environmental time-series data from the NEPTUNE observatory at the Barkley Canyon Upper Slope (BCUS) location to study how densities of *S. fragilis* respond to seasonal and inter-annual variability in oceanographic conditions. In particular, we draw focus to the 2013-2016 MHW that affected more than 2.5 million km^2 of the NEP (Bond et al. 2015). "The Blob" reportedly caused reduction in coastal upwelling, with consequent decrease in primary and secondary productivity, with a range of effects that restructured local and regional food-webs (Cavole et al. 2016; Brodeur et al. 2019). Since *S. fragilis* plays a key role in benthic-pelagic coupling and nutrient recycling over the shelf and slope, it is crucial to understand how this species is affected by large-scale, climate-driven ecosystem changes.

We contrasted the high frequency time-series observations from NEPTUNE against a 14-year, bi-annual bottom trawl survey conducted on the West Coast of Vancouver Island by Fisheries and Oceans Canada (DFO). The trawl survey database was used to extract *S. fragilis* densities and distribution across a broader spatial scale and along a depth gradient to be used as a

possible predictor of local population fluctuations quantified from video imagery at the single fixed location of the seafloor observatory. In addition, we also used climatology data of sea-surface temperature (SST) and colour irradiance (as a proxy for chlorophyll-*a*) from an offshore meteorological buoy and from the MODIS Aqua OceanColour satellite, respectively to understand the broader oceanographic effects of "The Blob" in the region. We hypothesized that 1) density of *S. fragilis* on the continental margin declined during "The Blob" due to reduced upwelling food supply disruption, and 2) depth distribution of *S. fragilis* shoaled over time due to the expanding OMZ.

2.2 Methods

2.2.1 Study site

The study area was located on the continental slope off Vancouver Island adjacent to the northern flank of Barkley Canyon (Figure 2.1A). This canyon incises the continental shelf from 200 m depth at its head (Allen et al. 2001) and reaches 2,660 m at the Cascadia Basin, providing a link between the continental margin and an abyssal plain. At the surface, near-shore, NE-SE wind-driven current flows advect over the canyon undisturbed (Allen et al. 2001). Flow along the shelf (above the benthic boundary layer) is inhibited by the canyon wall, upsetting the geostrophic balance, reducing Coriolis forces, and creating an up-canyon pressure gradient (Allen et al. 2001). This unbalance causes flow to be advected over and into the canyon, where stretching generates cyclonic vorticity, turning the flow up-canyon (Allen et al. 2001). When flow reaches the down-stream wall of the canyon, anti-cyclonic vorticity causes water to be advected into the canyon or up onto the shelf (Allen et al. 2001). Deeper water that flows into the canyon causes lifting of isopycnal layers, balancing out the pressure gradient and slowing the up-canyon flow (Allen et al. 2001). This lifting also induces cyclonic vorticity in the deep-water

layer near the mouth of the canyon. During upwelling, stronger up-canyon flow lifts the depth of the pycnocline above the canyon by half, forcing cold water and nutrients closer to the surface from the subpycnocline and enhancing primary productivity (Allen et al. 2001). In summary, seasonal upwelling-favourable winds in summer result in a net movement of deep, low oxygen water from the OMZ onto the slope. In winter when downwelling winds are dominant, deep wind-driven mixing forces oxygen-rich surface water down onto the slope. Short-lived phytoplankton blooms also occur during winter/downwelling conditions, and rapidly export particulate carbon through the main canyon axis (Thomsen et al. 2017). Aside from the seasonal fluctuations of the upper boundary, the dissolved oxygen levels and the main depth boundaries of the OMZ are relatively stable. The full details of the flow regime around Barkley Canyon can be found in Allen et al. (2001).

This study was conducted at the Barkley Canyon Upper Slope site (BCUS), on the slope about three kilometers from the canyon and connected to the network at 396 m depth (Fig. 1A; 48° 25' 37.2"N, 126° 10' 29.7"W). The seafloor at the BCUS site is characterized by soft sediments and a high abundance of *S. fragilis*, solariellidae snails, and rockfish (*Sebastes* spp., Chauvet 2018).

2.2.2 Estimating *S. fragilis* densities from imagery

We analyzed footage from a video camera mounted on the BCUS platform from 2013-2020 (Figure 2.1B, C). Four different high-definition video camera systems have been used during the entire 7-year study period (Table 2.1). The footage quality progressively improved as each new camera system deployed followed the NEPTUNE observatory's continuous progress towards better configuration of seafloor instrument platforms, digital infrastructure, software controls, and data archiving. In all systems, the camera was mounted on a galvanized steel tripod

and attached to a Remote Ocean Systems (ROS) pan and tilt system, allowing for 360˚ of pan angle rotation and thus covering the seafloor in all directions (Chauvet 2018; De Leo et al. 2018). Between years, the camera tripod configurations changed slightly, with the final height of the camera lenses above the seabed varying between 40-95 cm, thus altering the total imaged area of the seafloor (ranging from 0.5 m^2 to 14.93 m^2; Table 2.1). Two ROS LED lights (100 W, >406 lm, De Leo et al. 2018) provided illumination during video recordings. The cameras followed the same recording schedule since June 15, 2012 (i.e., recording five-minute videos every two hours, changing to an hourly recording interval on September 19, 2019). This recording schedule was designed to minimize the impact of artificial lighting on the behaviour of benthic organisms (Widder et al. 2005) and was optimized for detecting sea urchin abundance patterns (Robert and Juniper 2012). We analyzed 4 video sequences each day (0000-0005, 0600-0605, 1200-1205, and 1800-1805 UTC) in order to account for diurnal and tidal variation (Aguzzi and Company 2010). In each video, the number of *S. fragilis* present was counted and densities obtained by dividing the total count of individuals by the total area of imaged seafloor, which varied among the four camera deployments, and expressed in sea urchins per meters squared (see Table 2.1). *S. fragilis* were manually counted using ONC's SeaTube web-based video playback interface (https://data.oceannetworks.ca/SeaTube). All video imagery data used in the present study are freely accessible for playback and download at https://data.oceannetworks.ca/DataSearch.

Unfortunately, two fishing trawling incidents damaged some of the observatory seafloor infrastructure, including the node supplying power to the instruments on one occasion, and another directly hitting the BCUS platform with the seafloor video camera. These events resulted in relatively long stretches of missing data. Due to the trawling incidents, the resulting video time series was broken down, and for the purpose of a meaningful multi-year comparative

analysis, we split the dataset into 4 segments (2013-2014, 2014-2015, 2018, and 2019-2020), corresponding to a total of 565 days. Video data time series from each year at least partially covered late summer, fall and winter conditions (Table 2.1).

S. fragilis has a patchy distribution on the continental slope (Robert and Juniper 2012; Campanyà-Llovet et al. 2018), which could influence abundance and density estimates obtained using imagery from fixed-position observatories. Thus, we used the full field of view available in each sampling interval (ranging from 0.5-15 m^2 depending on deployment, Table 2.1) to cover as much of the seafloor around the observatory as possible. Field of views were calculated following the trigonometric approach of Wakefield and Genin (1987) and Nakajima et al. (2014) using the known height of each camera above the seabed, and the horizontal and vertical acceptance angles of each camera (Table 2.1). The procedure for calculating the area covered by each camera is outlined in the supplemental material (Appendix 1.1).

2.2.3 Environmental data from the seafloor and sea-surface

Environmental data were obtained from instrument sensors mounted on the BCUS platform at 396 m depth (Figure 2.1B) as well as from a nearby (46.6 km away) meteorological buoy and the MODIS satellite (Table 2.2). Dissolved oxygen concentration (mL L^{-1}) was collected from a Sea-Bird SBE 63 Dissolved Oxygen Sensor. Salinity (psu) was collected from a Conductivity-Temperature-Depth (CTD) sensor (Sea-Bird SBE 16plus V2 SEACAT C-T Recorder). These data were collected at a rate of 1 measurement every second.

Benthic boundary layer currents (BBLc) were measured in m s^{-1} as *u* (east-west) and *v* (north-south) vectors from an upward-looking Nortek Aquadop 2 MHz Acoustic Doppler Current-Profiler (ADCP). The ADCP collected data in 1.43 cm range bins from the sonar transducer head, from approximately 20 cm above the seabed, up to 1.5 m above the seabed, and

we averaged current velocities across the full range for each time point (Grant Garner, University of Victoria, pers comm.). We then calculated the current direction (˚True) and magnitude of the resulting current velocity vector from the *u* and *v* velocity components. Temperature (˚C) and pressure (dbar) were also obtained from the ADCP since its time-series had fewer missing values due to instrument issues during the study period than the CTD. We also collected the backscatter (Hz) from the ADCP as a proxy for particulate matter in the water column immediately above the seafloor. The ADCP data were collected at a rate of 1 measurement every 10 seconds.

We used 8-day averaged satellite chlorophyll-*a* concentration data from MODIS, NASA Earth Observations Goddard Ocean Colour Group (https://oceancolor.gsfc.nasa.gov/l3/order/) for an area around BCUS (Figure S2.1) to quantify temporal variability in sea surface primary productivity. The 8-day average allowed for more reliable coverage and helped account for the effects of cloud cover. The chlorophyll-*a* time-series was derived by averaging the chlorophyll-*a* concentration over the entire area for which points were extracted (Figure S2.1; Chauvet et al., 2018).

Following Chauvet et al. (2018), we acquired SST from the Fisheries and Oceans La Perouse Bank Buoy 46206 (48° 49' 48"N, 126° 0' 0"W, http://www.meds-sdmm.dfo-mpo.gc.ca/). To match the temporal resolution of the chlorophyll-*a* time series, we averaged the SST data into 8-day bins. Then to assess the effect of SST anomalies, such as the 2013-2016 “Blob” event (Bond et al. 2015; Cavole et al. 2016), we calculated anomalous SST (SSTa) as the difference between each 8-day-binned SST measurement and the average SST from the entire buoy time series (1985-2020).

All environmental time series (except chlorophyll-*a*) were averaged in 6-hour bins corresponding to the sampling period and frequency of the video time-series.

2.2.4 Bottom Trawl Surveys (2004-2018)

Every other year since 2004, DFO in collaboration with the Canadian Groundfish Research and Conservation Society has conducted fisheries-independent synoptic bottom trawl surveys on the continental shelf and slope on the West Coast of Vancouver Island (Figure S2.1; Anderson et al. 2019). These surveys followed a random depth-stratified sampling design with sampling conducted in 2 km x 2 km blocks on the Canadian Coast Guard research vessel *W.E. Ricker*, or a chartered industry vessel. These data are available under an Open Government License and can be accessed online (https://open.canada.ca/data/en/dataset/557e42ae-06fe-426d-8242-c3107670b1de).

The trawl survey recorded the total catch (number of individuals) of animals found in each tow. For each trawl tow that recorded *S. fragilis*, we determined the total area (m^2) covered by multiplying the width of the trawl doors (m) by the distance covered (m). We then calculated the density of *S. fragilis* in each trawl by dividing the total number of *S. fragilis* caught in all trawls by the total area covered (indiv. m^{-2}). This information was used to calculate mean density for each survey year (2004-2018). For some tows, a catch weight was recorded without a corresponding catch count. In these cases, we imputed a value of 1 and we assumed that at least one sea urchin was present in the catch since a weight was measured. Bottom depth (m) was reported as the modal bottom depth for each trawl tow. For each survey year, we determined the upper and lower depth limits, the mean and median depth, and the upper and lower 25% quantiles of the depth distribution.

2.2.5 Data analysis

2.2.5.1 Environmental predictor variables and density of S. fragilis

We used generalized additive models (GAMs) to characterize temporal trends in sea urchin density, and model possible responses to environmental change within and between years. GAMs are an extension of generalized linear models that allow for non-linear trends to be modeled using smooth functions f_j of covariates x_j (hereafter "smoothers", Wood 2011). In general, these models take the form:

$$E(Y) = g^{-1}\left(\beta_0 + \sum_{j=1}^{J} f_j(x_j)\right), \qquad \textit{Eq. 2.1}$$

Where E(Y) is the expected value of the response, g^{-1} is the inverse-link function for the distribution of Y, and β_0 is an intercept term. Smooths are represented as the sum of K basis functions ($b_{j,k}$), multiplied by some coefficients ($\beta_{j,k}$),

$$f_j(x_j) = \sum_{i=1}^{K} \beta_{j,k} b_{j,k}(x_j). \qquad \textit{Eq. 2.2}$$

In practice, K represents the upper limit on the complexity of the smoother (Wood 2011). When estimating the coefficients of each smoother, a "wiggliness penalty" needs to be applied to prevent the model overfitting the data (Wood 2011). The mgcv package (Wood 2011) in R (R Core Team 2020) enables automatic estimation of smoothness parameters using a variety of algorithms (Wood et al. 2016). Here, we fit GAMs using Restricted Maximum Likelihood Estimation (REML) to select smoothness parameters, since it is generally considered to be the most stable compared to other fitting procedures (Wood 2011). To preserve the inherent count-distribution of the sea urchin abundance data, and to account for possible overdispersion (Zuur et

al. 2009), we fit all models with a negative-binomial distribution and log-link function. The mgcv package is suitable for extended distribution families and has built-in automatic dispersion parameter estimation via the nb() function (Zuur et al. 2009; Wood et al. 2016).

To determine within- and between-year trends in sea urchin density, we first modeled the data using only sampling time (ST) and sample year as covariates. We fit 5 temporal models: A global smoother for ST (model G), year-level smoothers for ST (model I and model S), and a global smoother with year-level smoothers for ST (model GS and model GI) following Pedersen et al. (2019). Model G includes only a global smoother, which fits a single shared smooth for ST for all years. Models I and GI allowed the shape and wiggliness penalty of the ST smooth to vary between years using *by = Year*, whereas models S and GS assumed all years had the same wiggliness but varied in shape using the factor smooth basis via *bs = "fs"* (Pedersen et al. 2019). We set the number of basis functions at $k = 5$ for global ST smooth and $k = 12$ for year-level ST smooths to avoid fitting smoothers that were too wiggly, and to determine the relative importance of global versus between-year temporal variation (Pedersen et al. 2019). We selected the best temporal model using Aikike's Information Criteria (AIC, Burnham et al. 2002). Modeling sea urchin abundance as a smooth function of ST and year was sufficient to account for any temporal autocorrelation present in the time series (Figure S2.1).

Finally, we added global smooths of dissolved oxygen, BBLc magnitude, and ADCP backscatter (as a proxy for particulate organic matter; Chanson et al. 2008) to the best temporal model to determine average *S. fragilis* response to environmental change (Table 2.3). Including temporally-correlated environmental covariates in a model that already has a smoother for time requires that the environmental smoothers explain variation above and beyond the temporal smooth (Hayes et al. 2020). After fitting models, we tested for concurvity, the ability of a smooth

function of one variable to be reconstructed by the smooth function of another variable; essentially the nonlinear analogue of collinearity (Buja et al. 1989; Morlini 2006). We used the select = TRUE argument when fitting models with both global and year-level smooths (Pedersen et al. 2019). This helps to perform variable selection by adding an extra penalty to each smoother, allowing mgcv to penalize model terms to a zero effect (Marra and Wood 2011). We fit each smooth using the thin-plate-regression-spline (TPRS) basis (Wood 2003), since they are the default for mgcv and perform well with fixed *k* (Pedersen et al. 2019). In each model we also included the camera field of view (m^2) as an offset term to standardize abundance between years.

To investigate how the 2013-2016 "Blob" altered ocean dynamics, in particular benthic dissolved oxygen concentrations, we also fit a separate Generalized Additive Mixed-Model (GAMM) to model changes in benthic dissolved oxygen at BCUS over the entire study period (2013-2020). GAMM allows explicit specification of temporal autocorrelation structures (Lin and Zhang 1999) and allowed us to model seasonal and interannual variation and account for residual temporal autocorrelation. For the temporal model, we included a smooth for ST and week of year (WoY), and combinations of global and year-level smoothers. We also included an autoregressive (AR) correlation structure that allowed the previous two terms to be correlated with the response, known as AR(2), which was chosen by comparing residual autocorrelation plots from models fit with different temporal dependence structures (Figure S2.2). After we determined the best fitting temporal model, we then included global smooths of surface chlorophyll-*a* and SSTa to determine their influence on benthic oxygen over time. For these models, benthic oxygen and SSTa were binned to an 8-day average to align with the sampling

frequency of chlorophyll-*a*. We followed the same model specification and selection procedures outlined above.

We also fit a GAMM to model the relationship between surface chlorophyll-*a* and sea-surface temperature anomalies over the entire study period (2013-2020). We modeled surface chlorophyll-*a* as a function of smooths of week of year and SSTa, with a year-level random effect smooth. This allowed us to further examine the effect of "The Blob" on surface productivity, and how food export to the seafloor may have been affected. We followed the same model specification and selection procedures outline above.

2.2.5.2 Trawl surveys

To examine changes in density of *S. fragilis* and depth distribution over time, we first tested for normality using the Shapiro-Wilk normality test in R (Shapiro and Wilk 1965). Both density and capture depth violated the assumption of normality, so we used non-parametric tests to determine differences between survey years. We used the Kruskal-Wallis Rank Sum test (Kruskal and Wallis 1952) to test for differences in mean density across sample years, and Dunn's rank comparisons post-hoc test (Dunn 1964) with Bonferroni correction for multiple comparisons from the PMCMRplus package (Pohlert 2021) in R to determine in which years density of *S. fragilis* differed on the continental margin. We used the Komolgorov-Smirnov test (Conover 1971) to test for differences in the distribution of capture depth between pairs of survey years, as well as between trawls where *S. fragilis* was captured and all trawls conducted to account for the possibility that any changes in depth distribution were caused by differences in trawling depth. We then used linear regression to determine how strong the relationship was between each depth parameter (upper and lower limits, mean and median depth, and 25% and 75% quantiles) and time.

2.3 Results

2.3.1 Temporal patterns of sea urchin density

S. fragilis was observed in 1,245 out of 2,228 videos (56%). Sea urchin density was highly variable over time, ranging from 0 to 54 indiv. m^{-2} (Figure 2.2). Temporal patterns of density within years were characterized by extended periods of zero or few sea urchins followed by pulses of greater density (> 2 indiv. m^{-2}) lasting between a few days and a few weeks, then returning to low density (Figure 2.1). In 2013-2014, densities of *S. fragilis* showed four distinct peaks, in late-September-early-October, mid-October, late-November, and late January. In 2014-2015, we observed two density peaks, at the beginning and end of September. In 2018, we observed four to five density peaks at the end of August-beginning of September, end of September (this might be two pulses that blur together), mid-October, and mid-November. Unfortunately, this time-series ends on November 23, 2018, and no video data were available for winter 2018. In 2019-2020, there were three to four density peaks; mid-November, mid-December, and end of December to mid-January (this might be two pulses that blur together).

Between years, *S. fragilis* displayed the lowest densities during the marine heatwave in 2014-2015 (0.157 +/- 0.012 indv. m^{-2}) and in 2018 (1.283 +/- 0.131 indv. m^{-2}) shortly after the heat anomaly had subsided. The highest average densities occurred in 2019-2020 (2.104 +/-0.21 indv. m^{-2}) and in 2013-2014 (1.488 +/- 0.19 indv. m^{-2}) well after the cessation of, and at the very onset of the marine heat wave, respectively.

2.3.2 Pink sea urchin density model fit / model selection

GAMs that allowed the temporal trend in sea urchin density to vary by year (models I, S, GS, and GI) performed better than the model that included only a global smooth for sampling time, ST (model G) (Table 2.3). The best temporal model was model I, which allowed each year-level

smooth of ST to have its own wiggliness penalty (Table 32.). Adding environmental covariates improved model performance, and once again model I had the best fit with a global smooth for dissolved oxygen, bottom current (BBLc) magnitude, and ADCP backscatter (Figure 2.3; Table 2.3). Higher values of dissolved oxygen (>1.23 mL L^{-1}, Figure 2.3A) were linearly associated with higher sea urchin densities, while lower sea urchin densities were linked to high levels of backscatter (Figure 2.3B). Sea urchin density was also negatively associated with the global smooth of BBLc magnitude (i.e. a negative effect of fast-moving currents on sea urchin densities), however this term did not result in any significant improvements to the final model ($p = 0.035$, Figure 2.3C, Table 2.4). Although this term is statistically significant, caution is warranted when interpreting marginally significant smooth terms in GAMs as p-values are calculated without considering the uncertainty in estimating smoothing parameters (Wood et al. 2016).

The final model that included temporal and environmental smooths resulted in strong coherence ($R^2 = 0.739$) between observed and predicted values for 2019-2020 (Figure S2.3). However, the model is conservative at high sea urchin densities in early years, consistently under-predicting in 2013-2014 and 2014-2015 (Figure S2.3). The model under-fit extreme values of sea urchin densities and over-predicts a run of zeros in 2018 but does well at moderate densities that characterized most of the time series.

2.3.3 Environmental models

2.3.3.1 Seafloor dissolved oxygen GAMM

Dissolved oxygen concentration (hereafter, [DO]) at the seafloor at BCUS varied seasonally and interannually, ranging from 0.80 – 1.89 mL L^{-1} (Figure 2.4). [DO] increased from 2013 until

early 2016 commensurate with the onset and duration of the marine heat wave that affected the study area (Figure 2.4). The GAMM fit for weekly benthic oxygen as a function of week of year, surface chlorophyll-*a*, and sea-surface temperature anomaly provided a good fit to the dissolved oxygen time series (R^2_{adj} = 0.639, Figure 2.4). Benthic [DO] varied seasonally, with low oxygen in summer and high oxygen in autumn and winter across years (Figure 2.5A). Benthic [DO] was negatively associated with surface chlorophyll-*a* concentration throughout our study period (Figure 2.5B, Figure 2.6, Table 2.5). [DO] was below the 2013-2020 mean on average when surface chlorophyll-*a* was greater than 2.5 mg m^{-3} (Figure 2.6). A negative relationship of benthic oxygen and sea-surface temperature anomaly was also evident in the GAMM (not shown); however, this relationship was not statistically significant.

2.3.3.2 Surface chlorophyll-a GAMM

GAMM revealed seasonal changes in surface productivity above BCUS, with high chlorophyll-*a* concentration observed in late Spring and Summer and low chlorophyll-*a* concentration in the Autumn and Winter (Figure 2.7A). We also detected a negative, non-linear relationship between chlorophyll-*a* and warm-water anomalies (Figure 2.7B).

2.3.4 Trawl Survey data (2004-2018)

From 2004-2018, approximately 675 individuals of *S. fragilis* were caught in the benthic trawl surveys. We found statistically significant evidence of a decline in the mean *S. fragilis* density off Vancouver Island (Chi.sq(7) = 74.527, $p < 0.001$). *S. fragilis* density peaked in 2008, and declined until 2016, with a slight increase in 2018 (Figure 2.8, Table 2.6). It is worth noting that the decline of *S. fragilis* densities started between 2010-2012, before the onset of the marine

heat wave in the region. However, densities during and after the temperature anomaly never returned to pre-2012 levels (Figure 2.8, Table 2.6).

The depth distribution of *S. Fragilis* changed across the survey years (Figure 2.9, Table 2.6). The upper limit of *S. fragilis* shoaled from 119.0 m to 70.0 m at a rate of 3.5 m yr^{-1} on average (Figure 2.10A). The upper 25% quantile of *S. fragilis* depth distribution also shoaled from 144.5 m to 116.5 m, a rate of 2 m yr^{-1} on average, and exhibited lower variability than the upper limit (Figure 2.10B). A two-sample Komolgorov-Smirnov (K-S) test indicated that the upper limit and 25% quantiles of *S. fragilis* depth distribution come from a different probability distribution than the same parameters measured in all species trawls (Table 2.7). The linear regression results further indicated the shoaling trend in upper limit and 25% quantile is only present in the *S. fragilis* trawls and is absent from the all-species trawls (Figure 2.10A, B, Table 2.7). A two-sample K-S test also indicated that the lower limit of *S. fragilis* differs from the all-species trawls, however this was not corroborated by the linear regression (Table 2.7, Table 2.8). The 75% quantile, lower-limit, mean, and median depth also appear to shoal over time, though these trends were not statistically significant and were indistinguishable from the trend in all trawls (Figure 2.10C-F, Table 2.7).

2.4 Discussion

Pink sea urchin densities varied within and between years at the Barkley Canyon Upper Slope (BCUS) site, with lower densities following the 2013-2016 NEP marine heat wave anomaly (MHW) or the so-called warm "Blob" (Kintisch 2015), and recovery to pre-blob levels in 2018. *S. fragilis* densities were positively associated with dissolved oxygen concentration across all years, with this variable fluctuating both seasonally and interannually. Dissolved

oxygen was negatively associated with surface chlorophyll-*a* concentrations, which, in turn, was negatively associated with the sea-surface temperature anomalies recorded during the period of abnormally high temperatures in the NEP. By contrast, ADCP backscatter (as a proxy for particulate organic matter) was negatively associated with *S. fragilis* density. Together, these results suggest *S. fragilis* density at BCUS is mediated by two controlling variables – food availability and oxygen, which are in turn influenced by ocean warming, coastal upwelling dynamics, and local hydrodynamics.

The broad-scale environmental shifts caused by the 2013-2016 MHW, with remarkable effects over ecosystem functioning and productivity, have been well described elsewhere (Cavole et al. 2016; Yang et al. 2018). However, its effects on deep-sea benthic ecosystems and community structure have only been addressed in a single study at the long-term abyssal monitoring site Station M off the California Margin (Kuhnz et al. 2020). Our results indicated a complex interplay of environmental control over *S. fragilis* population by a concert of variables that ultimately regulate food availability and metabolic acclimation under nearly permanent hypoxic conditions in the slope offshore Vancouver Island. The combination of our observatory and bottom trawl survey data seems to corroborate a recent study that showed that *S. fragilis* is undergoing habitat expansion, extending its range upslope and over the shelf following the shoaling of the NEP OMZ (Sato et al. 2017). Under low dissolved oxygen concentrations (13–42 μmol kg^{-1}) found at the OMZ core (450-900 m) off the California margin, *S. fragilis* experience drastic reduction in reproductive fitness expressed in terms of suppressed gonadal development (Sato et al. 2018). In addition, the study pointed to reduced hardness and stiffness of the calcitic endoskeleton coupled with increased porosity and pore size in individuals collected in these same OMZ core areas, which are also characterized by low pH, ranging from 7.57-7-59 (Sato et

al. 2018). The authors therefore predicted that *S. fragilis* may be potentially vulnerable to crushing predators if these conditions of warming, acidification and deoxygenation become more widespread in the future.

The bottom trawl survey data covering an area of 760 km^2 and a depth gradient of nearly 400 m indicated *S. fragilis* has expanded into shallower water at a rate of 2.0 m yr^{-1} from 2004-2018 (Figure 2.9, Figure 2.10), similar to the shoaling documented in Sato et al. (2017). In contrast to Sato et al. (2017), the lower limits of pink sea urchin depth distribution in the upper 400 m off Vancouver Island remained stable over time, suggesting range expansion into favourable conditions rather than range shifting away from a physiological limit, although deeper trawls are needed to investigate the lower limits of the depth range of *S. fragilis* in this region of the NEP. Furthermore, the trawl survey data indicated the density of *S. fragilis* on the continental shelf was declining at least 2 years prior to the 2013-2016 MHW but has yet to recover to pre-2012 levels. Thus, while the MHW was likely not the direct cause of pink sea urchin density decline on the continental shelf off Vancouver Island, it has likely inhibited their survival, recruitment, and population recovery through food limitation (Sato et al. 2018; Starko et al. 2019; McPherson et al. 2021).

2.4.1 Within- and between-year variation of sea urchin density

S. fragilis is a detritivore that feeds on fresh phytodetritus, kelp and other macroalgae detritus, and other organic matter on the seafloor, and it forms large feeding aggregations on the continental slope (Boolootian et al. 1959; De Leo et al. 2017; Campanyà-Llovet et al. 2018). Within each year, we observed alternating periods of few (0-1 indiv. m^{-2}) sea urchins and "spikes" of many (>2 indv. m^{-2}) sea urchins, which likely reflect the patchy distribution of food on the continental slope. We also observed large aggregations of *S. fragilis* around small seafloor

depressions (R.C., pers obs.) that likely promoted patchiness in the accumulation of organic matter (Campanyà-Llovet et al. 2018). This patchy distribution pattern is consistent with observations from previous studies of *S. fragilis* on continental margin settings off British Columbia (De Leo et al. 2017; Campanyà-Llovet et al. 2018) and further south at the Oregon margin (Sumich and McCauley 1973).

Observed sea urchin density patterns could also be an artifact of differences in activity levels within or between sampling days, whereby higher (lower) mobility during certain times could inflate (depress) the interpreted density – a common issue in time-lapse imagery studies with limited spatial coverage (here, 0.5 m^2 – 14.93 m^2; Aguzzi and Company 2010). In the present study, we noted one period of high mobility (R.C. pers obs.) at the end of 2019 (Figure 2D), in which a large aggregation of sea urchins moved through the field of view over a three-week period. We sampled at four evenly spaced intervals throughout a 24-hour period each day, and during a similar seasonal period across years to minimize bias due to differences in activity levels related to the day-night or seasonal cycles. However, we cannot fully constrain the effect of activity levels on density estimates with a single fixed camera. Thus, density estimates from the platform should be considered in the context of the visible field of view (0.5 m^2 – 14.93 m^2), while density patterns observed in the trawl survey data are representative of the continental shelf.

Sea urchins are important for nutrient cycling through locomotion and bioturbation, and consumption of detritus (Boolootian et al. 1959). Indeed, large aggregations of feeding sea urchins can influence the spatial distribution and patchiness of nutrients on the continental margin (Campanyà-Llovet et al. 2018). *S. fragilis* may preferentially feed on high C:N ratio patches, and directly influence the composition of nutrients in the sediment (Campanyà-Llovet et

al. 2018). Their locomotion and feeding aggregations also change the distribution and mixing depth of nutrients within sediments, which affects infaunal communities that are also key for nutrient cycling (Campanyà-Llovet et al. 2018). Bioturbation by sea urchins has also been shown to influence oxygen circulation in sediment pore water (Vopel et al. 2007) affecting sediment redox potential and nutrient flux at the sediment-surface interface (Morford and Emerson 1999). All these processes release essential nutrients into the water column, which contribute to surface and coastal productivity. As warming events become more common and deoxygenation continues (Whitney et al. 2007; Pierce et al. 2012; Ross et al. 2020), the density and distribution of *S. fragilis* is likely to change, with direct consequences for biogeochemical cycling on the continental margin.

We found positive relationships between *S. fragilis* density and dissolved oxygen concentration across all years. Previous studies have documented changes in the distribution of *S. fragilis* commensurate with the shoaling OMZ in the Southern California Bight (Sato et al. 2017), suggesting a tolerance to low oxygen. Similarly, De Leo et al. (2017) found *S. fragilis* distributed from 300 m to 1400 m depth along the continental slope near BCUS, a range that includes the OMZ. However, aside from high density (>50 indiv./ 500 m) feeding aggregations observed between 500 - 600 m at the edge of the OMZ, the density of *S. fragilis* was up to 2 orders of magnitude higher outside the OMZ (DO ~ 1.4 mL/L) than inside the OMZ (DO < 0.5 mL/L; De Leo et al. 2017). This suggests that *S. fragilis* can tolerate low oxygen, but prefers a higher oxygen environment, which agrees with previous studies describing a competitive advantage of *S. fragilis* over other less-resilient shelf-inhabiting urchin species (Sato et al. 2017). Higher pink sea urchin densities also highlight a possible OMZ 'edge effect' proposed by Levin (2003), where benthic faunal densities may exhibit a maximum near the upper and lower

boundaries of OMZs at specific oxygen concentrations that may represent a physiological threshold or preference.

ADCP backscatter was negatively associated with density of *S. fragilis*. If ADCP backscatter could be considered as a proxy for sinking organic matter (Chanson et al. 2008), a positive relationship of density with organic matter deposition on the seafloor would be expected. While many types of particles and organisms are detected in ADCP backscatter (Hoitink and Hoekstra 2005; Lara-Lopez and Neira 2008; Chanson et al. 2008; Dwinovantyo et al. 2017; De Leo et al. 2018; Haalboom et al. 2021), at least some of this backscatter is likely due to particle resuspension from sediment disturbance. Resuspension of phytodetritus and other particulate organic matter deposited on the seafloor can occur when bottom currents are between 0.08 - 0.16 m/s (Beaulieu 2003). Although our GAM analysis did not find any statistically significant evidence of a direct link between BBLc magnitude and the density of *S. fragilis*, phytodetritus resuspension is possible within the range of BBLc observed in our study (Figure S2.3). Bottom trawling is also known to contribute to sediment resuspension and high turbidity in benthic habitats (Puig et al. 2014). Barkley Canyon is located near active fishing grounds, and there have been three major trawl collisions with the NEPTUNE observatory infrastructure over the last ~8 years. Furthermore, direct measurements of turbidity and chlorophyll-*a* by a vertical profiling system also connected to the NEPTUNE cabled observatory at BCUS, have shown that bottom nepheloid layer (BNL) detachments can be associated with bottom trawling activities in the area (Arjona-Camas *et al*., [in-press]). For detritivores that primarily feed on drifting macroalgae and other phytodetritus, like *S. fragilis* (Harrold et al. 1998), regular resuspension events could reduce opportunities for feeding on fresh organic matter, resulting in lower sea urchin densities. In late-summer and fall, fast currents of the of the California Undercurrent

(CUC) that flow northwestward along the continental margin may be a significant source of particle resuspension and advection (Hickey 1979; Arjona-Camas *et al*., [in-press]), preclude organic matter deposition in the first place, forcing much of the sinking organic matter down-slope or into nearby submarine canyons (Baker and Hickey 1986). Indeed, the sediments at the head of Barkley Canyon (200 m) near our study site have the lowest quantity and quality of organic matter compared to sediments throughout the rest of the canyon (Campanyà-Llovet et al. 2018). In addition, from all NEPTUNE instrument platforms in Barkley Canyon and Upper Slope that possess a seafloor video camera, kelp macroalgae detritus is observed in much greater concentrations deeper in the slope at Barkley Node (620 m) and inside the canyon topography at Barkley MidEast (987 m) and Barkley Axis (970 m) (De Leo, FC, unpublished observations). The negative association of the density of *S. fragilis* with high ADCP backscatter may therefore be related to low organic matter deposition caused by fall storms, along-margin currents, and intense bottom trawling activity that contribute to high sediment resuspension and BNL formation at slope depths on the continental margin.

2.4.2 *S. fragilis* response to the 2013-2016 marine heatwave

We observed the highest sea urchin density before and well after the MHW in 2013-2014 and 2019-2020, and the lowest density of urchins during the MHW in 2014-2015 and following the MHW in 2018. The MHW has been reported to reduce overall productivity in the region. Thermal stratification in the upper ocean reduced coastal upwelling (Leising et al. 2015; Tseng et al. 2017), surface primary productivity (McGowan 1998; Yang et al. 2018), and organic matter flux to the seafloor (Smith Jr. 1999; Smith et al. 2018). Additionally, the higher seafloor dissolved oxygen concentration we observed during the MHW indicates reduced upwelling of water from the OMZ (Barth et al. 2018), and lower respiration as a result of low food export to

the seafloor (Drazen et al. 1998). The latter is also corroborated by the negative relationship between surface chlorophyll-*a* and benthic oxygen in our GAMM. Hence, despite observing a positive relationship between *S. fragilis* and dissolved oxygen at BCUS, which would suggest that we could expect higher sea urchin density at BCUS during the MHW, the low density in 2014-2015 and in 2018 may be explained by lower food availability.

If warming-induced thermal stratification reduced upwelling and food availability on the seafloor, we expect that the relative proportion of food settling at the upper slope may be lower compared to non-blob years (Kuhnz et al. 2020). Consequently, *S. fragilis* may move down-slope in search of food, which could explain reduced density at BCUS during 2014-2015. ROV surveys that found higher density of *S. fragilis* outside the OMZ (De Leo et al. 2017) were conducted in early August, when food availability at the benthos was still high following the spring and summer phytoplankton blooms. Further, *S. fragilis* has been observed aggregating within the OMZ when macroalgal detritus is available (Yee et al., in preparation). Together with our findings, this suggests that *S. fragilis* may exhibit a foraging-respiration trade-off strategy - preferring higher oxygen in shallow water during autumn and early winter when food availability is low and migrating down-slope into the OMZ in late summer when food is plentiful. During the 2013-2016 MHW when oxygen at BCUS was highest (Figure 2.4), dissolved oxygen concentration further down the slope was likely also higher than average, allowing *S. fragilis* to forage in deeper water for longer than under normal conditions. Observations of *S. fragilis* at the Barkley Node (643 m) have also demonstrated aggregation on kelp falls, though these effects are masked by increasing dissolved oxygen (Connor Yee, pers. comm.). A video camera was added at the Barkley Node in August 2019 and is located just down-slope from the BCUS platform. These instrument platforms, spanning a depth gradient (400-620 m) on the slope adjacent to

Barkley Canyon, could be used in concert during future studies to examine if *S. fragilis* is indeed more abundant in deeper water during warm-water anomalies.

Kelp export from the coast is a significant component of the diet of *S. fragilis* (Sato et al. 2018; Campanyà-Llovet et al. 2018). Kelp diversity and abundance in nearby Barkley Sound was significantly reduced following the 2013-2016 MHW (Starko et al. 2019), which would limit this food source on the continental slope. Kelp forests in some regions have been slow to recover following the MHW (McPherson et al. 2021), indicating possible long-term reduction of food export to the continental margin. Food limitation in the deep sea affects energy intensive processes like reproductive capacity and calcification rates (Sato et al. 2018), which influence recruitment and abundance of sea urchins (Zhao et al. 2013; Filbee-Dexter and Scheibling 2014). Specifically, the ability of individuals of *S. fragilis* to calcify and undergo energetically demanding reproduction processes such as gametogenesis (Sato et al. 2018) (Sato et al., 2018) and metamorphosis from planktonic larva to benthic juvenile (Dorey et al. 2022) likely be affected further under future ocean warming and acidification scenarios (McBride et al. 1997; Taylor et al. 2014), reducing overall population size and making individuals more vulnerable to crushing predators like crabs and fish (Sato et al. 2018; Asnaghi et al. 2020).

High mortality as a consequence of the MHW is another possible explanation for the low pink sea urchin densities observed in 2014-2015 and 2018. However, this explanation was not corroborated by the trawl survey data, which revealed significant temporal trends in the depth distribution, but not the density, of pink sea urchins across the continental slope off Vancouver Island. Although the density of *S, fragilis* appeared to decline from 2012-2016 (Figure 8A, Table 6), densities remained within the range of variation observed across all other years. This high variability suggests that pink sea urchin distribution may be patchy on the scale of the

continental shelf, consistent with the highly mobile nature of *S. fragilis* (Robert and Juniper 2012). Together, these observations suggest a mobility mechanism, rather than mortality, is likely responsible for the observed differences in pink sea urchin density at the BCUS platform.

Another important limitation of cabled seafloor observatories is the spatial scale at which observations can be made. These platforms are designed for high temporal frequency to the exclusion of spatial resolution. Consequently, correlations between sea urchin density and environmental variables measured within the small field of view of the camera may not generalize to the continental slope. Thus, caution is warranted when interpreting and scaling results taken only from a single fixed-point observatory. Additional data sources and future research using time-lapse cameras at different locations (e.g., Barkley Node) could lend support to our results. However, the trends observed in the present study are consistent with previous findings on the response of *S. fragilis* to broad-scale oceanographic trends (Sato et al. 2017, 2018).

2.4.3 Decadal distribution shifts (from bottom trawl surveys)

Although we did not observe a decline in dissolved oxygen at BCUS over the study period (2013-2020), previous studies in the NEP have documented deoxygenation and OMZ expansion on a decadal scale (Whitney et al. 2007; Pierce et al. 2012; Ross et al. 2020). Given our results and those of Sato et al. (2017; 2018), we expect the depth distribution of *S. fragilis* to shoal off Vancouver Island on a decadal scale as the OMZ continues to expand. Interestingly, the observed shoaling of pink sea urchin upper limit and 25% quantile (Figure 2.9) was not followed by a concomitant increase in pink sea urchin density (Figure 2.8). This discrepancy may be explained by an overall decrease in pink sea urchin density on the shelf, which may have persisted due to the effects of the 2013-2016 MHW. The expected shoaling of pink sea urchins in

response to deoxygenation will likely be modulated by the increasing prevalence, duration, and severity of warm-water anomalies that disrupt seasonal upwelling and food availability on the continental margin. The extent to which future SST anomalies may influence *S. fragilis* density and distribution should be considered to understand the consequences for coastal and deep-sea benthopelagic coupling in the NEP.

2.5 Conclusion

S. fragilis is a slow-moving (average 7.31 - 26.9 cm h^{-1}; Robert and Juniper 2012; Barry et al. 20114) calcifying organism and is susceptible to ocean change. Under future climate change scenarios, the distribution of *S. fragilis* on the continental margin may be affected - migrating into deeper water during periods of weak upwelling and shoaling over decades as deoxygenation continues. The density of *S. fragilis* may also be affected due to ocean warming disrupting food availability at the benthos, and acidification reducing their defense and reproductive capacity (Sato *et al*., 2018). This is turn may influence nutrient cycling on the slope, affecting infaunal community composition, biogeochemical cycling, and surface productivity. Long-term monitoring of the continental margin on multiple spatial and temporal scales is therefore critical to predict how these important marine ecosystems will respond to future ocean change.

2.6 Acknowledgements

Ocean Networks Canada is funded through the Canada Foundation for Innovation-Major Science Initiative (CFI-MSI) fund 30199. We are thankful for the support from ONC's marine and digital operations staff for servicing and maintaining the NEPTUNE observatory and for the curation and quality control of all oceanographic data streams used in this study. We also thank

the Department of Fisheries and Oceans (DFO) and the Institute of Ocean Sciences (IOS), in Sidney, BC, Canada, for the publicly and freely available data from the long-term Line P monitoring program. RC was supported by an Early Career Faculty Award Grant to Dr. Katleen Robert from the Marine Environmental Observation, Prediction and Response Network (MEOPAR) and a Canada Research Chair (Ocean Mapping) to PI KR. We also thank M.E.C., J.A.M.M., P.K., K.C., S.N., A.J.C.S., and A.Y-S. for their feedback on early drafts of the manuscript.

2.7 References

Aguzzi, J., and Company, J.B. 2010. Chronobiology of Deep-Water Decapod Crustaceans on Continental Margins. *In* Advances in Marine Biology. Elsevier. pp. 155–225. doi:10.1016/B978-0-12-381015-1.00003-4.

Allen, S.E., and de Madron, X.D. 2009. A review of the role of submarine canyons in deep-ocean exchange with the shelf. Ocean Sci.: 14.

Allen, S.E., Vindeirinho, R.E., Thomson, R.E., Foreman, M.G.G., and Mackas, D.L. 2001. Physical and biological processes over a submarine canyon during an upwelling event. Canadian Journal of Fisheries and Aquatic Sciences **58**(4): 671–684.

Anderson, S.C., Keppel, E.A., and Edwards, A.M. 2019. A reproducible data synopsis for over 100 species of British Columbia groundfish. DFO Can. Sci. Advis. Sec. Res. Doc. Available from https://www.dfo-mpo.gc.ca/csas-sccs/Publications/ResDocs-DocRech/2019/2019_041-eng.pdf [accessed 5 May 2021].

Arntz, W.E., Gallardo, V.A., Gutiérrez, D., Isla, E., Levin, L.A., Mendo, J., Neira, C., Rowe, G.T., Tarazona, J., and Wolff, M. 2006. El Niño and similar perturbation effects on the benthos of the Humboldt, California, and Benguela Current upwelling ecosystems. Adv. Geosci. **6**: 243–265. doi:10.5194/adgeo-6-243-2006.

Asnaghi, V., Chindris, A., Leggieri, F., Scolamacchia, M., Brundu, G., Guala, I., Loi, B., Chiantore, M., and Farina, S. 2020. Decreased pH impairs sea urchin resistance to predatory fish: A combined laboratory-field study to understand the fate of top-down processes in future oceans. Marine Environmental Research **162**: 105194. doi:10.1016/j.marenvres.2020.105194.

Auth, T.D., Daly, E.A., Brodeur, R.D., and Fisher, J.L. 2018. Phenological and distributional shifts in ichthyoplankton associated with recent warming in the northeast Pacific Ocean. Glob Change Biol **24**(1): 259–272. doi:10.1111/gcb.13872.

Baker, E.T., and Hickey, B.M. 1986. Contemporary sedimentation processes in and around an active West Coast submarine canyon. Marine Geology **71**(1–2): 15–34. doi:10.1016/0025-3227(86)90031-9.

Barry, J.P., Lovera, C., Buck, K.R., Peltzer, E.T., Taylor, J.R., Walz, P., Whaling, P.J., and Brewer, P.G. 2014. Use of a Free Ocean CO_2 Enrichment (FOCE) System to Evaluate the Effects of Ocean Acidification on the Foraging Behavior of a Deep-Sea Urchin. Environ. Sci. Technol. **48**(16): 9890–9897. doi:10.1021/es501603r.

Barth, J., Fram, J., Dever, E., Risien, C., Wingard, C., Collier, R., and Kearney, T. 2018. Warm Blobs, Low-Oxygen Events, and an Eclipse: The Ocean Observatories Initiative Endurance Array Captures Them All. Oceanog **31**(1): 90–97. doi:10.5670/oceanog.2018.114.

Bates, A.E., Lee, R.W., Tunnicliffe, V., and Lamare, M.D. 2010. Deep-sea hydrothermal vent animals seek cool fluids in a highly variable thermal environment. Nat Commun **1**(1): 14. doi:10.1038/ncomms1014.

Batten, S.D., Raitsos, D.E., Danielson, S., Hopcroft, R., Coyle, K., and McQuatters-Gollop, A. 2018. Interannual variability in lower trophic levels on the Alaskan Shelf. Deep Sea Research Part II: Topical Studies in Oceanography **147**: 58–68. doi:10.1016/j.dsr2.2017.04.023.

Beaulieu, S.E. 2003. Resuspension of phytodetritus from the sea floor: A laboratory flume study. Limnol. Oceanogr. **48**(3): 1235–1244. doi:10.4319/lo.2003.48.3.1235.

Best, M.M.R., Bornhold, B.D., Juniper, S.K., and Barnes, C.R. 2007. NEPTUNE Canada Regional Cabled Observatory: Science Plan. *In* OCEANS 2007. IEEE, Vancouver, BC. pp. 1–7. doi:10.1109/OCEANS.2007.4449316.

Bett, B.J., Malzone, M.G., Narayanaswamy, B.E., and Wigham, B.D. 2001. Temporal variability in phytodetritus and megabenthic activity at the seabed in the deep Northeast Atlantic. Progress in Oceanography **50**(1–4): 349–368. doi:10.1016/S0079-6611(01)00066-0.

Billett, D.S.M., Bett, B.J., Reid, W.D.K., Boorman, B., and Priede, I.G. 2010. Long-term change in the abyssal NE Atlantic The 'Amperima Event revisited. : 12.

Billett, D.S.M., Lampitt, R.S., Rice, A.L., and Mantoura, R.F.C. 1983. Seasonal sedimentation of phytoplankton to the deep-sea benthos. Nature **302**(5908): 520–522. doi:10.1038/302520a0.

Birchenough, S.N.R., Reiss, H., Degraer, S., Mieszkowska, N., Borja, Á., Buhl-Mortensen, L., Braeckman, U., Craeymeersch, J., De Mesel, I., Kerckhof, F., Kröncke, I., Parra, S., Rabaut, M., Schröder, A., Van Colen, C., Van Hoey, G., Vincx, M., and Wätjen, K. 2015. Climate change and marine benthos: a review of existing research and future directions in the North Atlantic. WIREs Clim Change **6**(2): 203–223. doi:10.1002/wcc.330.

Bond, N.A., Cronin, M.F., Freeland, H., and Mantua, N. 2015. Causes and impacts of the 2014 warm anomaly in the NE Pacific: Geophys. Res. Lett. **42**(9): 3414–3420. doi:10.1002/2015GL063306.

Boolootian, R.A., Giese, A.C., Tucker, J.S., and Farmanfarmaian, A. 1959. A contribution to the biology of a deep sea echinoid, Allocentrotus fragilis (Jackson). The Biological Bulletin **116**(3): 362–372. doi:10.2307/1538946.

Brodeur, R.D., Auth, T.D., and Phillips, A.J. 2019. Major Shifts in Pelagic Micronekton and Macrozooplankton Community Structure in an Upwelling Ecosystem Related to an Unprecedented Marine Heatwave. Front. Mar. Sci. **6**: 212. doi:10.3389/fmars.2019.00212.

Buja, A., Hastie, T., and Tibshirani, R. 1989. Linear smoothers and additive models. The Annals of Statistics **17**(2): 453–555.

Burnham, K.P., Anderson, D.R., and Burnham, K.P. 2002. Model selection and multimodel inference: a practical information-theoretic approach. *In* 2nd ed. Springer, New York.

Campanyà-Llovet, N., Snelgrove, P.V.R., and De Leo, F.C. 2018. Food quantity and quality in Barkley Canyon (NE Pacific) and its influence on macroinfaunal community structure. Progress in Oceanography **169**: 106–119. doi:10.1016/j.pocean.2018.04.003.

Cavole, L.M., Demko, A., Diner, R., Giddings, A., Koester, I., Pagniello, C., Paulsen, M.-L., Ramirez-Valdez, A., Schwenck, S., Yen, N., Zill, M., and Franks, P. 2016. Biological Impacts of the 2013–2015 Warm-Water Anomaly in the Northeast Pacific: Winners, Losers, and the Future. Oceanog **29**(2). doi:10.5670/oceanog.2016.32.

Chanson, H., Takeuchi, M., and Trevethan, M. 2008. Using turbidity and acoustic backscatter intensity as surrogate measures of suspended sediment concentration in a small subtropical estuary. Journal of Environmental Management **88**(4): 1406–1416. doi:10.1016/j.jenvman.2007.07.009.

Chauvet, P. 2018. Etude de la dynamique temporelle et environnementale contrôlant la mégafaune profonde vivant dans le Canyon de Barkley grâce à l'utilisation de l'observatoire Ocean Network Canada. PhD, Université de Bretagne occidentale, Brest.

Chauvet, P., Metaxas, A., Hay, A.E., and Matabos, M. 2018. Annual and seasonal dynamics of deep-sea megafaunal epibenthic communities in Barkley Canyon (British Columbia,

Canada): A response to climatology, surface productivity and benthic boundary layer variation. Progress in Oceanography **169**: 89–105. doi:10.1016/j.pocean.2018.04.002.
Chauvet, P., Metaxas, A., and Matabos, M. 2019. Interannual Variation in the Population Dynamics of Juveniles of the Deep-Sea Crab Chionoecetes tanneri. Front. Mar. Sci. **6**: 50. doi:10.3389/fmars.2019.00050.
Chavez, F.P., and Messié, M. 2009. A comparison of Eastern Boundary Upwelling Ecosystems. Progress in Oceanography **83**(1–4): 80–96. doi:10.1016/j.pocean.2009.07.032.
Conover, W.J. 1971. Practical Nonparametric Statistics. John Wiley & Sons, Ltd, New York.
Couch, C.S., Burns, J.H.R., Liu, G., Steward, K., Gutlay, T.N., Kenyon, J., Eakin, C.M., and Kosaki, R.K. 2017. Mass coral bleaching due to unprecedented marine heatwave in Papahānaumokuākea Marine National Monument (Northwestern Hawaiian Islands). PLoS ONE **12**(9): e0185121. doi:10.1371/journal.pone.0185121.
De Leo, F.C., Gauthier, M., Nephin, J., Mihály, S., and Juniper, S.K. 2017. Bottom trawling and oxygen minimum zone influences on continental slope benthic community structure off Vancouver Island (NE Pacific). Deep Sea Research Part II: Topical Studies in Oceanography **137**: 404–419. doi:10.1016/j.dsr2.2016.11.014.
De Leo, F.C., Ogata, B., Sastri, A.R., Heesemann, M., Mihály, S., Galbraith, M., and Morley, M.G. 2018. High-frequency observations from a deep-sea cabled observatory reveal seasonal overwintering of Neocalanus spp. in Barkley Canyon, NE Pacific: Insights into particulate organic carbon flux. Progress in Oceanography **169**: 120–137. doi:10.1016/j.pocean.2018.06.001.
Delorme, N.J., and Sewell, M.A. 2014. Temperature and salinity: two climate change stressors affecting early development of the New Zealand sea urchin Evechinus chloroticus. Mar Biol **161**(9): 1999–2009. doi:10.1007/s00227-014-2480-0.
Domke, L., Lacharité, M., Metaxas, A., and Matabos, M. 2017. Influence of an oxygen minimum zone and macroalgal enrichment on benthic megafaunal community composition in a NE Pacific submarine canyon. Mar Ecol **38**(6): e12481. doi:10.1111/maec.12481.
Dorey, N., Butera, E., Espinel-Velasco, N., and Dupont, S. 2022. Direct and latent effects of ocean acidification on the transition of a sea urchin from planktonic larva to benthic juvenile. Sci Rep **12**(1): 5557. doi:10.1038/s41598-022-09537-7.
Doya, C., Aguzzi, J., Pardo, M., Matabos, M., Company, J.B., Costa, C., Mihaly, S., and Canals, M. 2014. Diel behavioral rhythms in sablefish (Anoplopoma fimbria) and other benthic species, as recorded by the Deep-sea cabled observatories in Barkley canyon (NEPTUNE-Canada). Journal of Marine Systems **130**: 69–78. doi:10.1016/j.jmarsys.2013.04.003.
Drazen, J.C., Baldwin, R.J., and Smith, K.L. 1998. Sediment community response to a temporally varying food supply at an abyssal station in the NE pacific. Deep Sea Research Part II: Topical Studies in Oceanography **45**(4–5): 893–913. doi:10.1016/S0967-0645(98)00007-1.
Dunn, O.J. 1964. Multiple Comparisons Using Rank Sums. Technometrics **6**(3): 241–252. doi:10.1080/00401706.1964.10490181.
Durden, J.M., Bett, B.J., Huffard, C.L., Pebody, C., Ruhl, H.A., and Smith, K.L. 2020. Response of deep-sea deposit-feeders to detrital inputs: A comparison of two abyssal time-series sites. Deep Sea Research Part II: Topical Studies in Oceanography **173**: 104677. doi:10.1016/j.dsr2.2019.104677.

Dwinovantyo, A., Manik, H.M., Prartono, T., Susilohadi, and Ilahude, D. 2017. Estimation of suspended sediment concentration from Acoustic Doppler Current Profiler (ADCP) instrument: A case study of Lembeh Strait, North Sulawesi. IOP Conf. Ser.: Earth Environ. Sci. **54**: 012082. doi:10.1088/1755-1315/54/1/012082.

Edwards, M.S. 2004. Estimating scale-dependency in disturbance impacts: El Niños and giant kelp forests in the northeast Pacific. Oecologica **138**: 436–447. doi:10.1007/s00442-003-1452-8.

Filbee-Dexter, K., and Scheibling, R. 2014. Detrital kelp subsidy supports high reproductive condition of deep-living sea urchins in a sedimentary basin. Aquat. Biol. **23**(1): 71–86. doi:10.3354/ab00607.

Fredriksen, R., Christiansen, J.S., Bonsdorff, E., Larsen, L.-H., Nordström, M.C., Zhulay, I., and Bluhm, B.A. 2020. Epibenthic megafauna communities in Northeast Greenland vary across coastal, continental shelf and slope habitats. Polar Biol **43**(10): 1623–1642. doi:10.1007/s00300-020-02733-z.

Gage, J.D., and Tyler, P.A. 1991. Deep-Sea Biology: A Natural History of Organisms at the Deep-sea Floor. Cambridge University Press, Cambridge.

Genin, A. 2004. Bio-physical coupling in the formation of zooplankton and fish aggregations over abrupt topographies. Journal of Marine Systems **50**(1–2): 3–20. doi:10.1016/j.jmarsys.2003.10.008.

Gleason, L.U., and Burton, R.S. 2013. Phenotypic evidence for local adaptation to heat stress in the marine snail Chlorostoma (formerly Tegula) funebralis. Journal of Experimental Marine Biology and Ecology **448**: 360–366. doi:10.1016/j.jembe.2013.08.008.

Glover, A.G., Gooday, A.J., Bailey, D.M., Billett, D.S.M., Chevaldonné, P., Colaço, A., Copley, J., Cuvelier, D., Desbruyères, D., Kalogeropoulou, V., Klages, M., Lampadariou, N., Lejeusne, C., Mestre, N.C., Paterson, G.L.J., Perez, T., Ruhl, H., Sarrazin, J., Soltwedel, T., Soto, E.H., Thatje, S., Tselepides, A., Van Gaever, S., and Vanreusel, A. 2010. Temporal Change in Deep-Sea Benthic Ecosystems. *In* Advances in Marine Biology. Elsevier. pp. 1–95. doi:10.1016/B978-0-12-381015-1.00001-0.

Haalboom, S., de Stigter, H., Duineveld, G., van Haren, H., Reichart, G.-J., and Mienis, F. 2021. Suspended particulate matter in a submarine canyon (Whittard Canyon, Bay of Biscay, NE Atlantic Ocean): Assessment of commonly used instruments to record turbidity. Marine Geology **434**: 106439. doi:10.1016/j.margeo.2021.106439.

Harrold, C., Light, K., and Lisin, S. 1998. Organic enrichment of submarine-canyon and continental-shelf benthic communities by macroalgal drift imported from nearshore kelp forests. Limnol. Oceanogr. **43**(4): 669–678. doi:10.4319/lo.1998.43.4.0669.

Hayes, N.M., Haig, H.A., Simpson, G.L., and Leavitt, P.R. 2020. Effects of lake warming on the seasonal risk of toxic cyanobacteria exposure. Limnol Oceanogr **5**(6): 393–402. doi:10.1002/lol2.10164.

Heise, K. 2006. Oxidative stress during stressful heat exposure and recovery in the North Sea eelpout Zoarces viviparus L. Journal of Experimental Biology **209**(2): 353–363. doi:10.1242/jeb.01977.

Helly, J.J., and Levin, L.A. 2004. Global distribution of naturally occurring marine hypoxia on continental margins. Deep Sea Research Part I: Oceanographic Research Papers **51**(9): 1159–1168. doi:10.1016/j.dsr.2004.03.009.

Hickey, B.M. 1979. The California current system—hypotheses and facts. Progress in Oceanography **8**(4): 191–279. doi:10.1016/0079-6611(79)90002-8.

Hoitink, A.J.F., and Hoekstra, P. 2005. Observations of suspended sediment from ADCP and OBS measurements in a mud-dominated environment. Coastal Engineering **52**(2): 103–118. doi:10.1016/j.coastaleng.2004.09.005.

Honjo, S., Eglinton, T., Taylor, C., Ulmer, K., Sievert, S., Bracher, A., German, C., Edgcomb, V., Francois, R., Iglesias-Rodriguez, M.D., Van Mooy, B., and Rapeta, D. 2014. Understanding the Role of the Biological Pump in the Global Carbon Cycle: An Imperative for Ocean Science. oceanog **27**(3): 10–16. doi:10.5670/oceanog.2014.78.

Jackson, J.M., Johnson, G.C., Dosser, H.V., and Ross, T. 2018a. Warming From Recent Marine Heatwave Lingers in Deep British Columbia Fjord. Geophys. Res. Lett. **45**(18): 9757–9764. doi:10.1029/2018GL078971.

Jackson, R., Gabric, A., and Cropp, R. 2018b. Effects of ocean warming and coral bleaching on aerosol emissions in the Great Barrier Reef, Australia. Sci Rep **8**(1): 14048. doi:10.1038/s41598-018-32470-7.

Kelly, M.W., Pankey, M.S., DeBiasse, M.B., and Plachetzki, D.C. 2017. Adaptation to heat stress reduces phenotypic and transcriptional plasticity in a marine copepod. Funct Ecol **31**(2): 398–406. doi:10.1111/1365-2435.12725.

Kendzierska, H., Łukawska-Matuszewska, K., Burska, D., and Janas, U. 2020. Benthic fluxes of oxygen and nutrients under the influence of macrobenthic fauna on the periphery of the intermittently hypoxic zone in the Baltic Sea. Journal of Experimental Marine Biology and Ecology **530–531**: 151439. doi:10.1016/j.jembe.2020.151439.

Kintisch, E. 2015. 'The Blob' invades Pacific, flummoxing climate experts. Science **348**(6230): 17–18. doi:10.1126/science.348.6230.17.

Kruskal, W.H., and Wallis, W.A. 1952. Use of Ranks in One-Criterion Variance Analysis. Journal of the American Statistical Association **47**(260): 583–621. doi:10.1080/01621459.1952.10483441.

Kuhnz, L.A., Ruhl, H.A., Huffard, C.L., and Smith, K.L. 2020. Benthic megafauna assemblage change over three decades in the abyss: Variations from species to functional groups. Deep Sea Research Part II: Topical Studies in Oceanography **173**: 104761. doi:10.1016/j.dsr2.2020.104761.

Lampitt, R.S. 1985. Evidence for the seasonal deposition of detritus to the deep-sea floor and its subsequent resuspension. Deep Sea Research Part A. Oceanographic Research Papers **32**(8): 885–897. doi:10.1016/0198-0149(85)90034-2.

Lara-Lopez, A., and Neira, F.J. 2008. Synchronicity between zooplankton biomass and larval fish concentrations along a highly flushed Tasmanian estuary: assessment using net and acoustic methods. Journal of Plankton Research **30**(9): 1061–1073. doi:10.1093/plankt/fbn063.

Lebrato, M., Iglesias-Rodríguez, D., Feely, R.A., Greeley, D., Jones, D.O.B., Suarez-Bosche, N., Lampitt, R.S., Cartes, J.E., Green, D.R.H., and Alker, B. 2010. Global contribution of echinoderms to the marine carbon cycle: $CaCO_3$ budget and benthic compartments. Ecological Monographs **80**(3): 441–467. doi:10.1890/09-0553.1.

Leising, A.W., Schroeder, I.D., Bograd, S.J., Abell, J., Durazo, R., Gaxiola-Castro, G., Marinas, U.-F. de C., and Playitas, Z. 2015. State of the California Current 2014–15: Impacts of the warm-water "Blob." **56**: 38.

Levin, L.A. 2003. Oxygen minimum zone benthos: Adaptation and community response to hypoxia. Oceanography and Marine Biology: an Annual Review **41**: 1–45.

Levin, L.A., Liu, K.-K., Emeis, K.-C., Breitburg, D.L., Cloern, J., Deutsch, C., Giani, M., Goffart, A., Hofmann, E.E., Lachkar, Z., Limburg, K., Liu, S.-M., Montes, E., Naqvi, W., Ragueneau, O., Rabouille, C., Sarkar, S.K., Swaney, D.P., Wassman, P., and Wishner, K.F. 2015. Comparative biogeochemistry–ecosystem–human interactions on dynamic continental margins. Journal of Marine Systems **141**: 3–17. doi:10.1016/j.jmarsys.2014.04.016.

Levin, L.A., and Sibuet, M. 2012. Understanding Continental Margin Biodiversity: A New Imperative. Annu. Rev. Mar. Sci. **4**(1): 79–112. doi:10.1146/annurev-marine-120709-142714.

Lin, X., and Zhang, D. 1999. Inference in generalized additive mixed modelsby using smoothing splines. J Royal Statistical Soc B **61**(2): 381–400. doi:10.1111/1467-9868.00183.

Low, N.H.N., and Micheli, F. 2020. Short- and long-term impacts of variable hypoxia exposures on kelp forest sea urchins. Sci Rep **10**(1): 2632. doi:10.1038/s41598-020-59483-5.

Mackas, D.L., Kieser, R., Saunders, M., Yelland, D.R., Brown, R.M., and Moore, D.F. 1997. Aggregation of euphausiids and Pacific hake (Merluccius productus) along the outer continental shelf off Vancouver Island. Can. J. Fish. Aquat. Sci. **54**(9): 2080–2096. doi:10.1139/f97-113.

Marra, G., and Wood, S.N. 2011. Practical variable selection for generalized additive models. Computational Statistics & Data Analysis **55**(7): 2372–2387. doi:10.1016/j.csda.2011.02.004.

Matabos, M., Bui, A.O.V., Mihály, S., Aguzzi, J., Juniper, S.K., and Ajayamohan, R.S. 2014. High-frequency study of epibenthic megafaunal community dynamics in Barkley Canyon: A multi-disciplinary approach using the NEPTUNE Canada network. Journal of Marine Systems **130**: 56–68. doi:10.1016/j.jmarsys.2013.05.002.

McBride, S.C., Pinnix, W.D., Lawrence, J.M., Lawrence, A.L., and Mulligan, T.M. 1997. The Effect of Temperature on Production of Gonads by the Sea Urchin Strongylocentrotus franciscanus Fed Natural and Prepared Diets. J World Aquaculture Soc **28**(4): 357–365. doi:10.1111/j.1749-7345.1997.tb00282.x.

McCabe, R.M., Hickey, B.M., Kudela, R.M., Lefebvre, K.A., Adams, N.G., Bill, B.D., Gulland, F.M.D., Thomson, R.E., Cochlan, W.P., and Trainer, V.L. 2016. An unprecedented coastwide toxic algal bloom linked to anomalous ocean conditions. Geophys. Res. Lett. **43**(19). doi:10.1002/2016GL070023.

McGowan, J.A. 1998. Climate-Ocean Variability and Ecosystem Response in the Northeast Pacific. Science **281**(5374): 210–217. doi:10.1126/science.281.5374.210.

McKibben, S.M., Peterson, W., Wood, A.M., Trainer, V.L., Hunter, M., and White, A.E. 2017. Climatic regulation of the neurotoxin domoic acid. Proc Natl Acad Sci USA **114**(2): 239–244. doi:10.1073/pnas.1606798114.

McPherson, M.L., Finger, D.J.I., Houskeeper, H.F., Bell, T.W., Carr, M.H., Rogers-Bennett, L., and Kudela, R.M. 2021. Large-scale shift in the structure of a kelp forest ecosystem co-occurs with an epizootic and marine heatwave. Communications Biology **4**(298). doi:10.1038/s42003-021-01827-6.

Morford, J.L., and Emerson, S. 1999. The geochemistry of redox sensitive trace metals in sediments. Geochimica et Cosmochimica Acta **63**(11/12): 1735–1750.

Morlini, I. 2006. On Multicollinearity and Concurvity in Some Nonlinear Multivariate Models. JISS **15**(1): 3–26. doi:10.1007/s10260-006-0005-9.

Nakajima, R., Komuku, T., Yamakita, T., Lindsay, D.J., Jintsu-Uchifune, Y., Watanabe, H., Tanaka, K., Shirayama, Y., Yamamoto, H., and Fujikura, K. 2014. A new method for estimating the area of the seafloor from oblique images taken by deep-sea submersible survey platforms. JAMSTEC-R **19**(0): 59–66. doi:10.5918/jamstecr.19.59.

Oliver, E.C.J., Donat, M.G., Burrows, M.T., Moore, P.J., Smale, D.A., Alexander, L.V., Benthuysen, J.A., Feng, M., Sen Gupta, A., Hobday, A.J., Holbrook, N.J., Perkins-Kirkpatrick, S.E., Scannell, H.A., Straub, S.C., and Wernberg, T. 2018. Longer and more frequent marine heatwaves over the past century. Nat Commun **9**(1): 1324. doi:10.1038/s41467-018-03732-9.

Papiol, V., Hendrickx, M.E., and Serrano, D. 2017. Effects of latitudinal changes in the oxygen minimum zone of the northeast Pacific on the distribution of bathyal benthic decapod crustaceans. Deep Sea Research Part II: Topical Studies in Oceanography **137**: 113–130. doi:10.1016/j.dsr2.2016.04.023.

Pedersen, E.J., Miller, D.L., Simpson, G.L., and Ross, N. 2019. Hierarchical generalized additive models in ecology: an introduction with mgcv. PeerJ **7**: e6876. doi:10.7717/peerj.6876.

Pierce, S.D., Barth, J.A., Shearman, R.K., and Erofeev, A.Y. 2012. Declining Oxygen in the Northeast Pacific*. Journal of Physical Oceanography **42**(3): 495–501. doi:10.1175/JPO-D-11-0170.1.

Pohlert, T. 2021. PMCMRplus: Calculate Pairwise Multiple Comparisons of Mean Rank Sums Extended. Available from https://CRAN.R-project.org/package=PMCMRplus.

Puig, P., Palanques, A., and Martín, J. 2014. Contemporary Sediment-Transport Processes in Submarine Canyons. Annu. Rev. Mar. Sci. **6**(1): 53–77. doi:10.1146/annurev-marine-010213-135037.

R Core Team. 2020. R: A language and environment for statistical computing. R Foundation for Statistical Computing, Vienna, Austria. Available from https://www.Rproject.org/.

Ramos-Musalem, K., and Allen, S.E. 2019. The Impact of Locally Enhanced Vertical Diffusivity on the Cross-Shelf Transport of Tracers Induced by a Submarine Canyon. Journal of Physical Oceanography **49**: 24.

Ritzman, J., Brodbeck, A., Brostrom, S., McGrew, S., Dreyer, S., Klinger, T., and Moore, S.K. 2018. Economic and sociocultural impacts of fisheries closures in two fishing-dependent communities following the massive 2015 U.S. West Coast harmful algal bloom. Harmful Algae **80**: 35–45. doi:10.1016/j.hal.2018.09.002.

Robert, K., and Juniper, S. 2012. Surface-sediment bioturbation quantified with cameras on the NEPTUNE Canada cabled observatory. Mar. Ecol. Prog. Ser. **453**: 137–149. doi:10.3354/meps09623.

Ross, T., Du Preez, C., and Ianson, D. 2020. Rapid deep ocean deoxygenation and acidification threaten life on Northeast Pacific seamounts. Glob Change Biol: gcb.15307. doi:10.1111/gcb.15307.

Rossi, V., López, C., Hernández-García, E., Sudre, J., Garçon, V., and Morel, Y. 2009. Surface mixing and biological activity in the four Eastern Boundary Upwelling Systems. Nonlin. Processes Geophys. **16**(4): 557–568. doi:10.5194/npg-16-557-2009.

Ruhl, H.A. and Smith Jr., Kenneth L. 2004. Shifts in Deep-Sea Community Structure Linked to Climate and Food Supply. Science **305**(5683): 513–515. doi:10.1126/science.1099759.

Sato, K.N., Andersson, A.J., Day, J.M.D., Taylor, J.R.A., Frank, M.B., Jung, J.-Y., McKittrick, J., and Levin, L.A. 2018. Response of Sea Urchin Fitness Traits to Environmental

Gradients Across the Southern California Oxygen Minimum Zone. Front. Mar. Sci. **5**: 258. doi:10.3389/fmars.2018.00258.

Sato, K.N., Levin, L.A., and Schiff, K. 2017. Habitat compression and expansion of sea urchins in response to changing climate conditions on the California continental shelf and slope (1994–2013). Deep Sea Research Part II: Topical Studies in Oceanography **137**: 377–389. doi:10.1016/j.dsr2.2016.08.012.

Scannell, H.A., Pershing, A.J., Alexander, M.A., Thomas, A.C., and Mills, K.E. 2016. Frequency of marine heatwaves in the North Atlantic and North Pacific since 1950: FREQUENCY OF MARINE HEATWAVES SINCE 1950. Geophys. Res. Lett. **43**(5): 2069–2076. doi:10.1002/2015GL067308.

Shapiro, S.S., and Wilk, M.B. 1965. An analysis of variance test for normality (complete samples). Biometrika **52**(3 and 4): 591–611. doi:10.1093/biomet/52.3-4.591.

Smith Jr., K.L. 1999. Long-Term Discrepancy Between Food Supply and Demand in the Deep Eastern North Pacific. Science **284**(5417): 1174–1177. doi:10.1126/science.284.5417.1174.

Smith, K.L., Kaufmann, R.S., and Baldwin, R.J. 1994. Coupling of near-bottom pelagic and benthic processes at abyssal depths in the eastern North Pacific Ocean. Limnology and Oceanography **39**(5): 1101–1118. doi:https://doi.org/10.4319/lo.1994.39.5.1101.

Smith, K.L., Kaufmann, R.S., and Wakefield, W.W. 1993. Mobile megafaunal activity monitored with a time-lapse camera in the abyssal North Pacific. Deep Sea Research Part I: Oceanographic Research Papers **40**(11–12): 2307–2324. doi:10.1016/0967-0637(93)90106-D.

Smith, K.L., Ruhl, H.A., Huffard, C.L., Messié, M., and Kahru, M. 2018. Episodic organic carbon fluxes from surface ocean to abyssal depths during long-term monitoring in NE Pacific. Proc Natl Acad Sci USA **115**(48): 12235–12240. doi:10.1073/pnas.1814559115.

Sorte, C.J.B., Fuller, A., and Bracken, M.E.S. 2010. Impacts of a simulated heat wave on composition of a marine community. Oikos **119**(12): 1909–1918. doi:10.1111/j.1600-0706.2010.18663.x.

Starko, S., Bailey, L.A., Creviston, E., James, K.A., Warren, A., Brophy, M.K., Danasel, A., Fass, M.P., Townsend, J.A., and Neufeld, C.J. 2019. Environmental heterogeneity mediates scale-dependent declines in kelp diversity on intertidal rocky shores. PLoS ONE **14**(3): e0213191. doi:https://doi.org/10.1371/journal.pone.0213191.

Sumich, J.L., and McCauley, J.E. 1973. Growth of a Sea Urchin, Allocentrotus fragilis, off the Oregon Coast. Pacific Science **27**(2): 156–167.

Suryan, R.M., Arimitsu, M.L., Coletti, H.A., Hopcroft, R.R., Lindeberg, M.R., Barbeaux, S.J., Batten, S.D., Burt, W.J., Bishop, M.A., Bodkin, J.L., Brenner, R., Campbell, R.W., Cushing, D.A., Danielson, S.L., Dorn, M.W., Drummond, B., Esler, D., Gelatt, T., Hanselman, D.H., Hatch, S.A., Haught, S., Holderied, K., Iken, K., Irons, D.B., Kettle, A.B., Kimmel, D.G., Konar, B., Kuletz, K.J., Laurel, B.J., Maniscalco, J.M., Matkin, C., McKinstry, C.A.E., Monson, D.H., Moran, J.R., Olsen, D., Palsson, W.A., Pegau, W.S., Piatt, J.F., Rogers, L.A., Rojek, N.A., Schaefer, A., Spies, I.B., Straley, J.M., Strom, S.L., Sweeney, K.L., Szymkowiak, M., Weitzman, B.P., Yasumiishi, E.M., and Zador, S.G. 2021. Ecosystem response persists after a prolonged marine heatwave. Sci Rep **11**. doi:10.1038/s41598-021-83818-5.

Taylor, J.R., Lovera, C., Whaling, P.J., Buck, K.R., Pane, E.F., and Barry, J.P. 2014. Physiological effects of environmental acidification in the deep-sea urchin

Strongylocentrotus fragilis. Biogeosciences **11**(5): 1413–1423. doi:10.5194/bg-11-1413-2014.

Thompson, B., and Riddle, M. 2005. Bioturbation behaviour of the spatangoid urchin Abatus ingens in Antarctic marine sediments. Mar. Ecol. Prog. Ser. **290**: 135–143. doi:10.3354/meps290135.

Thomsen, L., Aguzzi, J., Costa, C., De Leo, F., Ogston, A., and Purser, A. 2017. The Oceanic Biological Pump: Rapid carbon transfer to depth at Continental Margins during Winter. Sci Rep **7**(1): 10763. doi:10.1038/s41598-017-11075-6.

Trainer, V.L., Moore, S.K., Hallegraeff, G., Kudela, R.M., Clement, A., Mardones, J.I., and Cochlan, W.P. 2020. Pelagic harmful algal blooms and climate change: Lessons from nature's experiments with extremes. Harmful Algae **91**: 101591. doi:10.1016/j.hal.2019.03.009.

Tseng, Y.-H., Ding, R., and Huang, X. 2017. The warm Blob in the northeast Pacific—the bridge leading to the 2015/16 El Niño. Environ. Res. Lett. **12**(5): 054019. doi:10.1088/1748-9326/aa67c3.

Turner, J.T. 2015. Zooplankton fecal pellets, marine snow, phytodetritus and the ocean's biological pump. Progress in Oceanography **130**: 205–248. doi:10.1016/j.pocean.2014.08.005.

Vetter, E., and Dayton, P. 1999. Organic enrichment by macrophyte detritus, and abundance patterns of megafaunal populations in submarine canyons. Mar. Ecol. Prog. Ser. **186**: 137–148. doi:10.3354/meps186137.

Vopel, K., Vopel, A., Thistle, D., and Hancock, N. 2007. Effects of spatangoid heart urchins on O2 supply into coastal sediment. Mar. Ecol. Prog. Ser. **333**: 161–171. doi:10.3354/meps333161.

Wakefield, W.W., and Genin, A. 1987. The use of a Canadian (perspective) grid in deep-sea photography. Deep Sea Research Part A. Oceanographic Research Papers **34**(3): 469–478. doi:10.1016/0198-0149(87)90148-8.

Ware, D.M., and Thomson, R.E. 1991. Link Between Long-Term Variability in Upwelling and Fish Production in the Northeast Pacific Ocean. Can. J. Fish. Aquat. Sci. **48**(12): 2296–2306. doi:10.1139/f91-270.

Whitney, F.A., Freeland, H.J., and Robert, M. 2007. Persistently declining oxygen levels in the interior waters of the eastern subarctic Pacific. Progress in Oceanography **75**(2): 179–199. doi:10.1016/j.pocean.2007.08.007.

Widder, E.A., Robison, B.H., Reisenbichler, K.R., and Haddock, S.H.D. 2005. Using red light for in situ observations of deep-sea fishes. Deep Sea Research Part I: Oceanographic Research Papers **52**(11): 2077–2085. doi:10.1016/j.dsr.2005.06.007.

Wood, S.N. 2003. Thin plate regression splines. Journal of the Royal Statistical Society: Series B (Statistical Methodology) **65**(1): 95–114. doi:10.1111/1467-9868.00374.

Wood, S.N. 2011. Fast stable REML and ML estimation of semiparametric GLMs. Journal of the Royal Statistical Society: Series B (Statistical Methodology) **73**(1): 3–36. doi:https://doi.org/10.1111/j.1467-9868.2010.00749.x.

Wood, S.N., Pya, N., and Säfken, B. 2016. Smoothing Parameter and Model Selection for General Smooth Models. Journal of the American Statistical Association **111**(516): 1548–1563. doi:10.1080/01621459.2016.1180986.

Yang, B., Emerson, S.R., and Peña, M.A. 2018. The effect of the 2013–2016 high temperature anomaly in the subarctic Northeast Pacific (the "Blob") on net community production. Biogeosciences **15**(21): 6747–6759. doi:10.5194/bg-15-6747-2018.

Zhao, C., Liu, P., Zhou, H., Tian, X., and Chang, Y. 2013. Diel observation on the distribution of the sea urchin *Strongylocentrotus intermedius* under different food availability and shelter conditions in the laboratory. Marine and Freshwater Behaviour and Physiology **45**(6): 357–364. doi:10.1080/10236244.2013.763456.

Zuur, A.F., Ieno, E.N., Walker, N., Saveliev, A.A., and Smith, G.M. 2009. Mixed effects models and extensions in ecology with R. Springer New York, New York, NY. doi:10.1007/978-0-387-87458-6.

2.8 Tables

Table 2.1. Video camera deployments for each time-series sampling period at the Barkley Canyon Upper Slope site.

Date	Camera System, pixel resolution, frame rate	Camera mounting height (cm)	Field of view angles (horizontal, vertical˚)	Pan and tilt angles	Total seafloor area imaged (m^2)
2013-08-15 to 2014-02-03	SubC Imaging Dragonfish 1080p, 30 fps	45	54.7, 34.4	Fixed 45˚ tilt	0.5
2014-08-15 to 2015-01-12	SubC Imaging Dragonfish 1080p, 30 fps	45	54.7, 34.4	Fixed 63˚ tilt, 215.24˚ Pan	14.4
2018-08-15 to 2018-11-23	SubC Imaging Dragonfish 1080p, 30 fps	95	54.7, 34.4	76˚ tilt sweep	9.33
2019-09-14 to 2020-02-03	Axis Sony P134 SubAqua, 1080p, 23 fps	85	54.7, 34.4	76˚ tilt sweep, 180˚ pan sweep	14.93

Table 2.2. List of instruments, sampling frequencies, measured environmental variables, and their units for data collected at the upper slope of Barkley Canyon (48° 25' 37.2"N, 126° 10' 29.7"W), weather data collected from the La Perouse Bank buoy (48° 49' 48"N, 126° 0' 0"W), Tofino, British Columbia and MODIS satellite. Data were collected from August 15, 2013 to February 3, 2014, August 15, 2014 to January 15, 2015, August 15, 2018 to November 24, 2018, and September 11, 2019 to February 3, 2020.

Sampling Site	**Instruments**	**Measured variables**	**Sampling frequency**	**Units**
Seafloor data	2 MHz ADCP	v (Northward BBLc)	10 s	m/s
		u (Eastward BBLc)	10 s	m/s
		Temperature	10 s	˚C
		Pressure	10 s	dbar
	CTD	Backscatter	10 s	Hz
		Salinity	1 s	psu
	Oxygen optode	Oxygen	10 s	mL/L
Weather data (all years except 2018)	La Perouse Bank Meteorological buoy	SST	2 hr	˚C
Sea surface data	NASA Satellites	Chlorophyll-a	8 days	mg/m^3

Table 2.3. Akaike Information Criteria (AIC) table comparing Generalized Additive Model fits for Barkley Canyon Upper Slope sea urchin density. ΔAIC refers to the difference in AIC between each model and the best model for Temporal models and Temporal + environmental covariate (Env. Cov.) models. Global smooths in Temporal model + Environmental covariates are for dissolved oxygen, current magnitude, and ADCP backscatter.

Model	df	AIC	ΔAIC
Temporal models			
G: density ~ s(Time) + $Year_i$	16	9556	1015
I: density ~ $s(Time)_{Year}$ + $Year_i$	43	8540	0
S: density ~ s(Time, Year) + $Year_i$	43	8816	277
GS: density ~ s(Time) + s(Time, Year) + $Year_i$	43	8817	278
GI: density ~ s(Time) + $s(Time)_{Year}$ + $Year_i$	43	8544	4
Temporal model + Environmental covariates			
I + s(Oxygen) + s(Magnitude) + s(Backscatter)	39	7619	0
GI + s(Oxygen) + s(Magnitude) + s(Backscatter)	48	7631	11

Table 2.4. Model summary table for parametric and smooth terms of final generalized additive model for sea urchin abundance at Barkley Canyon Upper Slope.

Parametric term	**Estimate**	**Std. Error**	**Z Value**	**P-Value**
(Intercept)	-1.975	0.398	-4.966	0
Smooth terms	**EDF**	**Ref DF**	**Chi.sq**	**P-Value**
s(Time):Year2013-2014	10.31	10.857	223.025	<0.001
s(Time):Year2014-2015	1.002	1.003	114.322	<0.001
s(Time):Year2018	10.891	10.994	413.502	<0.001
s(Time):Year2019-2020	9.435	9.864	852.934	<0.001
s(Year)	1.647	3	30.003	<0.001
s(Oxygen)	1	1.001	46.168	<0.001
s(Magnitude)	1.001	1.002	4.468	0.035
s(Backscatter)	1.001	1.002	8.004	0.005

Table 2.5. Model summary table for parametric and smooth terms of final generalized additive mixed-model for benthic dissolved oxygen at Barkley Canyon Upper Slope.

Parametric term	**Estimate**	**Std. Error**	**Z Value**	**P-Value**
(Intercept)	1.007	0.043	23.348	<0.001
Year2014	0.155	0.051	3.066	0.002
Year2015	0.306	0.07	4.384	<0.001
Year2016	0.225	0.053	4.677	<0.001
Year2017	0.143	0.053	2.703	0.007
Year2018	0.012	0.051	0.24	0.81
Year2019	0.192	0.058	3.297	0.001
Year2020	0.402	0.104	3.875	<0.001
Smooth term	**EDF**	**Ref DF**	**Chi.sq**	**P-Value**
s(Week of year)	5.274	10	6.885	<0.001
s(Chlorophyll-a)	1	1	8.88	0.003
s(SSTa)	1	1	2.781	0.097

Table 2.6. Dunn's post-hoc multiple comparisons with Bonferroni correction for S. fragilis density over time from the West Coast Vancouver Island synoptic bottom trawl surveys. Komolgorov-Smirnov (K-S) comparison of S. fragilis depth distributions for each pair of survey years. Bold rows indicate statistical significance at the $\alpha = 0.05$ level.

Comparison	**Dunn's P-value**	**K-S Test statistic**	**K-S P-value**
2016 vs 2018	1.000	0.187	0.205
2014 vs 2018	1.000	0.135	0.488
2014 vs 2016	1.000	0.102	0.888
2012 vs 2018	0.079	0.269	0.007
2012 vs 2016	0.003	0.145	0.498
2012 vs 2014	0.771	0.199	0.096
2010 vs 2018	<0.001	0.259	0.084
2010 vs 2016	<0.001	0.168	0.589
2010 vs 2014	<0.001	0.157	0.608
2010 vs 2012	0.019	0.203	0.284
2008 vs 2018	0.008	0.260	0.031
2008 vs 2016	<0.001	0.155	0.539
2008 vs 2014	0.094	0.160	0.414
2008 vs 2012	1.000	0.149	0.504
2008 vs 2010	0.514	0.118	0.940
2006 vs 2018	0.001	0.307	0.006
2006 vs 2016	<0.001	0.195	0.260
2006 vs 2014	0.011	0.193	0.203
2006 vs 2012	1.000	0.174	0.307

2006 vs 2010	1.000	0.108	0.972
2006 vs 2008	1.000	0.098	0.967
2004 vs 2018	0.008	0.431	0.003
2004 vs 2016	<0.001	0.303	0.101
2004 vs 2014	0.053	0.319	0.055
2004 vs 2012	1.000	0.196	0.505
2004 vs 2010	1.000	0.256	0.331
2004 vs 2008	1.000	0.236	0.340
2004 vs 2006	1.000	0.256	0.251

Table S2.1. Model summary table for linear regression models for depth distribution parameters as a function of time, trawl contents (sea urchins only vs all species), and an interaction between time and trawl contents. Bold-face p-values indicate significance at the alpha = 0.05 level.

Parameter	Term	Estimate	Std. Error	t-value	p-value
Upper limit					
	Intercept	184.701	1516.675	0.122	0.905
	Time	-0.067	0.754	-0.089	0.930
	Sea urchinss only	7185.655	2144.902	3.350	0.006
	Time * Sea urchins only	-3.557	1.067	-3.335	0.006
25% Quantile					
	Intercept	-232.914	633.705	-0.368	0.720
	Time	0.170	0.315	0.538	0.600
	Sea urchins only	3509.680	896.195	3.916	0.002
	Time * Sea urchins only	-1.734	0.446	-3.891	0.002
75% Quantile					
	Intercept	2189.296	2692.747	0.813	0.432
	Time	-0.986	1.339	-0.736	0.476
	Sea urchins only	190.059	3808.119	0.050	0.961
	Time * Sea urchins only	-0.103	1.894	-0.054	0.958
Lower limit					
	Intercept	6679.105	6844.288	0.976	0.348
	Time	-3.094	3.403	-0.909	0.381
	Sea urchins only	-9093.783	9679.285	-0.940	0.366
	Time * Sea urchins only	4.471	4.813	0.929	0.371
Mean					
	Intercept	1302.642	1540.891	0.845	0.414

	Time	-0.563	0.766	-0.735	0.476
	Sea urchins only	2594.758	2179.149	1.191	0.257
	Time * Sea urchins only	-1.291	1.084	-1.191	0.257
Median					
	Intercept	776.404	1117.667	0.695	0.500
	Time	-0.314	0.556	-0.565	0.582
	Sea urchins only	3159.480	1580.620	1.999	0.069
	Time * Sea urchins only	-1.565	0.786	-1.991	0.070

2.9 Figures

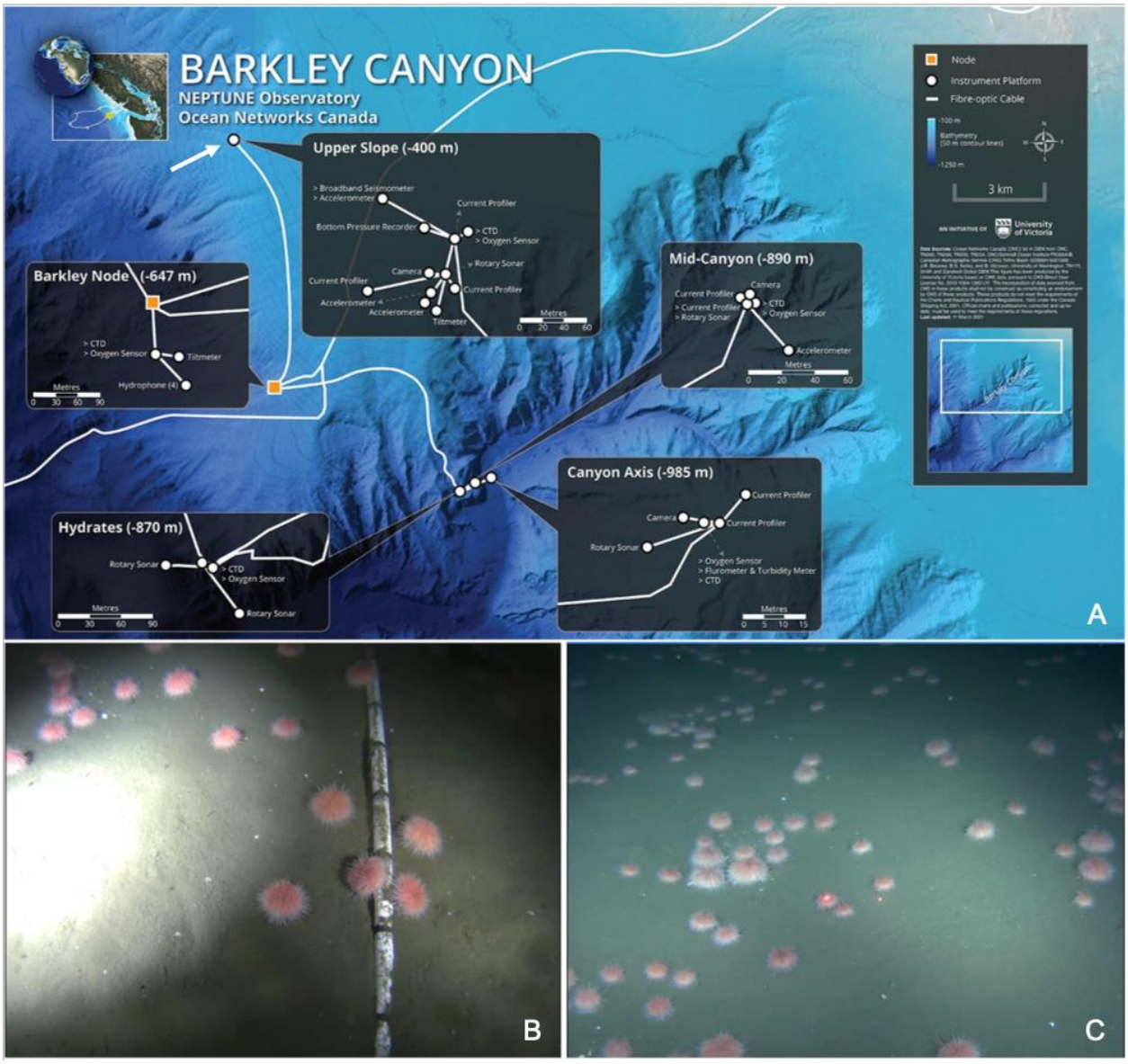

Figure 2.1. Map of the study area showing the NEPTUNE cabled observatory infrastructure at Barkley Canyon and Upper Slope (A). Examples of two seafloor camera fields of views for November 2013 (B), and January 2020 (C). White pole in (B) is a scale bar, with each horizontal black line measuring 10 cm. Red scaling laser points in (C) are calibrated to be 10 cm apart.

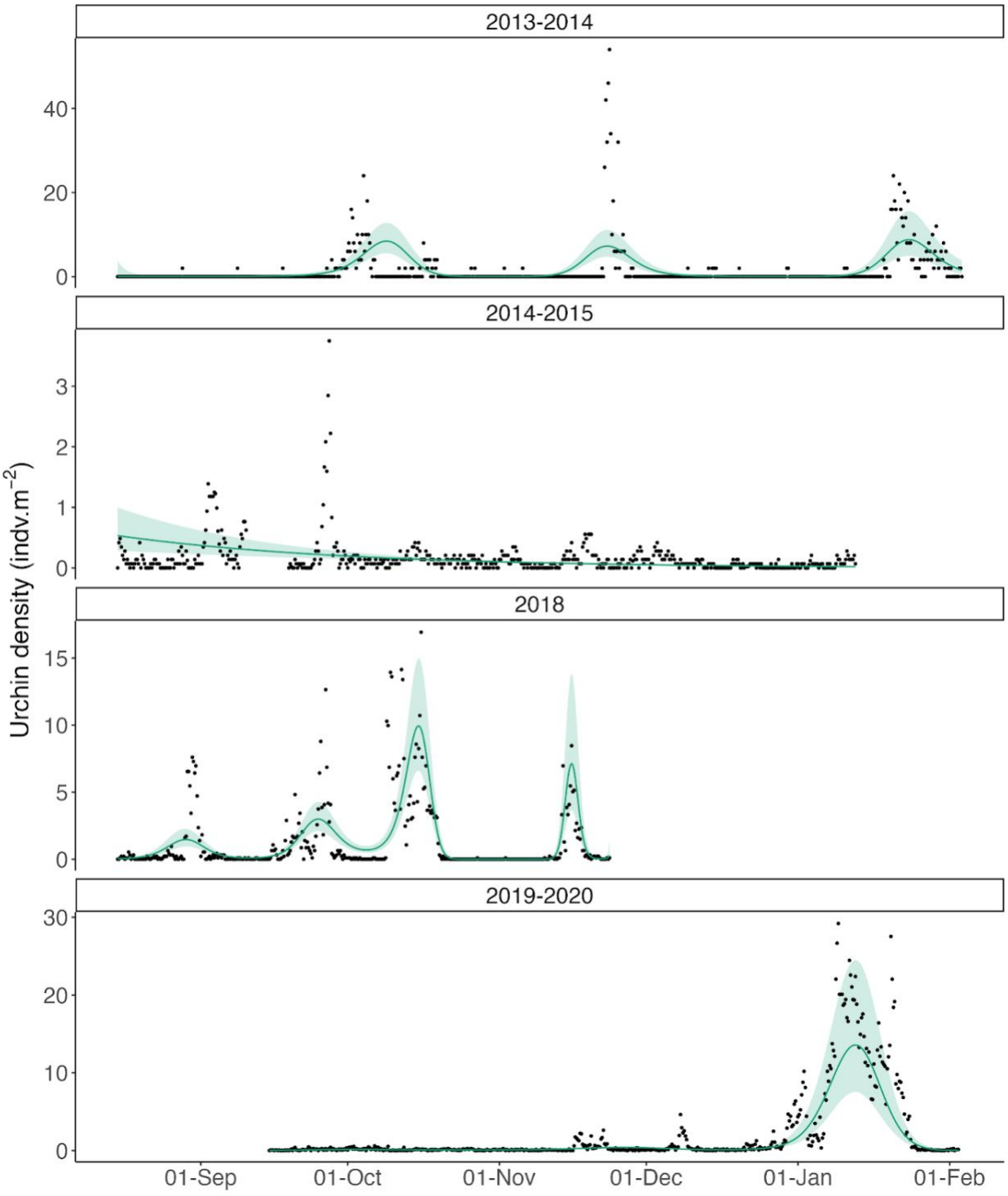

Figure 2.2. Observed pink sea urchin density (points) and predicted (solid lines) values from the highest-ranking environmental hierarchical generalized additive model for each year. Solid lines are the smooth mean trend of sea urchin abundance for each year, the ribbon is +/- pointwise 95% confidence interval.

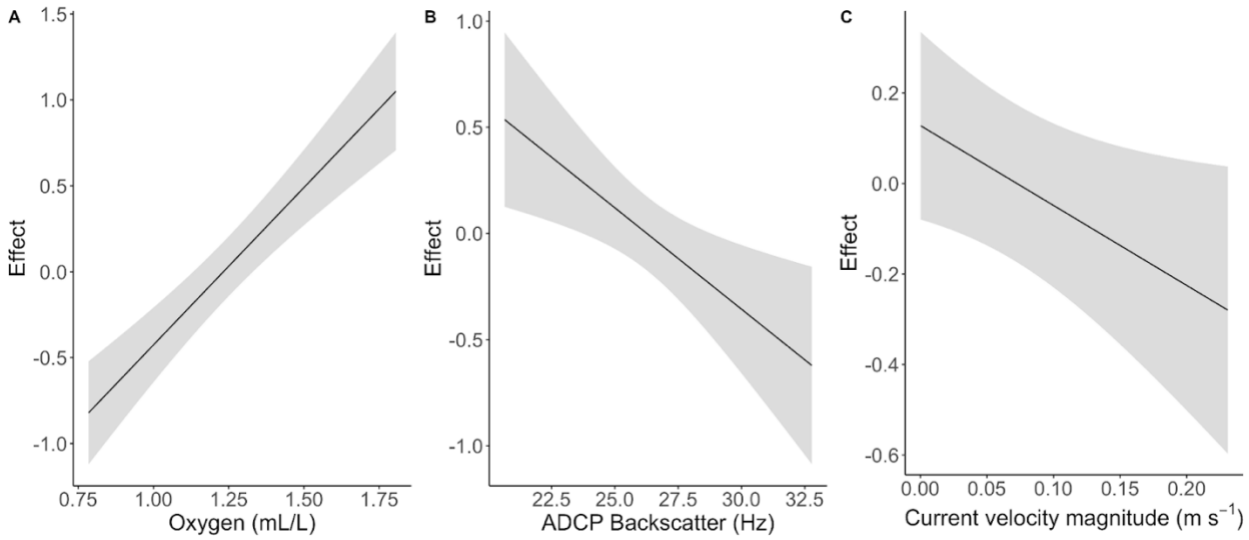

Figure 2.3. Global smooths for the effects of oxygen (A) and ADCP backscatter (B) on *S. fragilis* density from the final temporal and environmental covariate GAM.

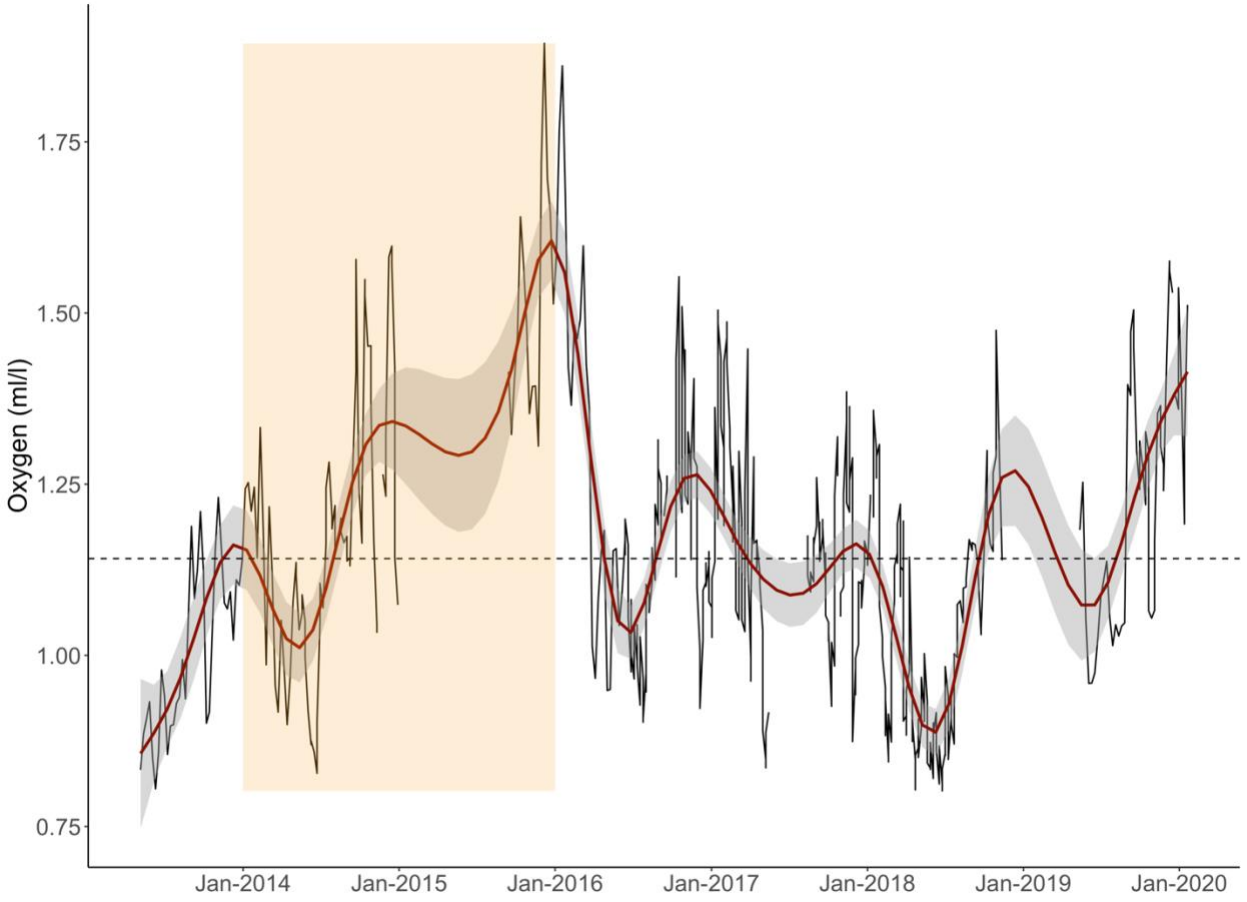

Figure 2.4. Weekly benthic dissolved oxygen concentration (solid black line) at Barkley Canyon Upper Slope from 2013-2020. Solid red line is the smoothed temporal trend of oxygen over time, grey ribbon is +/- standard error around the trend, and horizontal dashed line is the mean dissolved oxygen across the entire study period. Orange overlay represents the duration of the 2013-2016 “Blob”.

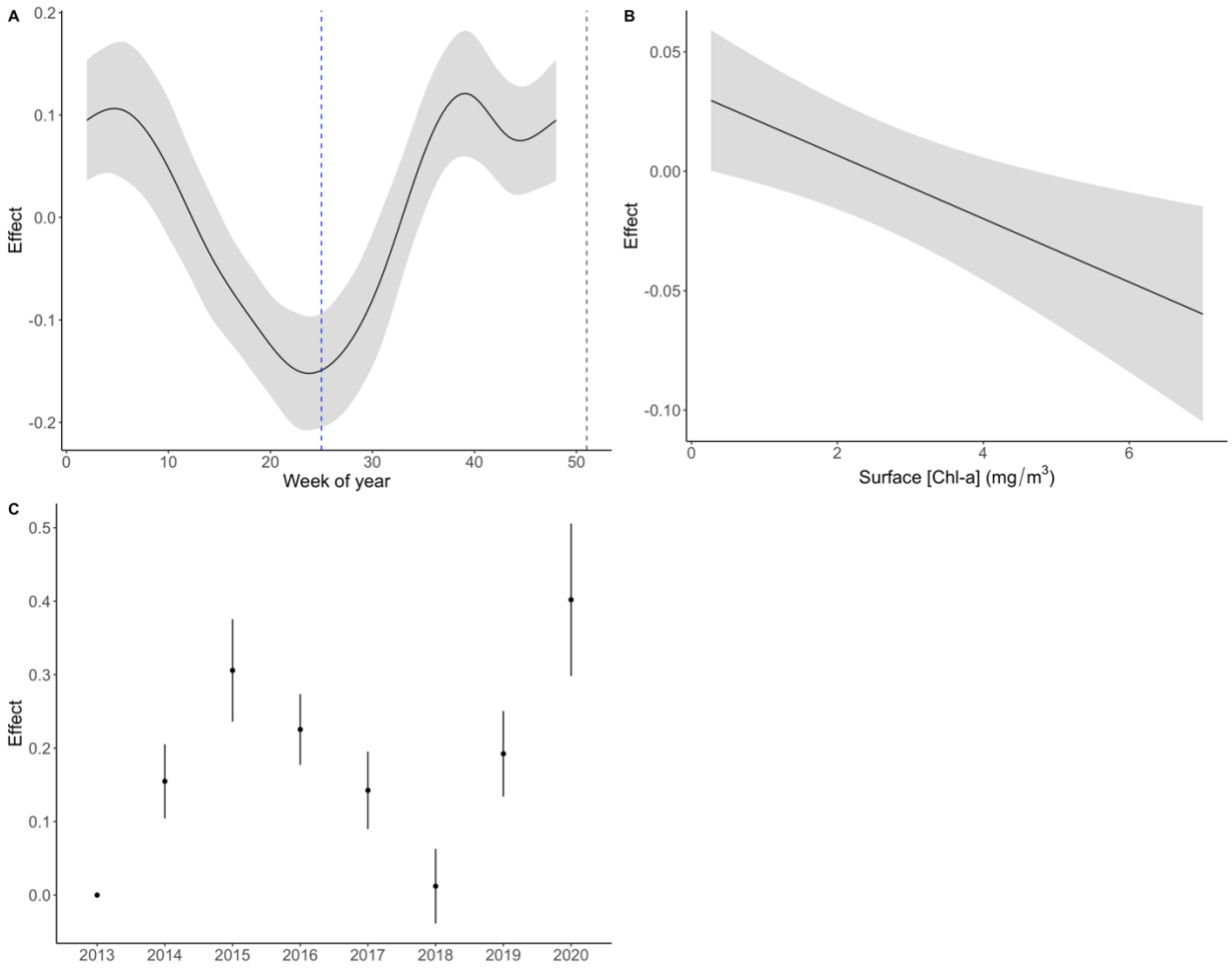

Figure 2.5. Smooth effects of week of year (A) and surface chlorophyll-a concentration (B). Lines are mean oxygen concentration, grey ribbons are +/- 95% confidence interval around the mean. Parametric fixed-effect of year (C), points represent the mean effect of each year relative to 2013, vertical lines are +/- 95% confidence interval around the mean effect. Vertical dashed lines in (A) are the average week of the onset of summer (blue) and winter (grey).

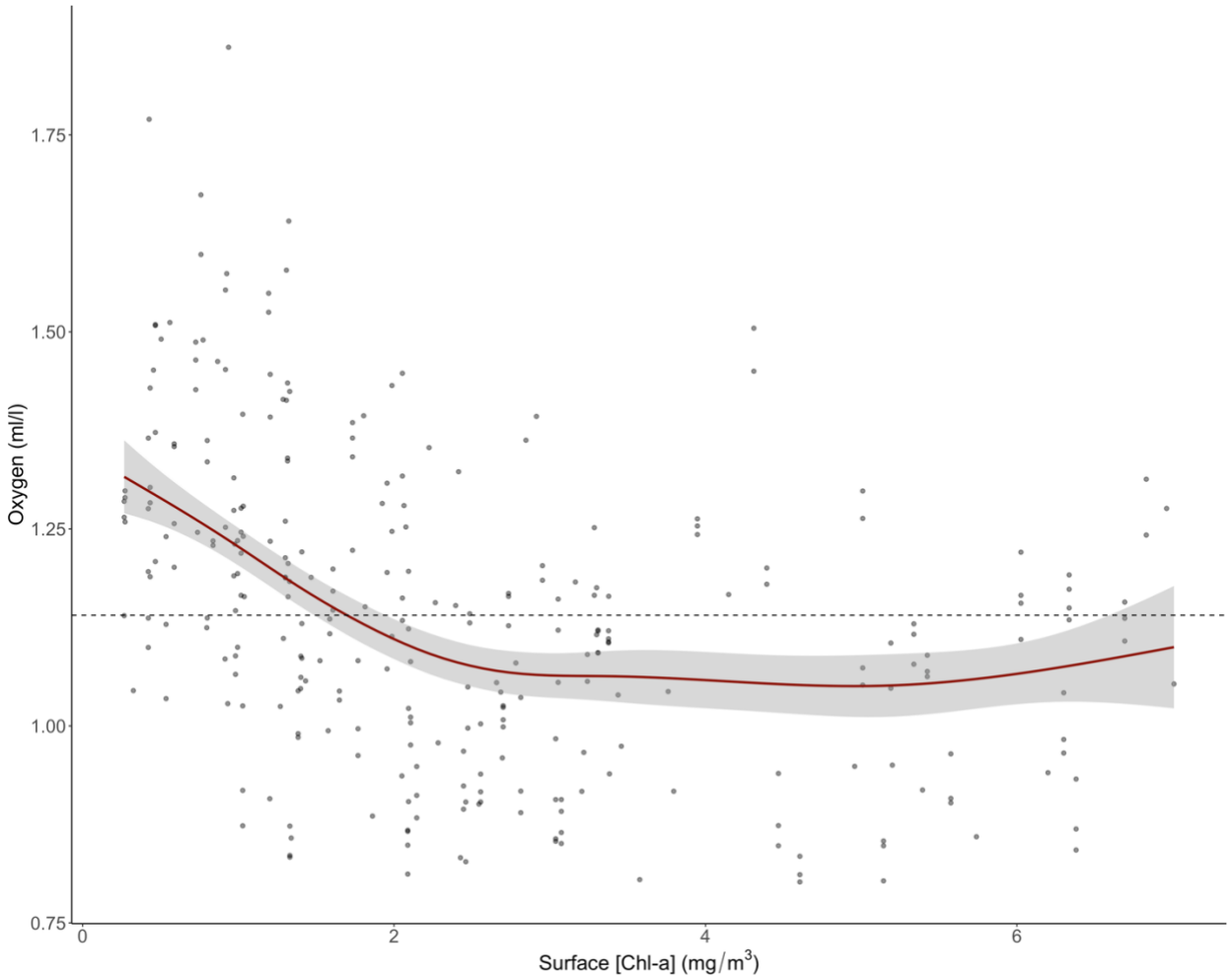

Figure 2.6. Predicted values of oxygen for weekly surface chlorophyll-a concentration on benthic dissolved oxygen at Barkley Canyon Upper Slope across the entire study period (2013-2020). Points are a scatter plot of dissolved oxygen and chlorophyll-a, solid red line is the smooth effect, grey ribbon is +/- 95% CI around the smooth. Horizontal dashed line is the mean dissolved oxygen concentration across the entire study period.

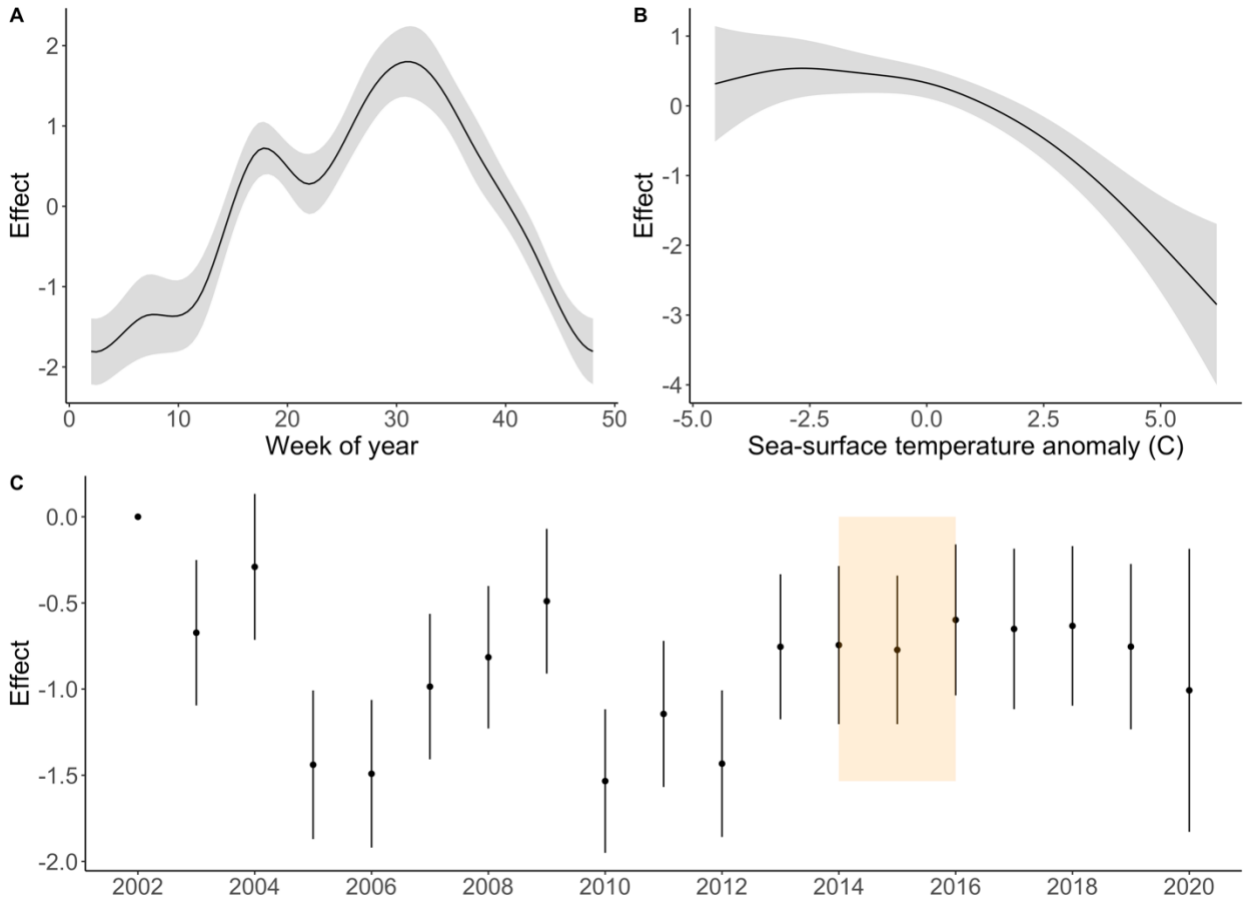

Figure 2.7. Smooth effects of week of year (A) and sea-surface temperature anomaly (B). Lines are mean chlorophyll-a concentration, grey ribbons are +/- 95% confidence interval around the mean. Parametric fixed-effect of year (C), points are the mean effect of each year relative to 2002, vertical lines are +/- 95% confidence interval around the mean effect. Orange overlay represents the duration of the 2013-2016 "Blob".

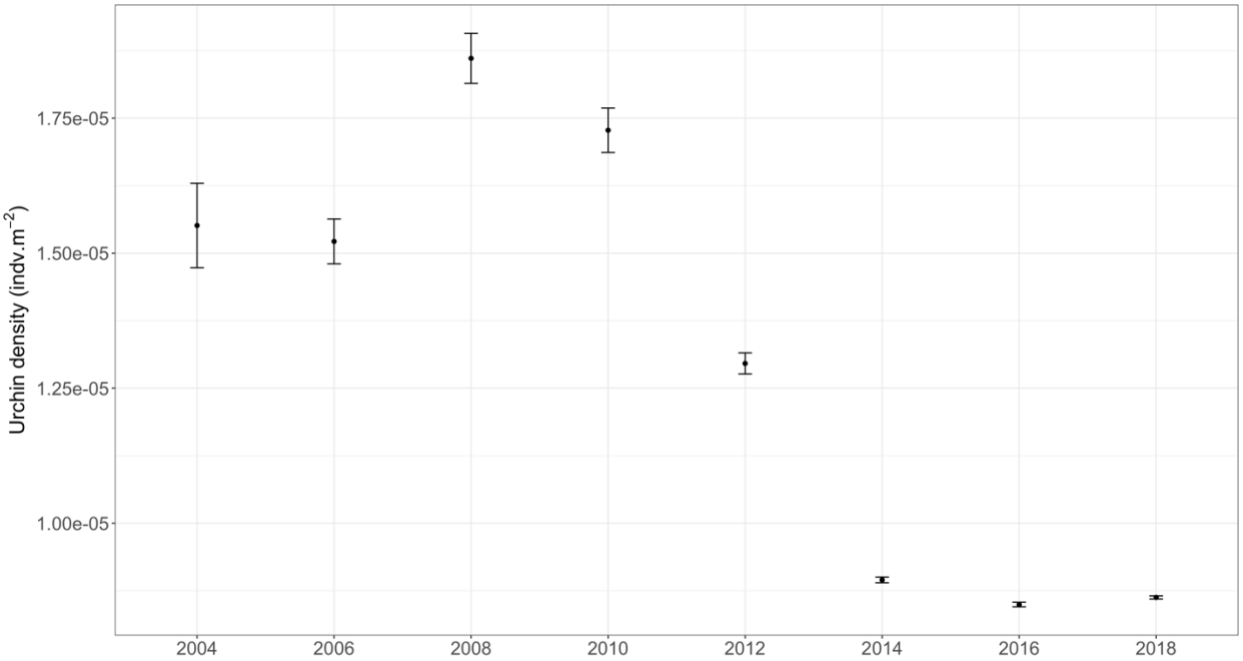

Figure 2.8. Mean +/- standard deviation of density of *S. fragilis* found in the West Coast Vancouver Island bi-annual trawl surveys from 2004-2018 considering the entire depth range of trawl samples. The orange band indicates the 2013-2016 "Blob".

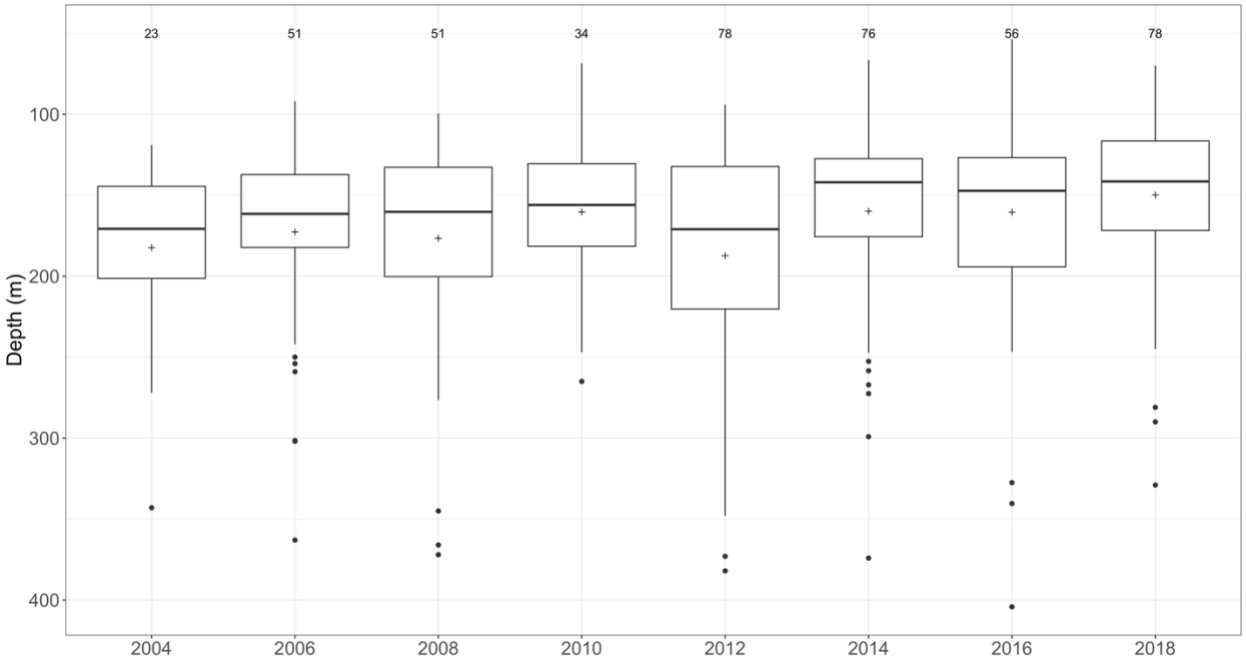

Figure 2.9. Depth-distribution statistics from 2004-2018 from the West Coast Vancouver Island bi-annual trawl surveys for trawls where pink sea urchins were caught (blue points) and for all trawls (red points). Coloured lines represent the least squares fitted line for a simple linear model for all trawls (red line) and trawls where pink sea urchins were caught (blue line). Grey bands represent 95% confidence intervals around the fitted line.

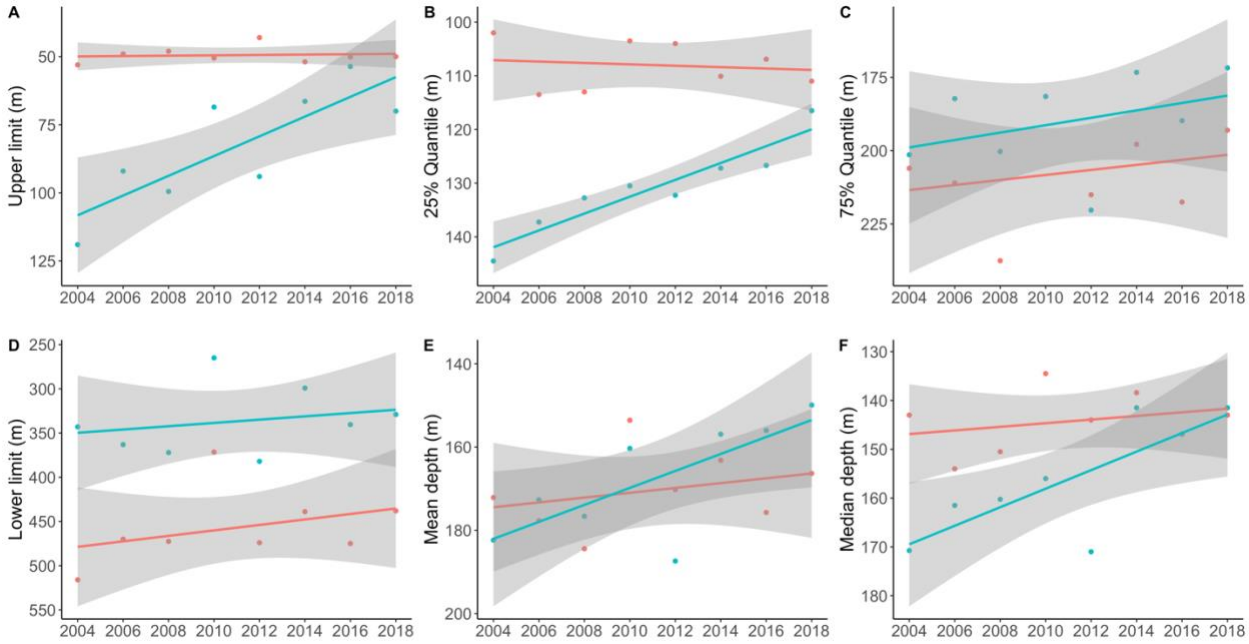

Figure 2.10. Box plot of depth distribution of *S. fragilis* obtained from the bi-annual West Coast Vancouver Island synoptic trawl survey from 2004-2018. Solid horizontal line indicates median depth, + symbol indicates mean depth, and dots indicate outliers that are greater than 1.5 times the distance between the 25% and 75% quartiles. Numbers above each box indicates the number of trawls in which *S. fragilis* was present for each survey year. Orange band indicates the 2013-2016 "Warm Blob". Two trawls found pink sea urchins at 800 m depth but were considered outliers and were subsequently excluded from analysis.

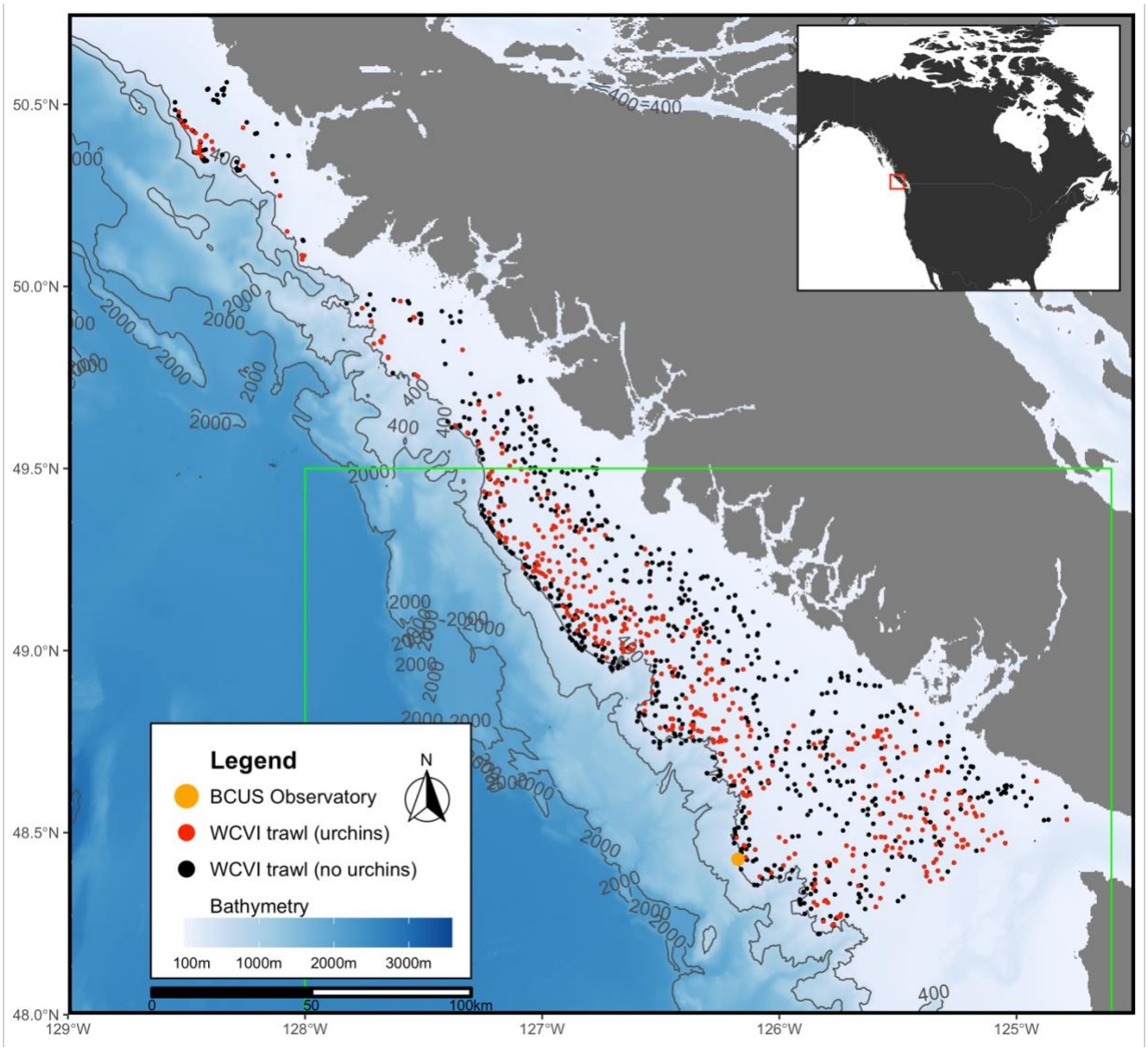

Figure S2.1. Map of the West coast of Vancouver Island. Depth contours shown at 400m and 2000m. Green box indicates the area from which Chlorophyll-a values were extracted from the MODIS OceanColour satellite (bottom-left corner at 48˚N, 128˚W, top-right corner at 49˚30'N, 124° 35' 59.99451"). Orange point indicates the location of the Barkley Canyon Upper Slope platform of the NEPTUNE observatory. Dots indicate the start position of all trawls from the 2004-2018 biannual West Coast Vancouver Island synoptic bottom trawl surveys, where black dots represent trawls that did not find any Strongylocentrotus fragilis and red dots represent those trawls that recorded at least one S. fragilis, including those for which 1) a count was recorded, or 2) a weight was recorded and a count was not (see Methods section 2.4 for more details). GEBCO Gridded Bathymetry data retrieved from https://download.gebco.net/.

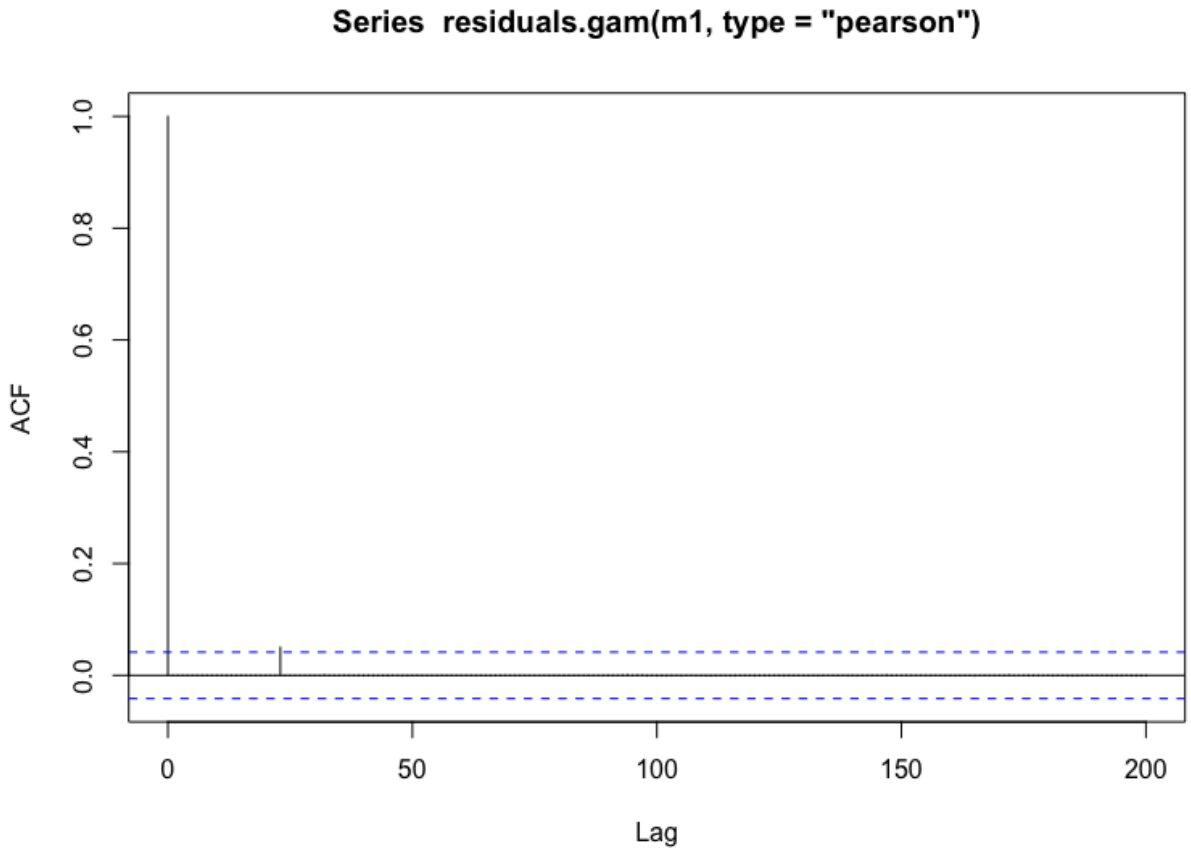

Figure S2.2. Autocorrelation plot for residuals of sea urchin temporal model I.

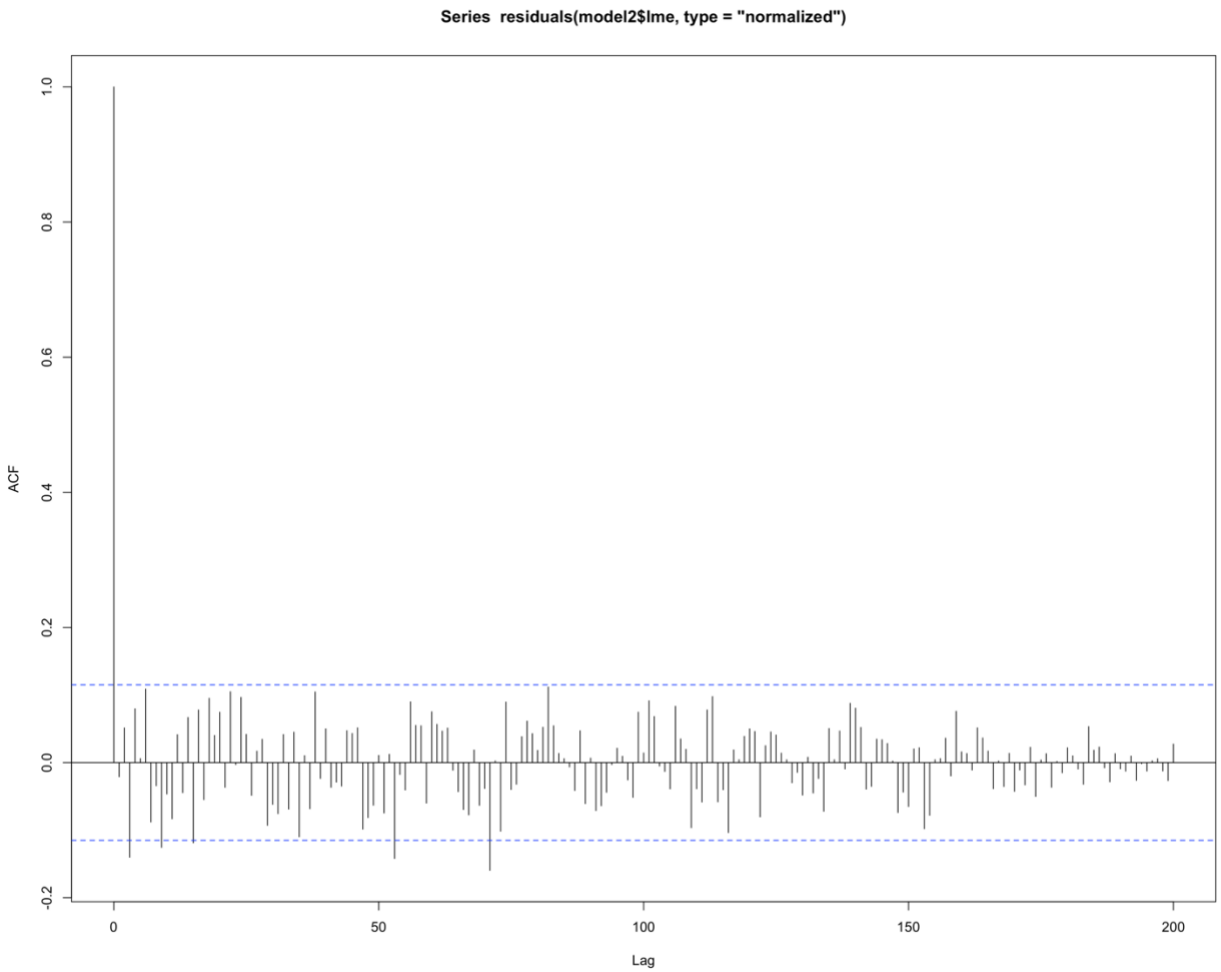

Figure S2.3. Autocorrelation function of benthic oxygen Generalized Additive Mixed-Model residuals. Dotted blue line indicates the threshold for significance at the alpha = 0.05 level.

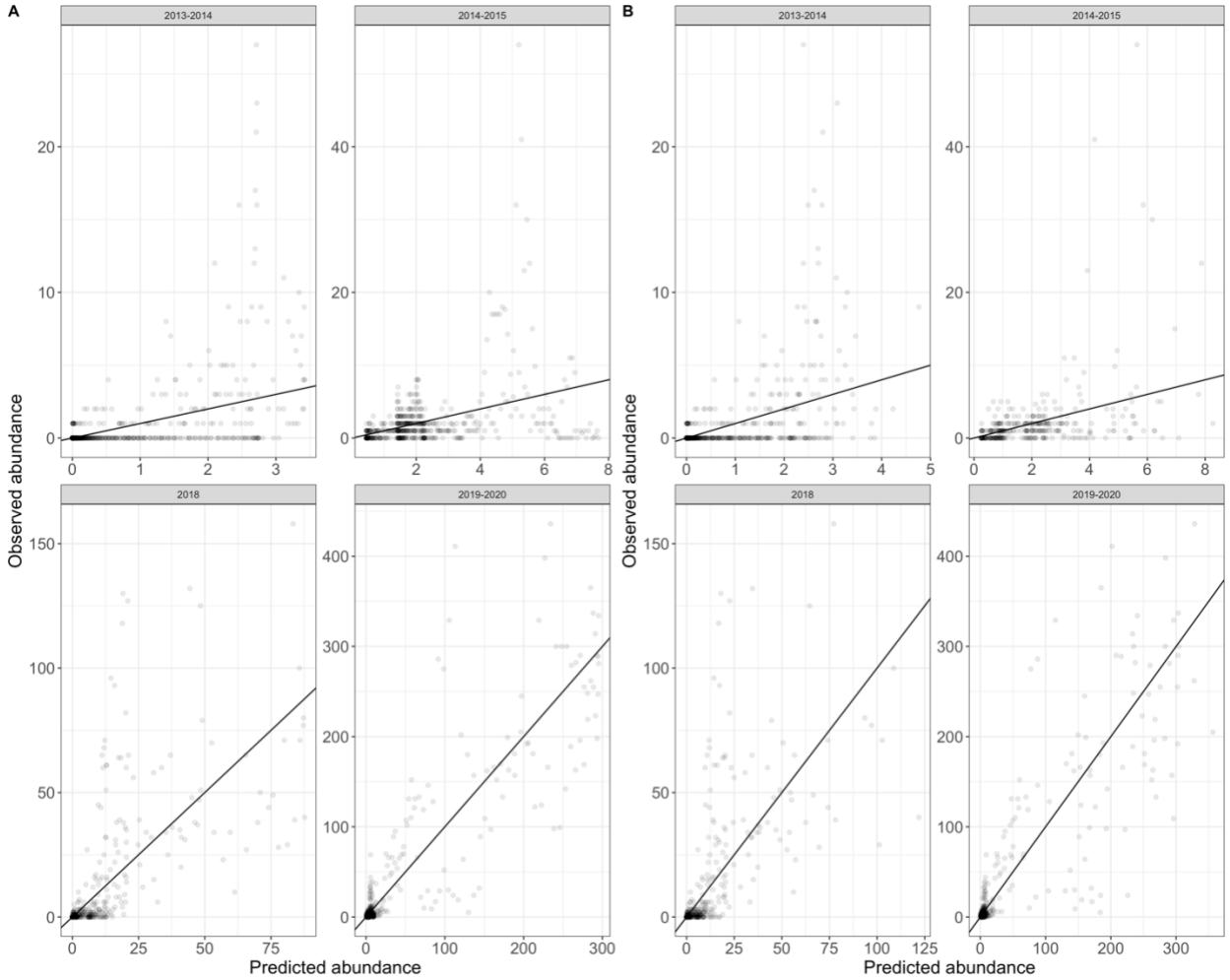

Figure S2.4. Predicted versus observed values (points) for temporal sea urchin model I (A) and final temporal + environmental covariate sea urchin model (B). Points are transparent to illustrate overlap between points. 1:1 line added for reference.

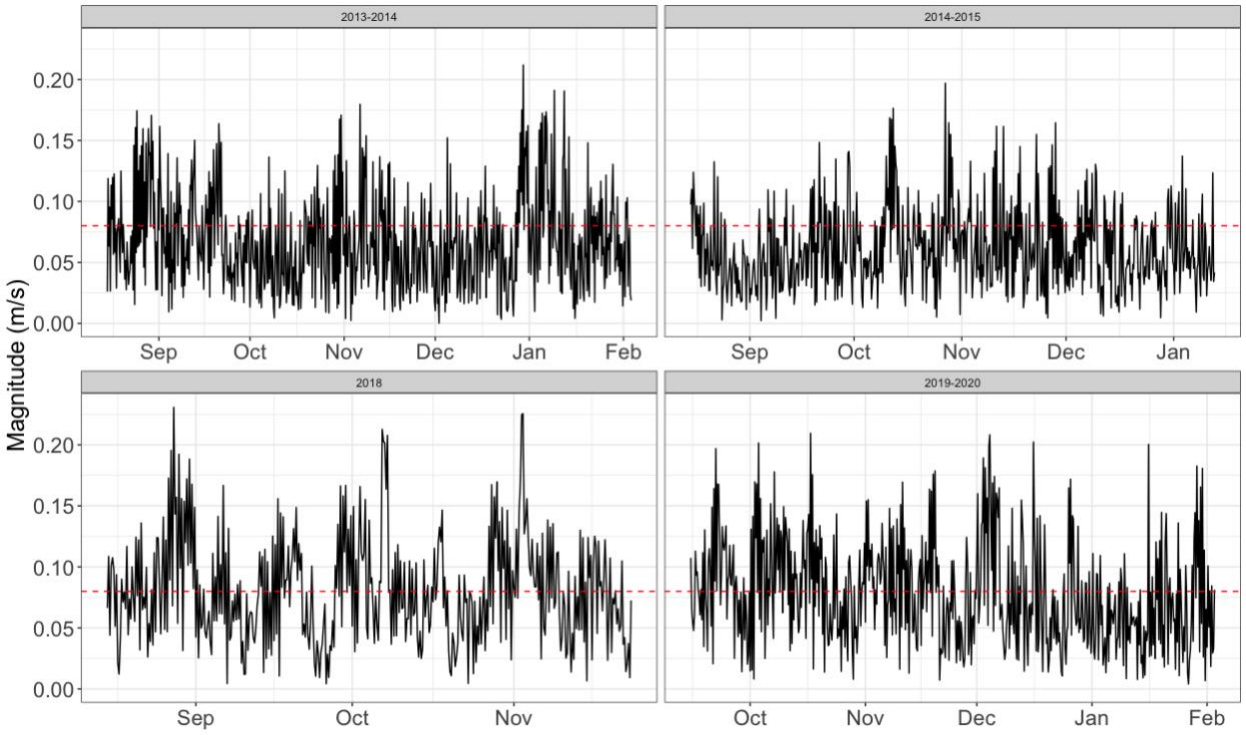

Figure S2.5. Benthic boundary layer currents (BBLc) magnitude (m/s) at Barkley Canyon Upper Slope. Red dashed line indicates the threshold above which resuspension of phytodetritus and other organic matter can occur.

Chapter 3: A first look at megabenthic community responses to seasonal change using the new Holyrood Subsea Observatory in Conception Bay, NL.

Abstract

Sub-Arctic seafloor communities rely on seasonal phytoplankton blooms for food, revealing a tight benthic-pelagic coupling. To maximize resource availability for offspring, organisms such as snow crabs, sea stars, and sea cucumbers synchronize their reproductive and feeding behaviours with spring blooms. Due to climate change, spring blooms are occurring earlier in sub-Arctic regions, leading to a possible mismatch between timing of resource availability and optimal environmental conditions, and important life-history behaviours. Here, we utilize high-frequency time-series observations from the Holyrood Subsea Observatory, a new cabled seafloor observatory deployed in Conception Bay, Newfoundland, Canada. We use hourly data collected from environmental sensors (Conductivity-Temperature-Depth, Acoustic Doppler Current Profiler, fluorometer), a near-surface mooring (fluorometer), and a video camera to identify and quantify abundance and diversity of benthic megafauna, and to determine how community composition changes from pre-bloom to full bloom conditions. Data analysis revealed striking temporal changes in benthic activity, with the notable emergence from the sediment of *Psolus phantapus* sea cucumbers (up to 289.9 ind. m^{-2}) coinciding with increased chlorophyll-a concentration and seawater temperature. At least three dense schools of forage fish, two Atlantic herring (79 and 144 ind. $frame^{-1}$) and one capelin (91 ind. $frame^{-1}$), were observed during the main bloom between May 5 and June 16. This study provides the first high-frequency *in situ* observations of benthic community response to seasonal food input in the region. The high temporal resolution made it possible to record the precise timing of the emergence of *Psolus phantapus* in relation to the timing of food input to the seafloor, which provides novel insight into how seasonal influxes of nutrients elicit responses in an understudied

suspension feeding holothuroid, and will serve as a baseline to monitor phenology as climate change progresses. Changes to the timing of spring blooms have implications for sub-Arctic fisheries productivity and ecosystem functioning, making continuous long-term monitoring of seafloor communities essential.

3.1 Introduction

Seasonal phytoplankton blooms drive biogeochemical cycling in the global ocean (Turner 2015), and support diverse marine communities from coastlines to the abyssal plain (Smith et al. 1994, 2008a; Wei et al. 2010; McClain et al. 2012; Woolley et al. 2016; Smith et al. 2018; Wei et al. 2020). Seafloor deposition of phytodetritus, fecal pellets, and other bloom-related organic material provides a crucial benthic-pelagic coupling of carbon and nutrients (Graf 1989; Smith et al. 1994; Turner 2015; Herbert et al. 2021), resulting in profound seasonal changes in the behaviour and structure of benthic communities (Billett et al. 1983, 2010; Lampitt 1985; Townsend and Cammen 1988). Indeed, many organisms have evolved life-history behaviours, such as reproduction, synchronized with the arrival of food at the seafloor (Himmelman 1975; Lightfoot et al. 1979; Tyler et al. 1982; Starr et al. 1990; Hamel et al. 1993; Smith et al. 2008b; Sumida et al. 2014). In a rapidly changing ocean, a mismatch in the timing of optimal conditions for proper gametogenesis and spring blooms that trigger spawning could have severe consequences for marine food webs (Ouellet et al. 2007; Koeller et al. 2009).

Cushing's match-mismatch hypothesis (MMH) posits that a consumer maximizes its fitness by synchronizing spawning with the timing of maximum resource availability (Cushing 1969, 1990). The precise timing of optimal spawning varies depending on larval feeding modality (Mercier and Hamel 2010), but in general larvae with greater access to food have a higher chance of surviving to adulthood and recruiting into the population (Cushing 1990). A

mismatch occurs when the timing of the resource does not match the timing of the behaviour, which can result in reduced fitness (Vikebø et al. 2021). Understanding the links between behavioural phenology and environmental change can improve predictions of the effects of climate change on marine environments (Durant et al. 2007). While the MMH was developed for fish, the theory is thought to hold when the resource controls consumer fitness (i.e., bottom-up control) and when the resource is only available seasonally.

For organisms with non-feeding larvae, like many benthic marine invertebrates, the MMH falls short in two major ways. First, food availability does not directly affect larval recruitment success, but rather may indirectly influence recruitment by alter the energy stores available for adults for reproductive processes like gametogenesis. For many organisms, such as echinoderms, gametogenesis occurs over an entire year; the gametes that are released during spawning developed from energy acquired from the previous years' spring bloom (Hamel et al. 1993). Second, "resources" should also include the physico-chemical conditions required for optimal gametogenesis, and the conditions required for spring-bloom initiation in addition to food availability. In this context, a mismatch could occur when annual cycles of temperature, photoperiod, and wind-driven mixing that control the strength, timing, and composition of spring phytoplankton blooms do not overlap with those conditions that optimize gametogenesis and reproduction processes, in addition to affecting the timing of food availability for adult individuals. Changes in bloom composition, and thus the quality of food deposition to the seafloor (Parrish et al. 2005; Dörner et al. 2020; Lowman et al. 2021) in response to ocean warming and acidification could alter gametogenesis (Parrish et al. 2009) and affect an organism's fitness.

In practice, there exists limited empirical justification for the MMH, owing to the challenge of collecting data at sufficient temporal resolutions to identify recruitment, abundance, and behaviour patterns, and comparing them to appropriate baselines (Kharouba and Wolkovich 2020). Thus, there is an opportunity for long-term *in situ* monitoring infrastructure to investigate phenological match-mismatch questions at the organismal level, particularly in the face of rapid ocean change.

Long-lived, slow-growing, and slow-moving heterotrophic benthic organisms are ideal study organisms for monitoring environmental change, and rely on food input from external sources (Wei et al. 2020). These characteristics mean that they integrate and directly respond to their physicochemical environment and may serve as indicators of changing conditions over time (Wei et al. 2020), although variability in how individuals within a benthic community change in response to their environment should be considered over the long-term. In the North Atlantic, several studies have documented the accumulation of organic matter on the seafloor and the resulting benthic response revealing particularly striking changes in echinoderm assemblages (Billett et al. 1983, 2001, 2010; Lampitt 1985; Campanyà-Llovet et al. 2021).

The coastal waters of Newfoundland and Labrador (NL) provide a particularly suitable environment in which to study the structuring role of spring bloom dynamics on benthic communities. The region is known for strong seasonality in temperature, photoperiod, wind-driven mixing, storms, sea ice, and salinity, all of which influence the timing of spring blooms (Stead and Thompson 2003; Marra et al. 2015; Janout et al. 2016; Almén and Tamelander 2020; Gronchi et al. 2021). Conception Bay, on the island of Newfoundland, is one coastal embayment in which the timing, composition, flux rates, and contribution to total productivity of the spring bloom are well understood (Redden 1994; Stead and Thompson 2003; Parrish et al. 2005;

Thompson et al. 2008), and the hydrodynamics have been similarly well-studied (de Young and Sanderson 1995). Here, the onset of the spring bloom usually occurs in mid-March – primarily diatoms requiring high silica availability (e.g., *Skeletonema costatum* and *Thalassiosira nordenskiodii*), prior to thermal stratification, and is primarily triggered by a reduction in wind-driven mixing, while a second "main" bloom peaks around mid-May, and consists primarily of chain- and mat-forming diatoms with a lower silica requirement (e.g., *Chaetoceros debilis*, *Chaetoceros socialis*, *Chaetoceros diadema*), and some unarmoured dinoflagellates (e.g., *Gymnodinium* sp.) (Stead and Thompson 2003; Thompson et al. 2008; C.H. McKenzie, unpublished data). The light regime and availability of inorganic nutrients are considered sufficient for bloom initiation as early as January-February, and early "slow-burn" spring blooms have been observed (Stead and Thompson 2003). There is considerable meteorological and oceanographic variability in the region during the winter; thus, while the general bloom characteristics have been well-described, the precise timing of bloom onset is still difficult to predict.

In Conception Bay, around 56% of seasonal primary production from the surface sinks to the seafloor, providing high-quality food input for the benthic fauna (Parrish et al. 2005; Thompson et al. 2008), meeting the energetic and reproductive cycle requirements of several benthic and hyperbenthic fauna (Hamel et al. 1993; Choe et al. 2003). However, ocean warming and acidification threaten this reliable food source, signalling an impending mismatch in behavioural phenology (Platt et al. 2003; Fuentes-Yaco et al. 2007; Koeller et al. 2009). Lengthening ice-free periods in the Labrador Sea are triggering earlier spring blooms (Kahru et al. 2011; Glen Harrison et al. 2013; Chan et al. 2017), while the quantity and quality of phytodetritus available to the seafloor may decline due to ocean acidification (Dörner et al.

2020). Carotenoids and polyunsaturated fatty acids obtained from bloom material are essential nutrients for proper gametogenesis and vitellogenesis in many suspension- and deposit-feeding benthic invertebrates (Parrish et al. 2009; Gianasi et al. 2017) so changes in bloom composition and size could have major implications for reproductive success. Rapidly changing climate conditions are narrowing the window to establish natural baselines against which ecological change can be measured, especially in cold-water marine systems that are particularly vulnerable to climate change (Tian et al. 2003).

The transition from winter to spring is an historically under-sampled and understudied period across a range of marine ecosystems, imposing significant knowledge gaps for marine science (Terrado et al. 2008). Stormy variable winter conditions and potential pack ice cover make traditional monitoring tools, such as plankton tows, sediment traps, benthic trawls, and drop-camera surveys virtually untenable. Similarly, the often-unrelenting cloud cover in the region precludes the use of satellite imagery to supplement temporally continuous estimates of sea surface conditions. Surface moorings can be a useful tool for *in situ* monitoring of environmental conditions but are also highly vulnerable to storms. In contrast, seafloor cabled observatories, although spatially limited, can provide the temporal resolution necessary to elucidate high-frequency and long-term patterns of benthic community responses to environmental variability (Mànuel-Làzaro et al. 2010; Matabos et al. 2011; Bergmann et al. 2011; Juniper et al. 2013; Doya et al. 2014; Taylor et al. 2017), and allow for seafloor data collection during otherwise challenging conditions.

The recent deployment of the Holyrood Subsea Observatory in Conception Bay, NL provides continuous monitoring infrastructure unprecedented in the region. Monitoring seasonal changes that may structure sub-Arctic benthic communities will provide a baseline against which

future change can be measured, and contribute to the study of long-term biotic and abiotic trends (Danovaro et al. 2020). Further, Conception Bay is home to several species of commercial interest, including snow crab (*Chionoecetes opilio* (Fabricius, 1788)), northern shrimp (*Pandalus borealis* Krøyer, 1838), capelin (*Mallotus villosus* (Müller, 1776)), and Atlantic herring (*Clupea harengus* Linnaeus, 1758), and one Species At Risk Act-listed species, the Atlantic wolffish (*Anarhichas lupus* Linnaeus, 1758; Novaczek et al. 2017), making it a desirable location for long-term monitoring infrastructure. In this study, our objectives were to 1) characterize the benthic community at this site, and 2) determine the processes that may contribute to variation in the local benthic community structure during the spring phytoplankton bloom.

3.2 Methods and Materials

3.2.1 Study site

Conception Bay, Newfoundland is a northeast facing coastal embayment that opens into the inshore branch of the Labrador current (Petrie and Anderson 1983) (Figure 3.1). Consequently, the bay experiences considerable seasonal variation in meteorological and oceanographic conditions, including prolonged cloud cover, strong storms, upstream sea-ice melt (Mertz et al. 1993), and a temperate latitude light regime (Thompson et al. 2008). The mean circulation, thermocline structure, and wind-forcing in Conception Bay have been well-described by de Young and Sanderson (1995), all of which contribute to the timing of the onset of the spring phytoplankton bloom (Thompson et al. 2008). A previous study has suggested no evidence of a seasonal signal in bottom water temperature, which ranges from -0.8˚C to -1.4˚C, although there is consistent deep-water exchange throughout the year that results in a seasonal change in density and salinity (de Young and Sanderson 1995). It is important to note that past oceanographic work was carried out in the main Bay and may not reflect conditions in the shallower near-shore area of the Holyrood Inlet at the southern head of Conception Bay where the cabled observatory is located. The head of the bay is sheltered from the winds in spring, resulting in reduced vertical mixing compared to the outer bay (de Young and Sanderson 1995), and likely experiences earlier stratification and possibly earlier onset of the spring bloom compared to the outer bay.

3.2.2 Data collection

3.2.2.1 Holyrood Subsea Observatory System

The Marine Institute's Holyrood Subsea Observatory System was deployed by Ocean Networks Canada (ONC) on February 14th, 2021, at 82 m depth at the mouth of the Holyrood Inlet of

Conception Bay, NL (Figure 3.1). The observatory is connected by a 4 km electro-optical cable to a shore station located at the Holyrood Marine Base in Holyrood, NL. After a commissioning phase, data acquisition began on February 21st, 2021, and, for this study, concluded on June 16th, 2021, although the observatory continues to collect data. All data collected from the observatory are available on Oceans 3.0 (https://data.oceannetworks.ca/DataSearch). The observatory is equipped with a diverse suite of instruments for collecting physical, chemical, and biological data near the seafloor. A SeaBird Microcat SBE37SIP Conductivity-Temperature-Depth (CTD) sensor measures temperature (˚C), salinity (psu), density (kg mL^{-3}), and pressure (dbar) at a rate of 1 Hz. An upward-facing Nortek AWAC 400 kHz Acoustic Doppler Current Profiler (ADCP) measures east-west (U-component) and north-south (V-component) current velocities, as well as backscatter intensity (Hz) from the water column. Backscatter has been used as a proxy for micronekton, plankton, particulate matter, and other bloom-associated material (Record and Young 2006; De Leo et al., 2018; Receveur et al. 2020). The ADCP collects data in 1 m range bins from 1.49 m to 35 m above the seafloor, at a frequency of 1 Hz. To reduce data download and processing time, ADCP data were retrieved from ONC's Oceans 3.0 (https://data.oceannetworks.ca/) with 10-minute ensemble period ping-averaging. A Turner Cyclops-7F fluorometer measures chlorophyll-*a* (µg mL^{-1}) in the water column at a rate of 1 Hz. To complement the seafloor data collection, we also deployed a YSI EXO2 multi-parameter sonde moored to a surface float at 30 m depth near the observatory to collect near-surface chlorophyll-*a* as relative fluorescence units (RFU) at a rate of 1 measurement every 15 minutes. RFU were converted to chlorophyll-*a* concentration (µg mL^{-1}) following Richoux et al. (2004), using a regression equation developed based on previously collected samples from Conception Bay. The range of seafloor environmental conditions observed is outlined in Table S3.1.

The observatory is also equipped with a SubC Imaging Rayfin HD video camera, as well as two Aquorea Mk3 LED Lights (up to 15000 lumen output each) to record benthic imagery. The camera and lights were fixed in position, with the camera mounted 44.11 cm above the seafloor with a fixed diagonal, horizontal, and vertical field of view of 70˚, 47.4, and 60.4 tangential to the seabed, respectively. To account for the uneven illumination field on the seafloor, we first calculated a Canadian (perspective) grid following Wakefield and Genin (1987). This allowed the distance from the bottom of the camera field of view to the top of the illuminated area to be estimated (80 cm). The illuminated camera field of view was then calculated to be approximately 0.89 m^2 (Appendix 1). The camera was programmed to turn on in tandem with the lights and record a five-minute video every hour.

3.2.2.2 Environmental data collection and processing

All environmental data (temperature, salinity, density, pressure, currents, backscatter, and chlorophyll fluorometry) were averaged to one-hour bins to match the sampling rate of the video data. We used wavelet analysis to identify the dominant frequencies or cycles behind the variation in the environmental data (Cazelles et al. 2008). Briefly, any time-series can be thought of as a combination of sine and cosine waves, each oscillating at a given frequency. The frequencies of the waves that make up an individual time-series can be identified by transforming from the time-domain (where the independent variable is time and the dependent variable is the observations of a time series) to the frequency-domain (where the independent variable is the frequency and the dependent variable is the spectrum, or strength, of a given frequency) using the Fast-Fourier Transform (FFT; Shumway and Stoffer 2016). In the frequency domain, we can assess the relative contribution of a given frequency to variation in the

time series. However, in complex ecological systems the dominant cycles of variation can change over time and may not be consistent throughout a time series. Here, we use the Morlet continuous wavelet transform (WaveletComp package, Rosch and Schmidbauer 2018) to identify the dominant cycles in the environment, at what time points they occur, and how these cycles change over time.

3.2.2.3 Video collection and faunal characterization

In each video, all visible megafauna within the illuminated field of view were counted and identified to the lowest taxonomic level possible to measure abundance and taxonomic richness. High-resolution taxonomic identification is challenging using underwater video where individuals were difficult to discern to the genus or species level. To reduce possible error, we occasionally grouped organisms to a higher taxonomic classification based on morphological similarity, known as morphotaxa (Howell et al. 2019). For example, several morphologically similar shrimp species occur in the Northwest Atlantic, identified here as caridean shrimp (Caridea spp.). In another example, the observed genus *Myoxocephalus* spp. likely consisted of a mix of *M. octodecemspinosus* and *M. scorpinus*, with other small sculpins identified to the family level (Cottidae). For mobile fauna that move in and out of the frame throughout a single video, the maximum number of individuals visible in a single frame (Max N) was used as the abundance for that video. Max N is commonly used for counting fish in video datasets and eliminates the possibility of double counting mobile individuals (Denney et al. 2017).

3.2.3 Statistical analysis

All statistical analyses were carried out using the R statistical software (R Core Team 2020).

3.2.3.1 Community characterization

Organism abundance data was Hellinger-transformed prior to community analysis using the *decostand* function in the vegan R package for community ecologists (Oksanen et al. 2020). This transformation is the square root of the relative abundance of each organism in an observation period, and preserves the Hellinger distance during Euclidian ordination analysis (Legendre and Gallagher 2001). Hellinger distance is more appropriate for analyzing community composition data that contains many zeros (Legendre and Gallagher 2001).

We calculated a Bray-Curtis distance matrix on the Hellinger-transformed abundance data and clustered community composition according to Ward's method (Ward.D2, after Murtagh and Legendre 2014), whereby clusters are created to minimize within-group variance (Borcard et al. 2011). The optimal number of clusters was determined by utilizing the Ward.D2 algorithm of Murtagh and Legendre (2014) to calculate a critical value for the silhouette index (Rousseeuw 1987). For each cluster in a set of clusters (minimum two, maximum six), a "silhouette width" was calculated that indicated whether dates fell well within a cluster or in between clusters (Rousseeuw 1987). The optimal number of clusters is that with the highest average silhouette width. This was implemented using the *NbClust* function from the vegan package (Oksanen et al. 2020). We then used non-metric multidimensional scaling to visualize the ordination in two dimensions, followed by ANOSIM and SIMPER analyses from the *vegan* package (Oksanen et al. 2020) to test for differences among identified groups and determine which species contributed most to the (dis)similarity, respectively. Environmental variables were standardized to zero mean and unit variance, and fit onto the ordination as vectors using the *envfit* function in the vegan package (Oksanen et al. 2020). The magnitude of the environmental

vector corresponds to the strength of correlation with the ordination (i.e. similarities among dates and species), and the direction represents the most rapidly changing gradient of each variable to maximize correlations with the ordination.

3.2.3.2 Biological rhythms and tidal periodicity

We used 24-hour-based waveform analysis to investigate the presence of daily or tidal activity rhythms in the most abundant megafauna, considered to be organisms observed more than two times per day on average.

To visualize tidal and diurnal cycles in organism abundance or visibility/emergence, we calculated the average abundance for each hour across five, 28-day time-series segments. We conducted a 24-hour-based waveform analysis to statistically determine any significant relationships between environmental and morphotaxa abundance cycles. First, we computed the Midline Estimating Statistic of Rhythm (MESOR; Aguzzi *et al*., 2013) for each organism, which was calculated by re-averaging waveform values over all the 28-day segments. Then, we overlayed the average hourly environmental data (temperature and pressure) to visualize possible cause-effect relationships. A significant relationship between abundance and environment was considered to exist when the average hourly abundance did not overlap with the MESOR for three consecutive hours and corresponded to a concomitant positive or negative change in either temperature or pressure during the same period (Aguzzi *et al*., 2013).

3.2.3.3 Changepoint analysis

We used the mcp R package (Lindeløv 2020) to identify change points in environmental and organism abundance time series. A change point, D , is a point along a dimension x_i where

the expected value, μ_i, of the observed series, y_i, changes from being defined by one function, $f_1(x_i, \beta_1)$, to another function, $f_2(x_i, \beta_2)$, where b are regression coefficients (Stephens, 1994; Carlin 1992). This can be conceptualized as a piecewise regression problem:

$$\mu_i = \begin{cases} f_1(x_i, \beta_1) & \text{if } x_i < \Delta \\ f_2(x_i, \beta_2) & \text{if } x_i > \Delta \end{cases} \qquad \textit{Eq. 3.1}$$

The mcp package uses a Bayesian inference approach with JAGS ('Just Another Gibbs Sampler', Plummer, 2003) to estimate the point in which a series switches from being predicted by one function to the next function. Briefly, Bayesian inference considers any quantity for which uncertainty exists, such as model parameters (here, change points), to be representable by a probability distribution (Lynch 2007). We are interested in the probability of a change point occurring at a certain time conditional on the observed data, which, in a Bayesian framework, is considered to be fixed (Lynch 2007). This conditional distribution is called the *posterior distribution* and is a function of our prior knowledge of the data and model parameters (change points), and the likelihood of the observed data given the change points. If we consider model parameters as change points, Bayes' theorem expressed in terms of probability distributions is:

$$f(\Delta|\text{data}) = \frac{f(\text{data}|\Delta) f(\Delta)}{f(\text{data})}, \qquad \textit{Eq. 3.2}$$

where $f(\Delta|\text{data})$ is the posterior distribution of the change point, Δ, $f(\text{data}|\Delta)$ is the likelihood function of Δ for our fixed data, $f(\Delta)$ reflects our prior beliefs about the possible values of Δ, which is scaled by some function of our data, $f(\text{data})$. Since $f(\text{data})$ does not depend on our change point Δ, Bayes' theorem can be re-written as:

$$f(\Delta|\text{data}) \propto f(\text{data}|\Delta) f(\Delta), \qquad \textit{Eq. 3.3}$$

where the posterior probability of our change point is proportional to our prior beliefs about the change point times the likelihood function for our data (Lynch 2007). Model parameters can then be estimated by drawing samples from the probability distribution of the known function (right-hand side of the proportionality in Eq. 3.3). The method of parameter estimation implemented in the mcp package is Markov Chain Monte Carlo (MCMC) simulation, which is a class of algorithms for random distribution sampling. Starting from an arbitrary point, samples are drawn from the known distribution, and assigned a probability based on their contribution to the expected value or variance. Several iterations of this process are performed concurrently to develop an ensemble of chains (in this study, we used 10,000 iterations of three chains). Model fit is determined based on whether the individual chains converge on the same result.

Models were fit for each time series by breaking the series into segments and regressing over time, specifying the functional form for each segment *a priori*. The number of segments was chosen *a priori* based on visual inspection of each series. The models were first fit with default uninformative priors for change points, which default to the t-tail prior for models with more than two change points (Lindeløv 2020). Then, priors were specified by restricting change points to intervals with uniform prior credence (i.e. a uniform probability that a change point occurs within the interval) where a change in functional form could be reasonably assumed. The mcp package allows for flexibility in modeled relationships; generalized linear mixed-model (GLMM) segments can be independently specified for each segment in the series, defining changes in mean, trend, variance, and autoregression or a combination of these (Lindeløv 2020). Environmental series were modeled with Gaussian error terms, while change points for abundance series were modeled with Poisson error terms with log link function. For all models, an AR(1) autoregressive term was included to account for temporal dependence among adjacent

observations. Model fit was evaluated by the Gelman-Rubin convergence diagnostic, where a value below 1.1 indicated MCMC chain convergence (Gelman and Rubin, 1992).

We compared the change points between environmental and abundance series to identify which environmental changes may trigger changes in abundance. For each change point in an abundance time series, we tested the hypotheses that it was contained within the interval of an environmental time series change point. Hypothesis tests were conducted using Savage-Dickey density ratios and Bayes Factors (BF) to determine support for the specified hypothesis. A BF greater than one indicated a stronger belief in the specified hypothesis relative to the prior, and $0 < BF < 1$ indicated support for the prior (Lindeløv 2020).

3.3 Results

3.3.1 Spring bloom conditions

3.3.1.1 Temperature and salinity

Late winter of 2021 in the Holyrood Inlet was characterized by cold seawater temperatures (below 0˚), with gradual warming already occurring in the region by late February (Figure 3.2A). The increasing mean temperature was followed by a period of high variability starting on March 3rd when benthic water temperature reached 0˚C. The period of variable and increasing temperature coincided with a mirrored decline in salinity (Figure 3.2B). Wavelet analysis identified daily cycles in both temperature and salinity, which were strongest in early March (Figure 3.2A, B, S3.1). This period of increasing temperature and decreasing salinity characterizes the “Pre-bloom” state in Holyrood Inlet.

3.3.1.2 Chlorophyll-a and turbidity

Chlorophyll-*a* concentration near the seabed started to increase around March 10th when the first photosynthetic material from the spring phytoplankton bloom reached the seafloor, marking the beginning of the "Bloom" period (Figure 3.2C). Chlorophyll-*a* continued to increase until April 1st – April 5th, when the concentration of photosynthetic material plateaued at 1.07 +/- 0.19 µg mL^{-3} (Figure 3.2C). Between April 3rd and 20th, chlorophyll-*a* stabilized and remained high, with a spike (3.95 µg mL^{-3}) observed on April 16th, whereafter chlorophyll-*a* declined. Following this decline, a period of high but plateaued chlorophyll-*a* concentration (0.59 +/- 0.14 µg mL^{-3}) at the seafloor persisted until May 5th (Figure 3.2C). After this point, the variability abruptly increased, and an increasing trend was observed until May 23rd, coinciding with a period of low salinity. A large spike in chlorophyll-*a* (6.22 µg mL^{-3}) was observed on May 23rd, again coinciding with an abrupt increase in salinity, followed by a decline in chlorophyll-*a* to 0.39 +/- 0.07 µg mL^{-3} at the end of the study period on June 16th (Figure 3.2C). The instrument measuring near-surface chlorophyll-*a* was deployed on April 2nd, and a first recorded peak (initial bloom onset likely occurred earlier) occurred on April 12th, with increased variance between April 10th and 15th (Figure 3.2D). This was followed by a period of stable chlorophyll-*a* around 0.24 µg mL^{-3}. A second period of high surface chlorophyll-*a* was recorded between May 1st and May 17th, with the maximum concentration observed on May 15th (Figure 3.2D). During this time, the bloom material sank through the water column with approximately an 8-day time lag between peak surface chlorophyll-*a* and peak benthic chlorophyll-*a*.

Water column backscatter intensity followed a similar pattern to benthic and surface chlorophyll-*a* concentrations during bloom-onset (Figure 3.2E), however this pattern was not observed throughout the entire bloom (i.e., low backscatter values were observed in May even though chlorophyll-*a* concentration remained high). We cannot directly partition the backscatter

among photosynthetic particles, zooplankton fecal pellets, and other suspended or sinking organic matter or organisms in the water column, as well as stirred particles resuspended by storms or water turbulence. However, backscatter intensity was highest during the initial bloom phase (end of March to early May) and during the main bloom (late-May until the end of our study period; Figure 3.2E). This suggests that at least some of the backscatter can be attributed to photosynthetic material sinking from the surface bloom. Increased backscatter following the main bloom is more likely related to zooplankton fecal pellets, and other organic matter related to the secondary production that dominates this phase.

3.3.2 Benthic community

3.3.2.1 Whole-community response

Twenty-nine different morphotaxa across five phyla (echinoderms, arthropods, chordates, cnidarians, molluscs; Table 3.1, Figure 3.3), were identified in approximately 254 hours of video (5 minutes x 3,044 videos). The most abundant organism during the study period was the suspension-feeding sea cucumber *Psolus phantapus*, which emerged from the sediment at the end of February and remained highly visible until the end of the study period (Figure 3.4A). Caridean shrimp and Ophiuroids were the next most common, declining in abundance over the study period (Figure 3.4B, C, Figure 3.6). It is important to note that the decline in these two morphotaxa may be an artifact of the large number of sea cucumbers obscuring the view of the seafloor and not necessarily evidence of decline. Three other taxa of commercial importance were present at the site: Clupeidae (likely *Clupea harengus*. Figure 3.4D), Osmeridae (likely *Mallotus villosus* and *Osmerus mordax*, Figure 3.4E), and snow crab (*Chionoecetes opilio,* Figure 3.4F). Both Clupeidae and Osmeridae were observed at low abundance of individuals

throughout the study period, but several large schools were observed in May and June (Figure 3.4D, E). *C. opilio* was observed sporadically throughout the study period, though in low abundance (Figure 3.4F).

The Bray-Curtis dendrogram illustrates two temporally adjacent periods of similar species composition identified through clustering: "Pre- and post-bloom" (PPB), which included February 21-March 16, and June 13-16, and "During bloom" (DB), which included March 17-June 12 (Figure 3.5A). The optimal number of clusters was determined by consensus of several algorithms. ANOSIM indicated these two groups were significantly different ($R = 0.9788$, $p < 0.0001$ on 9999 permutations). The dendrogram clustering was further supported by the nMDS ordination, which depicted the clustering of dates within the DB and PPB periods, with a stress value of 0.06 (Figure 3.5B). Temperature ($r^2 = 0.78$), density ($r^2 = 0.62$), salinity ($r^2 = 0.55$), and chlorophyll-*a* ($r^2 = 0.24$) were significantly correlated with the nMDS ordination (Figure 3.5B). DB was positively associated with chlorophyll-*a* and temperature, and negatively associated with salinity and density (Figure 3.5B). Most fish taxa were positively associated with temperature during the DB period, except for Gadidae, Clupeidae, and Stichaeidae, while the invertebrates, except for Buccinidae, Naticidae, and *Cancer* sp., were primarily associated with cooler temperatures (Figure 3.5B). *P. phantapus* was the primary species associated with the DB period and contributed most (28%) to the dissimilarity between DB and PPB, according to SIMPER analysis (Figure 3.6A, Table S3.2). In the PPB periods, the community was primarily composed of caridean shrimp and Ophiuroids, which contributed 22% and 18% to the dissimilarity, respectively (Figure 3.6A, Table S3.2). Clupeidae (5.6%), *Solaster endeca* (3.4%), and *Chionoecetes opilio* (3%), were also associated with the PPB periods (Table S3.2).

3.3.2.2 Psolus phantapus emergence

Psolus phantapus was present in low abundance (0-5 individuals) at the end of February, where only the tentacles of individuals were visible above the sediment surface. On February 28 the number of observed individuals increased slightly then returned to low numbers (Figure 3.7A). Here, *P. phantapus* bodies were partially visible but ultimately returned to the sediment without sustained emergence. This coincided with the beginning of the period of increasing and variable water temperature (Figure 3.7B, Table S3.5). The number of observed individuals of *P. phantapus* increased dramatically between March 6th (1 individual) to March 27th (210 individuals) during the period of increasing temperature and increasing chlorophyll-*a* concentration, coinciding with the first change point identified in the chlorophyll-*a* series (March 10th; Figure 3.7A). The number of observed individuals of *P. phantapus* plateaued and then declined between March 26th and April 24th, and then declined again between April 24th and May 18th (Figure 3.7A). This period was characterized by warm temperatures (0.34 – 0.38˚C) and high but declining chlorophyll-*a* concentration that plateaued around April 23rd (Figure 3.5C). Temperature also dipped to between 0.24˚C and 0.26˚C around May 5th, where it remained stable but variable on a daily scale for the remainder of the study period (Figure 3.7B). The number of observed individuals of *P. phantapus* increased again between May 18th and May 27th, during a period of variable and increasing chlorophyll-*a* concentration. The number of observed individuals of *P. phantapus* declined after May 27th until the end of the study period, following a period of declining chlorophyll.

3.3.3 Tidal periodicity, currents, and biological rhythms

Holyrood Inlet exhibited a diurnal tidal period (Figure 3.8A), which was supported by the wavelet analysis of the pressure series showing dominant frequency of approximately 12 hours

(Figure S3.1). Water currents in the lower 2 meters of the water column flow predominantly South-Southwest and Northeast (Figure 3.8B, C), and the North-South velocity component is stronger and more variable than the East-West component (Figure 3.8D, E). The N-S and E-W near-seabed current velocity components also exhibit high-frequency variation between 12 hours and 40 hours, with the strongest frequency occurring around 24 hours (Figure S3.1). The timing of high-frequency variation in current velocities varied across the study period, with the strongest daily cycles occurring at the beginning of March and the end of May (Figure S3.1).

The 24h-based waveform analysis indicated that Caridean shrimps exhibited diurnal variation in abundance over the study period, and were found to be more abundant at the seafloor at night (Figure 3.9). Caridean shrimps exhibited lowest visibility (mean abundance below MESOR) between 1 pm and 7pm in late February-early March and were most visible (mean abundance above MESOR) between 3am and 7am (Figure 3.9A-D). Shrimp abundance may also be slightly correlated with the tidal cycle during this early period (Figure 3.9A). The pattern of diurnal variation was generally consistent until mid-May, when average abundance levels could no longer be distinguished from the MESOR (Figure 3.9D).

Waveform analysis indicated that hourly *P. phantapus* visibility was highly variable over the study period (Figure 3.10A-D). During the April 21 period, *P. phantapus* was found to have a period of low visibility (levels below the MESOR) at 7 pm but did not constitute a significant difference as it was not sustained for at least three consecutive hours (Figure 3.10C). No other high-frequency emergence rhythms related to light or tidal cycles were evident in *P. phantapus*, or Ophiuroidea (not shown) during the study period.

3.4. Discussion

Over the course of the first Holyrood cabled-observatory deployment, we identified two distinct periods of similar visible composition corresponding to the timing of the spring phytoplankton bloom: Pre-and -post-bloom (February 21-March 16, and June 13-16), and during the bloom (March 17 to June 12). The difference between these periods was driven primarily by the emergence of the sea cucumber, *Psolus phantapus,* in early March, which reached upwards of 200 individuals visible in the field of view. To the best of our knowledge, there exists little data on the abundance and distribution of *P. phantapus* in the region (Coady 1973). The synchrony of *P. phantapus* emergence with the spring phytoplankton bloom likely represents a phenological adaptation to maximize resource consumption and energy availability for reproduction, growth, locomotion, and other metabolic processes.

3.4.1 Spring bloom dynamics

Considering historical data for Conception Bay, there is considerable variation in both the strength and timing of the spring bloom across years (Redden 1994; Stead and Thompson 2003; Thompson et al. 2008). Holyrood Inlet, at the head of Conception Bay, is considerably more sheltered than the outer bay, resulting in lower wind-driven mixing (de Young and Sanderson 1995), and possibly earlier bloom onset than the rest of the bay. However, capturing the onset of the bloom remains challenging as meteorological and oceanographic variability during the winter make the timing of precise conditions difficult to predict.

The spring phytoplankton bloom in Conception Bay is known to occur during cold water conditions prior to thermal stratification in the water column, with vertical stability of the bloom regulated by salinity (Stead and Thompson 2003; Thompson et al. 2008). Indeed, we observed a period of high variability in chlorophyll-*a* at the seafloor and near the surface that coincided with

low salinity (Figure 3.2B-D), and the arrival of bloom material at the seafloor in early March followed a period of increasing mean and variance of bottom water temperatures (Figure 3.2A). While the bloom was already well underway when we deployed the multi-parameter sonde, coupling historical flux rates with our benthic fluorometer data, we can estimate the date of bloom onset. The composition of the bloom changes throughout its duration, but consists primarily of chain-forming centric diatoms (Thompson et al. 2008) and was dominated by several species of *Chaetoceros* during the May 2021 bloom (C.H. McKenzie, unpublished data). Diatoms provide an important source of carotenoids and poly-unsaturated fatty acids essential for gametogenesis and vitellogenesis in echinoderms and other benthic invertebrates (Parrish et al. 2009; Gianasi et al. 2017). Vertical flux rates of mostly intact phytoplankton cells taken from depth-stratified sediment traps range between 20-23 m d^{-1} during the peak bloom (Thompson et al. 2008). Considering the first chlorophyll-*a* change point identified in our study was March 10th, and the depth of the observatory at 82 m, we would expect bloom material to take approximately 4 days to reach the seafloor. This places the onset of the 2021 spring phytoplankton bloom around March 6th.

We observed the maximum seafloor chlorophyll-*a* concentration of 6.22 µg mL^{-3} on May 19th. This peak was later and larger than previously recorded seasonal maxima in the region of 2.5 µg mL^{-3} in early May 1988 (Thompson et al. 2008), and 4.26 µg mL^{-3} and 5.09 µg mL^{-3} in the third week of April 1997 and 1998, respectively (Stead and Thompson 2003). Bloom material reaching the seafloor in Conception Bay is high in polyunsaturated fatty acids (Parrish et al. 2005), has low carbon:nitrogen and phaeopigment:chlorophyll-*a* ratios, and arrives at the seafloor relatively undegraded, accounting for around 56% of seasonal primary production

(Thompson et al. 2008). Thus, this fresh phytodetritus provides a seasonally available, high-quality food source for benthic fauna.

It is notable that the bloom material in Conception Bay does not accumulate on the seafloor, nor is it immediately degraded, but is either rapidly buried by deposit feeders or takes the form of diatom resting spores (Thompson et al. 2008). Unfortunately, sedimentation of phytodetritus could not be confirmed in the present study due to limitations of the camera angle and illumination field, although time-lapse and video cameras have been used successfully to measure phytodetritus accumulation on the seafloor in previous studies (e.g., Billett et al. 1983; Smith et al. 2008b). The first photographic evidence of phytodetritus accumulation on the seafloor in the North Atlantic was taken from the Porcupine Abyssal Plain, and also documented the first *in situ* community response to seasonal phytodetritus input to the seafloor in a mass-appearance of the holothuroid *Amperima rosea* (E. Perrier, 1886) in what is now known as the "Amperima event" (Billett et al. 1983). This event has been revisited several times since the 1980s (Billett et al. 2001, 2010; Campanyà-Llovet et al. 2021), demonstrating behavioural phenology in holothurians is closely linked with the spring phytoplankton bloom. Additionally, many laboratory studies have demonstrated seasonality in echinoderm reproduction (Hamel et al. 1993; Galley et al. 2008), activity rhythms (Singh et al. 1999; Mercier et al. 1999, 2011), and the role of phytoplankton in modulating behaviour (Galley et al. 2008). However, there exist few *in-situ* time-series of echinoderm response during seasonal phytoplankton blooms (Sumida et al. 2014).

Interestingly, other cold-water regions, such as the West Antarctic Peninsula, do not appear to exhibit seasonality in food availability at the seabed despite strong evidence of seasonal primary production and food availability in the water column; a phenomenon attributed

to the build-up of a "food bank" (Mincks et al. 2005; Mincks and Smith 2007; Smith et al. 2008b, 2012a). Although there has been no reported evidence of phytodetritus accumulation on the seabed during the spring and summer in Conception Bay, to our knowledge there have been no sediment samples collected during the winter months to test hypotheses related to winter food limitation at the benthos and facilitate comparison of food availability in the sediments across an entire year. Collecting sediment samples year-round could provide new insights into benthic-pelagic coupling and nutrient cycling dynamics of the sub-Arctic fjord of Conception Bay, and the potential effects of climate-induced changes to phytoplankton bloom timing, composition, and intensity on benthic megafauna that time their behaviours with seasonal food availability.

3.4.2 *Psolus* emergence and phenology

The sudden emergence of *P. phantapus* from within the sediments was unexpected, as there were no *P. phantapus* individuals visible on the sediment surface prior to the bloom, only their feeding tentacles were partially visible (R.C., pers. obs.). During the bloom, the sea cucumbers were occasionally observed moving through the sediment partially buried, though only one individual was ever observed to be fully exposed, emerging completely and then reburying itself over a 36-hour period (R.C., pers. obs.). The absence of visible movement prior to the bloom, followed by the sudden emergence of *P. phantapus* suggests these organisms exhibit a period of low activity immediately prior to the spring bloom, possibly to conserve energy during the resource-limited winter (Sun et al. 2020).

Regulating movement improves energy management for reproduction in ectotherms (Fossette et al. 2012), allowing for thermoregulation to maintain gamete viability during winter. Recent research by Ru et al. (2021) found plasticity in sea cucumber (*Apostichopus japonicus*)

movement, whereby movement is downregulated to conserve energy for reproduction. *P. phantapus* are free-spawning, with a lecithotrophic (i.e. yolk-bearing) pelagic larval stage that lasts at least 58 days (Mercier and Hamel 2010). A similar reproductive strategy has been documented in the related *P. fabricii*, also found in the region, albeit with a slightly shorter larval stage (55 days; Mercier and Hamel 2010). During a controlled mesocosm experiment, *P. phantapus* was shown to spawn in mid-April; spawning was recorded only during daylight hours, lasted less than a week, and generally occurred simultaneously in males and females (Mercier and Hamel 2010). Production of lecithotrophic larvae requires a high level of energy investment from females (Mincks and Smith 2007). In addition to storing energy directly in the gonads during feeding, holothuroids can build up energy reserves in their body walls and muscle bands, which can later be translocated for gonad and gamete development (David and MacDonald 2002). Since gametogenesis appears to occur from winter until spring spawning (Hamel et al. 1993), down-regulation of movement may be an energy management strategy to promote gamete development.

Abrupt changes in the mean and variability of environmental cues can trigger behavioural phenologies, particularly those related to reproduction (Tyler et al. 1982). Environmental cues initiating gametogenesis and spawning in echinoderms have been extensively studied, and include light intensity, salinity, turbidity, temperature, and phytoplankton blooms (Himmelman 1975; Tyler et al. 1982; Starr et al. 1990; Hamel et al. 1993; Mercier and Hamel 2009). Starr et al. (1990) suggested phytoplankton as the primary spawning cue for echinoderms since it directly signals food availability and encompasses environmental parameters that signal favourable conditions for larvae. Recent laboratory experiments have demonstrated that phytoplankton is a potent trigger of spawning in sea cucumbers (Gianasi et al. 2019) and may trigger spawning

independent of gonad maturity (Gianasi et al. 2017). Indeed, spawning of *Cucameria frondosa* can be artificially induced at least two months prior to their natural spawning window (Mercier and Hamel 2010). Interestingly, although the first changepoint we identified for *P. phantapus* occurred within hours of that measured for benthic chlorophyll-*a* (Table S3.3, Table S3.5), we also observed a small, earlier "pulse" emergence of *P. phantapus* immediately following an increase in mean and variance of bottom water temperature (Figure 3.4A, Figure 3.2A). This is consistent with previous research that has suggested a concert of environmental cues likely act in synergy to influence the timing of spawning in echinoderms (reviewed in. Mercier and Hamel 2009). In a closely-related sea cucumber, *P. fabricii*, gametogenesis begins to accelerate in March when water temperatures rise and food availability begins to increase (Hamel et al. 1993). This follows a period of little to no gametogenic activity through the autumn and winter months, when food availability is low, suggesting a resource-conservation strategy. This is also consistent with the hypothesis that an organism maximizes its fitness by spawning during periods of optimal resource availability in terms of 1) food available for adults to build energy stores, 2) food available for larva/juveniles to survive and recruit into the population, and 3) (Cushing 1990). Conversely, reproducing too early or too late could result in a mismatch, whereby resource availability is sub-optimal, and fitness may be reduced. The initial "pulse" emergence of *P. phantapus* may have been triggered by the increase in temperature, which may serve as an early warning that food will be available soon, allowing *P. phantapus* to emerge at the right time to maximize food consumption, recover energy lost to gametogenesis, and maximize juvenile survival.

While the reproductive cycle of *P. phantapus* has not been well-documented *in situ*, we observed *P. phantapus* with its tentacles extended into the water column between mid-March and

early June, with maximum extension observed in late-March and April (R.C. pers. obs.). Full-body elevation or "reaching" postures are common in free-spawning echinoderms during active reproduction (Mercier and Hamel 2010), likely improving probability of gamete dispersal. This observation supports synchrony between reproductive behaviour of *P. phantapus* and timing of the spring phytoplankton bloom in this system. Further, individuals of this species may relocate to other areas of the bay during the cold autumn to keep their gametes viable. A period of little-to-no movement could follow from January-March, when gametogenesis begins to accelerate (Hamel et al. 1993). However, a thermoregulatory-movement hypothesis alone may be insufficient to explain the emergence in Holyrood Inlet, where bottom water temperature varies little over a year, and where *P. phantapus* was not observed prior to emergence. We therefore suggest that *P. phantapus* down-regulates movement as a means of resource conservation during the winter months.

3.4.3 Tidal periodicity

Although diurnal cycles in burrowing, locomotion, and feeding activity relating to light intensity and photoperiod have been demonstrated for *P. phantapus* and other suspension-feeding holothuroids (Mercier et al. 1999, 2011; Mercier and Hamel 2010; Sun et al. 2020), we did not observe such a rhythm in our study. This may be a result of the large number of individuals observed in the field of view, potentially aliasing patterns in the behaviour of individual sea cucumbers (Figure 3.10). Although previous studies have investigated activity and feeding behaviours in controlled laboratory environments (Mercier et al. 1999, 2011; Aguzzi et al. 2006; Mercier and Hamel 2010; Duchêne 2017), these behaviours could be further investigated *in-situ* by monitoring a subset of individual sea cucumbers using the Holyrood Subsea Observatory. There is some debate as to the utility of underwater video for behavioural

studies when artificial lighting is used to illuminate a study area (Widder et al. 2005; Sun et al. 2019; Zheng et al. 2021; Geoffroy et al. 2021), so caution would be warranted in interpreting results from such a study. Different light sources (e.g., red light) as well as acoustic cameras could be installed at this site in the future to determine the magnitude of disturbance from the recording schedule. However, interpreting behaviours of benthic fauna in a laboratory environment outside the context in which they typically exist also presents challenges. Combining *in-situ* and laboratory techniques would bolster the findings of both methods and provide a more holistic understanding of the behaviour of understudied species.

We did observe diurnal periodicity in the caridean shrimp at our study site, with activity levels appearing to correlate with the photoperiod. Day-night cycles in activity levels have been well-documented for many shrimp species (Company and Sardà 1997; Aguzzi et al. 2007a, 2007b; García et al. 2008; Koeller et al. 2009), which often migrate vertically through the water column to feed during the night. We also observed that the number of hours where activity levels were above and below the MESOR declined as the photoperiod lengthened.

3.4.4 Other taxa

Chemical communication among conspecifics and between taxa during reproduction has been demonstrated in other holothuroid and echinoderm species (Mercier and Hamel 2010; Marquet et al. 2018). Indeed, a spawning window similar to that observed in *P. phantapus* has also been documented in ophiuriods (April 10^{th}-14^{th}), and the boreal sun star *Solaster endeca* (April 12^{th}-14^{th}; Mercier and Hamel 2010), both of which were present at the study site before the bloom. While the abundance of other echinoderms and Caridean shrimp was observed to decline during the bloom, this observation could be an artifact of the large number of *P. phantapus* obscuring the view of the seafloor. Therefore, while it is possible these species are

also synchronizing their behaviours with the timing of the spring phytoplankton bloom, further research is required to determine whether there are detectable changes in their abundance or behaviours seasonally.

We documented several commercially important species present at the study site, including snow crab (*Chionoecetes opilio*), capelin (*Mallotus villosus*), and Atlantic herring (*Clupea haregnus*). Snow crab supports an important fishery in Newfoundland and Labrador, but has experienced a decline in recent years (Mullowney et al. 2014). Despite decades of study, the complex life-history dynamics of snow crab, including reproduction, mating, molting, and ontogenetic and seasonal migration, remain unresolved (Mullowney et al. 2018). Although we observed low density of *C. opilio* in the Holyrood Inlet (Figure 3.4, this study; Charmley et al. 2022), ontogenetic migration across a depth gradient of a related species, *C. tanneri*, has been recently documented using cabled seafloor observatories off the coast of British Columbia (Chauvet et al. 2019). Although Conception Bay is at the upper limit of snow crab distribution (Mullowney et al. 2018), expanding future monitoring from the Holyrood Subsea Observatory to include the deeper-basin of Conception Bay proper could enhance our understanding of near-shore snow crab abundance and distribution patterns, and support fisheries management efforts in Conception Bay.

We also observed several large groups of Clupeidae and Osmeridae during the peak of the bloom in mid-May, which may be explained by the match-mismatch hypothesis, although we cannot make general inferences regarding the behavioural phenologies of these fish given the small, fixed field of view (0.89 m^2) of our study. In early summer, capelin aggregate in near-shore waters prior to spawning on the beach in a process known as “rolling” (Leggett and Frank 1990). Historically, Atlantic herring also spawn in spring, with a second recruitment pulse in

early autumn (Melvin et al. 2009). In recent years, Atlantic herring populations in Newfoundland have undergone a shift from predominately Spring-spawning to Autumn-spawning, likely relating to warming ocean temperature affecting the phenology of copepods, a primary food source for larval herring (Melvin et al. 2009; Wilson et al. 2018). While fixed seafloor observatories alone are not usually optimized for monitoring pelagic fishes with large ranges, there is increasing development of underwater imagery technology (e.g., stereo cameras) as a less-invasive method for quantifying fish density, abundance, body size, and distribution (Doya et al. 2014; Denney et al. 2017; Aguzzi et al. 2020a, 2020b).

3.5 Conclusions and future directions

Many questions remain regarding the activity levels of *P. phantapus* throughout the year. One hypothesis is that they are in a low-activity (e.g., not feeding) state to conserve energy when phytoplanktonic food is scarce through the sparse winter months. Previous research found changes in digestive cell morphology and increased digestive enzyme activity of the bivalve *Yolida hyperborea* in the region coincident with the input of fresh algae in the spring, suggesting an "activation of a formerly depressed digestive system" after a period of little food consumption (late-summer through winter) (Stead and Thompson 2003). Conducting similar research for *P. phantapus* could provide additional evidence relating to the low-activity hypothesis and help explain their sudden emergence in late-winter and early spring.

Although the Holyrood Subsea Observatory provides unprecedented temporal resolution to seafloor data collection in Conception Bay, the spatial limitations of a fixed cabled observatory preclude investigation of spatial patterns. There are three promising avenues of research to address this challenge. First, acoustic tagging of sea cucumbers could provide insight

into their movements throughout the year. Sea cucumbers often expel invasive tags from their body walls making this a challenging task (Reichenbach 1999; Shiell 2006; Cieciel et al. 2009). However, recent research has had success with acoustic PIT tagging in a closely related and morphologically similar suspension-feeding holothuroid species of commercial interest, *Cucamaria frondosa* (Gianasi et al. 2015). To our knowledge, this has not been tested in *Psolus* sea cucumbers, and could provide insight into their distribution when they cannot be directly observed. Second, combining vessel-based or autonomous seafloor mapping and drop-camera ground truthing data could enhance spatial coverage of the benthos in the region. Seasonal habitat mapping has recently been conducted in Holyrood Inlet, with notable differences in the visibility above the substratum and distribution of *P. phantapus* throughout the year (Charmley et al. 2022). Coupling high-frequency time-series with habitat mapping across multiple years could provide the temporal resolution necessary to investigate *P. phantapus* behaviour, and the spatial coverage required to examine broad-scale distribution shifts. Finally, installing additional monitoring stations along a depth gradient into the main basin of Conception Bay would improve spatial coverage and enable monitoring of depth-distribution trends in commercially important species like snow crab. Expanded observing capacity of this nature could also support the monitoring of species' invasions (McKenzie et al. 2016) or range expansions from the deeper shelf or slope into shallower water, as seen in the lithodid crab *Neolithodes yaldwyni* in the West Antarctic Peninsula (Smith et al. 2012b).

The long-term deployment of the Holyrood Subsea Observatory will facilitate a multi-year comparison of bloom dynamics and benthic response in the region. In winter 2022, we have already observed several events that merit further investigation, including the influx of a warm water mass (M. Kott, pers. comm.), and two intense turbidity events during the winter storm

season (S. Mihaly, pers. comm.). At the time of writing, we have again observed the emergence of *P. phantapus* coincident with the 2022 spring phytoplankton bloom (R.C. pers. obs.). Leveraging high-frequency, year-round, and continuous *in situ* monitoring will improve our understanding of these complex ecological and oceanographic phenomena.

Tools like the Holyrood Subsea Observatory allow for unprecedented access to the seafloor in Conception Bay, providing continuous data year-round. Coupling this high-resolution time series data from the seafloor with surface buoys, seasonal spatial surveys, sediment trap or sediment core samples, and gliders could maximize coverage in the region and allow for high-resolution monitoring in space and time. This approach could facilitate observations of recurring patterns and improve our understanding of sub-Arctic benthic megafauna and their responses to environmental change.

3.6 Acknowledgements

This project and R. Command were supported by an Early Career Faculty Award Grant to Dr. Katleen Robert from the Marine Environmental Observation, Prediction and Response Network (MEOPAR) and a Canada Research Chair (Ocean Mapping) to PI K. Robert. The Holyrood Subsea Observatory platform was jointly funded by Atlantic Canada Opportunities Agency (ACOA) and the Marine Institute of Memorial University of Newfoundland. Ocean Networks Canada is funded through Canada Foundation for Innovation-Major Science Initiative (CFI-MSI) fund 30199. We also thank ONC's marine and digital operations staff for servicing and maintaining the NEPTUNE observatory and for the curation and quality control of all oceanographic data streams used in this study. In particular, the efforts by S. Kerschtien and S. Wagner to troubleshoot issues with the acquisition of video imagery were key. We thank

Fisheries and Oceans Canada for supplying the multiparameter sonde, H. Lambert and K. Matheson for instrument support, and A. Templeman and K. Regular for deploying and recovering the sonde.

3.7 References

Aguzzi, J., Chatzievangelou, D., Company, J.B., Thomsen, L., Marini, S., Bonofiglio, F., Juanes, F., Rountree, R., Berry, A., Chumbinho, R., Lordan, C., Doyle, J., del Rio, J., Navarro, J., De Leo, F.C., Bahamon, N., García, J.A., Danovaro, P.R., Francescangeli, M., Lopez-Vazquez, V., and Gaughan, P. 2020a. The potential of video imagery from worldwide cabled observatory networks to provide information supporting fish-stock and biodiversity assessment. ICES Journal of Marine Science: fsaa169. doi:10.1093/icesjms/fsaa169.

Aguzzi, J., Chiesa, J.J., Caprioli, R., Cascione, D., Magnifico, G., Rimatori, V., and Costa, C. 2006. Preliminary evidences of circadian fan activity rhythm in *Sabella spallanzanii* (Gmelin, 1791) (Polychaeta: Sabellidae). Sci. Mar. **70**(4): 727–734. doi:10.3989/scimar.2006.70n4727.

Aguzzi, J., Company, J., Abelló, P., and García, J. 2007a. Ontogenetic changes in vertical migratory rhythms of benthopelagic shrimps Pasiphaea multidentata and P. sivado. Mar. Ecol. Prog. Ser. **335**: 167–174. doi:10.3354/meps335167.

Aguzzi, J., López-Romero, D., Marini, S., Costa, C., Berry, A., Chumbinho, R., Ciuffardi, T., Fanelli, E., Pieretti, N., Del Río, J., Stefanni, S., Mirimin, L., Doyle, J., Lordan, C., and Gaughan, P. 2020b. Multiparametric monitoring of fish activity rhythms in an Atlantic coastal cabled observatory. Journal of Marine Systems **212**: 103424. doi:10.1016/j.jmarsys.2020.103424.

Aguzzi, J., Ramirez-Llodra, E., Telesnicki, G., and Camps, M. 2007b. Day-night activity rhythm of the cold seep shrimp *Alvinocaris stactophila* (Caridea: Alvinocarididae) from the Gulf of Mexico. J. Mar. Biol. Ass. **87**(5): 1175–1180. doi:10.1017/S0025315407057311.

Almén, A.-K., and Tamelander, T. 2020. Temperature-related timing of the spring bloom and match between phytoplankton and zooplankton. Marine Biology Research **16**(8–9): 674–682. doi:10.1080/17451000.2020.1846201.

Bergmann, M., Soltwedel, T., and Klages, M. 2011. The interannual variability of megafaunal assemblages in the Arctic deep sea: Preliminary results from the HAUSGARTEN observatory (79°N). Deep Sea Research Part I: Oceanographic Research Papers **58**(6): 711–723. doi:10.1016/j.dsr.2011.03.007.

Billett, D.S.M., Bett, B.J., Reid, W.D.K., Boorman, B., and Priede, I.G. 2010. Long-term change in the abyssal NE Atlantic The 'Amperima Event revisited. : 12.

Billett, D.S.M., Bett, B.J., Rice, A.L., Thurston, M.H., Galéron, J., Sibuet, M., and Wolff, G.A. 2001. Long-term change in the megabenthos of the Porcupine Abyssal Plain (NE Atlantic). Progress in Oceanography **50**(1–4): 325–348. doi:10.1016/S0079-6611(01)00060-X.

Billett, D.S.M., Lampitt, R.S., Rice, A.L., and Mantoura, R.F.C. 1983. Seasonal sedimentation of phytoplankton to the deep-sea benthos. Nature **302**(5908): 520–522. doi:10.1038/302520a0.

Borcard, D., Gillet, F., and Legendre, P. 2011. Numerical Ecology with R. Springer New York, New York, NY. doi:10.1007/978-1-4419-7976-6.

Campanyà-Llovet, N., Le Guitton, M., and Watson, S.-A. 2021. Long-term and seasonal changes in the life-history biology of the abyssal holothurian Pseudostichopus aemulatus from the Porcupine Abyssal Plain (North-East Atlantic). Deep Sea Research Part I: Oceanographic Research Papers **174**: 103537. doi:10.1016/j.dsr.2021.103537.

Cazelles, B., Chavez, M., Berteaux, D., Ménard, F., Vik, J.O., Jenouvrier, S., and Stenseth, N.C. 2008. Wavelet analysis of ecological time series. Oecologia **156**(2): 287–304. doi:10.1007/s00442-008-0993-2.

Chan, P., Halfar, J., Adey, W., Hetzinger, S., Zack, T., Moore, G.W.K., Wortmann, U.G., Williams, B., and Hou, A. 2017. Multicentennial record of Labrador Sea primary productivity and sea-ice variability archived in coralline algal barium. Nat Commun **8**(1): 15543. doi:10.1038/ncomms15543.

Charmley, K., Baker, K., and Robert, K. 2022. Seasonal Change Between Benthic Habitat Maps in a Sub-Arctic Ecosystem. Virtual.

Chauvet, P., Metaxas, A., and Matabos, M. 2019. Interannual Variation in the Population Dynamics of Juveniles of the Deep-Sea Crab Chionoecetes tanneri. Front. Mar. Sci. **6**: 50. doi:10.3389/fmars.2019.00050.

Choe, N., Deibel, D., Thompson, R., Lee, S., and Bushell, V. 2003. Seasonal variation in the biochemical composition of the chaetognath Parasagitta elegans from the hyperbenthic zone of Conception Bay, Newfoundland. Mar. Ecol. Prog. Ser. **251**: 191–200. doi:10.3354/meps251191.

Cieciel, K., Pyper, B.J., and Eckert, G.L. 2009. Tag Retention and Effects of Tagging on Movement of the Giant Red Sea Cucumber Parastichopus californicus. North American Journal of Fisheries Management **29**(2): 288–294. doi:10.1577/M07-194.1.

Coady, L.W. 1973, March. Aspects of the reproductive biology of *Cucamaria frondosa* (Gunnerus, 1770) and *Psolus fabricii* (Duben and Koren, 1846) (Echinodermata: Holothuroidea) in shallow waters of the Avalon Peninsula, Newfoundland. M.Sc., Memorial University of Newfoundland, St. John's, NL. Available from https://research.library.mun.ca/7249/3/Coady_LawrenceWilliam.pdf [accessed 17 March 2022].

Company, J.B., and Sardà, F. 1997. Reproductive patterns and population characteristics in five deep-water pandalid shrimps in the Western Mediterranean along a depth gradient (150-1100 m). Mar. Ecol. Prog. Ser. **148**: 49–58. doi:10.3354/meps148049.

Cushing, D.H. 1969. The Regularity of the Spawning Season of Some Fishes. ICES Journal of Marine Science **33**(1): 81–92. doi:10.1093/icesjms/33.1.81.

Cushing, D.H. 1990. Plankton production and year-class strength in fish populations: an update of the match/mismatch hypothesis. Advances in Marine Biology **26**: 249–293.

Danovaro, R., Fanelli, E., Aguzzi, J., Billett, D., Carugati, L., Corinaldesi, C., Dell'Anno, A., Gjerde, K., Jamieson, A.J., Kark, S., McClain, C., Levin, L., Levin, N., Ramirez-Llodra, E., Ruhl, H., Smith, C.R., Snelgrove, P.V.R., Thomsen, L., Van Dover, C.L., and Yasuhara, M. 2020. Ecological variables for developing a global deep-ocean monitoring and conservation strategy. Nat Ecol Evol **4**(2): 181–192. doi:10.1038/s41559-019-1091-z.

David, V.M.M., and MacDonald, B.A. 2002. Seasonal biochemical composition of tissues from *Cucumaria frondosa* collected in the Bay of Fundy, Canada: feeding activity and reproduction. J. Mar. Biol. Ass. **82**(1): 141–147. doi:10.1017/S0025315402005258.

Denney, C., Fields, R., Gleason, M., and Starr, R. 2017. Development of New Methods for Quantifying Fish Density Using Underwater Stereo-video Tools. JoVE (129): 56635. doi:10.3791/56635.

Dörner, I., Hauss, H., Aberle, N., Lohbeck, K., Spisla, C., Riebesell, U., and Ismar-Rebitz, S. 2020. Ocean acidification impacts on biomass and fatty acid composition of a post-bloom marine plankton community. Mar. Ecol. Prog. Ser. **647**: 49–64. doi:10.3354/meps13390.

Doya, C., Aguzzi, J., Pardo, M., Matabos, M., Company, J.B., Costa, C., Mihaly, S., and Canals, M. 2014. Diel behavioral rhythms in sablefish (Anoplopoma fimbria) and other benthic species, as recorded by the Deep-sea cabled observatories in Barkley canyon (NEPTUNE-Canada). Journal of Marine Systems **130**: 69–78. doi:10.1016/j.jmarsys.2013.04.003.

Duchêne, J.-C. 2017. Activity Rhythm Measurement in Suspension Feeders. *In* Marine Animal Forests. *Edited by* S. Rossi, L. Bramanti, A. Gori, and C. Orejas. Springer International Publishing, Cham. pp. 761–785. doi:10.1007/978-3-319-21012-4_18.

Durant, J., Hjermann, D., Ottersen, G., and Stenseth, N. 2007. Climate and the match or mismatch between predator requirements and resource availability. Clim. Res. **33**: 271–283. doi:10.3354/cr033271.

Fossette, S., Schofield, G., Lilley, M.K.S., Gleiss, A.C., and Hays, G.C. 2012. Acceleration data reveal the energy management strategy of a marine ectotherm during reproduction: Accelerometry reveals turtle energy management strategy. Functional Ecology **26**(2): 324–333. doi:10.1111/j.1365-2435.2011.01960.x.

Fuentes-Yaco, C., Koeller, P.A., Sathyendranath, S., and Platt, T. 2007. Shrimp (Pandalus borealis) growth and timing of the spring phytoplankton bloom on the Newfoundland?Labrador Shelf. Fisheries Oceanogr **16**(2): 116–129. doi:10.1111/j.1365-2419.2006.00402.x.

Galley, E.A., Tyler, P.A., Smith, C.R., and Clarke, A. 2008. Reproductive biology of two species of holothurian from the deep-sea order Elasipoda, on the Antarctic continental shelf. Deep Sea Research Part II: Topical Studies in Oceanography **55**(22–23): 2515–2526. doi:10.1016/j.dsr2.2008.07.002.

García, Company, and Aguzzi. 2008. The circadian behavioural regulation of the shrimp, Processa canaliculata Leach, 1815 (Decapoda, Processidae) in relation to depth, ontogeny, and the reproductive cycle. Crustac **81**(11): 1301–1316. doi:10.1163/156854008X369492.

Geoffroy, M., Langbehn, T., Priou, P., Varpe, Ø., Johnsen, G., Le Bris, A., Fisher, J.A.D., Daase, M., McKee, D., Cohen, J., and Berge, J. 2021. Pelagic organisms avoid white, blue, and red artificial light from scientific instruments. Sci Rep **11**(1): 14941. doi:10.1038/s41598-021-94355-6.

Gianasi, B.L., Hamel, J.-F., and Mercier, A. 2019. Triggers of spawning and oocyte maturation in the commercial sea cucumber Cucumaria frondosa. Aquaculture **498**: 50–60. doi:10.1016/j.aquaculture.2018.08.030.

Gianasi, B.L., Parrish, C.C., Hamel, J.-F., and Mercier, A. 2017. Influence of diet on growth, reproduction and lipid and fatty acid composition in the sea cucumber *Cucumaria frondosa*. Aquac Res **48**(7): 3413–3432. doi:10.1111/are.13168.

Gianasi, B.L., Verkaik, K., Hamel, J.-F., and Mercier, A. 2015. Novel Use of PIT Tags in Sea Cucumbers: Promising Results with the Commercial Species Cucumaria frondosa. PLoS ONE **10**(5): e0127884. doi:10.1371/journal.pone.0127884.

Glen Harrison, W., Yngve Børsheim, K., Li, W.K.W., Maillet, G.L., Pepin, P., Sakshaug, E., Skogen, M.D., and Yeats, P.A. 2013. Phytoplankton production and growth regulation in the Subarctic North Atlantic: A comparative study of the Labrador Sea-Labrador/Newfoundland shelves and Barents/Norwegian/Greenland seas and shelves. Progress in Oceanography **114**: 26–45. doi:10.1016/j.pocean.2013.05.003.

Graf, G. 1989. Benthic-pelagic coupling in a deep-sea benthic community. Nature **341**(6241): 437–439. doi:10.1038/341437a0.

Gronchi, E., Jöhnk, K.D., Straile, D., Diehl, S., and Peeters, F. 2021. Local and continental-scale controls of the onset of spring phytoplankton blooms: Conclusions from a proxy-based model. Global Change Biology **27**(9): 1976–1990. doi:10.1111/gcb.15521.

Hamel, J.F., Himmelman, J.H., and Dufresne, L. 1993. Gametogenesis and Spawning of the Sea Cucumber *Psolus fabricii* (Duben and Koren). The Biological Bulletin **184**(2): 125–143. doi:10.2307/1542223.

Herbert, L.C., Michaud, A.B., Laufer-Meiser, K., Hoppe, C.J.M., Zhu, Q., Aller, R.C., Jørgensen, B.B., and Wehrmann, L.M. 2021. Tight benthic-pelagic coupling drives seasonal and interannual changes in iron-sulfur cycling in Arctic fjord sediments (Kongsfjorden, Svalbard). Journal of Marine Systems: 103645. doi:10.1016/j.jmarsys.2021.103645.

Himmelman, J.H. 1975. Phytoplankton as a stimulus for spawning in three marine invertebrates. Journal of Experimental Marine Biology and Ecology **20**(2): 199–214. doi:10.1016/0022-0981(75)90024-6.

Howell, K.L., Davies, J.S., Allcock, A.L., Braga-Henriques, A., Buhl-Mortensen, P., Carreiro-Silva, M., Dominguez-Carrió, C., Durden, J.M., Foster, N.L., Game, C.A., Hitchin, B., Horton, T., Hosking, B., Jones, D.O.B., Mah, C., Laguionie Marchais, C., Menot, L., Morato, T., Pearman, T.R.R., Piechaud, N., Ross, R.E., Ruhl, H.A., Saeedi, H., Stefanoudis, P.V., Taranto, G.H., Thompson, M.B., Taylor, J.R., Tyler, P., Vad, J., Victorero, L., Vieira, R.P., Woodall, L.C., Xavier, J.R., and Wagner, D. 2019. A framework for the development of a global standardised marine taxon reference image database (SMarTaR-ID) to support image-based analyses. PLoS ONE **14**(12): e0218904. doi:10.1371/journal.pone.0218904.

Janout, M.A., Hölemann, J., Waite, A.M., Krumpen, T., von Appen, W.-J., and Martynov, F. 2016. Sea-ice retreat controls timing of summer plankton blooms in the Eastern Arctic Ocean: Eastern Arctic Plankton Blooms. Geophys. Res. Lett. **43**(24): 12,493-12,501. doi:10.1002/2016GL071232.

Juniper, S.K., Matabos, M., Mihály, S., Ajayamohan, R.S., Gervais, F., and Bui, A.O.V. 2013. A year in Barkley Canyon: A time-series observatory study of mid-slope benthos and habitat dynamics using the NEPTUNE Canada network. Deep Sea Research Part II: Topical Studies in Oceanography **92**: 114–123. doi:10.1016/j.dsr2.2013.03.038.

Kahru, M., Brotas, V., Manzano-Sarabia, M., and Mitchell, B.G. 2011. Are phytoplankton blooms occurring earlier in the Arctic? Global Change Biology **17**(4): 1733–1739. doi:10.1111/j.1365-2486.2010.02312.x.

Kharouba, H.M., and Wolkovich, E.M. 2020. Disconnects between ecological theory and data in phenological mismatch research. Nat. Clim. Chang. **10**(5): 406–415. doi:10.1038/s41558-020-0752-x.

Koeller, P., Fuentes-Yaco, C., Platt, T., Sathyendranath, S., Richards, A., Ouellet, P., Orr, D., Skúladóttir, U., Wieland, K., Savard, L., and Aschan, M. 2009. Basin-scale coherence in phenology of shrimps and phytoplankton in the North Atlantic Ocean. Science **324**(5928): 791–793. doi:10.1126/science.1170987.

Lampitt, R.S. 1985. Evidence for the seasonal deposition of detritus to the deep-sea floor and its subsequent resuspension. Deep Sea Research Part A. Oceanographic Research Papers **32**(8): 885–897. doi:10.1016/0198-0149(85)90034-2.

Legendre, P., and Gallagher, E.D. 2001. Ecologically meaningful transformations for ordination of species data. Oecologia **129**(2): 271–280. doi:10.1007/s004420100716.

Leggett, W.C., and Frank, K.T. 1990. The Spawning of the Capelin. Sci Am **262**(5): 102–107. doi:10.1038/scientificamerican0590-102.

Lightfoot, R.H., Tyler, P.A., and Gage, J.D. 1979. Seasonal reproduction in deep-sea bivalves and brittlestars. Deep Sea Research Part A. Oceanographic Research Papers **26**(8): 967–973. doi:10.1016/0198-0149(79)90110-9.

Lindeløv, J.K. 2020. mcp: An R Package for Regression With Multiple Change Points. preprint, Open Science Framework. doi:10.31219/osf.io/fzqxv.

Lowman, H.E., Emery, K.A., Dugan, J.E., and Miller, R.J. 2021. Nutritional quality of giant kelp declines due to warming ocean temperatures. Oikos: oik.08619. doi:10.1111/oik.08619.

Lynch, S.M. 2007. Introduction to applied Bayesian statistics and estimation for social scientists. Springer, New York.

Mànuel-Làzaro, A., Nogueras, M., and Del Río, J. 2010. OBSEA: an Expandable Seafloor Observatory. Sea Technology **51**(7): 37.

Marquet, N., Hubbard, P.C., da Silva, J.P., Afonso, J., and Canário, A.V.M. 2018. Chemicals released by male sea cucumber mediate aggregation and spawning behaviours. Sci Rep **8**(1): 239. doi:10.1038/s41598-017-18655-6.

Marra, J.F., Dickey, T.D., Plueddemann, A.J., Weller, R.A., Kinkade, C.S., and Stramska, M. 2015. Phytoplankton bloom phenomena in the North Atlantic Ocean and Arabian Sea. ICES Journal of Marine Science **72**(6): 2021–2028. doi:10.1093/icesjms/fsu241.

Matabos, M., Aguzzi, J., Robert, K., Costa, C., Menesatti, P., Company, J.B., and Juniper, S.K. 2011. Multi-parametric study of behavioural modulation in demersal decapods at the VENUS cabled observatory in Saanich Inlet, British Columbia, Canada. Journal of Experimental Marine Biology and Ecology **401**(1–2): 89–96. doi:10.1016/j.jembe.2011.02.041.

McClain, C.R., Allen, A.P., Tittensor, D.P., and Rex, M.A. 2012. Energetics of life on the deep seafloor. Proc. Natl. Acad. Sci. U.S.A. **109**(38): 15366–15371. doi:10.1073/pnas.1208976109.

McKenzie, C., Matheson, K., Caines, S., and Wells, T. 2016. Surveys for non-indigenous tunicate species in Newfoundland, Canada (2006 – 2014): a first step towards understanding impact and control. MBI **7**(1): 21–32. doi:10.3391/mbi.2016.7.1.04.

Melvin, G.D., Stephenson, R.L., and Power, M.J. 2009. Oscillating reproductive strategies of herring in the western Atlantic in response to changing environmental conditions. ICES Journal of Marine Science **66**(8): 1784–1792. doi:10.1093/icesjms/fsp173.

Mercier, A., Battaglene, S.C., and Hamel, J.-F. 1999. Daily burrowing cycle and feeding activity of juvenile sea cucumbers Holothuria scabra in response to environmental factors. Journal of Experimental Marine Biology and Ecology **239**(1): 125–156. doi:10.1016/S0022-0981(99)00034-9.

Mercier, A., and Hamel, J. 2009. Chapter 3 Spawning. *In* Advances in Marine Biology. Elsevier. pp. 73–168. doi:10.1016/S0065-2881(09)55003-1.

Mercier, A., and Hamel, J.-F. 2010. Synchronized breeding events in sympatric marine invertebrates: role of behavior and fine temporal windows in maintaining reproductive isolation. Behavioral Ecology and Sociobiology **64**(11): 1749–1765. Springer.

Mercier, A., Sun, Z., Baillon, S., and Hamel, J.-F. 2011. Lunar Rhythms in the Deep Sea: Evidence from the Reproductive Periodicity of Several Marine Invertebrates. J Biol Rhythms **26**(1): 82–86. SAGE Publications Inc. doi:10.1177/0748730410391948.

Mertz, G., Narayanan, S., and Helbig, J. 1993. The freshwater transport of the labrador current. Atmosphere-Ocean **31**(2): 281–295. doi:10.1080/07055900.1993.9649472.

Mincks, S.L., and Smith, C.R. 2007. Recruitment patterns in Antarctic Peninsula shelf sediments: evidence of decoupling from seasonal phytodetritus pulses. Polar Biol **30**(5): 587–600. doi:10.1007/s00300-006-0216-4.

Mincks, S.L., Smith, C.R., and DeMaster, D.J. 2005. Persistence of labile organic matter and microbial biomass in Antarctic shelf sediments: evidence of a sediment 'food bank.' Mar Ecol Prog Ser **300**: 3–19.

Mullowney, D., Morris, C., Dawe, E., Zagorsky, I., and Goryanina, S. 2018. Dynamics of snow crab (Chionoecetes opilio) movement and migration along the Newfoundland and Labrador and Eastern Barents Sea continental shelves. Rev Fish Biol Fisheries **28**(2): 435–459. doi:10.1007/s11160-017-9513-y.

Mullowney, D.R.J., Dawe, E.G., Colbourne, E.B., and Rose, G.A. 2014. A review of factors contributing to the decline of Newfoundland and Labrador snow crab (Chionoecetes opilio). Rev Fish Biol Fisheries **24**(2): 639–657. doi:10.1007/s11160-014-9349-7.

Murtagh, F., and Legendre, P. 2014. Ward's Hierarchical Agglomerative Clustering Method: Which Algorithms Implement Ward's Criterion? J Classif **31**(3): 274–295. doi:10.1007/s00357-014-9161-z.

Novaczek, E., Devillers, R., Edinger, E., and Mello, L. 2017. High-resolution seafloor mapping to describe coastal denning habitat of a Canadian species at risk: Atlantic wolffish (*Anarhichas lupus*). Can. J. Fish. Aquat. Sci. **74**(12): 2073–2084. doi:10.1139/cjfas-2016-0414.

Oksanen, J., Blanchet, F.G., Friendly, M., Kindt, R., Legendre, P., McGlinn, D., Minchin, P.R., O'Hara, R.B., Simpson, G.L., Solymos, P., Stevens, M.H.H., Szoecs, E., and Wagner, H. 2020. vegan: Community Ecology Package. Available from https://CRAN.R-project.org/package=vegan.

Ouellet, P., Savard, L., and Larouche, P. 2007. Spring oceanographic conditions and northern shrimp Pandalus borealis recruitment success in the north-western Gulf of St. Lawrence. Mar. Ecol. Prog. Ser. **339**: 229–241. doi:10.3354/meps339229.

Parrish, C., Deibel, D., and Thompson, R. 2009. Effect of sinking spring phytoplankton blooms on lipid content and composition in suprabenthic and benthic invertebrates in a cold ocean coastal environment. Mar. Ecol. Prog. Ser. **391**: 33–51. doi:10.3354/meps08148.

Parrish, C., Thompson, R., and Deibel, D. 2005. Lipid classes and fatty acids in plankton and settling matter during the spring bloom in a cold ocean coastal environment. Mar. Ecol. Prog. Ser. **286**: 57–68. doi:10.3354/meps286057.

Petrie, B., and Anderson, C. 1983. Circulation on the newfoundland continental shelf. Atmosphere-Ocean **21**(2): 207–226. doi:10.1080/07055900.1983.9649165.

Platt, T., Fuentes-Yaco, C., and Frank, K.T. 2003. Spring algal bloom and larval fish survival. Nature **423**(6938): 398–399. doi:10.1038/423398a.

R Core Team. 2020. R: A language and environment for statistical computing. R Foundation for Statistical Computing, Vienna, Austria. Available from https://www.Rproject.org/.

Receveur, A., Kestenare, E., Allain, V., Ménard, F., Cravatte, S., Lebourges-Dhaussy, A., Lehodey, P., Mangeas, M., Smith, N., Radenac, M.-H., and Menkes, C. 2020. Micronekton distribution in the southwest Pacific (New Caledonia) inferred from shipboard-ADCP backscatter data. Deep Sea Research Part I: Oceanographic Research Papers **159**: 103237. doi:10.1016/j.dsr.2020.103237.

Record, N.R., and Young, B. de. 2006. Patterns of diel vertical migration of zooplankton in acoustic Doppler velocity and backscatter data on the Newfoundland Shelf. Can. J. Fish. Aquat. Sci. **63**(12): 2708–2721. doi:10.1139/f06-157.

Redden, A. 1994, May. Grazer-mediated chloropigment degradation and the vertical flux of spring bloom production in Conception Bay, Newfoundland. PhD, Memorial University of Newfoundland. Available from https://research.library.mun.ca/945/1/Redden_AnnaM.pdf [accessed 2 February 2020].

Reichenbach, N. 1999. Ecology and Fishery Biology of Holothuria fuscogilva in the Maldives, Indian Ocean (Echinodermata: Holothuroidea). Bulletin of Marine Science **64**(1): 103–113.

Richoux, N.B., Deibel, D., and Thompson, R.J. 2004. Population biology of hyperbenthic crustaceans in a cold water environment (Conception Bay, Newfoundland). I. Mysis mixta (Mysidacea). Marine Biology **144**(5): 881–894. doi:10.1007/s00227-003-1249-7.

Rosch, A., and Schmidbauer, H. 2018. WaveletComp 1.1: A guided tour through the R package. : 58.

Rousseeuw, P.J. 1987. Silhouettes: A graphical aid to the interpretation and validation of cluster analysis. Journal of Computational and Applied Mathematics **20**: 53–65. doi:10.1016/0377-0427(87)90125-7.

Ru, X., Zhang, L., and Yang, H. 2021. Plasticity of Locomotor Activity Permits Energy Homeostasis During Reproduction in a Female Sea Cucumber. Front. Mar. Sci. **8**: 748571. doi:10.3389/fmars.2021.748571.

Shiell, G.R. 2006. Effect of invasive tagging on the activity of *Holothuria whitmaei* [Echinodermata: Holothuroidea]: A suitable mark-recapture method for short-term field studies of holothurian behaviour. Marine and Freshwater Behaviour and Physiology **39**(2): 153–162. doi:10.1080/10236240600688789.

Shumway, R.H., and Stoffer, D.S. 2016. Time Series Analysis and Its Applications. *In* 4th edition. Springer.

Singh, R., MacDonald, B., Thomas, M., and Lawton, P. 1999. Patterns of seasonal and tidal feeding activity in the dendrochirote sea cucumber Cucumaria frondosa (Echinodermata:Holothuroidea) in the Bay of Fundy, Canada. Mar. Ecol. Prog. Ser. **187**: 133–145. doi:10.3354/meps187133.

Smith, C., Deleo, F., Bernardino, A., Sweetman, A., and Arbizu, P. 2008a. Abyssal food limitation, ecosystem structure and climate change. Trends in Ecology & Evolution **23**(9): 518–528. doi:10.1016/j.tree.2008.05.002.

Smith, C., DeMaster, D., Thomas, C., Srsen, P., Grange, L., Evrard, V., and DeLeo, F. 2012a. Pelagic-Benthic Coupling, Food Banks, and Climate Change on the West Antarctic Peninsula Shelf. oceanog **25**(3): 188–201. doi:10.5670/oceanog.2012.94.

Smith, C.R., Grange, L.J., Honig, D.L., Naudts, L., Huber, B., Guidi, L., and Domack, E. 2012b. A large population of king crabs in Palmer Deep on the west Antarctic Peninsula shelf and potential invasive impacts. Proc. R. Soc. B. **279**(1730): 1017–1026. doi:10.1098/rspb.2011.1496.

Smith, C.R., Mincks, S., and DeMaster, D.J. 2008b. The FOODBANCS project: Introduction and sinking fluxes of organic carbon, chlorophyll-a and phytodetritus on the western Antarctic Peninsula continental shelf. Deep Sea Research Part II: Topical Studies in Oceanography **55**(22–23): 2404–2414. doi:10.1016/j.dsr2.2008.06.001.

Smith, K.L., Kaufmann, R.S., and Baldwin, R.J. 1994. Coupling of near-bottom pelagic and benthic processes at abyssal depths in the eastern North Pacific Ocean. Limnology and Oceanography **39**(5): 1101–1118. doi:https://doi.org/10.4319/lo.1994.39.5.1101.

Smith, K.L., Ruhl, H.A., Huffard, C.L., Messié, M., and Kahru, M. 2018. Episodic organic carbon fluxes from surface ocean to abyssal depths during long-term monitoring in NE Pacific. Proc Natl Acad Sci USA **115**(48): 12235–12240. doi:10.1073/pnas.1814559115.

Starr, M., Himmelman, J.H., and Therriault, J.-C. 1990. Direct Coupling of Marine Invertebrate Spawning with Phytoplankton Blooms. Science **247**(4946): 1071–1074. doi:10.1126/science.247.4946.1071.

Stead, R.A., and Thompson, R.J. 2003. The effect of the sinking spring diatom bloom on digestive processes of the cold-water protobranch *Yoldia hyperborea*. Limnol. Oceanogr. **48**(1): 157–167. doi:10.4319/lo.2003.48.1.0157.

Sumida, P.Y.G., Smith, C.R., Bernardino, A.F., Polito, P.S., and Vieira, D.R. 2014. Seasonal dynamics of megafauna on the deep West Antarctic Peninsula shelf in response to variable phytodetrital influx. R. Soc. open sci. **1**(3): 140294. doi:10.1098/rsos.140294.

Sun, J., Chi, X., Yang, M., Ding, J., Shi, D., Yu, Y., Chang, Y., and Zhao, C. 2019. Light intensity regulates phototaxis, foraging and righting behaviors of the sea urchin Strongylocentrotus intermedius. PeerJ **7**. doi:10.7717/peerj.8001.

Sun, J., Hamel, J.-F., Stuckless, B., Small, T.J., and Mercier, A. 2020. Effect of light, phytoplankton, substrate types and colour on locomotion, feeding behaviour and microhabitat selection in the sea cucumber Cucumaria frondosa. Aquaculture **526**: 735369. doi:10.1016/j.aquaculture.2020.735369.

Taylor, J., Krumpen, T., Soltwedel, T., Gutt, J., and Bergmann, M. 2017. Dynamic benthic megafaunal communities: Assessing temporal variations in structure, composition and diversity at the Arctic deep-sea observatory HAUSGARTEN between 2004 and 2015. Deep Sea Research Part I: Oceanographic Research Papers **122**: 81–94. doi:10.1016/j.dsr.2017.02.008.

Terrado, R., Lovejoy, C., Massana, R., and Vincent, W.F. 2008. Microbial food web responses to light and nutrients beneath the coastal Arctic Ocean sea ice during the winter–spring transition. Journal of Marine Systems **74**(3–4): 964–977. doi:10.1016/j.jmarsys.2007.11.001.

Thompson, R., Deibel, D., Redden, A., and McKenzie, C. 2008. Vertical flux and fate of particulate matter in a Newfoundland fjord at sub-zero water temperatures during spring. Mar. Ecol. Prog. Ser. **357**: 33–49. doi:10.3354/meps07277.

Tian, R., Deibel, D., Thompson, R., and Rivkin, R. 2003. Modeling of climate forcing on a cold-ocean ecosystem, Conception Bay, Newfoundland. Mar. Ecol. Prog. Ser. **262**: 1–17. doi:10.3354/meps262001.

Townsend, D.W., and Cammen, L.M. 1988. Potential Importance of the Timing of Spring Plankton Blooms to Benthic-Pelagic Coupling and Recruitment of Juvenile Demersal Fishes. Biological Oceanography **5**(3): 215–228. doi:https://doi.org/10.1080/01965581.1987.10749514.

Turner, J.T. 2015. Zooplankton fecal pellets, marine snow, phytodetritus and the ocean's biological pump. Progress in Oceanography **130**: 205–248. doi:10.1016/j.pocean.2014.08.005.

Tyler, P.A., Grant, A., Pain, S.L., and Gage, J.D. 1982. Is annual reproduction in deep-sea echinoderms a response to variability in their environment? Nature **300**: 747–750.

Vikebø, F.B., Broch, O.J., Endo, C.A.K., Frøysa, H.G., Carroll, J., Juselius, J., and Langangen, Ø. 2021. Northeast Arctic Cod and Prey Match-Mismatch in a High-Latitude Spring-Bloom System. Front. Mar. Sci. **8**: 767191. doi:10.3389/fmars.2021.767191.

Wakefield, W.W., and Genin, A. 1987. The use of a Canadian (perspective) grid in deep-sea photography. Deep Sea Research Part A. Oceanographic Research Papers **34**(3): 469–478. doi:10.1016/0198-0149(87)90148-8.

Wei, C., Cusson, M., Archambault, P., Belley, R., Brown, T., Burd, B.J., Edinger, E., Kenchington, E., Gilkinson, K., Lawton, P., Link, H., Ramey-Balci, P.A., Scrosati, R.A., and Snelgrove, P.V.R. 2020. Seafloor biodiversity of Canada's three oceans: Patterns, hotspots and potential drivers. Divers Distrib **26**(2): 226–241. doi:10.1111/ddi.13013.

Wei, C., Rowe, G., Hubbard, G., Scheltema, A., Wilson, G., Petrescu, I., Foster, J., Wicksten, M., Chen, M., Davenport, R., Soliman, Y., and Wang, Y. 2010. Bathymetric zonation of deep-sea macrofauna in relation to export of surface phytoplankton production. Mar. Ecol. Prog. Ser. **399**: 1–14. doi:10.3354/meps08388.

Widder, E.A., Robison, B.H., Reisenbichler, K.R., and Haddock, S.H.D. 2005. Using red light for in situ observations of deep-sea fishes. Deep Sea Research Part I: Oceanographic Research Papers **52**(11): 2077–2085. doi:10.1016/j.dsr.2005.06.007.

Wilson, C.J., Murphy, H.M., Bourne, C., Pepin, P., and Robert, D. 2018. Feeding ecology of autumn-spawned Atlantic herring (Clupea harengus) larvae in Trinity Bay, Newfoundland: Is recruitment linked to main prey availability? Journal of Plankton Research **40**(3): 255–268. doi:10.1093/plankt/fby003.

Woolley, S.N.C., Tittensor, D.P., Dunstan, P.K., Guillera-Arroita, G., Lahoz-Monfort, J.J., Wintle, B.A., Worm, B., and O'Hara, T.D. 2016. Deep-sea diversity patterns are shaped by energy availability. Nature **533**(7603): 393–396. doi:10.1038/nature17937.

de Young, B., and Sanderson, B. 1995. The circulation and hydrography of conception bay, Newfoundland. Atmosphere-Ocean **33**(1): 135–162. doi:10.1080/07055900.1995.9649528.

Zheng, Q., Teo, H.C., and Koh, L.P. 2021. Artificial Light at Night Advances Spring Phenology in the United States. Remote Sensing **13**(3): 399. doi:10.3390/rs13030399.

3.8 Tables

Table 3.1. Average (+/- standard deviation) and maximum count and density (abundance/area where area is 0.89 m^2) observed per video at the Holyrood Subsea Observatory over the study period (Feb 21 – Jun 16, 2021).

Species	Mean Count	Max Count	Mean Density	Max Density
Arthropoda				
Cancer sp.	0 (0.02)	1	0 (0.023)	1.124
Caridean shrimp	5.876 (7.03)	41	6.603 (7.899)	46.067
Chionoecees opilio	0.169 (0.417)	3	0.19 (0.469)	3.371
Decapoda sp.	0.003 (0.058)	1	0.004 (0.065)	1.124
Hyas sp.	0.034 (0.187)	2	0.039 (0.21)	2.247
Pagarus sp.	0.011 (0.129)	3	0.012 (0.145)	3.371
Chordata				
Anarhichas lupus	0 (0.02)	1	0 (0.023)	1.124
Clupeidae	0.305 (3.527)	144	0.342 (3.963)	161.798
Cottidae spp.	0.041 (0.213)	2	0.046 (0.239)	2.247
Cyclopterus lumpus	0.001 (0.029)	1	0.001 (0.033)	1.124
Pleuronectidae spp.	0.018 (0.138)	2	0.021 (0.155)	2.247
Gadidae sp.	0.013 (0.115)	1	0.015 (0.129)	1.124
Myoxocephalus sp.	0.028 (0.164)	1	0.031 (0.184)	1.124
Osmeridae sp.	0.176 (1.99)	91	0.198 (2.236)	102.247
Phoca sp.	0.003 (0.054)	1	0.003 (0.061)	1.124
Stichaeidae sp.	0.084 (0.348)	9	0.095 (0.391)	10.112
UNID Actinopteri	0.003 (0.058)	2	0.003 (0.065)	2.247
Zoarcidae sp.	0.007 (0.082)	1	0.008 (0.092)	1.124
Cnidaria				
UNID Cnidaria	0.072 (0.28)	3	0.081 (0.314)	3.371
Echinodermata				
Ctenodiscus crispatus	0.176 (0.532)	9	0.198 (0.598)	10.112
Ophiuroidea spp.	7.532 (3.833)	18	8.463 (4.307)	20.225
Psolus cf. *phantapus*	81.289 (70.155)	258	91.335 (78.826)	289.888
Solaster endeca	0.142 (0.349)	1	0.159 (0.392)	1.124
Strongylocentrotus dobrachiensis	0.151 (0.358)	1	0.17 (0.403)	1.124
UNID Asteroidea	0.001 (0.035)	1	0.001 (0.04)	1.124
Mollusca				
Buccinidae sp.	0.205 (0.545)	9	0.231 (0.613)	10.112
Naticidae sp.	0.005 (0.074)	1	0.006 (0.083)	1.124
Nudibranchia sp.1	0.02 (0.139)	1	0.022 (0.156)	1.124
Nudibranchia sp.2	0.003 (0.065)	2	0.004 (0.073)	2.247

Table S3.1. Range and mean +/- SD for environmental variables from the Holyrood Underwater Observatory over the entire study period (Feb 21 – Jun 16, 2021).

Variable	**Units**	**Minimum**	**Mean**	**StDev**	**Maximum**
Near-seabed chlorophyll-a	$\mu g\ mL^{-3}$	0.215	0.817	0.708	6.449
Temperature	˚C	-0.201	0.225	0.156	0.466
Salinity	psu	32.182	32.299	0.053	32.407
Density	$kg\ m^{-3}$	1026.204	1026.310	0.049	1026.418
Pressure	dbar	81.801	82.764	0.287	83.747
Backscatter	Hz	60.745	73.841	5.089	87.459
East-West current velocity	$m\ s^{-1}$	-0.092	0.005	0.020	0.104
North-South current velocity	$m\ s^{-1}$	-0.210	-0.008	0.036	0.179
Current velocity magnitude	$m\ s^{-1}$	0.014	0.046	0.022	0.232
Current direction	˚True	18.495	188.126	68.804	335.359

Table S3.2. SIMPER analysis results.

Taxa	Average	SD	Ratio	ava	avb	Cumulative Sum	P-Value
Psolus phantapus	0.143	0.054	2.689	0.379	0.934	0.283	0.001
Caridean shrimp	0.114	0.043	2.627	0.601	0.169	0.506	0.001
Ophiuroidea	0.093	0.030	3.073	0.603	0.249	0.686	0.001
Clupeidae	0.027	0.018	1.528	0.120	0.030	0.739	0.001
Solaster endeca	0.017	0.023	0.766	0.063	0.012	0.773	0.001
Chionoecetes opilio	0.015	0.011	1.343	0.079	0.033	0.802	0.001
Buccinidae	0.015	0.015	0.994	0.063	0.044	0.831	0.011
Osmeridae	0.014	0.020	0.680	0.059	0.033	0.858	0.004
Stichaeidae	0.009	0.007	1.173	0.034	0.018	0.875	0.005
Cnidaria sp.	0.008	0.011	0.748	0.028	0.012	0.891	0.028
Ctenodiscus crispatus	0.008	0.006	1.353	0.050	0.039	0.908	0.084
Strongylocentrotus droebachiensis	0.008	0.012	0.639	0.016	0.019	0.923	0.709
Hyas sp	0.006	0.007	0.865	0.019	0.013	0.935	0.128
Cottidae sp	0.006	0.007	0.761	0.013	0.014	0.946	0.827
Myoxocephalus sp.	0.005	0.007	0.797	0.016	0.012	0.957	0.211
Gadidae	0.004	0.005	0.872	0.015	0.004	0.965	0.004
Nudibranchia sp.1	0.004	0.006	0.673	0.014	0.004	0.973	0.009
Flatfish	0.004	0.006	0.638	0.010	0.008	0.980	0.432
Pagarus sp.	0.002	0.005	0.476	0.007	0.003	0.984	0.223
Zoarcidae	0.002	0.005	0.463	0.006	0.004	0.989	0.354
Decapoda sp.	0.002	0.005	0.391	0.008	0.000	0.993	0.001
Naticidae	0.002	0.004	0.402	0.005	0.002	0.996	0.138
Nudibranchia sp.2	0.001	0.005	0.276	0.005	0.000	0.998	0.001
Phoca sp.	0.001	0.002	0.283	0.000	0.002	0.999	1.000
Cyclopterus lumpus	<0.001	0.001	0.153	<0.001	0.001	1.000	1.000
Anarhicus lupus	<0.001	0.001	0.109	<0.001	<0.001	1.000	1.000
Cancer sp.	<0.001	<0.0001	0.109	<0.001	<0.001	1.000	1.000

Table S3.3. Chlorophyll-*a* change points. Mean, Lower, and Upper represent the average and the 95% confidence interval around each variable. For the change points (cp 1 to cp 5) the values are given as a "time step", where a one-unit increase in time step equals one hour and time zero is February 21st, 2021 at 00:00:00 UTC. The terms "ar1" and "int" refer to the auto-regressive and the intercept terms, respectively. The "time" terms refer to the slope, and the sigma terms refer to a change in the variation around the trend.

Variable	Mean	Lower	Upper	Rhat	n.eff
ar1_2	0.753	0.728	0.777	1.007	3823
cp_1	415.642	400.003	445.008	1.014	1127
cp_2	1002.862	955.849	1049.912	1.001	5261
cp_3	1407.289	1400.106	1412.850	1.981	14
cp_4	1770.646	1768.361	1772.000	1.001	1999
cp_5	2201.946	2200.001	2205.353	1.050	817
int_1	0.275	0.256	0.294	1.001	3670
int_4	0.662	0.580	0.740	1.010	5188
int_6	1.317	1.071	1.561	1.005	1482
time_2	0.001	0.001	0.001	1.008	1137
time_3	0.001	0.001	0.001	1.013	1089
time_6_E2	0.000	0.000	0.000	1.003	1559
sigma_1	0.203	0.196	0.210	1.002	4952
sigma_5	0.583	0.560	0.607	1.000	5457

Table S3.4. Temperature change points. Mean, Lower, and Upper represent the average and the 95% confidence interval around each variable. For the change points (cp 1 to cp 5) the values are given as a "time step", where a one-unit increase in time step equals one hour and time zero is February 21st, 2021 at 00:00:00 UTC. The terms "ar1" and "int" refer to the auto-regressive and the intercept terms, respectively. The "time" terms refer to the slope, and the sigma terms refer to a change in the variation around the trend.

Name	Mean	Lower	Upper	Rhat	n.eff
ar1_1	0.922	0.908	0.937	1.003	2550
cp_1	253.515	201.207	289.360	1.014	161
cp_2	826.837	800.001	866.069	1.001	1114
cp_3	999.837	953.811	1048.851	1.002	3957
cp_4	1534.544	1467.699	1599.994	1.068	81
cp_5	1730.870	1700.003	1787.361	1.009	489
int_1	-0.167	-0.189	-0.145	1.009	555
int_4	0.361	0.344	0.376	1.002	3168
int_5	0.364	0.318	0.407	1.051	136
int_6	0.253	0.242	0.264	1.001	5596
time_1	0.000	0.000	0.000	1.017	264
time_2	0.001	0.001	0.001	1.003	482
time_3	0.000	0.000	0.000	1.002	3016
time_5_E2	0.000	0.000	0.000	1.024	237
sigma_1	0.012	0.011	0.013	1.001	2874
sigma_2	0.016	0.015	0.016	1.000	5057

Table S3.5. *Psolus phantapus* change points. Mean, Lower, and Upper represent the average and the 95% confidence interval around each variable. For the change points (cp 1 to cp 5) the values are given as a "time step", where a one-unit increase in time step equals one hour and time zero is February 21st, 2021 at 00:00:00 UTC. The terms "ar1" and "int" refer to the auto-regressive and the intercept terms, respectively. The "time" terms refer to the slope.

Name	Mean	Lower	Upper	Rhat	n.eff
ar1_1	0.000	0.000	0.000	NaN	0
cp_1	400.073	400.000	400.224	1.009	1915
cp_2	811.487	809.071	813.683	1.027	300
cp_3	1500.321	1500.000	1500.959	1.002	1734
cp_4	2064.355	2050.001	2077.488	1.000	6381
cp_5	2299.947	2299.840	2300.000	1.001	1644
int_1	2.124	2.096	2.148	1.062	151
int_5	4.895	4.885	4.905	1.001	2776
time_2	0.008	0.008	0.008	1.072	91
time_3	-0.001	-0.001	-0.001	1.004	792
time_4	-0.003	-0.003	-0.003	1.001	2477
time_6	-0.004	-0.004	-0.004	1.001	2839

3.9 Figures

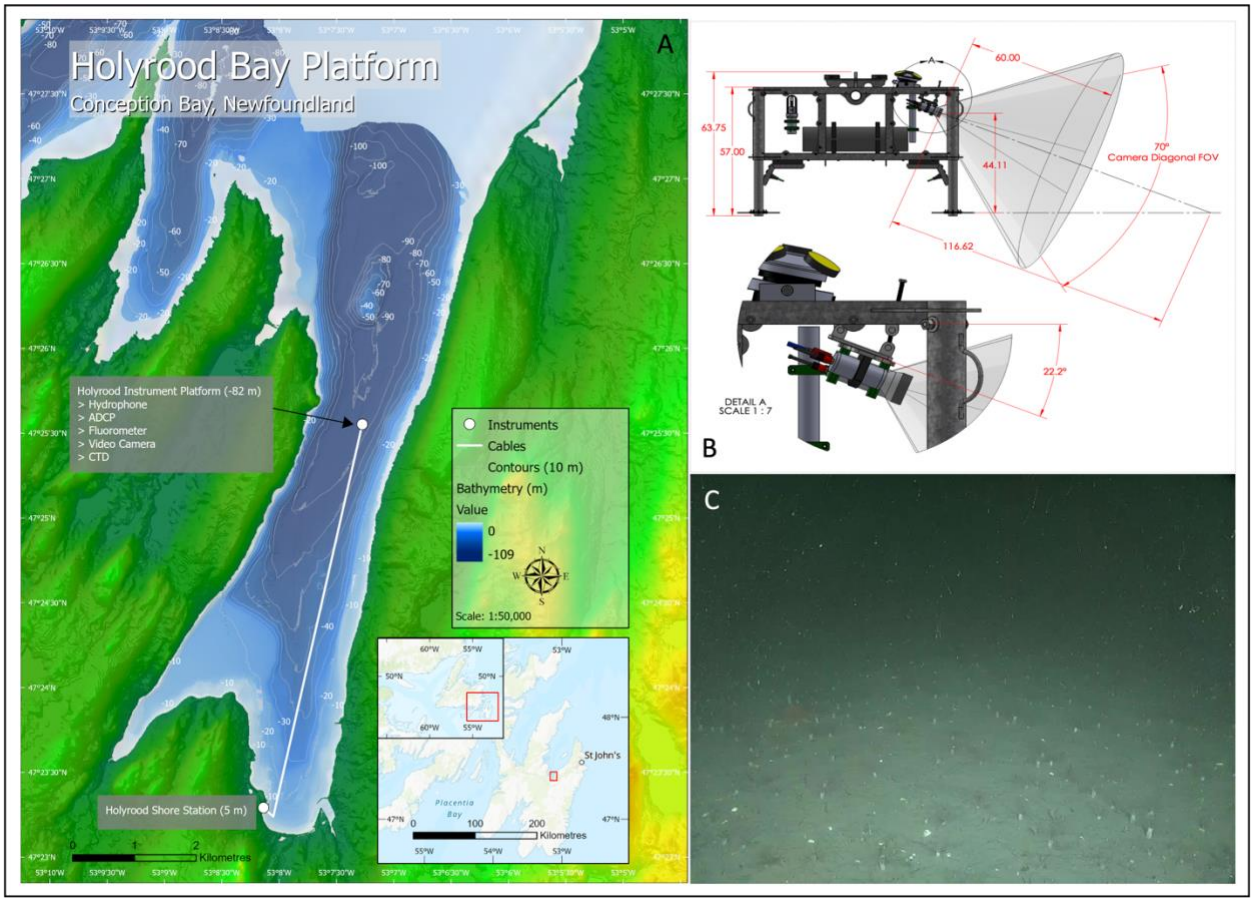

Figure 3.1. (A) Map of the Holyrood Inlet of Conception Bay showing the location of the Holyrood Subsea Observatory (HSO) at 82 m depth. Bathymetry measured at 10 m resolution. (B) Schematic of the HSO instrument platform illustrating the size of the platform and the camera mounting parameters. (C) Example field of view from the HSO.

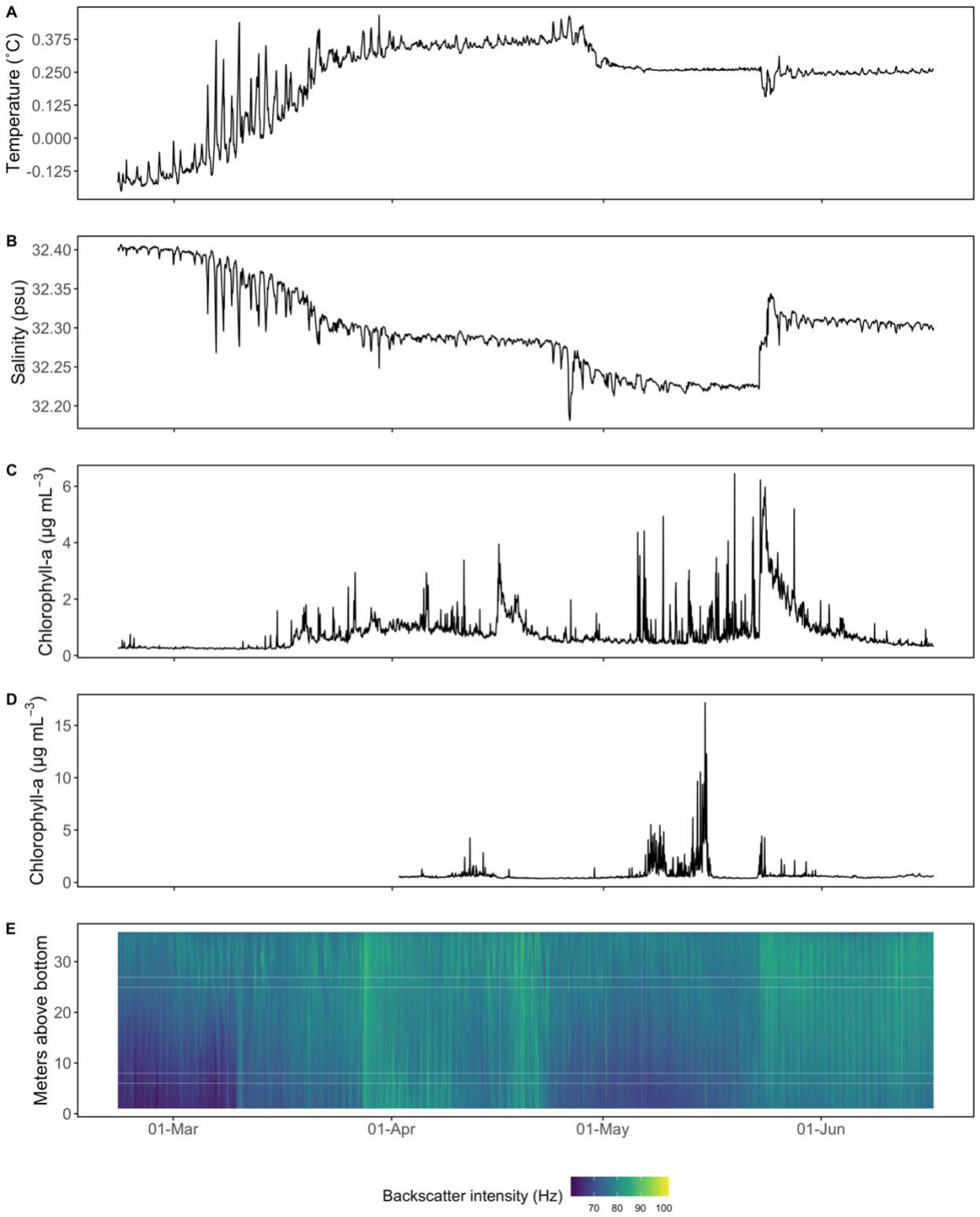

Figure 3.2. Observed environmental time series over the study period at the Holyrood Underwater Observatory at 82 m depth. (A) temperature (˚C), (B) salinity (psu), (C) near-seabed chlorophyll-*a* (µg mL^{-3}), (D) near-surface chlorophyll-*a* (µg mL^{-3}), and (E) backscatter (Hz).

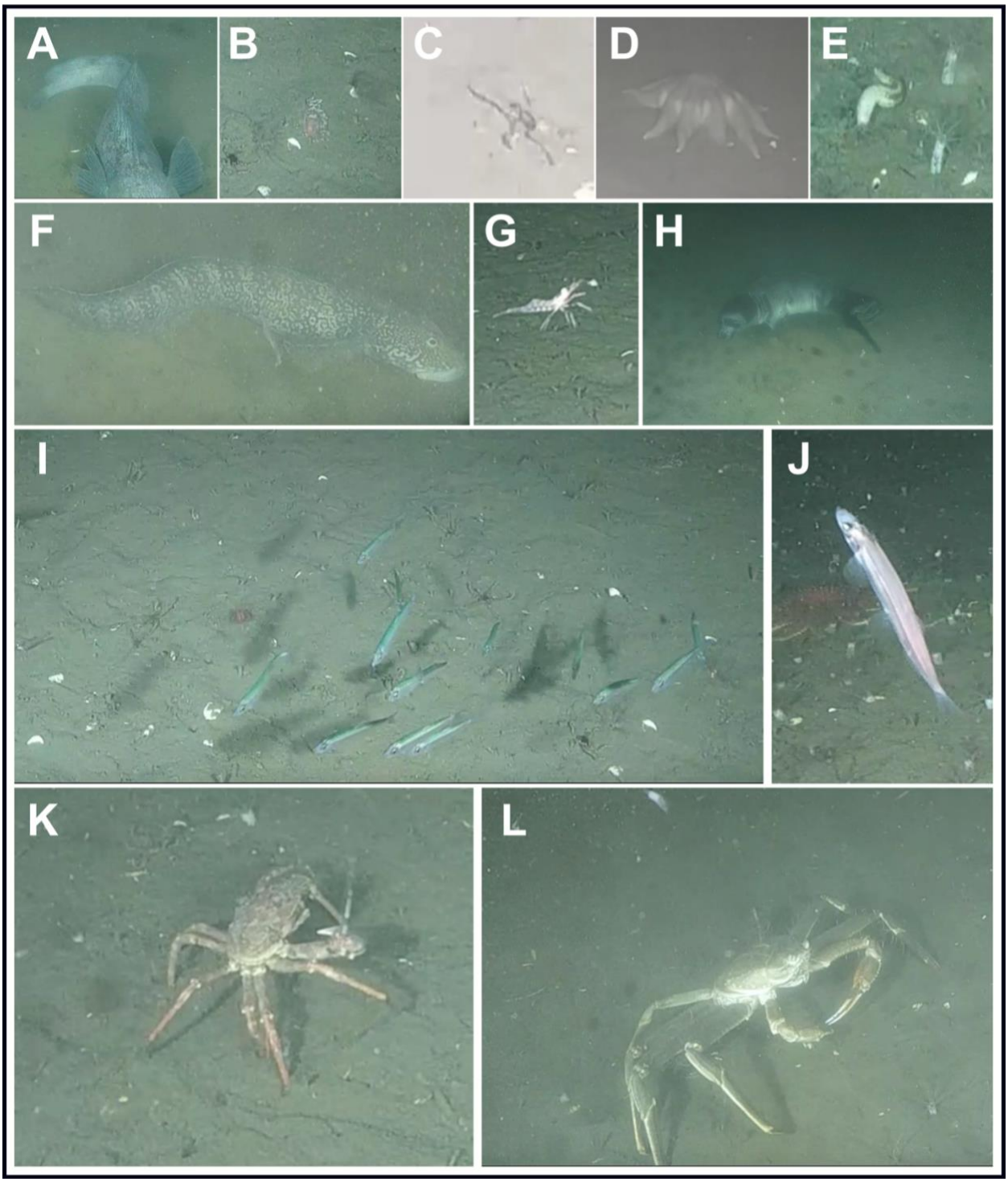

Figure 3.3. Photographic atlas of the most common taxa observed at the Holyrood Subsea Observatory between February 21 and June 16, 2021. (A) *Anarhichas lupus*, (B) Nudibranchia sp.1, (C) Ophiuroidea spp., (D) *Solaster endeca*, (E) *Psolus* cf. *phantapus*, (F) Zoarcidae sp., (G) Caridea spp., (H) *Phoca* sp., (I) school of Clupeidae, (J) Osmeridae (*Mallotus villosus*), (K) *Hyas* sp., (L) *Chionoecetes opilio*.

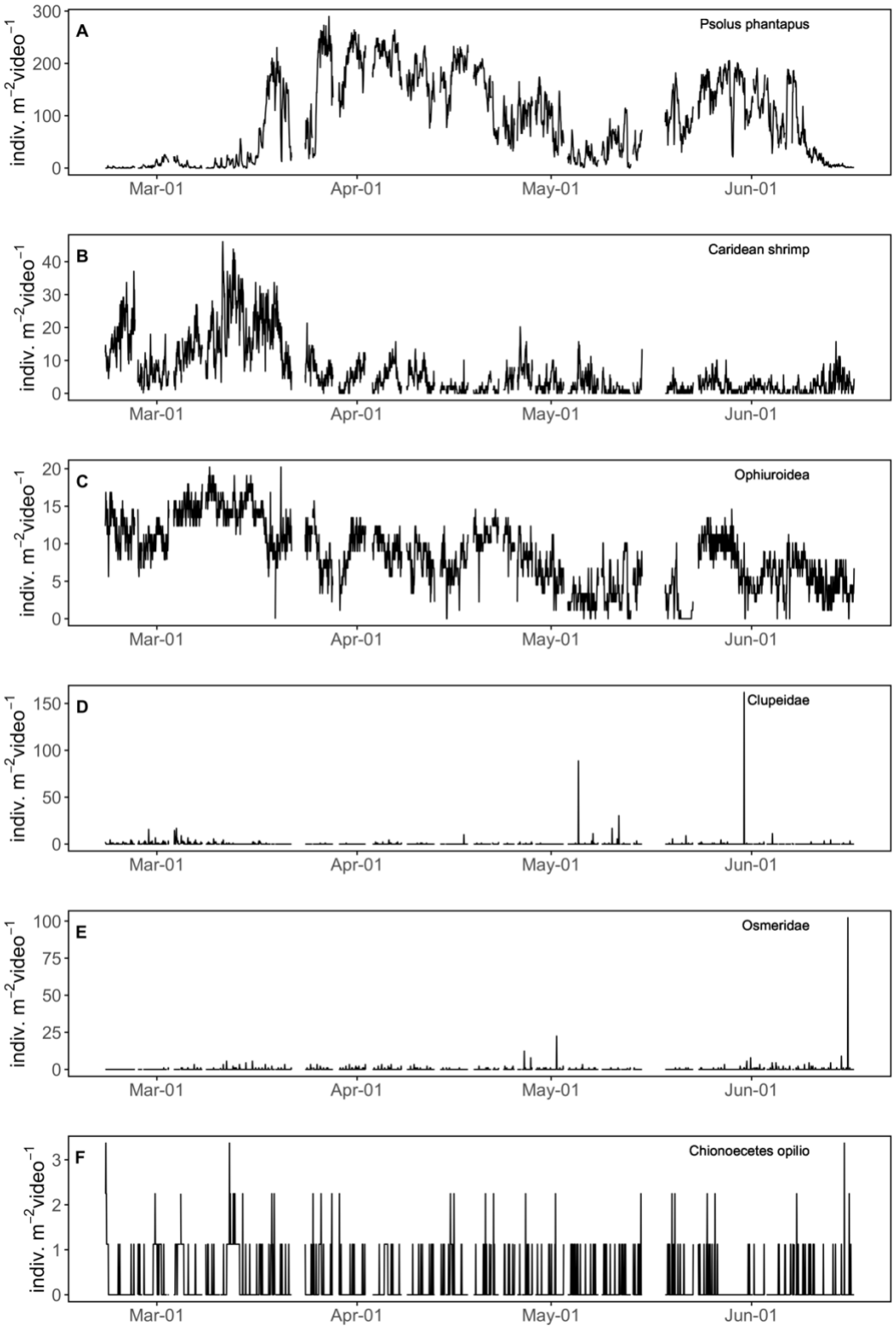

Figure 3.4. Time series of obsereved counts of the most common morphotaxa over the study period at the Holyrood Subsea Observatory. (A) *Psolus phantapus*, (B) Caridean shrimp, (C) Ophiuroidea, (D) Clupeidae, (E) Osmeridae, and (F) *Chionoecetes opilio.*

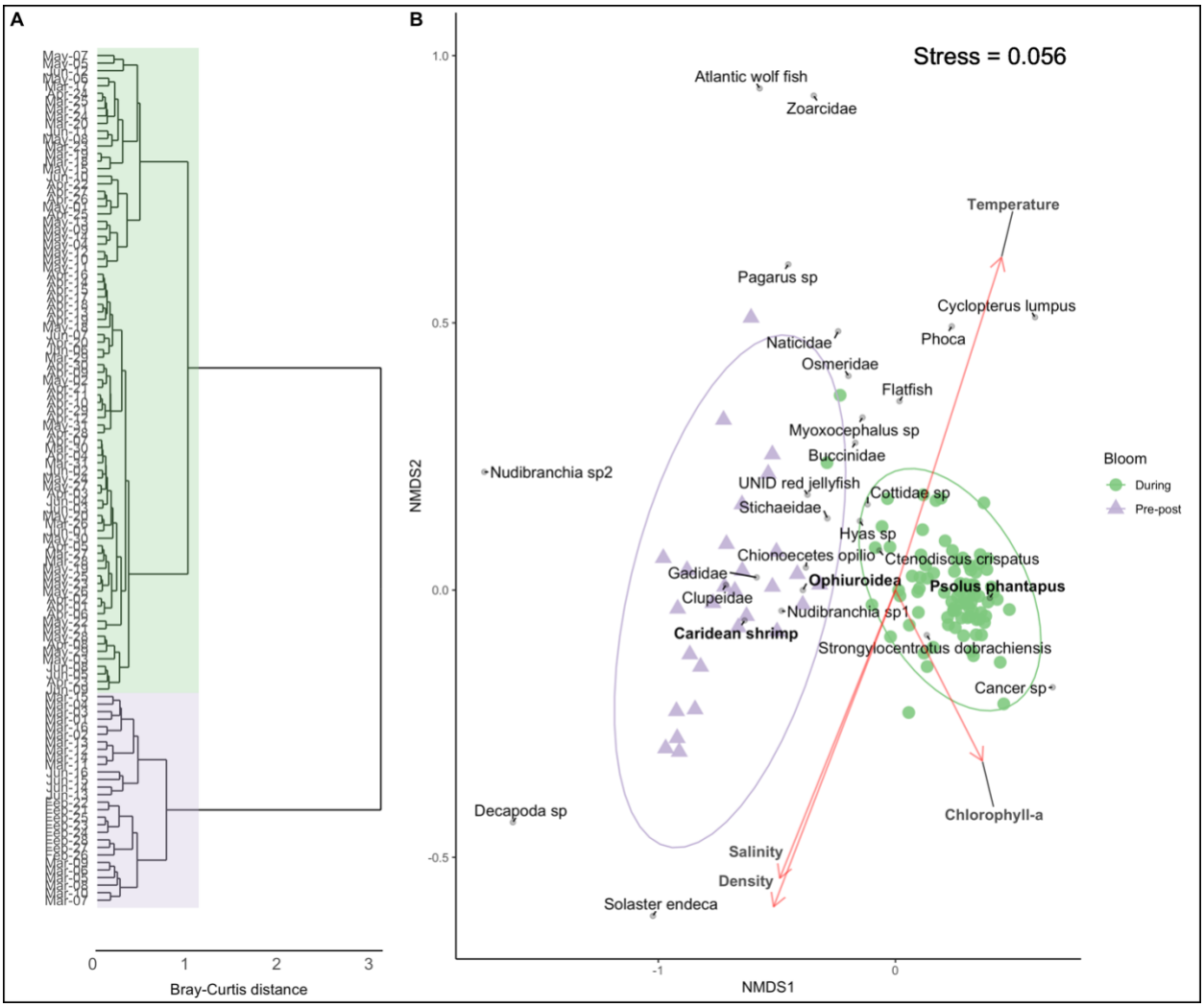

Figure 3.5. Graphical ordination of daily observations using the Bray-Curtis dissimilarity matrix, based on Hellinger-transformed visual count data from the Holyrood Subsea Observatory. (A) Dendrogram. (B) Non-metric multidimensional scaling showing the "During" and "Pre-post" bloom groups (coloured ellipses) identified by the dendrogram. Environmental variables were fitted onto the ordination. Arrows show direction of increasing values of each variable and the magnitude is proportional to the amount of correlation between the environmental variable and the ordination.

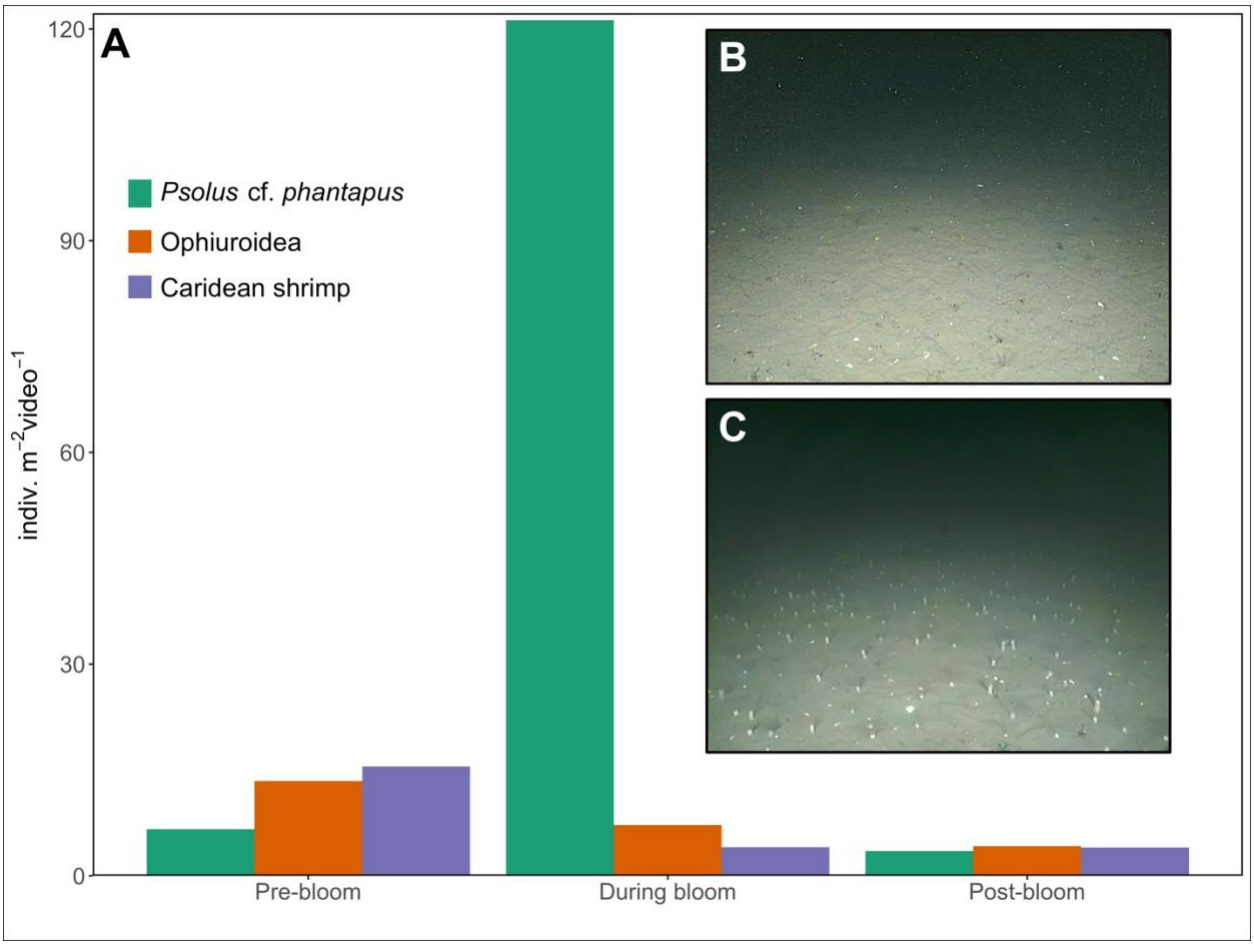

Figure 3.6. Visible counts of dominant taxa during the spring phytoplankton bloom, and pre-and-post bloom (A). *In-situ* image from the Holyrood Subsea Observatory pre- (B) and during (C) the 2021 spring phytoplankton bloom. Images B and C are colour-corrected to improve contrast between seafloor and sea cucumbers and reduce the vignette effect caused by the lights.

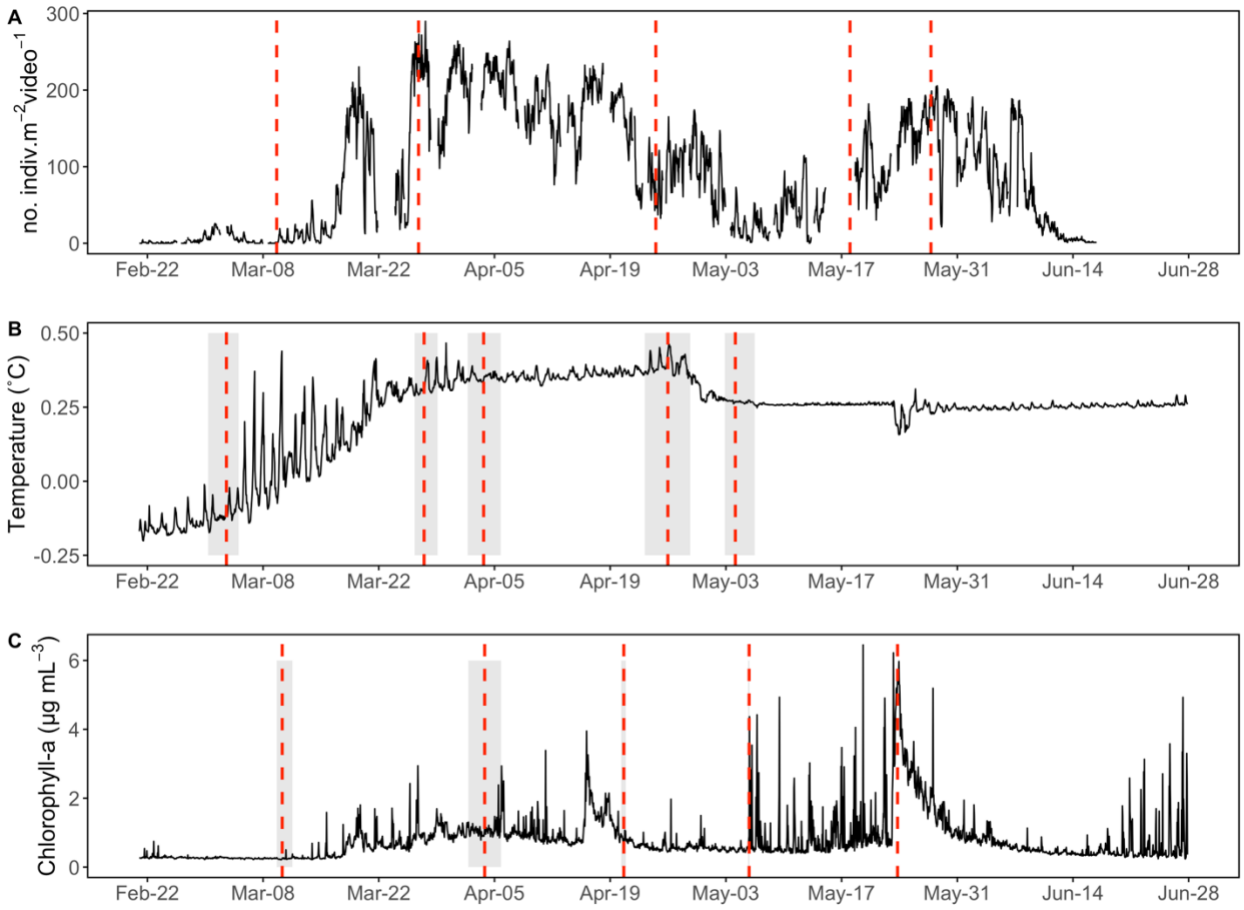

Figure 3.7. Daily averaged time series of *Psolus phantapus* (A), temperature (B), and chlorophyll-*a* (C), at the Holyrood Subsea Observatory. Black lines are time series, vertical dashed lines are the mean change points identified from the models. Grey bands represent 95% confidence intervals around the identified change point.

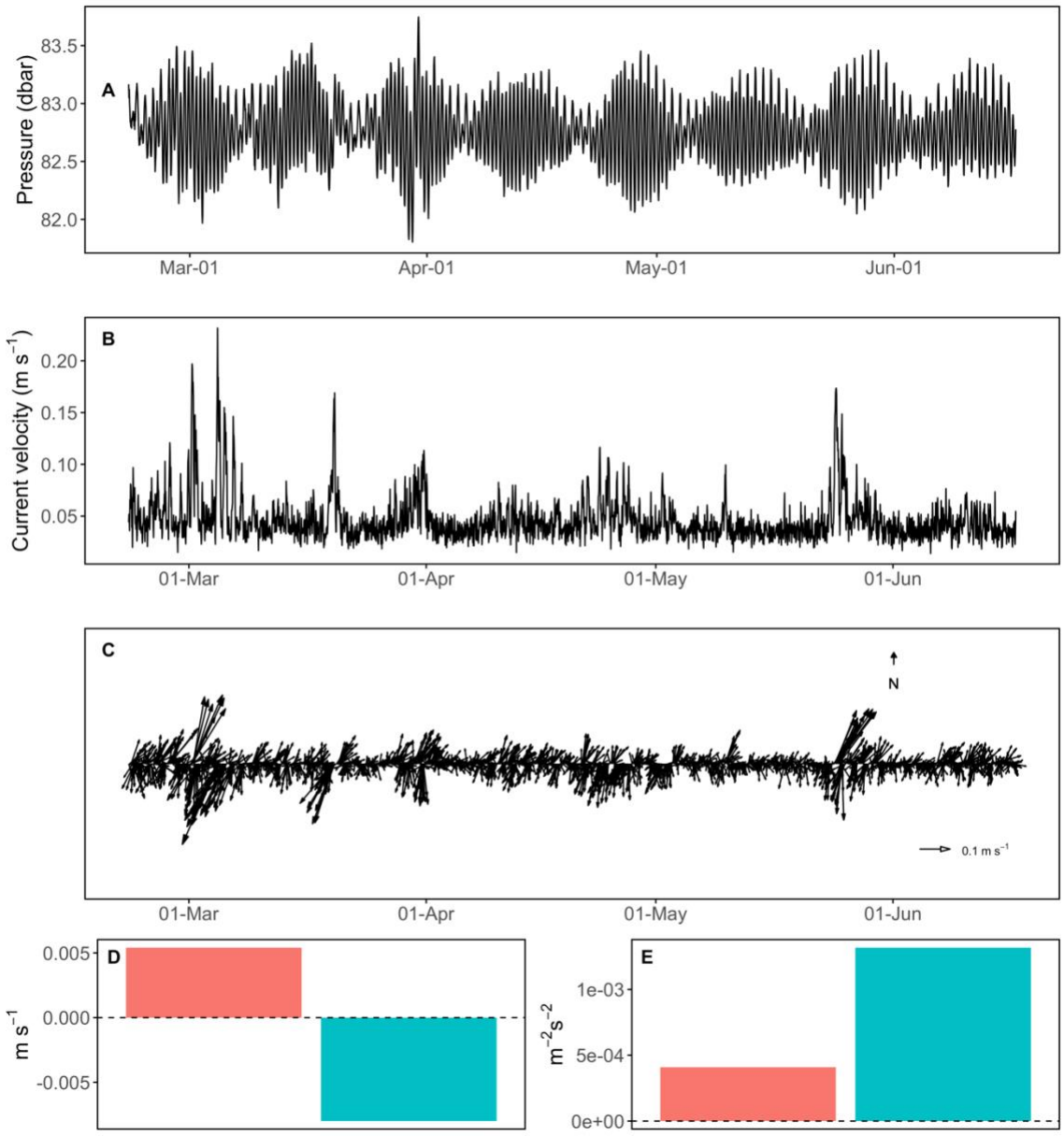

Figure 3.8. Data from the 400kHz ADCP at Holyrood Subsea Observatory. Time series of (A) pressure (dbar), and (B) current velocity magnitude (m s^{-1}) and (C) direction (˚True) between 1.49 m and 2.0 m above bottom. Bar plots show mean current velocity (D), and variation (E) over the entire time series for East-West (red) and North-South (blue) velocity components. All current data represent the near-seabed currents, and are the average values between 1.49 m and 2.0 m above bottom.

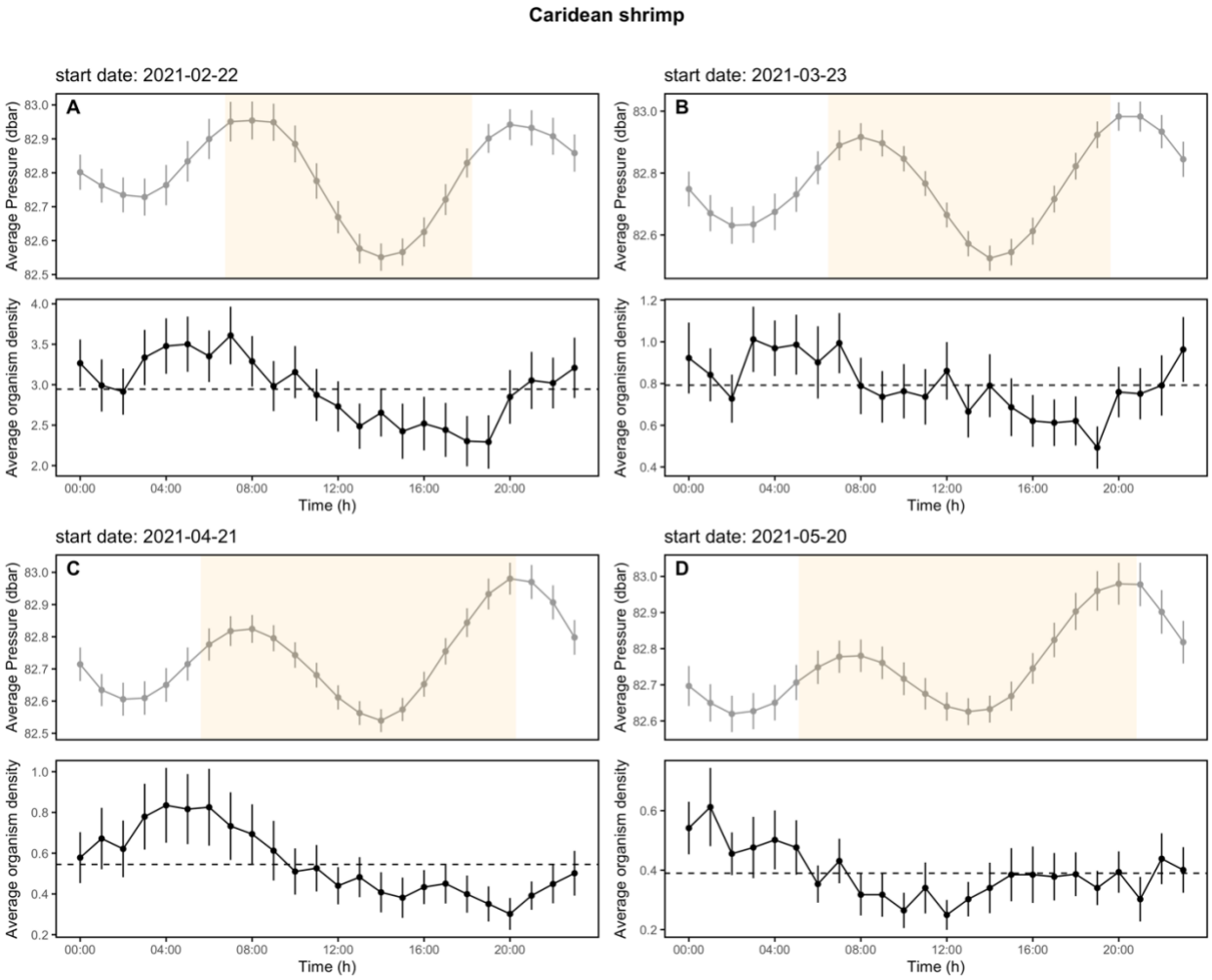

Figure 3.9. Waveform analysis for caridean shrimp. Points and vertical lines represent hourly measurements (pressure or counts) averaged over 28 days and standard error, respectively. Horizontal dashed line indicates the Midline Estimating Statistic of Rhythm, and the yellow rectangle denotes daylight hours.

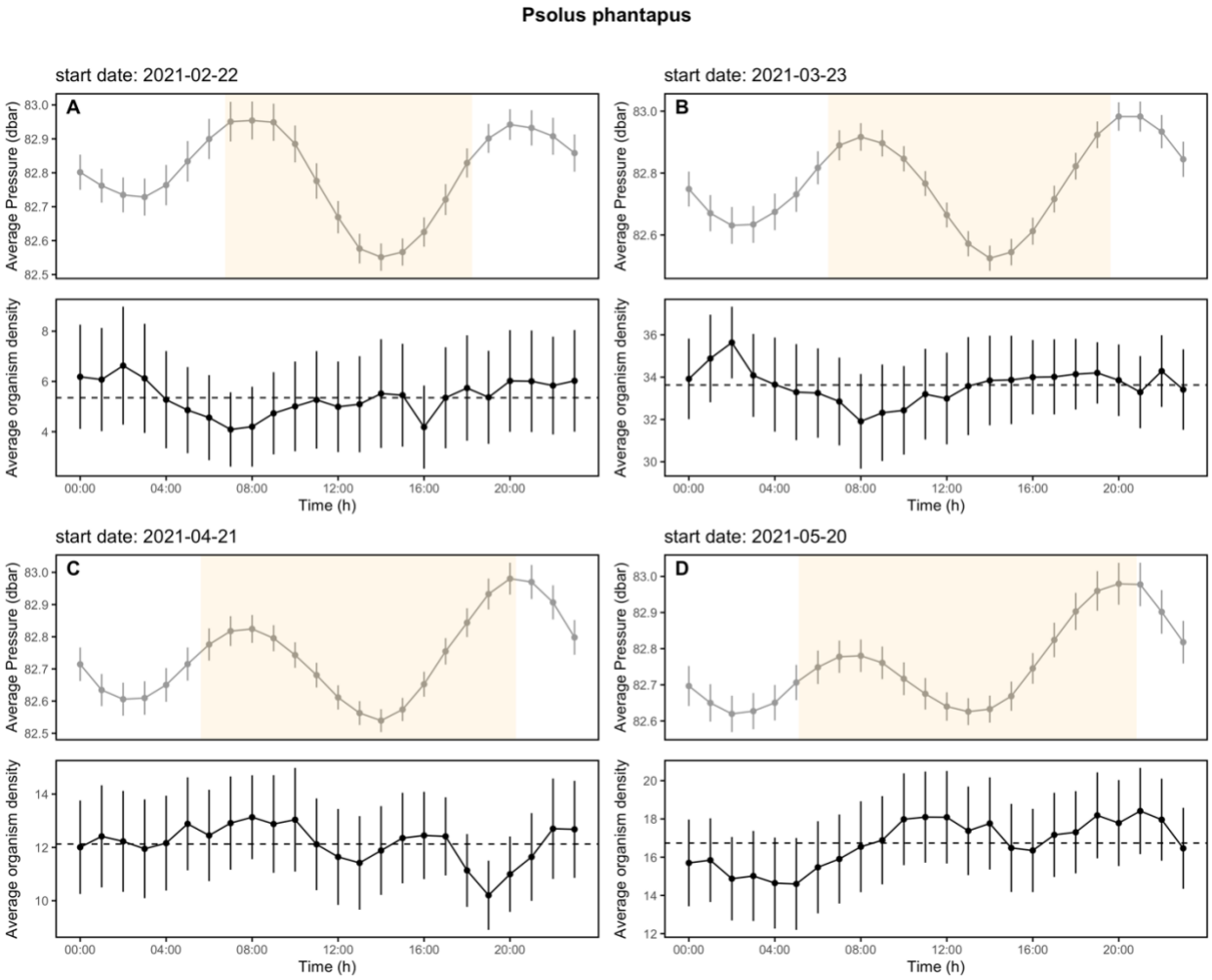

Figure 3.10. Waveform analysis for *Psolus phantapus*. Points and vertical lines represent hourly measurements (pressure or counts) averaged over 28 days and standard error, respectively. Horizontal dashed line indicates the Midline Estimating Statistic of Rhythm, and the yellow rectangle denotes daylight hours.

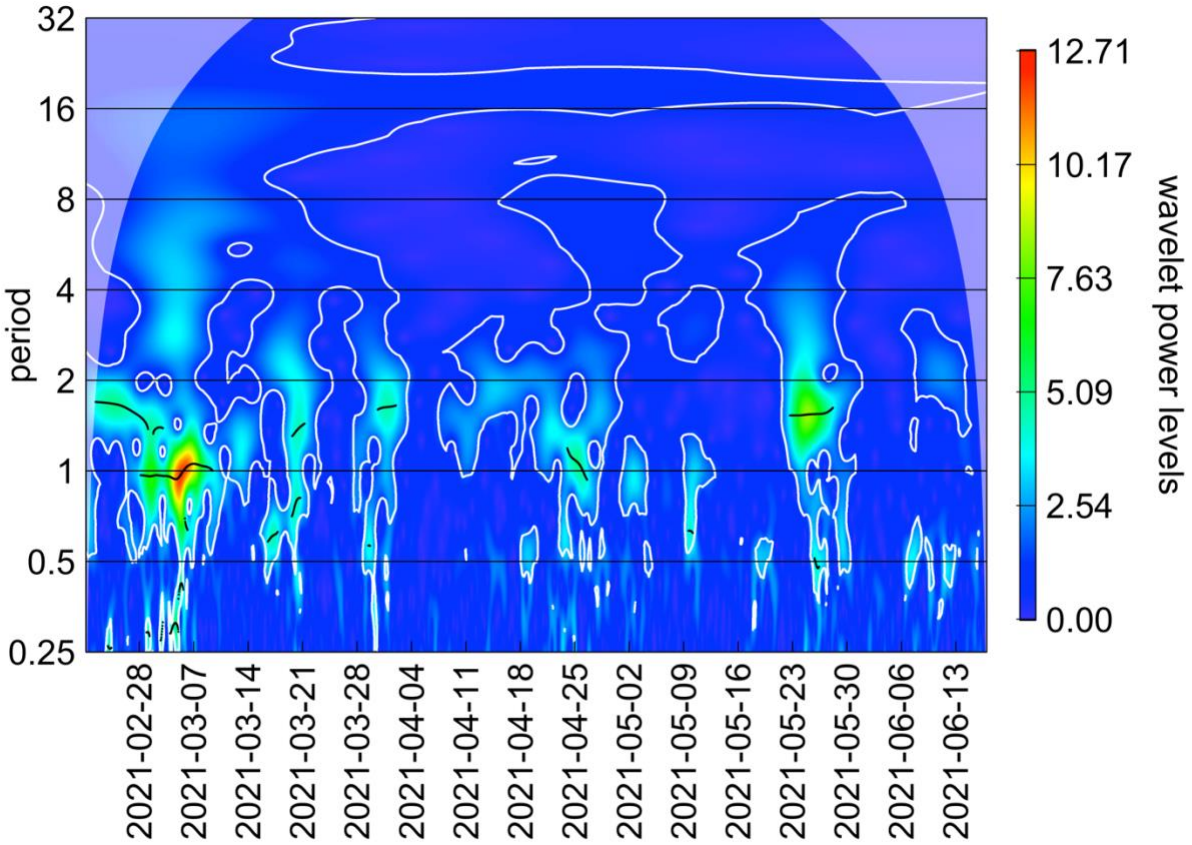

Figure S3.1. Wavelet transform of U (East-West) near seabed current velocity time series. Time (weekly intervals) is depicted on the x-axis, and the period (in days), or the amount of time for a single cycle to occur, is depicted on the y-axis. Colour indicates the wavelet power, or the strength of the periodic signal at a given time (red indicates a strong signal, blue indicates a weak signal). White lines indicate regions of statistically significant at the $\alpha = 0.05$ level.

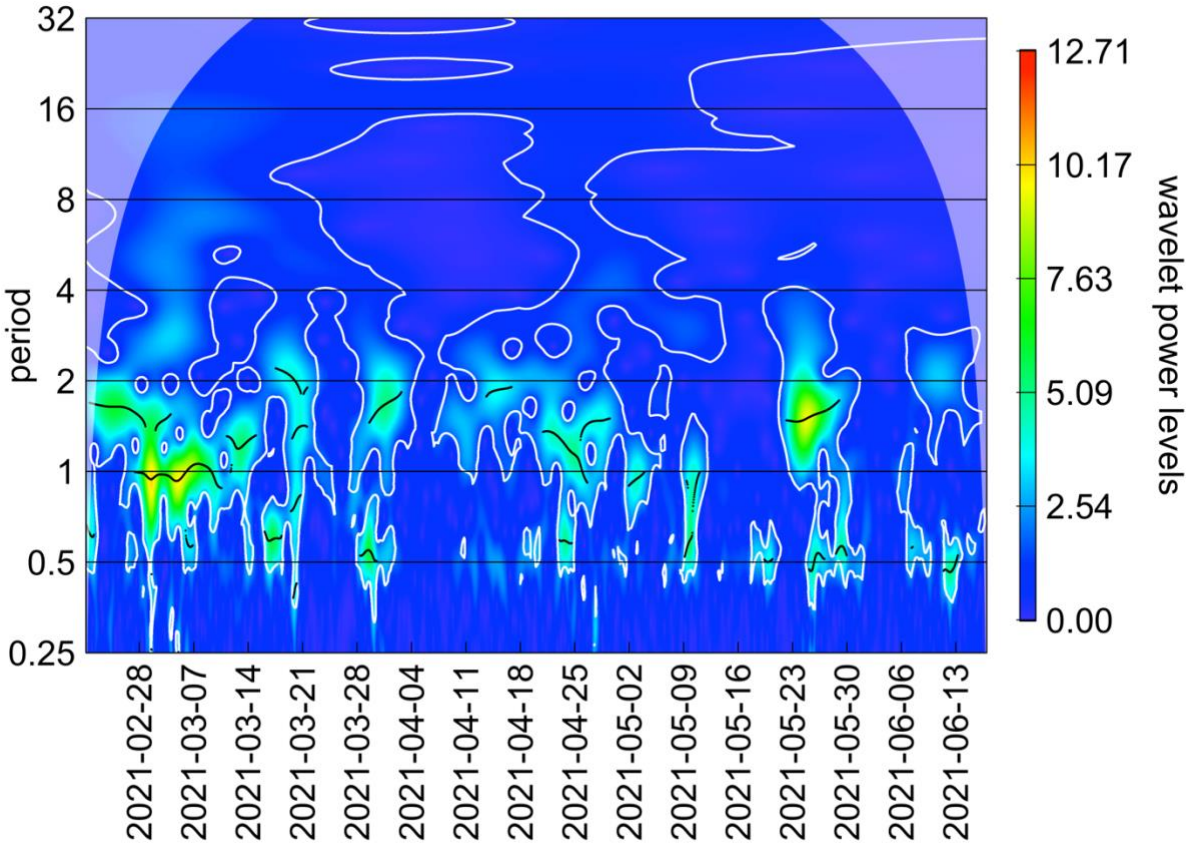

Figure S3.2. Wavelet transform of V (North-South) near seabed current velocity time series. Time (weekly intervals) is depicted on the x-axis, and the period (in days), or the amount of time for a single cycle to occur, is depicted on the y-axis. Colour indicates the wavelet power, or the strength of the periodic signal at a given time (red indicates a strong signal, blue indicates a weak signal). White lines indicate regions of statistically significant at the $\alpha = 0.05$ level.

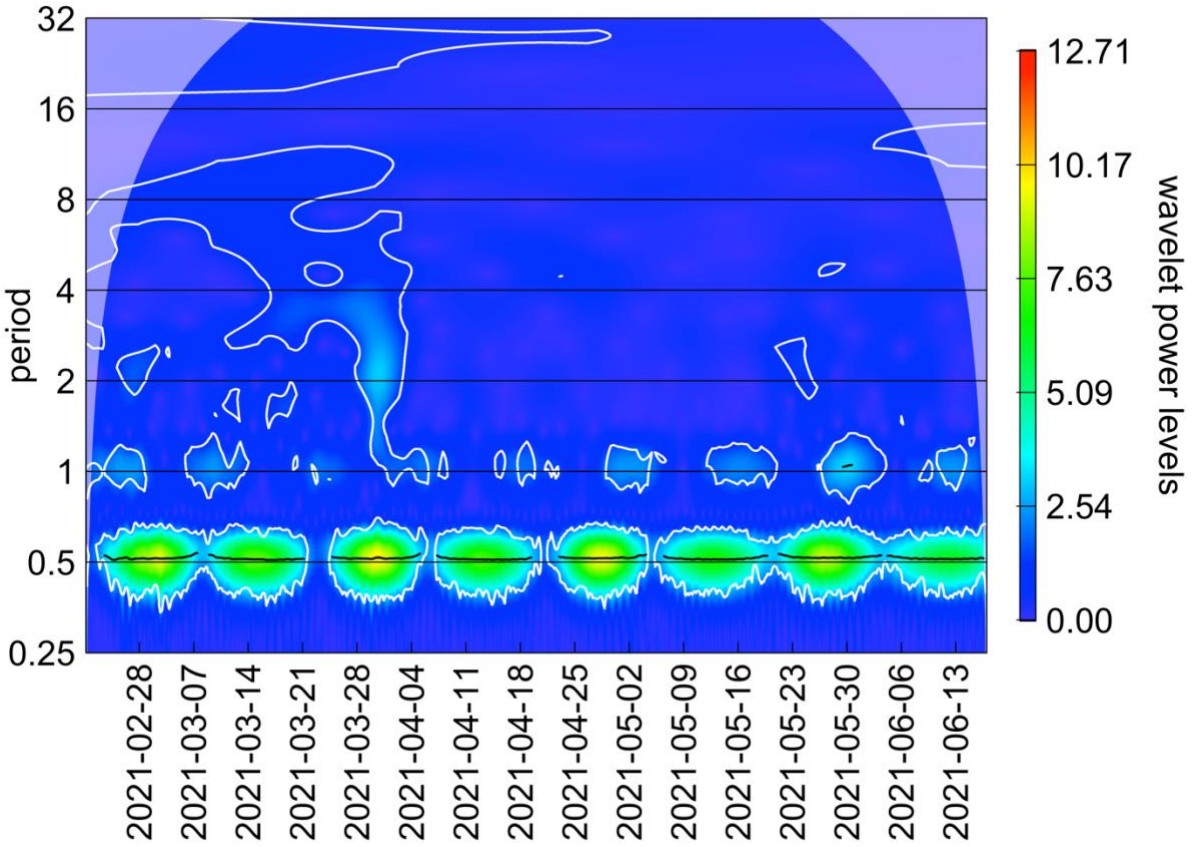

Figure S3.3. Wavelet transform of pressure time series. Time (weekly intervals) is depicted on the x-axis, and the period (in days), or the amount of time for a single cycle to occur, is depicted on the y-axis. Colour indicates the wavelet power, or the strength of the periodic signal at a given time (red indicates a strong signal, blue indicates a weak signal). White lines indicate regions of statistically significant at the $\alpha = 0.05$ level.

Chapter 4: Conclusion

Climate change is altering the abundance, composition, and timing of food availability to seafloor communities (Smith et al. 2008; Kahru et al. 2011). This is increasingly evident off the coast of British Columbia as loss of kelp subsidies to the continental margin adversely affects pink sea urchins (Filbee-Dexter and Scheibling 2014; Starko et al. 2019; McPherson et al. 2021). In Conception Bay, this may manifest as changes to the timing and strength of the spring phytoplankton bloom and result in a mismatch between food availability and important life history behaviours. Changes in food availability could fundamentally alter the abundance and distribution of key benthic species, and depending on the behaviours and ecological roles of those species would have far reaching implications for the structure and function of seafloor ecosystems (McClain et al. 2012; Woolley et al. 2016; Ani and Robson 2021). For example, pink sea urchins contribute to nutrient cycling as detritivores and by turning over surface sediments through locomotion (Boolootian et al. 1959; Robert and Juniper 2012). *Psolus* sea cucumbers are large burrowers that also contribute to bioturbation and bioirrigation, and consume phytodetritus and other organic matter that reach the seafloor from surface waters (Sun 2019). Changes in the abundance and distribution of these key species could directly and indirectly influence oxygen penetration depth, nutrient turnover, sediment properties, and associated infaunal communities.

Advances in ocean observing technology over the past two decades have enabled changes in seafloor ecosystems to be studied in high temporal resolution over the long-term (Levin et al. 2019). The case studies presented in this thesis highlight the utility of cabled seafloor observatories as tools for studying temporal dynamics of the abundance, behaviour, biodiversity, and distribution of epibenthic megafauna. In particular, these case studies quantify the precise timing of ecological phenomena *in situ* and species' relationships with environmental change over different time scales in two ocean systems. This thesis also highlighted opportunities to

integrate other data sources, such as bottom trawl surveys, to address some of the spatial limitations of seafloor observatories.

Chapter one examined the spatial and temporal scales of variation in physical and chemical ocean processes, and how they structure biological processes and influence the ecology of epibenthic megafauna in myriad ways. Considering the role of anthropogenic climate change in modifying these dynamics, high-resolution data collection in seafloor environments is necessary to understand the current state of marine populations and ecosystems, and how they may respond to future conditions. Although many methods are available for studying seafloor fauna, such as ROVs, drop-cameras, and bottom-contact fishing gear, the temporal resolution is inherently limited; high-frequency patterns, such as organism-level emergence behaviours or a population-level response to pulse disturbances, cannot be resolved. Cabled seafloor observatories provide the continuous data collection at high temporal resolution to capture these patterns in addition to long-term trends. This type of sampling is becoming increasingly useful as climate change affects ecosystem level properties, allowing for detailed monitoring to assess those impacts over time.

Chapter two assessed seasonal and interannual population dynamics of the deep-sea pink sea urchin *Strongylocentrotus fragilis* at the continental margin off the west coast of Vancouver Island, British Columbia using the Barkley Upper Slope platform of the NEPTUNE observatory. The density of *S. fragilis* on the continental margin was negatively affected by the 2013-2016 marine heatwave (Kintisch 2015) likely due to reduced kelp subsidies from coastal waters. A complex relationship was found between pink sea urchin density, dissolved oxygen, and sediment resuspension at the seafloor, likely resulting from seasonal upwelling dynamics mediated by the marine heatwave, as well as trawling and storm events that contribute to

nepheloid layer formation on the upper slope. The spatial limitation of the cabled observatory was addressed by analyzing biannual benthic trawl surveys from the continental shelf near the observatory and along the west coast of Vancouver Island. The decline in pink sea urchin density occurred over a large area, and that pink sea urchins appear to be undergoing a range-expansion into shallower water, similar to that observed in Southern California by Sato et al. (2017). It has been previously suggested that the proximal cause of this shoaling is the expansion of the oxygen minimum zone in the Northeast Pacific Ocean (Sato et al. 2017).

Pink sea urchins are detritivores that play an important role in nutrient cycling on the continental margin (Robert and Juniper 2012). They are also slow-moving, calcifying organisms that are particularly vulnerable to ocean acidification (Taylor et al. 2014; Barry et al. 2014). Additionally, the coastal kelps that pink sea urchins rely on for food are threatened by ocean warming and the increasing frequency and intensity of marine heatwaves (Starko et al. 2019; McPherson et al. 2021). NEPTUNE and other permanent cabled seafloor observatory networks enable high-resolution time-series data to be collected over multiple years. From these data it is possible to determine how populations respond to both pulse (e.g., marine heatwaves) and climate change-related (e.g., deoxygenation, ocean warming, ocean acidification) disturbances. The limited spatial resolution of cabled observatories can be augmented by including previously collected bottom trawl data to provide a more holistic understanding of how important continental margin megafauna are affected by ocean change in both space and time.

The new Holyrood Subsea Observatory deployed in Holyrood Inlet, Conception Bay, Newfoundland and Labrador, was used to characterize the epibenthic megafaunal community and their response to seasonal food input from the spring phytoplankton bloom. A marked shift in the dominant seafloor species visible in the field of view was driven by changes in seafloor

temperature and benthic chlorophyll-*a* concentration during the winter-spring transition. The unexpected emergence of the sea cucumber *Psolus phantapus* in the camera's field of view also accounted for much of the dissimilarity between the seafloor community observed during the bloom, and pre- and post-bloom. Bayesian changepoint models showed evidence for synchrony between *Psolus* emergence and the increase in seafloor temperature and the arrival of photosynthetic material to the seafloor from the spring phytoplankton bloom. The results presented in this thesis are the first from the Holyrood Subsea Observatory, which serve as a baseline characterization of the current state of the seafloor community in the inlet during the winter-spring transition. As the HSO infrastructure is intended for long-term deployment, additional data collected in other seasons and across years will enables comparisons of both environmental and biological variability patterns over time.

Augmenting existing observatory platforms will improve our ability to monitor ocean change and understand potential future outcomes for seafloor fauna. Ocean acidification is increasingly threatening marine fauna (Feely et al. 2016; Ashur et al. 2017), and fisheries (Wilson et al. 2020). New sensors, such as *p*CO2 and pH, that monitor ocean carbonate chemistry will be important for understanding the effects of ocean acidification, particularly on populations of calcifying megafauna like *S. fragilis* (Taylor et al. 2014; Barry et al. 2014). These instruments will be especially useful in Oxygen Minimum Zones where pCO_2 is already elevated, affecting important zooplankton species that provide a crucial carbon source to the deep sea (Hildebrandt et al. 2016; Garzke et al. 2016; Hammill et al. 2018; De Leo et al. 2018).

The high temporal resolution of seafloor observatories comes at a cost of spatial coverage. This limitation can be overcome by making use of additional sampling methods, such as bottom trawls (as in Chapter 2), ROVs, AUVs, gliders, drop cameras, other observatories, and

remote sensing technologies. At Barkley Canyon, ROV surveys have documented pink sea urchins feeding within the OMZ, and the recent addition of a video camera at the Barkley Node downslope from the BCUS platform will provide additional insight into the potential downslope migration of *S. fragilis* when food is scarce, or upwelling is disrupted. In Conception Bay, a complementary research project used a drop camera system to collect video-based species assemblage and distribution data in combination with multibeam echosounder data to build seasonal, full-coverage benthic habitat maps (Charmley et al. 2022). This will facilitate comparisons of biodiversity estimates from different sampling methods and enhance the spatial coverage of seafloor monitoring in the Holyrood Inlet.

Although the use of underwater imagery is a less invasive method of seafloor data collection than bottom-contact fishing gear (Matabos et al. 2016; Durden et al. 2016), there are several challenges that need to be overcome. First, the scales at which imagery are collected does always not match the scales of oceanographic and ecological processes. Imagery studies generally suffer from low spatial resolution and little to no replication of sampling efforts in space. Cabled seafloor observatories and autonomous landers make it possible to collect high-temporal resolution imagery at the expense of spatial coverage. It would be possible to deploy multiple landers or fixed platforms equipped with cameras in an area to improve spatial coverage, and networks of camera systems have already been established in several regions around the world (e.g., HAUSTGARTEN, NEPTUNE, VENUS, OBSEA, EMSO). Higher spatial resolution can be achieved using ROV or drop-camera transect surveys, even producing high-pixel resolution photomosaics of the seafloor. However, this type of sampling is rarely repeated due to budget constraints and offers only a temporal snapshot of an ecosystem. One possible solution lies in the development of autonomous underwater vehicles (AUVs) and gliders

designed for long-term deployment at fixed underwater docking stations. Such systems could be equipped with cameras and oceanographic sensors and programmed to conduct surveys over a specified area at a particular sampling interval, then return to the docking station to recharge and transmit data (Hobson et al. 2007). Advances in computer vision (CV) and underwater robotics are supporting these developments (e.g., Hobson et al. 2007; Kimball et al. 2018; Yazdani et al. 2020), which will reduce costs associated with ship-time, enable sampling during typically sub-optimal conditions (e.g., stormy winters), and improve both the spatial and temporal coverage of marine ecosystems.

Another limitation of imagery-based studies is the storage and processing of the massive quantities of video data collected by imaging platforms; it is impossible for manual annotation to keep pace with the volume of video data collected each day. Recent developments in CV and artificial intelligence have enabled machine-assisted annotation of images and video (Schoening et al. 2012; Piechaud et al. 2019; Stanchev et al. 2020; Chen and Liu 2020; McIntosh et al. 2020; Harrison et al. 2021), but require large amounts of labelled data to train effective models. To fill that need, open-source platforms like FathomNet have been developed for researchers and ocean enthusiasts alike to provide a repository of image annotations to crowd-source data for training models (Katija et al. 2022). FathomNet also allows users to upload pre-trained machine learning models to make them freely available to the wider research community to help address the bottleneck of image processing (Appendix 2).

Cameras deployed long term are subject to biofouling that may obscure the camera lens, particularly shallow-water coastal observatories that are installed within the photic zone (Bailey et al. 2019; Aguzzi et al. 2020). Image quality is also a major challenge and is influenced by turbidity, natural and artificial light, and camera angle with respect to the seafloor, among other

factors, all of which affect data availability and quality. Furthermore, artificial lighting may have negative effects on underwater fauna (Herring et al. 1999), and yield biased abundance estimates and behavioural observations in species that exhibit phototaxis (Widder et al. 2005; Chauvet et al. 2018; Geoffroy et al. 2021). Optimizing camera position and sampling schedules to capture species and processes of interest is a crucial component for underwater imagery collection. Additionally, many taxa cannot be identified to species based on an *in situ* image alone, thus the taxonomic resolution possible from imagery-based studies is inherently limited. While *in situ* imagery cannot fully replace physical sampling for biodiversity studies, the high temporal resolution possible from seafloor observatories and the low-impact of other sources of imagery cement cameras as invaluable tools for ecosystem monitoring.

Seafloor observatories provide unprecedented temporal resolution for data collection and are a powerful approach to monitoring the benthos. Augmenting existing observatories with new sensors to measure ocean acidification at depth and developing docking stations for underwater gliders and automated underwater vehicles to enhance spatial coverage are two promising avenues to advance ocean observing research. Additionally, designing sampling and monitoring plans that explicitly incorporate sampling efforts over both space (e.g., acoustic surveys with drop cameras, trawl surveys) and time (e.g., fixed-point observatories) will improve our capacity to capture current ecological patterns and assess future changes. Making use of as many approaches as possible in a given location will provide a more holistic understanding of the ecosystem and inform management and conservation in the face of increasing human pressure.

4.1 References

Aguzzi, J., Iveša, N., Gelli, M., Costa, C., Gavrilovic, A., Cukrov, N., Cukrov, M., Cukrov, N., Omanovic, D., Štifanić, M., Marini, S., Piria, M., Azzurro, E., Fanelli, E., and Danovaro,

R. 2020. Ecological video monitoring of Marine Protected Areas by underwater cabled surveillance cameras. Marine Policy **119**: 104052. doi:10.1016/j.marpol.2020.104052.

Ani, C.J., and Robson, B. 2021. Responses of marine ecosystems to climate change impacts and their treatment in biogeochemical ecosystem models. Marine Pollution Bulletin **166**: 112223. doi:10.1016/j.marpolbul.2021.112223.

Ashur, M.M., Johnston, N.K., and Dixson, D.L. 2017. Impacts of Ocean Acidification on Sensory Function in Marine Organisms. Integrative and Comparative Biology **57**(1): 63–80. doi:10.1093/icb/icx010.

Bailey, K., Steinberg, C., Davies, C., Galibert, G., Hidas, M., McManus, M.A., Murphy, T., Newton, J., Roughan, M., and Schaeffer, A. 2019. Coastal Mooring Observing Networks and Their Data Products: Recommendations for the Next Decade. Front. Mar. Sci. **6**: 180. doi:10.3389/fmars.2019.00180.

Barry, J.P., Lovera, C., Buck, K.R., Peltzer, E.T., Taylor, J.R., Walz, P., Whaling, P.J., and Brewer, P.G. 2014. Use of a Free Ocean CO $_2$ Enrichment (FOCE) System to Evaluate the Effects of Ocean Acidification on the Foraging Behavior of a Deep-Sea Urchin. Environ. Sci. Technol. **48**(16): 9890–9897. doi:10.1021/es501603r.

Boolootian, R.A., Giese, A.C., Tucker, J.S., and Farmanfarmaian, A. 1959. A contribution to the biology of a deep sea echinoid, Allocentrotus fragilis (Jackson). The Biological Bulletin **116**(3): 362–372. doi:10.2307/1538946.

Charmley, K., Baker, K., and Robert, K. 2022. Seasonal Change Between Benthic Habitat Maps in a Sub-Arctic Ecosystem. Virtual.

Chauvet, P., Metaxas, A., Hay, A.E., and Matabos, M. 2018. Annual and seasonal dynamics of deep-sea megafaunal epibenthic communities in Barkley Canyon (British Columbia, Canada): A response to climatology, surface productivity and benthic boundary layer variation. Progress in Oceanography **169**: 89–105. doi:10.1016/j.pocean.2018.04.002.

Chen, S., and Liu, Y. 2020. Migration Learning Based on Computer Vision and Its Application in Ocean Image Processing. Journal of Coastal Research **104**(sp1). doi:10.2112/JCR-SI104-051.1.

De Leo, F.C., Ogata, B., Sastri, A.R., Heesemann, M., Mihály, S., Galbraith, M., and Morley, M.G. 2018. High-frequency observations from a deep-sea cabled observatory reveal seasonal overwintering of Neocalanus spp. in Barkley Canyon, NE Pacific: Insights into particulate organic carbon flux. Progress in Oceanography **169**: 120–137. doi:10.1016/j.pocean.2018.06.001.

Durden, J.M., Schoening, T., Althaus, F., Friedman, A., Garcia, R., Glover, A.G., Greinert, J., Jacobsen Stout, N., Jones, D.O.B., Jordt, A., Kaeli, J.W., Kuhnz, L.A., Lindsay, D., Morris, K.J., Nattkemper, T.W., Osterloff, J., Ruhl, H.A., Singh, H., Tran, M., and Bett, B.J. 2016. Perspectives in visual imaging for marine biology and ecology: From acquisition to understanding. Oceanography and Marine Biology: an Annual Review **54**: 1–72. doi:10.1201/9781315368597.

Feely, R.A., Alin, S.R., Carter, B., Bednaršek, N., Hales, B., Chan, F., Hill, T.M., Gaylord, B., Sanford, E., Byrne, R.H., Sabine, C.L., Greeley, D., and Juranek, L. 2016. Chemical and biological impacts of ocean acidification along the west coast of North America. Estuarine, Coastal and Shelf Science **183**: 260–270. doi:10.1016/j.ecss.2016.08.043.

Filbee-Dexter, K., and Scheibling, R. 2014. Detrital kelp subsidy supports high reproductive condition of deep-living sea urchins in a sedimentary basin. Aquat. Biol. **23**(1): 71–86. doi:10.3354/ab00607.

Garzke, J., Hansen, T., Ismar, S.M.H., and Sommer, U. 2016. Combined Effects of Ocean Warming and Acidification on Copepod Abundance, Body Size and Fatty Acid Content. PLoS ONE **11**(5): e0155952. doi:10.1371/journal.pone.0155952.

Geoffroy, M., Langbehn, T., Priou, P., Varpe, Ø., Johnsen, G., Le Bris, A., Fisher, J.A.D., Daase, M., McKee, D., Cohen, J., and Berge, J. 2021. Pelagic organisms avoid white, blue, and red artificial light from scientific instruments. Sci Rep **11**(1): 14941. doi:10.1038/s41598-021-94355-6.

Hammill, E., Johnson, E., Atwood, T.B., Harianto, J., Hinchliffe, C., Calosi, P., and Byrne, M. 2018. Ocean acidification alters zooplankton communities and increases top-down pressure of a cubozoan predator. Glob Change Biol **24**(1): e128–e138. doi:10.1111/gcb.13849.

Harrison, D., De Leo, F.C., Gallin, W.J., Mir, F., Marini, S., and Leys, S.P. 2021. Machine Learning Applications of Convolutional Neural Networks and Unet Architecture to Predict and Classify Demosponge Behavior. Water **13**(18): 2512. doi:10.3390/w13182512.

Herring, P.J., Gaten, E., and Shelton, P.M.J. 1999. Are vent shrimps blinded by science? Nature **398**(6723): 116–116. doi:10.1038/18142.

Hildebrandt, N., Sartoris, F.J., Schulz, K.G., Riebesell, U., and Niehoff, B. 2016. Ocean acidification does not alter grazing in the calanoid copepods Calanus finmarchicus and Calanus glacialis. ICES Journal of Marine Science **73**(3): 927–936. doi:10.1093/icesjms/fsv226.

Hobson, B.W., McEwen, R.S., Erickson, J., Hoover, T., McBride, L., Shane, F., and Bellingham, J.G. 2007. The Development and Ocean Testing of an AUV Docking Station for a 21" AUV. *In* OCEANS 2007. IEEE, Vancouver, BC. pp. 1–6. doi:10.1109/OCEANS.2007.4449318.

Kahru, M., Brotas, V., Manzano-Sarabia, M., and Mitchell, B.G. 2011. Are phytoplankton blooms occurring earlier in the Arctic? Global Change Biology **17**(4): 1733–1739. doi:10.1111/j.1365-2486.2010.02312.x.

Katija, K., Orenstein, E., Schlining, B., Lundsten, L., Barnard, K., Sainz, G., Boulais, O., Cromwell, M., Butler, E., Woodward, B., and Bell, K.C. 2022, March 10. FathomNet: A global image database for enabling artificial intelligence in the ocean. arXiv. Available from http://arxiv.org/abs/2109.14646 [accessed 17 May 2022].

Kimball, P.W., Clark, E.B., Scully, M., Richmond, K., Flesher, C., Lindzey, L.E., Harman, J., Huffstutler, K., Lawrence, J., Lelievre, S., Moor, J., Pease, B., Siegel, V., Winslow, L., Blankenship, D.D., Doran, P., Kim, S., Schmidt, B.E., and Stone, W.C. 2018. The ARTEMIS under-ice AUV docking system. Journal of Field Robotics **35**(2): 299–308. doi:10.1002/rob.21740.

Kintisch, E. 2015. 'The Blob' invades Pacific, flummoxing climate experts. Science **348**(6230): 17–18. doi:10.1126/science.348.6230.17.

Levin, L.A., Bett, B.J., Gates, A.R., Heimbach, P., Howe, B.M., Janssen, F., McCurdy, A., Ruhl, H.A., Snelgrove, P., Stocks, K.I., Bailey, D., Baumann-Pickering, S., Beaverson, C., Benfield, M.C., Booth, D.J., Carreiro-Silva, M., Colaço, A., Eblé, M.C., Fowler, A.M., Gjerde, K.M., Jones, D.O.B., Katsumata, K., Kelley, D., Le Bris, N., Leonardi, A.P., Lejzerowicz, F., Macreadie, P.I., McLean, D., Meitz, F., Morato, T., Netburn, A., Pawlowski, J., Smith, C.R., Sun, S., Uchida, H., Vardaro, M.F., Venkatesan, R., and

Weller, R.A. 2019. Global Observing Needs in the Deep Ocean. Front. Mar. Sci. **6**: 241. doi:10.3389/fmars.2019.00241.

Matabos, M., Best, M., Blandin, J., Hoeberechts, M., Juniper, S.K., Pirenne, B., Robert, K., Ruhl, H.A., Sarrazin, J., and Vardaro, M. 2016. Seafloor Observatories. *In* Biological Sampling in the Deep Sea. *Edited by* M.R. Clark, M. Consalvey, and A.A. Rowden. John Wiley & Sons, Ltd, Chichester, UK. pp. 306–337. doi:10.1002/9781118332535.ch14.

McClain, C.R., Allen, A.P., Tittensor, D.P., and Rex, M.A. 2012. Energetics of life on the deep seafloor. Proc. Natl. Acad. Sci. U.S.A. **109**(38): 15366–15371. doi:10.1073/pnas.1208976109.

McIntosh, D., Marques, T.P., Albu, A.B., Rountree, R., and De Leo, F. 2020, November 28. Movement Tracks for the Automatic Detection of Fish Behavior in Videos. arXiv. Available from http://arxiv.org/abs/2011.14070 [accessed 25 July 2022].

McPherson, M.L., Finger, D.J.I., Houskeeper, H.F., Bell, T.W., Carr, M.H., Rogers-Bennett, L., and Kudela, R.M. 2021. Large-scale shift in the structure of a kelp forest ecosystem co-occurs with an epizootic and marine heatwave. Communications Biology **4**(298). doi:10.1038/s42003-021-01827-6.

Piechaud, N., Hunt, C., Culverhouse, P., Foster, N., and Howell, K. 2019. Automated identification of benthic epifauna with computer vision. Mar. Ecol. Prog. Ser. **615**: 15–30. doi:10.3354/meps12925.

Robert, K., and Juniper, S. 2012. Surface-sediment bioturbation quantified with cameras on the NEPTUNE Canada cabled observatory. Mar. Ecol. Prog. Ser. **453**: 137–149. doi:10.3354/meps09623.

Sato, K.N., Levin, L.A., and Schiff, K. 2017. Habitat compression and expansion of sea urchins in response to changing climate conditions on the California continental shelf and slope (1994–2013). Deep Sea Research Part II: Topical Studies in Oceanography **137**: 377–389. doi:10.1016/j.dsr2.2016.08.012.

Schoening, T., Bergmann, M., Ontrup, J., Taylor, J., Dannheim, J., Gutt, J., Purser, A., and Nattkemper, T.W. 2012. Semi-Automated Image Analysis for the Assessment of Megafaunal Densities at the Arctic Deep-Sea Observatory HAUSGARTEN. PLoS ONE **7**(6): e38179. doi:10.1371/journal.pone.0038179.

Smith, C., Deleo, F., Bernardino, A., Sweetman, A., and Arbizu, P. 2008. Abyssal food limitation, ecosystem structure and climate change. Trends in Ecology & Evolution **23**(9): 518–528. doi:10.1016/j.tree.2008.05.002.

Stanchev, L., Egbert, H., and Ruttenberg, B. 2020. Automating Deep-Sea Video Annotation Using Machine Learning. *In* 2020 IEEE 14th International Conference on Semantic Computing (ICSC). pp. 17–24. doi:10.1109/ICSC.2020.00010.

Starko, S., Bailey, L.A., Creviston, E., James, K.A., Warren, A., Brophy, M.K., Danasel, A., Fass, M.P., Townsend, J.A., and Neufeld, C.J. 2019. Environmental heterogeneity mediates scale-dependent declines in kelp diversity on intertidal rocky shores. PLoS ONE **14**(3): e0213191. doi:https://doi.org/10.1371/journal.pone.0213191.

Sun, J. 2019. A study of dendrochirotid sea cucumbers with a focus on Cucumaria frondosa and its potential use in integrated multi-trophic aquaculture. PhD, Memorial University of Newfoundland, St. John's, NL.

Taylor, J.R., Lovera, C., Whaling, P.J., Buck, K.R., Pane, E.F., and Barry, J.P. 2014. Physiological effects of environmental acidification in the deep-sea urchin

Strongylocentrotus fragilis. Biogeosciences **11**(5): 1413–1423. doi:10.5194/bg-11-1413-2014.

Widder, E.A., Robison, B.H., Reisenbichler, K.R., and Haddock, S.H.D. 2005. Using red light for in situ observations of deep-sea fishes. Deep Sea Research Part I: Oceanographic Research Papers **52**(11): 2077–2085. doi:10.1016/j.dsr.2005.06.007.

Wilson, T.J.B., Cooley, S.R., Tai, T.C., Cheung, W.W.L., and Tyedmers, P.H. 2020. Potential socioeconomic impacts from ocean acidification and climate change effects on Atlantic Canadian fisheries. PLoS ONE **15**(1): e0226544. doi:10.1371/journal.pone.0226544.

Woolley, S.N.C., Tittensor, D.P., Dunstan, P.K., Guillera-Arroita, G., Lahoz-Monfort, J.J., Wintle, B.A., Worm, B., and O'Hara, T.D. 2016. Deep-sea diversity patterns are shaped by energy availability. Nature **533**(7603): 393–396. doi:10.1038/nature17937.

Yazdani, A.M., Sammut, K., Yakimenko, O., and Lammas, A. 2020. A survey of underwater docking guidance systems. Robotics and Autonomous Systems **124**: 103382. doi:10.1016/j.robot.2019.103382.

Appendix 1: Field of view calculations

A1.1 Barkley Canyon Upper Slope

2013 field of view

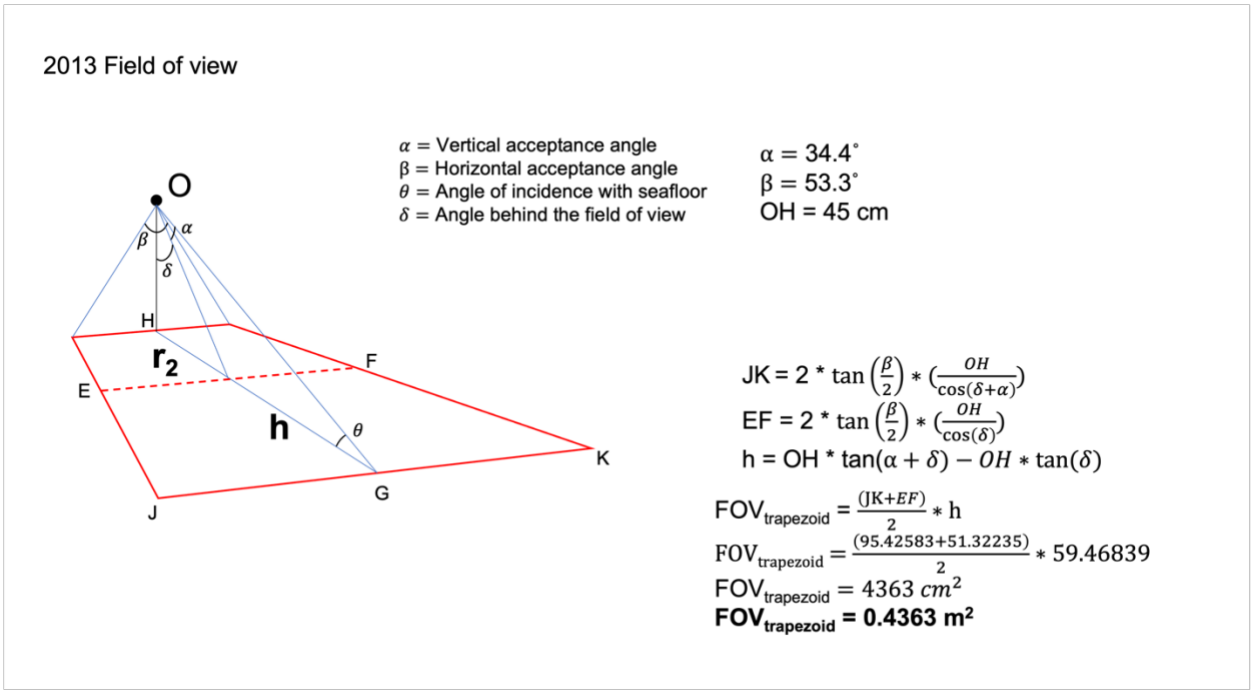

This field of view is calculated as the area of a trapezoid, where the width of the top and bottom are determined by doubling the tangent of one half the horizontal acceptance angle multiplied by the ratio of the camera height to the cosine of the angle incident with the camera lens at the top and bottom of the visible field of view (defined by the vertical acceptance angles. The calculated value was close to that reported in Chauvet (2018), so we used their previously published value of 0.5 m^2.

2014-2015 field of view

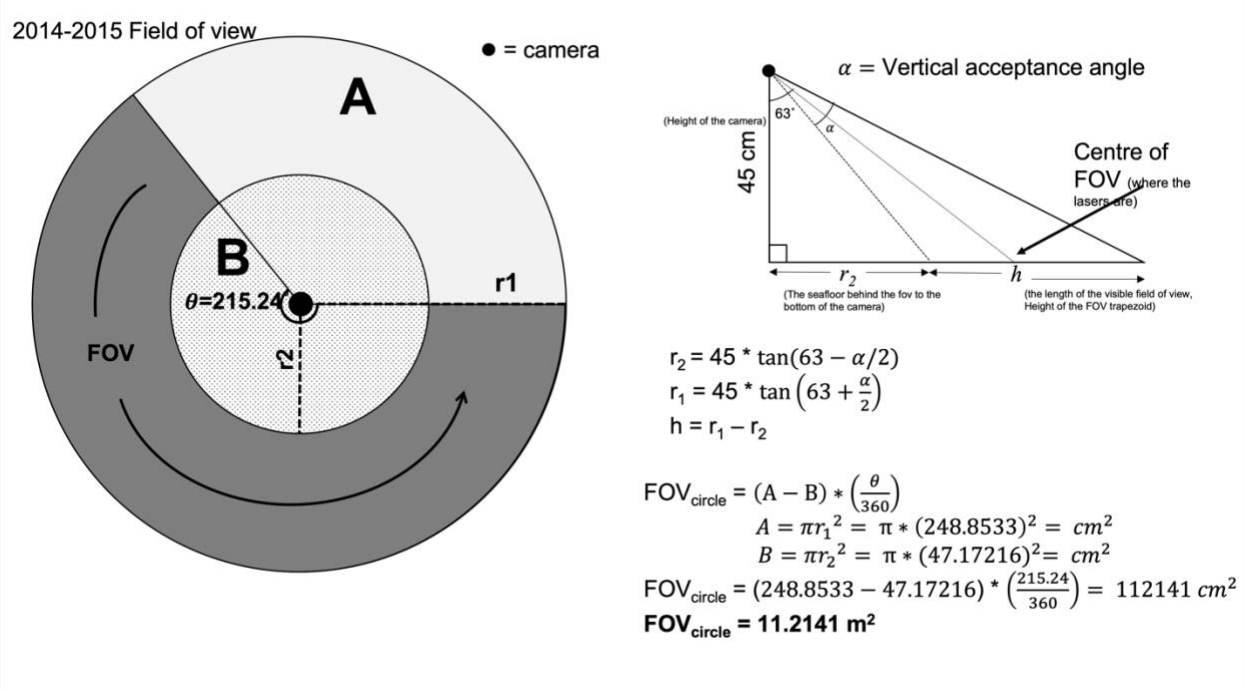

The area covered by the 215.24˚ pan angle can be calculated by subtracting the area of a large circle by the area of a small circle (non-visible area), where the radius of the large circle is defined by the camera height multiplied by tangent of the known fixed tilt angle of the camera plus one half the vertical acceptance angle, and the area of the small circle is defined by the camera height multiplied by tangent of the known fixed tilt angle of the camera minus one half the vertical acceptance angle. The difference between the large and small circle leaves the visible area of the seafloor for a 360˚ pan. This area is multiplied by the fraction of a circle corresponding to the total pan angle (215.24˚/360˚) to get the fraction of the total area that is visible to the camera.

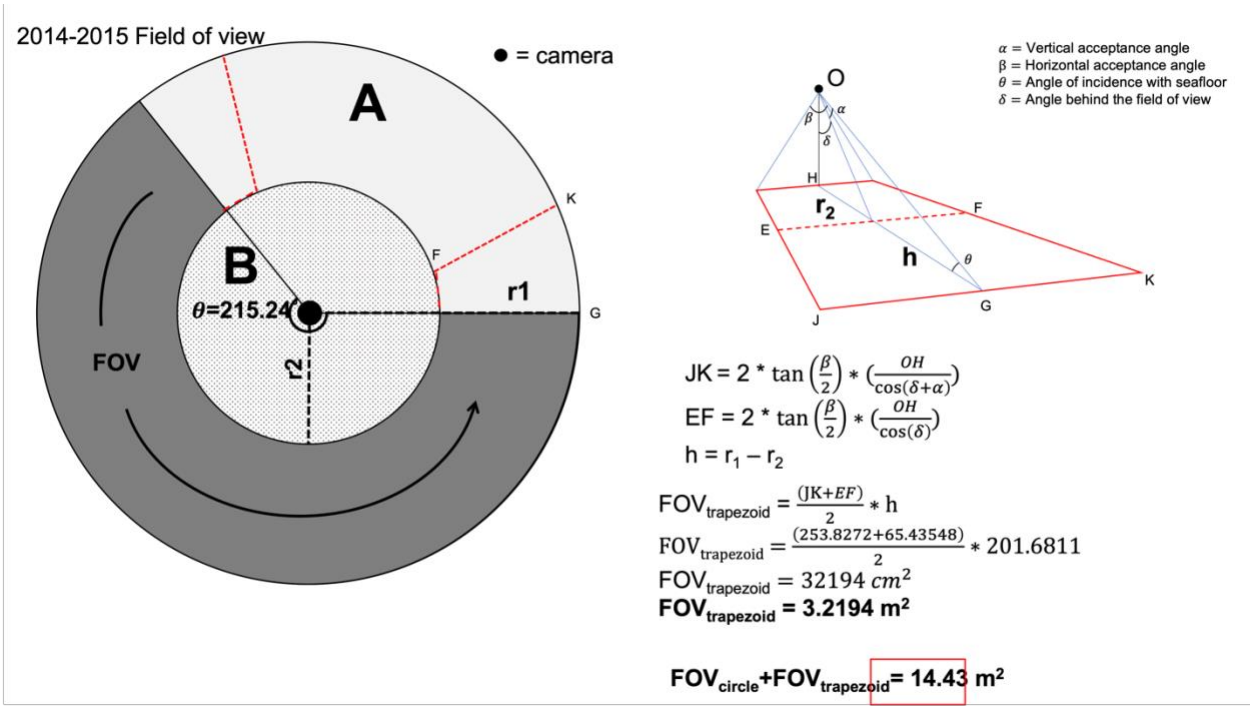

Since the pan angles are based on the position at the center of the field of view, we need to add the area to the right and left of the start and end positions, respectively (i.e., one still frame, oblique field of view). This is calculated as the area of a trapezoid, where the width of the top and bottom are determined by doubling the tangent of one half the horizontal acceptance angle multiplied by the ratio of the camera height to the cosine of the angle incident with the camera lens at the top and bottom of the visible field of view (defined by the vertical acceptance angles). The trapezoid area is then added to the circle area, to reach the full area visible in the field of view in 2014.

2018 field of view

2018 Field of view

α = Vertical acceptance angle
β = Horizontal acceptance angle
θ = Angle of incidence with seafloor
γ = Angle at the top of FOV

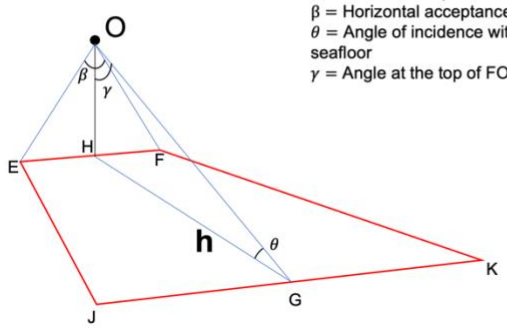

$\beta = 53.3^{\circ}$
$\gamma = 76^{\circ}$
OH = 95 cm

$JK = 2 * \tan\left(\frac{\beta}{2}\right) * \left(\frac{OH}{\cos(\gamma)}\right)$

$EF = 2 * \tan\left(\frac{\beta}{2}\right) * OH$

$h = OH * \tan(\gamma)$

$FOV_{trapezoid} = \frac{(JK+EF)}{2} * h$

$FOV_{trapezoid} = \frac{(394.1453+95.35239)}{2} * 381.0242$

$FOV_{trapezoid} = 93255.24 cm^2$

$FOV_{trapezoid}$ = 9.33 m^2

In 2018, the camera starts pointing straight down, tilts up to 90˚, and then tilts back to straight down. Here, we chose the angle at the top of the field of view to be 76˚ (angle at the center of the field of view, marked by the lasers) as this provided adequate lighting to see and count *Strongylocentrotus fragilis* but serves as a cut off to define a standardized field of view. The field of view area is calculated as the area of a trapezoid, where the width of the top and bottom are determined by doubling the tangent of one half the horizontal acceptance angle multiplied by the ratio of the camera height to the cosine of the angle incident with the camera lens at the top of the visible field of view (defined by the chosen stopping angle of 76˚). The trapezoid area is the full visible field of view used to count *S. fragilis* in 2018

2019-2020 field of view

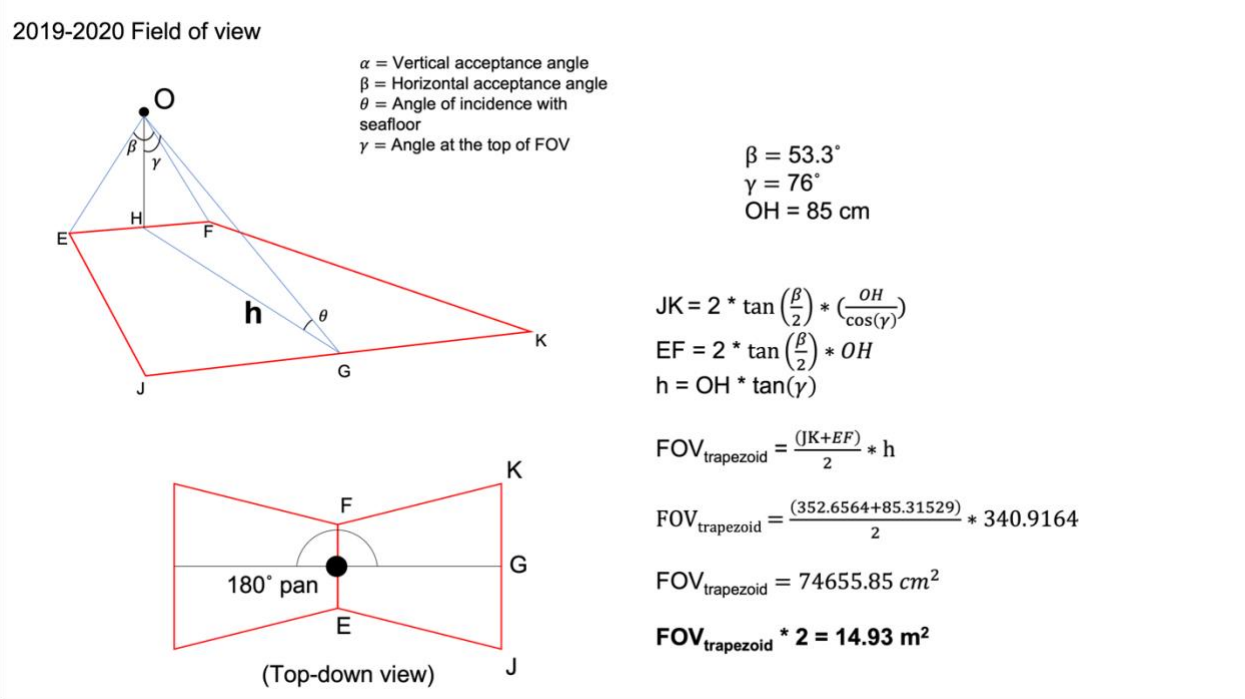

In 2019-2020, the camera starts pointing straight down, tilts up to 90˚, and then tilts back to straight down. Here, we chose the angle at the top of the field of view to be 76˚ (angle at the center of the field of view, marked by the lasers) as this provided adequate lighting to see and count *Strongylocentrotus fragilis* but serves as a cut off to define a standardized field of view. The field of view area is calculated as the area of a trapezoid, where the width of the top and bottom are determined by doubling the tangent of one half the horizontal acceptance angle multiplied by the ratio of the camera height to the cosine of the angle incident with the camera lens at the top of the visible field of view (defined by the chosen stopping angle of 76˚). As the 180˚ occurs when the camera is pointing 90˚, there is no visible seafloor area during the pan. When the camera pan finishes, the visible seafloor represents a new visible area and was assumed to be equal to the first area. Thus, the trapezoid area was doubled to account for both sides of the observatory visible in 2019-2020. This doubled area was used to count *S. fragilis* in 2019-2020.

A1.2 Holyrood Subsea Observatory

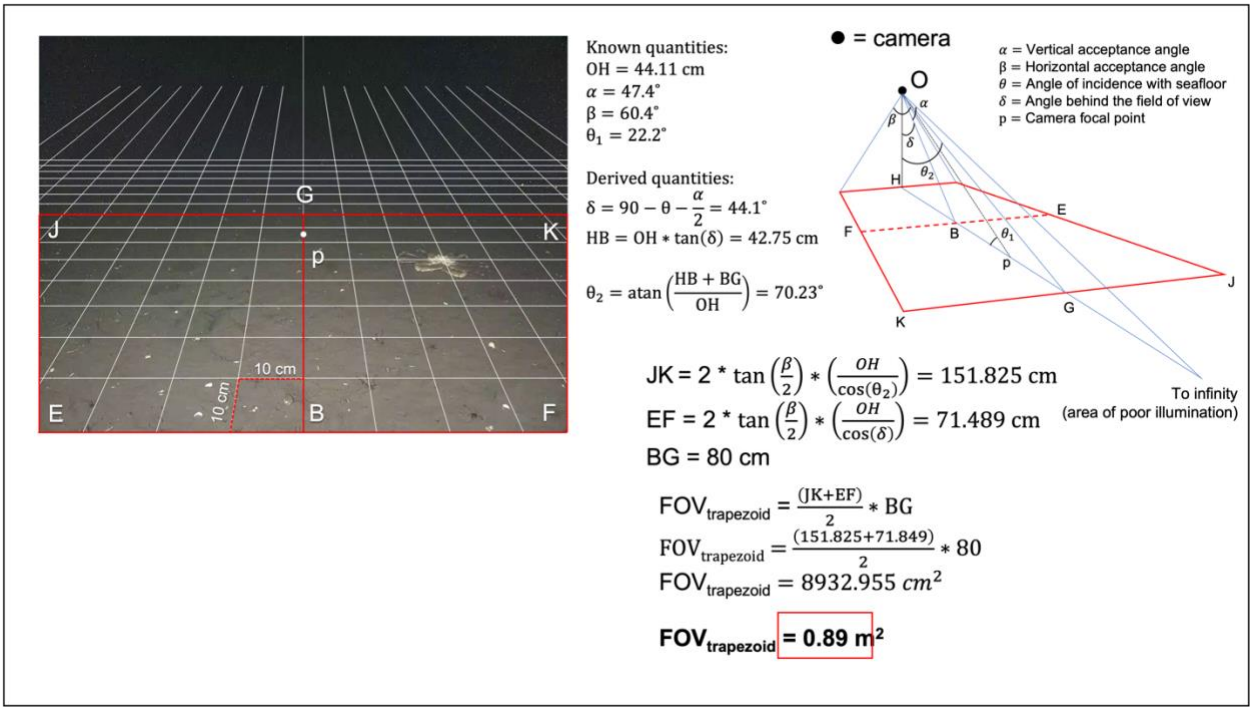

In order to account for the poor illumination field, a perspective grid was calculated following Wakefield & Genin (1987). The camera was calibrated such that the focal point, p, occurs at the intersection of diagonal lines drawn from corner to corner of the field of view. This point occurs a real distance of about 116 cm in a straight line from the camera lens; about 108 cm from the camera base parallel to the seafloor. Each grid cell represents 10cm x 10cm of real distance on the seafloor. The height of the trapezoid, BG, was determined by counting the grid cells to the top of the illuminated area. This distance was determined to be 80 cm.

The visible field of view was then calculated as the area of a trapezoid, where the width of the top and bottom are determined by doubling the tangent of one half the horizontal acceptance angle multiplied by the ratio of the camera height to the cosine of the angle incident with the camera lens at the top and bottom of the visible field of view (defined by the vertical acceptance angle (bottom) and adjusted for the height of the illumination field determined using the perspective grid (top)).

Appendix 2: Drowning in Data: How artificial intelligence could throw us a life ring

This essay has been published in Journal of Ocean Technology (2021, Volume 16, Issue 3) and was written by Rylan J. Command, with intellectual and editorial input from Dr. Katleen Robert (co-author), and editing by Dawn Roche (editor, Journal of Ocean Technology).


WINCH LOWER
WINCH UPPER
ARGUS DOWN
ARGUS BUTT
HERC BUTT
WINCH HOLD
WINCH STORE
ARGUS UTIL
ARGUS DASH
ARGUS ZEUS
HERC BROW

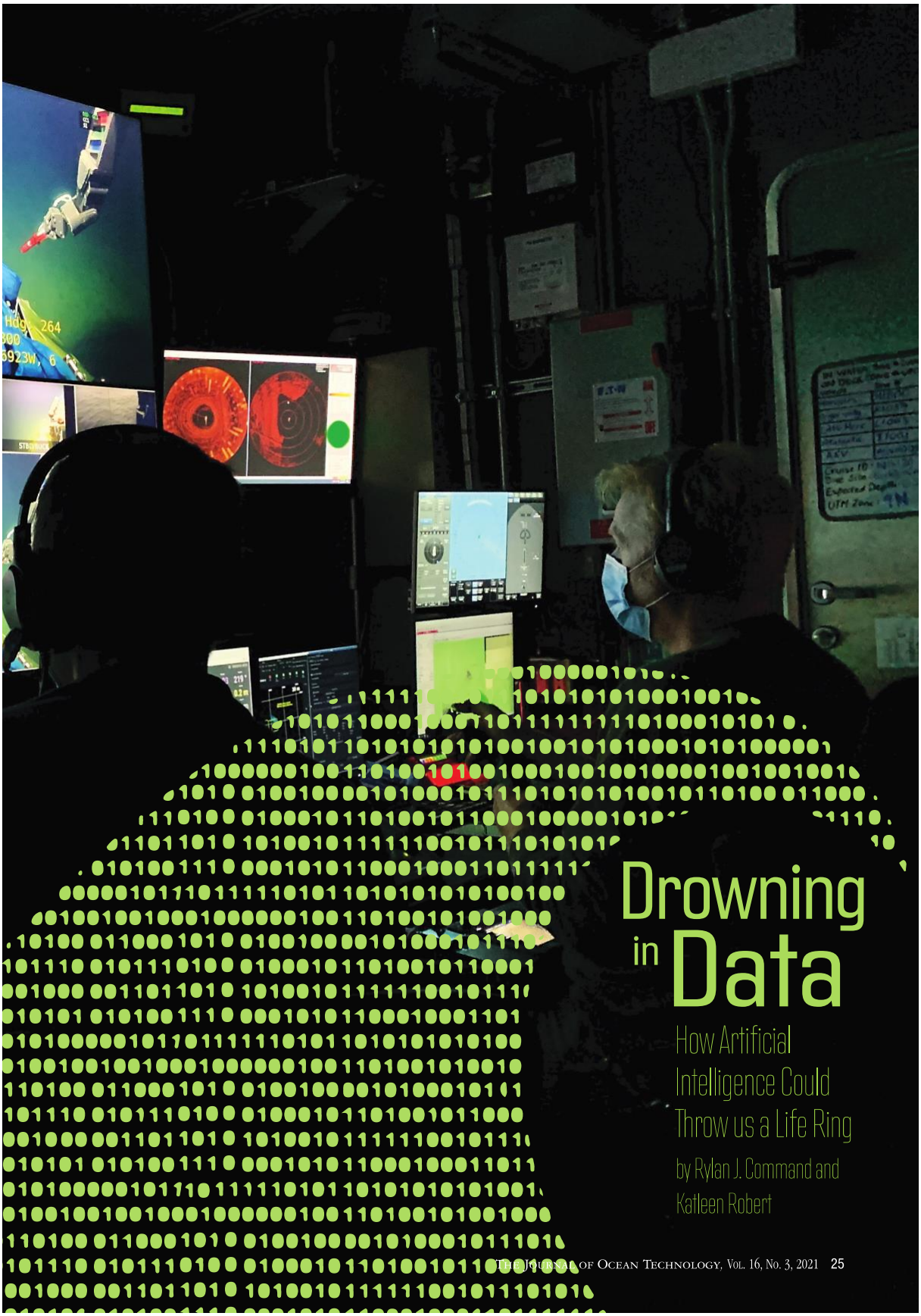

Drowning in Data

How Artificial Intelligence Could Throw us a Life Ring

by Rylan J. Command and Katleen Robert

Introduction

The amount of daily data collected by ocean observing systems is massive. The National Ocean and Atmospheric Administration (NOAA) in the United States collects around 20 terabytes of ocean data every day, and projects that its archives will store over 250 petabytes (PB) of ocean data by 2030. To put that in perspective, 200 PB is the estimated volume of all written material that has ever been printed. Ever. In addition to the sheer volume, ocean data comes in many different flavours covering the biological, chemical, and physical nature of the ocean. The instrument types needed to collect this information are numerous, including temperature loggers, oxygen sensors, fluorometers, turbidity monitors, acoustic Doppler current profilers, hydrophones, satellites and many more. All of these data types present their own challenges for interpreting and understanding oceanography from surface to seafloor. Free, open-source software has been developed to assist in processing oceanographic data to elucidate spatial and temporal patterns in the ocean. However, this wealth of collected environmental data is only the tip of the iceberg.

Advances in camera and image capture technologies and infrastructure for long-term deployments have led to a revolution in underwater data collection. From opportunistic time-lapse imagery to near real-time, high-definition video, our ability to collect high quality time-series of the seafloor has never been greater. However, this revolution has generated a looming question: Who is going to watch it all? There is so much biological information contained in a single image – what species are present? How many species are there? What are they doing? What sort of habitat do they live in? How do they interact with their habitat? Furthermore, video and imagery data files are large, requiring massive storage capacity, which is energy intensive and expensive.

As the saying goes, a picture is worth a thousand words. To give a real-world example, a seven-year oxygen sensor dataset collected at 1 observation/second takes up around 14 GB when saved as a series of comma-separated values. In contrast, a single five-minute high-resolution video clip (fast becoming the industry standard in seafloor observing systems) is around 180 MB. Seven years of these videos collected hourly is about 11,000 GB – or 785 times larger than the oxygen text files. How many words are those pictures worth?

The Need for Automated Video Analysis

Because each video or image contains so much information, they are incredibly time-consuming and labour intensive to process. Video and imagery collected from seafloor observatories are commonly used to identify the organisms present in a particular area. Marine plants and animals provide numerous ecosystem services from which humans benefit, such as food production, water filtration, recycling nutrients, and producing the oxygen we breathe. Data collected on the diversity of marine life helps inform fisheries management, marine spatial planning, ecosystem health assessments, and foster a connection with an otherwise unseen environment. Analyzing this data often requires expert knowledge or training to reliably identify the species of interest. Manual identification of organisms in video is time consuming and represents a large bottleneck.

During co-author Command's master degree studies at the Marine Institute of Memorial University of Newfoundland and Labrador, he had the opportunity to work with Ocean Networks Canada's (ONC) seafloor observatories off the coast of British Columbia, and the Marine Institute's newly installed cabled observatory in Holyrood, Newfoundland. At both sites, he studied temporal trends in the abundance of large seafloor organisms (Figure 1). As an example, 2,228 videos (~389 GB of data) required three months of work to count a single species of sea urchin. To put that in perspective, ONC alone collects roughly 10 GB of underwater videos daily.

Figure 1: Images from Ocean Networks Canada's cabled observatories co-author Command used for his master degree research. Left: The deepsea pink urchin Strongylocentrotus fragilis at the Barkley Canyon Upper Slope node of the NEPTUNE cabled observatory off Vancouver Island, British Columbia. Right: The northern sunstar, Solaster endeca, and the sea cucumber, most likely Psolus phantapus, at the Holyrood Bay Underwater Network in Conception Bay, Newfoundland and Labrador. Distance between the lasers in the left image is 10 cm.

Advances in artificial intelligence are already making computer vision tasks faster and more efficient, and more accurate than ever. Pre-trained models, open access software and code, large libraries of labelled data, and large communities are working together to share research and push the cutting edge of artificial intelligence. From particle counts and object tracking, to automated classification of organisms using complex algorithms modelled on the human brain, combinations of machine learning and computer vision approaches are rapidly improving our ability to process video and imagery data.

To Supervise or not to Supervise?

Two main categories of machine learning are used to automate image analysis – supervised and unsupervised learning – each of which lends themselves to different tasks. Supervised learning requires the model to be trained on a labelled data set to learn, for example, which image belongs to which category (i.e., fish versus crab). Once the model has been trained, it is put to the test on a batch of previously unseen images to see how well it can recognize and correctly classify each image (i.e., how often does the model say fish = fish versus fish = crab). To accomplish this, an expert must first create the labelled data set by assigning categories to pixels within a series of images collected from an observatory, for example. By putting in the time upfront, a researcher can train a supervised learning model to recognize species, and (hopefully) correctly classify unseen images into the correct categories.

One major limitation of supervised learning is the time-consuming nature of creating the labelled dataset in the first place. The minimum amount of data needed for a high-performing model depends on many factors, but a general rule of thumb is to make sure the amount of training data is at least 10 times the number of features used for training. For underwater images, there are often dozens of features extracted from an image relating to size, shape, texture, and colour that can inform classification, so the minimum training data size can be on the order of 1,000-10,000 images. Additionally, the model can only identify images and make predictions for the labels (i.e., species) for which it was trained. Expanding the labelled dataset to include a new species and retrain the model is time consuming.

Figure 2: Images of the black coral Leiopathes sp. taken from the ROV Holland I on the 2018 Tectonic Ocean Spreading at the Charlie-Gibbs Fracture Zone (TOSCA) expedition to the Charlie-Gibbs Fracture Zone on the Mid-Atlantic Ridge. Each of these images likely contains different species of the genus Leiopathes; however, distinguishing them in images may be impossible, requiring genetic techniques.

Where supervised learning requires a labelled dataset to learn to assign labels, unsupervised learning looks for patterns in an unlabelled dataset and clusters similar items together based on some criteria. The major challenge with unsupervised learning is defining the criteria with which clusters should be separated. This can be done by extracting features from an image, such as colour, shape, and texture, and separating images into groups based on how (dis)similar they are. Automated feature extraction using computer vision software (i.e., opencv in C++ or Python) is becoming more accessible and more efficient, and unsupervised learning is particularly useful for pattern recognition tasks.

There are several drawbacks with unsupervised learning for images. First, there is the computational complexity of working with very large, unlabelled datasets that are required to produce the desired outcome. Second, clustering algorithms are often difficult to interpret as there is often limited or zero capacity to determine the criteria by which a particular clustering decision was made. Finally, clusters created with unsupervised learning may be inaccurate and often require extensive validation by experts or with available "groundtruth" data. This is especially problematic when different species have very similar features, making it difficult to accurately distinguish between two different clusters of organisms that may have different ecological niches (i.e., consume different foods, are active at different times of day, etc.) but similar features in an image (Figure 2). This last point becomes especially challenging in underwater imagery, where variable lighting conditions may reduce image quality and make it more difficult to differentiate features among similar species.

The Power of the (Artificial) Brain

Artificial neural networks (ANNs; Figure 3) are one promising avenue of machine learning. These algorithms are based on the architecture of the human brain, and consist of layers of nodes (or neurons) connected by weighting functions (or synapses). An input is fed into the network, and passes through a series of weighting functions in each layer that determines if the information should be passed to the next layer, or stop. The output of each layer is determined by an activation function, which is influenced by the relative importance

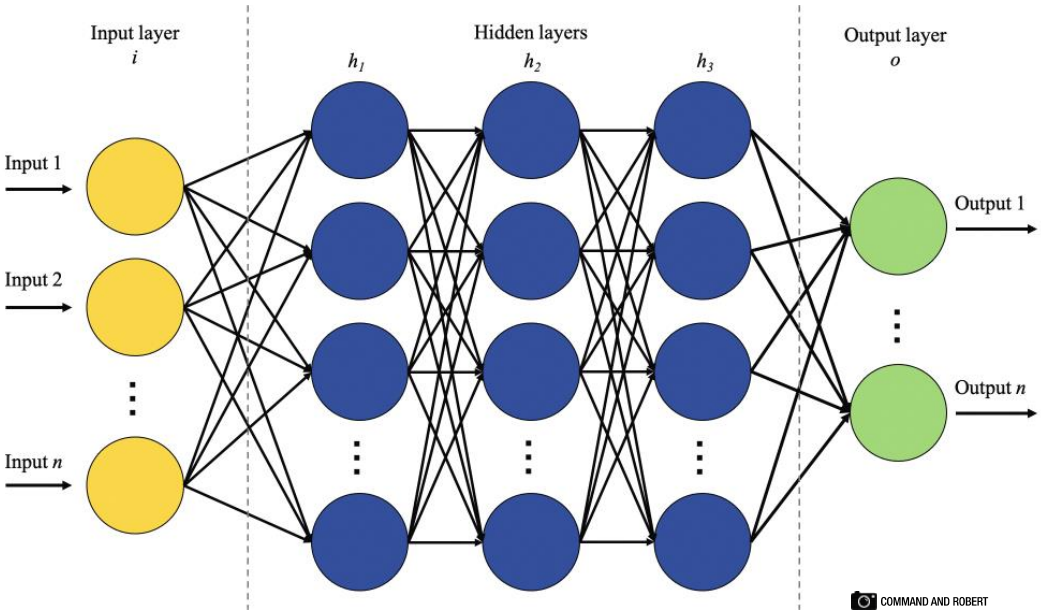

Figure 3: Structure of an artificial neural network (ANN). Input variables are fed into the network at the input layer and a calculation is performed. A series of weights and mathematical functions are applied, and errors are calculated to determine if the output, or signal, of a layer continues to the next layer. The weights and decisions made are not directly observable from the input and output of the network, so these are referred to as "hidden layers." Finally, the output layer takes as inputs the result of the hidden layers and calculates the final output of the network.

of each input, and becomes the input for the next layer. The network continues in this way to identify features based on thresholding criteria at each layer and produces an output – either a classification probability or a value. The weights for each node are determined through training and backpropagation, where the result is fed backwards through the network to fine-tune the weights and improve the model – this process is repeated numerous times to adjust weights to produce the expected output. This is computationally costly and time consuming, but with the help of hardware improvements over the past decade, has become more feasible and accessible.

Convolutional neural networks (CNNs; Figure 4) are a subset of ANNs that are particularly suited to deriving features from images. CNNs make use of convolution and pooling, steps that feed into and train a layered ANN to extract information and classify images or objects in a video. The convolution step defines what the important features are in an image, such as edges. The pooling step shrinks the information in a given frame by taking averages or finding maxima of nearby pixels for a sample window of a certain size, which is applied across an entire frame – essentially keeping only the important features as defined by the convolution step. By combining these steps of finding important features and removing the noise, information is passed through the network; convolution and pooling steps are repeated multiple times to condense the information contained in a frame and flatten the input image to be fed into the ANN. Most, if not all, modern computer vision models incorporate CNNs.

The possible applications for this technology are virtually limitless given the amount of video data collected daily by ocean observing systems. These models have been applied to fish identification for fisheries management and stock assessment, classification of algae species from plankton tows to monitor phytoplankton blooms, and environmental

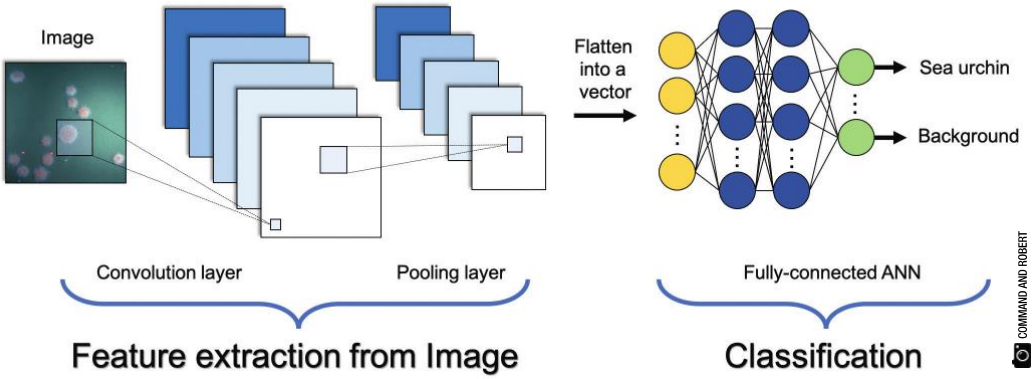

Figure 4: Diagram of a convolutional neural network (CNN). Convolutions are a class of mathematical functions that describe the amount of overlap between two functions as one is shifted over the other (i.e., it "blends" the functions). CNNs use a series of convolution and pooling steps to filter and reduce the dimensions of an input matrix, and are particularly well suited to extracting features from images. The result of a CNN is often fed into the input layer of an ANN that provides the classification step.

monitoring of marine energy projects such as wind or oil and gas platforms. These models are usually purpose-built but could be trained on similar datasets to address other problems from basic ecology to assessing responses to climate change.

This approach has been applied to the identification of deepsea pink urchins (*Strongylocentrotus fragilis*) from underwater video with 99% accuracy – the same species for which co-author Command manually sifted through 2,228 videos over the course of three months to count. This species lends itself well to computer vision tasks as it is easily distinguished from the background and other nearby organisms by its pink colour and unique morphology.

Computer Vision Underwater

Computer vision software has been optimized for object tracking and identification of day-to-day objects and situations, such as traffic and faces, to make light work of everyday situations (think self-driving cars and facial recognition). However, unique challenges exist for computer vision tasks in the marine environment. Variable or uneven lighting conditions due to high turbidity and particle loading create distorted or hazy images. Camera lenses can also become obscured through fouling by algae. Light attenuation with depth and the use of artificial lighting can also produce variable lighting conditions, with optical backscatter and colour fading making species identification more difficult. Addressing these challenges requires careful pre-processing of video and image data. Image processing pipelines to deal with each of these challenges are needed, but so far are only available on a case-by-case basis.

One possible way to improve predictions for some species would be to incorporate known life-history traits and ecologies into machine learning models. Spatiotemporal data about diel vertical migration and burrow emergence, or seasonal spawning and migration patterns using video timestamps and GPS tracking of instruments could help a model learn which organisms are likely to be present at a given site at a given time, and improve accuracy.

You Can Help

Machine learning models and CNNs can help information flow faster by automating some of the processing tasks, like object detection and classification, but only after training on a large dataset of labelled images. Labelling

these images is likely the most time-consuming part of the analysis, and cannot be automated without having a large, labelled dataset in the first place. How do we overcome this paradox of image analysis? This is where you come in.

Over the course of your internet use, you most likely have come across Google's image CAPTCHA. This usually shows up as the final "security check" before submitting an online form. For this check, Google shows you a grid of images and asks you to select only images with a stop sign or a crosswalk, or something similar. Have you ever wondered why these images are always related to traffic? Google is making use of perhaps the most efficient way to create a massive, labelled dataset – crowd sourcing annotations – to train their driverless car algorithms.

A few similar applications exist for identifying species in underwater images, and studies have been done to compare the performance of experts, machine learning algorithms, and trained volunteers (i.e., "the crowd"). Ocean Networks Canada's "Digital Fishers" is a crowd-sourced ocean science observation game where players label deepsea videos from ONC's cabled observatories and remotely operated vehicle dives. The player progresses through the game with each level unlocking more information about organisms and asking for more complex annotations. These crowd-sourced annotations directly contribute to ONC's database, creating a labelled dataset to train machine learning algorithms to automatically identify deepsea organisms from which scientists will be able to extract valuable information.

The fields of computer vision and artificial intelligence have the potential to unlock the bottleneck on underwater image and video processing and analysis. Given the current rate of ocean data collection, and the upcoming investment in ocean research brought by the United Nations Decade of Ocean Science for Sustainable Development, we certainly have our work cut out for us.

Rylan Command is a graduate student in the 4D Oceans Lab in the School of Ocean Technology; he is in the M.Sc. Fisheries Science and Technology program at the Fisheries and Marine Institute of Memorial University of Newfoundland and Labrador. His research focuses on temporal trends in the abundance, behaviour, biodiversity, and distribution of seafloor megafauna using underwater cabled observatories. His goal is to measure the response of benthic megafauna to rapid change over time to understand the role of anomalies, like marine heatwaves, and seasonal changes, like the spring phytoplankton bloom, in structuring marine communities. He is also interested in fisheries and food systems, and the ways in which humans use and distribute marine resources globally. He hopes to use available ocean data to engage broadly with both scientific and non-scientific audiences.

Dr. Katleen Robert in an Assistant Professor within the School of Ocean Technology at the Fisheries and Marine Institute of Memorial University where she holds a Canada Research Chair in Ocean Mapping. Her research aims at developing quantitative and repeatable approaches to map seafloor habitats. Her focus has been on examining fine-scale species-environment relationships using benthic imagery and multibeam sonars to build full coverage predictive maps. She is also interested in how benthic environments change temporally, and has been dappling with data from seafloor cabled-observatories since she started as a graduate student. Her hope is to one day merge these two research streams to produce maps showing the spatio-temporal heterogeneity of benthic habitats.